IntechOpen

Cement Based Materials

Edited by Hosam El-Din M. Saleh and Rehab O. Abdel Rahman

CEMENT BASED MATERIALS

Edited by **Hosam El-Din M. Saleh**
and **Rehab O. Abdel Rahman**

Cement Based Materials
http://dx.doi.org/10.5772/intechopen.71134
Edited by Hosam El-Din M. Saleh and Rehab O. Abdel Rahman

Contributors

Majed Aldahdooh, Chameera Dussantha Udawattha, Rangika Halwatura, Halim Hammi, Mohd Mustafa Al Bakri Abdullah, Liew Yun Ming, Heah Cheng Yong, Muhammad Faheem Mohd Tahir, Fariborz M. Tehrani, Nathan Miller, Dmitriy Kochkarev, Tatyana Galinska, Tatiana Pyatina, Toshifumi Sugama, Wafa Abdelmajeed Labib, Elena Cerro-Prada, Erdem Şahin, Stanislav Boldyryev, Mohammad Hajmohammadian Baghban, Hosam Saleh, Sung Hwang, Rouzbeh Shahsavari, Narasimhulu K, Ravindra Gettu

First published in London, United Kingdom, 2018 by IntechOpen
eBook (PDF) Published by IntechOpen, 2019
IntechOpen is the global imprint of INTECHOPEN LIMITED, registered in England and Wales, registration number: 11086078, The Shard, 25th floor, 32 London Bridge Street
London, SE19SG – United Kingdom
Printed in Croatia

British Library Cataloguing-in-Publication Data
A catalogue record for this book is available from the British Library

Additional hard and PDF copies can be obtained from orders@intechopen.com

Cement Based Materials
Edited by Hosam El-Din M. Saleh and Rehab O. Abdel Rahman

p. cm.

Print ISBN 978-1-78984-153-4

Online ISBN 978-1-78984-154-1

eBook (PDF) ISBN 978-1-83881-514-1

Meet the editors

Hosam Saleh is a professor of Radioactive Waste Management at the Department of Radioisotope, Atomic Energy Authority, Egypt. He received his MSc and PhD degrees in Physical Chemistry from the Cairo University. He is interested in studying the innovative economic and environment-friendly techniques for the management of hazardous and radioactive wastes. He has authored many peer-reviewed scientific papers and chapters. He is an editor of several books related to valuable international publishers.

Rehab O. Abdel Rahman is an associate professor of Chemical Nuclear Engineering at the Atomic Energy Authority, Egypt. She received her PhD degree in Nuclear Engineering from Alexandria University. She contributed to the publication of more than 30 peer-reviewed scientific papers, 8 book chapters, and 4 books. She is an honored scientist at the Academy of Scientific Research and Technology (ASRT) and serves as a verified reviewer in several journals and a managing editor of the International Journal of Environment and Waste Management (IJEWM) and International Journal of English and Education (IJEE).

Contents

Preface

Cement-based materials are hydraulic binders. Upon hydration, they produce materials with improved physical and mechanical properties. The nature of the cement-based materials allows its utilization in several applications today.

The book at hand, *Cement-Based Materials*, was compiled to represent advances in the development and application of these materials in different fields, which aim to ensure their sustainability. Carefully selected authorships from different countries contributed in this book.

Within this book, the recent research activities in four topics related to "cement-based materials" are included, namely, properties of cement-based materials, green cement, calcium phosphate cement, and alkali-activated cement. The book is dedicated to researchers and undergraduate students who are involved in these fields; we hope that this book is helpful and provides inspiration for readers during their work/studies. In addition, we strongly believe that the issue also attracts the attention of representatives of the cement industry and cement-based materials.

We provided the introductory chapter on cement-based materials, their properties, and their applications, with a special reference to the hydration chemistry.

We are tremendously optimistic that the exploratory and scientific attempts collected and summarized in the book at hand will encourage researchers all over the globe to deepen their activities in this field and to attract the interest of undergraduates as well as of progressive representatives from the relevant industrial sectors. Primarily, these activities shall boost the impatiently desired breakthrough of "cement" manufacturing processes, which reasonably merit this designation.

We especially acknowledge Ms. Anita Condic, Author Service Manager, for her successful cooperation, exceptional efforts, and prompt reply to our requests. Again, we would like to thank cordially all the contributors to this concern for their supreme work.

Hosam El-Din M. Saleh, PhD and Rehab O. Abdel Rahman, PhD
Atomic Energy Authority
Egypt

Section 1

Properties of Cement Based Material

Chapter 1

Introductory Chapter: Properties and Applications of Cement-Based Materials

Hosam M. Saleh and Rehab O. Abdel Rahman

Additional information is available at the end of the chapter

http://dx.doi.org/10.5772/intechopen.73784

1. Introduction

Cement-based materials have been used to support human civilizations many decades ago. With the increasing advancement of human activities, these materials were modified to maintain their roles in our lives. The main function of cement is to act as hydraulic binder, which increases the bond between fragmented particles, so it can enable their use in different fields. The resulted material will have different physical and mechanical properties from the initial materials. These changed properties are attributed to the exothermic hydration reactions that are initiated upon mixing the binder with water. The liberated localized heat will lead irreversible rearrangement of water molecules within the framework microstructure [1–3]. Ordinary Portland Cement (OPC) is the most widely used cement. It is prepared by crushing, milling, and mixing calcium, iron, silica, alumina, and sulfate sources with certain amounts. Then, hydraulic cement is passed to the kiln to produce clinker, which is subsequently cooled and pulverized. Portland cement is categorized into eight subgroups according to the ASTM C150, namely normal (type I), moderate sulfate resistance (type II), high early strength (type III), low heat of hydration (type IV), high sulfate resistance (type V), normal, moderate sulfate resistance, and high early resistance with air entraining (types IA, IIA, IIIA), respectively [4]. There are four principal unhydrated phases present in all OPC types, namely tricalcium silicate (Ca_3SiO_5), dicalcium silicate (Ca_2SiO_4), tricalcium aluminate ($Ca_3Al_2O_5$), and calcium aluminoferrite ($Ca_4Al_nFe_{2-n}O_7$). The formula of each of these minerals can be broken down into the basic calcium, silicon, aluminum, and iron oxides (**Table 1**). Cement chemists use abbreviated nomenclature based on oxides of various elements to indicate chemical formulae of relevant species, that is, C = CaO, S = SiO_2, A = Al_2O_3, and F = Fe_2O_3. Hence, traditional cement nomenclature abbreviates each oxide as shown in **Table 1** [1].

The composition of cement is varied depending on the application. A typical example of cement contains 50–70% C3S, 15–30% C2S, 5–10% C3A, 5–15% C4AF, and 3–8% other additives or minerals (such as oxides of calcium and magnesium). It is the hydration of the calcium silicate, aluminate, and aluminoferrite minerals that cause the hardening, or setting, of cement. The ratio of C3S to C2S helps to determine how fast the cement will set, with faster setting occurring with higher C3S contents. Lower C3A content promotes resistance to sulfates. Higher amounts of ferrite lead to slower hydration. The ferrite phase causes the brownish gray color in cements, so that "white cements" (i.e., those that are low in C4AF) are often used for esthetic purposes. The calcium aluminoferrite (C4AF) forms a continuous phase around the other mineral crystallites, as the iron containing species act as a fluxing agent in the rotary kiln during cement production and are the last to solidify around the others. **Figure 1** shows a typical cement grain.

It is worth noting that a given cement grain will not have the same size or even necessarily contain all the same minerals as the next grain. The heterogeneity exists not only within a given particle, but extends from grain to grain, batch to batch, and plant to plant.

Modifications of cement-based materials are usually carried out by testing the effect of different additives and/or admixtures on certain physicochemical properties that can affect the overall performance of the material [1, 3]. Additives might be classified based on their [3]:

1. Origin—natural igneous, natural sedimentary, industrial waste, or modified soil
2. Particle size—coarse or fine
3. Density—light or heavy
4. Activity—inert, chemically active, physically active, and physically and chemically active
5. Specific surface—low, average, high, ultra, and nano dispersion.

Depending on the amount of used additive to cement ration, cement-based material could be divided into blended cement or modified cement. Blended cement is a class of additive-cement system that contains more than 15% additive. ASTM identified five classes of blended hydraulic cement as follows: Ordinary Portland Cement (OPC)-blast furnace slag (IS type), OPC-Pozzolan (IP and P types), Pozzolan-modified-OPC (I(PM) type), Slag cement (S type), and Slag-modified OPC (SM type) [4]. Modified cement contains less than 15% mineral additives. On the other hand, there are different classifications for the tested/used admixture as follows [2, 3]:

Mineral	Chemical formula	Oxide composition	Abbreviation
Tricalcium silicate (alite)	Ca_3SiO_5	$3CaO.SiO_2$	C3S
Dicalcium silicate (belite)	Ca_2SiO_4	$2CaO.SiO_2$	C2S
Tricalcium aluminate	$Ca_3Al_2O_4$	$3CaO.Al_2O_3$	C3A
Tetracalcium aluminoferrite	$Ca_4Al_nFe_{2-n}O_7$	$4CaO.Al_nFe_{2-n}O_3$	C4AF

Table 1. Chemical formula and cement nomenclature for major unhydrated OPC phases.

1. Their effects on setting time and water requirements: ASTM C494, BS 5075, and CAN 3A2662M78 classify admixture according to their role in reducing the amount of water only or reduce the waste and act as retarders or accelerator.

2. Their technological characteristics: used in France, Germany, and Russia where the admixture effect on the setting time, rheology, air content, hardening, workability, cement properties and special properties are used to classify the admixture.

3. Classification is based on the chemical properties of the admixture themselves, that is, soluble and insoluble in water. Under this classification, the admixture is categorized based on their effects.

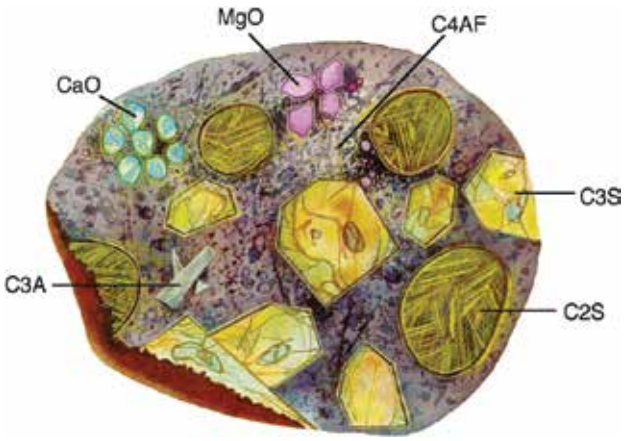

Figure 1. A pictorial representation of a cross section of a cement grain. Adapted from Cement Microscopy, Halliburton Services, Duncan, OK.

	Aluminates	**Phosphate**	**Sulfoaluminate**
Components	Calcium source Limestone Alumina source bauxite, high-alumina slags	Acid-base reactions in the presence of liquid activators containing phosphate anions	Calcium source: lime, Alumina source: bauxite, kaolin Sulfate source: gypsum
CO_2 emission	Low	—	Low
Setting	Fast	Fast	Fast
Strength	High	High adhesive, bending and compressive strength	High early strength
Working condition resistance			
Freeze–thaw	High	—	High
Heat	High	High	—
Chemical	High	High	High in sulfate and magnesium

Table 2. Comparison between different alternative cement and OPC properties.

Almost all the historical applications of cement as hydraulic binders relied on the use of pozzolanic materials with additives, and currently, alternative cements were developed to substitute Ordinary Portland Cement in certain application or to overcome Portland cement drawbacks. These materials include aluminate cements, phosphate cements, sulfoaluminate cements, and alkali-activated cements [3]. The later represent a vast category of subsets of materials that differ based on the alkaline activator of the aluminosilicate system. **Table 2** lists a comparison between the aluminate cements, phosphate cements, sulfoaluminate cements, and OPC [3].

2. OPC hydration chemistry

The hydration reactions of cement-based materials are complex, especially when chemically active additives/admixtures are used. However, it is generally accepted that the principal products of hydration of OPC are calcium-silicate-hydrate gel (CSH), which composed of mixture of tobermorite, jennite, and afwillite (60–70%); portlandite (CH) (20–25%); and other minor phases (approximately 5–15%) [1]. The principal reactions involved may be represented by the following two idealized equations:

$$\underset{\text{(alite)}}{2C_3S} + 6H \rightarrow \underset{\text{C-S-H gel}}{C_3S_2H_3(\text{C-S-H})} + 3CH \tag{1}$$

$$\underset{\text{(belite)}}{2C2S} + 4H \rightarrow \underset{\text{C-S-H gel}}{C_3S_2H_3(\text{C-S-H})} + CH \tag{2}$$

The stoichiometry of these reactions clearly shows that the hydration of 1 mol of tricalcium silicate yields 1.5 mol of Ca^{2+} ions (Reaction 1) and the hydration of 1 mol of di-calcium silicate yields 0.5 mol of Ca^{2+} ions (Reaction 2); these ions are released into pore solution with the formation of C-S-H phase. Cement hydration reaction progression occurs at three distinct periods, which are dormant, setting, and hardening. In the first (within few minutes from the reaction initialization) period, aluminate and ferrite phases react with gypsum to form an amorphous gel at the cement grains surface and short ettringite rods. In the second period (hours later), more portlandite and ettringite are formed and C—S—H formation begins. At the last period, the reaction slows down and internal C—S—H continues to grow near alite surface. The hydration rate is dependent on water and/or ion diffusion rate to anhydrous surface, so the timescale for each period and the development of hydrated phases in each time period are dependent on the hydration conditions, cement composition, and the presence of additives [1, 3].

3. Properties of cement-based materials

Cement-based materials are complex systems that have transient physical and mechanical properties. This phenomenon is related to the slow aging process in colloidal hydration

products [2]. In this section, the properties of cement-based material and the factors that affect them are overviewed.

3.1. Hydration heat

Heat is generated as a result of the exothermic hydration reaction, which will subsequently depend on the chemical and physical properties of unhydrated cement system. One of the important physical characteristics is the particle size distribution of the cement. The heat of hydration increases if the ration of fine materials increases, where the average fineness is in the range of 0.3–0.5 m^2/g. This is related to the increased available surface for reaction which subsequently leads to higher early strength [5].The heat of hydration plays a role in determining the setting time, as the release of this heat increases the rate of hardening. It should be noted that aluminates and sulfoaluminate cements have higher heat of hydration than OPC.

3.2. Setting time

Hydration reactions of cement-based materials are characterized by having initial and final setting times. The duration of setting is dependent on the chemical compositions and fineness of the binder and additives and on the ambient temperature. In specific cases, retardates are used to increase the setting time, so extended workability could be achieved. Retardation is applied in hot weather, cementing oil wells, pumping the paste over long distances, and if special finishing is required. It should be noted that in some cases, early strength development is reduced as a result of retarder addition. Free lime, gypsum, and alkali sulfate are used to slow OPC setting time. On the other hand, in some cases, accelerated hydration reaction with small setting time and early age strength development is required. This could be achieved by lowering the water to cement ration via using water reducer, curing at higher temperature or using accelerators [4].

3.3. Strength strain

Strength-strain relationship differs depending on the composition of the cement-based material, and for hardened cement pastes, the relationship is nearly linear, which reflects the brittleness of the material. On the other hand, hardened concretes continue to deform plastically after exceeding maximum load. The development of the strength-strain relationship in the complex heterogeneous system of cement-based material is affected by:

1. The porosity of hardened material, where the increase in porosity reduce the strength.
2. The chemical interaction and mechanical interlocking between the hydraulic binder and the additives.
3. Effect of hydraulic binder composition, that is, calcium, alumina, sulfate, alkali, and silica ration.
4. Effect of curing temperature, as it increases ultimate strength is reduced.
5. Production and testing conditions, including mixing composition, curing, and load humidity

3.4. Soundness

It is the ability of the hardened cement paste to retain its original volume, and the presence of free lime or magnesium oxide can reduce the soundness of the cement-based materials.

4. Cement composites

Different materials are used as additive to cement to improve the cement characterizations. The mechanical properties of the newly formulated composites were improved. Cement-waste fiber composite was produced due to the incorporation of waste fibers in cementitious materials and used in radioactive waste immobilization [6–9]. Polymers also were impregnated with cement to increase the durability and reduce the porosity of cement, producing favorable composite suitable for many applications and resistive to various aggressive conditions [10–15]. Natural additives such as clay were mixed progressively with cement to treat the retardation property of organic solvent with cement [16, 17].

5. Applications of cement-based materials

5.1. Construction

The application of OPC and its blends is widely applied in construction engineering. **Table 3** illustrates the use of different OPC and OPC blend types in constructions. Aluminate cement concrete is applied in the construction of industrial floors and refractory castables, where the floor must resist chemical, heat, and corrosion [4]. Moreover, decorative tiles, building bricks, and light concrete were performed [18]. Sulfate cement is used in repairing pavement and concrete structures and for places where aggressive chemicals exist.

Purpose	OPC	OPC blend	Applications
General use	I	IS, IP, I(PM), I (SP), S, P	For all uses including pavements, floors, reinforced concrete buildings, bridges, pipe, precast concrete products
Resist sulfate attack	II	IS, IP, P, I(PM), I(SM)	Where moderate sulfate concentration exists, that is, drainage structure, sea structures, and soil structure should be used at low water to cement ration
	V	—	High sulfate concentration media
Early strength	III	—	Used in cold weather to shorten the curing period
Hydration heat	IV	p	Low heat of hydration is required in massive concrete structures, such as large gravity dams
	II	IS, IP, I(PM), I (SM)	Moderate heat of hydration is required, in large structure in warm places, that is, large piers, large foundations, and thick retaining walls

Table 3. OPC and OPC-blend applications in construction [1, 3, 4].

5.2. Environmental aspects

The application of cement-based material in environmental protection and restoration is increasing, and they are used in radiation shielding in nuclear industry, cutoff walls in remediation activities, stabilization of contaminated soil, engineering barriers in disposal facilities, and waste immobilization matrices [19–34]. This wide range of applications is supported by their technical properties, where they have low diffusion coefficients and have available sorption sites; their alkaline environments reduce the mobility of different contaminants and flexibility of modification. In nuclear and radioactive waste industries, they are used as shield due to their good self-shielding performance, and they are suitable to solidify different radioactive waste streams, that is, sludge, emulsified organic liquid, fragmented solids, and exhausted ion exchangers, due to their chemical, radiological, thermal, mechanical, and physical stability. The economic value of these materials plays an important role in their widespread applications, as they are inexpensive and readily available, and has reduced operational cost (which is related to the simplicity of operation and operation at ambient temperature) [20–30]. To ensure the sustainability of these materials for the intended use, they need to be tested to evaluate their strength, radiation, biological and thermal stabilities, free water content, porosity, permeability, corrosion, leaching, dissolution rates, and release mechanisms.

6. Conclusion

The continuous widespread applications of cement-based materials to support human civilization is attributed to their simple modification ability. Different types of hydraulic binder were modified to address the needs to have functional constructions in different environments. With the continuous need to protect the environment from the effect of contaminated sites, either water or soil, cement-based materials were applied in different areas. There is still a need to enhance the performance of these materials in different applications, and this could be achieved by:

1. Testing the effect of industrial wastes as additives on OPC and alternate cements to increase the productive use of these wastes.
2. A quantitative assessment of the effect of additive on the microstructure of the produced material.
3. Developing models that could be used to predict the long-term behavior of the materials, either physical models or mathematical models.

Author details

Hosam M. Saleh* and Rehab O. Abdel Rahman

*Address all correspondence to: hosamsaleh70@yahoo.com

Atomic Energy Authority, Egypt

References

[1] Abdel Rahman RO, Ojovan MI. Recent trends in the evaluation of cementitious material in radioactive waste disposal, Ch (9). In: Wang LK, Wang MS, Hung YT, Shammas NK, editors. Handbook of Environmental Engineering, Vol 17, Natural Resources and Control Processes. Switzerland: Springer; 2016. pp. 401-448. DOI: 10.1007/978-3-319-26800-2_9 http://link.springer.com/chapter/10.1007/978-3-319-26800-2_9/fulltext.html

[2] Hewlett PC. Lea's Chemistry of Cement and Concrete. Amsterdam: Elsevier Science; 2006

[3] Abdel Rahman RO, Rakhimov RZ, Rakhimova NR, Ojovan MI. Cementitious Materials for Nuclear Waste Immobilisation, Wiley, New York; 2014. ISBN: 9781118512005. http://eu.wiley.com/WileyCDA/WileyTitle/productCd-1118512006,subjectCd-CH50.html

[4] Kosmatka SH, Kerkhoff B, William C. Panarese, Design and Control of Concrete Mixtures. 14th ed. USA: Portland Cement Association; 2003

[5] Abdel Rahman RO. Radioactive Waste. Rijeka, Croatia: InTech; 2012. ISBN 978-953-51-0551-0 http://www.intechopen.com/books/radioactive-waste (book editor)

[6] Eskander SB, Saleh HM, Fahmy HM. Incorporation of the spinning wastes in cement and mortars. Journal of Radiation Research and Applied Science. 2009;**2**(1):119-136

[7] Eskander, Saleh HM. Cement mortar-degraded spinney waste composite as a matrix for immobilizing some low and intermediate level radioactive wastes: Consistency under frost attack. Journal of Nuclear Materials. 2012;**420**(1–3):491-496

[8] Saleh HM, Eskander SB. Characterizations of mortar-degraded spinney waste composite nominated as solidifying agent for radwastes due to immersion processes. Journal of Nuclear Materials. 2012;**430**(1–3):106-113

[9] Fahmy HM, Eskander SB, Saleh HM. Applications of Recycled Textile Wastes in Cement Composite: Mortar-Spinney Wastes Composite. Germany: LAP Lambert Academic Publishing; 2012. ISBN 978-3-659-23099-8

[10] Saleh HM, Tawfik ME, Bayoumi TA. Chemical stability of seven years aged cement–PET composite waste form containing radioactive borate waste simulates. Journal of Nuclear Materials. 2011;**411**(1–3):185-192

[11] Eskander SB, Bayoumi TA, Saleh HM. Performance of aged cement-polymer composite immobilizing borate waste simulates during flooding scenarios. Journal of Nuclear Materials. 2012;**420**(1–3):175-181

[12] Ghattas NK, Eskander SB, Bayoumi TA, Saleh HM. Cement-polymer composite containers for radioactive wastes disposal. International Journal of Chemical and Environmental Engineering Systems. 2012;**3**(2):17-25

[13] Saleh HM, Bayoumi TA, Shatta HA. Mechanical and chemical characterizations of polyester modified cement immobilizing nuclear wastes. Advances in Chemical Science. 2012; **1**(1):12-17

[14] Saleh HM, Shatta HA. Immobilization of simulated borate radioactive waste solution in cement-poly(methylmethacrylate) composite: Mechanical and chemical characterizations. Journal of Nuclear Chemistry. 2013;**2013**:7

[15] Saleh HM. Composite materials for the improvement of radioactive waste containers: Structures and characterization. Journal of Nuclear Energy Science & Power Generation Technology. 2013;**S1-006**

[16] Eskander SB, Bayoumi TA, Saleh HM. Leaching behavior of cement-natural clay composite incorporating real spent radioactive liquid scintillator. Progress in Nuclear Energy. 2013;**67**:1-6

[17] Bayoumi TA, Saleh HM, Eskander SB. Solidification of hot real radioactive liquid scintillator waste using cement-clay composite. Monatshefte fur Chemie–Chemical Monthly. 2013;**144**(12):1751-1.3758

[18] Saleh HM, Eskander SB, Fahmy HM. Mortar composite based on wet oxidative degraded cellulosic spinney waste fibers. International Journal of Environmental Science and Technology. 2014;**11**(5):1297-1.3304

[19] Abdel Rahman RO, Saleh HEM. Nuclear Material Performance. Rijeka, Croatia: InTech; 2016. ISBN 978-953-51-4676-6, DOI: 10.5772/61411. http://www.intechopen.com/books/nuclear-material-performance

[20] Abdel Rahman RO. Planning and implementation of radioactive waste management system. Ch (1). In: Abdel Rahman RO, editor. Radioactive Waste. Rijeka, Croatia: InTech; 04/2012. ISBN: 978-953-51-0551-0. http://www.intechopen.com/books/radioactive-waste/-planning-and-implementation-of-radioactive-waste-management-system

[21] Abdel Rahman RO, Kozak MW, Hung YT. Radioactive pollution and control, Ch (16). In: Hung YT, Wang LK, Shammas NK, editors. Handbook of Environment and Waste Management. Singapore: World Scientific Publishing Co; Feb 2014. pp. 949-1027 http://dx.doi.org/10.1142/9789814449175_0016

[22] Abdel Rahman RO. Introduction to current trends in nuclear material research and technology, Ch (1). In: Abdel Rahman RO, Saleh HEM, editors. Nuclear Material Performance. Rijeka, Croatia: Intech; 2016. pp. 3-14. DOI: 10.5772/61411 http://www.intechopen.com/books/nuclear-material-performance/introductory-chapter-introduction-to-current-trends--in-nuclear-material-research-and-technology

[23] Abdel Rahman RO, Guskov A, Kozak M, Hung YT. Recent evaluation of early radioactive disposal practice, Ch (8). In: Wang LK, Wang MS, Hung YT, Shammas NK, editors. Handbook of Environmental Engineering, Vol 17, Natural Resources and Control Processes. Switzerland: Springer; 2016. pp. 371-400. DOI: 10.1007/978-3-319-26800-2_8 http://link.springer.com/chapter/10.1007/978-3-319-26800-2_8/fulltext.html

[24] Abdel Rahman RO, Ojovan MI. Application of nano-materials in radioactive waste management. In: Zhang TC, Gurjar BR, Govil JN, editors. Environmental Science and Engineering. Vol: 10, Industrial Processes & Nanotechnology Ch (15); LLC, USA: Studium Press; 2017: 361-378. ISBN 10:1-62699-098-0

[25] El-Kamash AM, Mohamed RO, Nagy ME, Khalill MY. Modeling and validation of radionuclides releases from an engineered disposal facility. International Journal of Waste Management and Environmental Restoration. 2002;**22**(4):373-393

[26] Abdel Rahman RO, El-Kamash AM, Zaki AA. Modeling the Long Term Leaching Behavior of 137Cs, 60Co, and 152,154Eu Radionuclides from Cement- Clay Matrices. Hazardous Materials. 2007;**145**:372-380

[27] Abdel Rahman RO, Zaki AA. Assessment of the leaching characteristics of incineration ashes in cement matrix. Chemical Engineering Journal. 2009;**155**:698-708

[28] Abdel Rahman RO, Zaki AA. Comparative study of leaching conceptual models: Cs leaching from different ILW cement based matrices. Chemical Engineering Journal. 2011; **173**:722-736

[29] Abdel Rahman RO, Zein DH, Abo Shadi H. Assessment of strontium immobilization in cement–bentonite matrices. Chemical Engineering Journal. 2013;**228**:772-780

[30] Abdel Rahman RO, Zein DH, Abo Shadi H. Cesium binding and leaching from single and binary contaminant cement-bentonite matrices. Chemical Engineering Journal. 2014;**245**: 276-287

[31] Abdel Rahman RO, Ojovan MI. Leaching tests and modelling of cementitious wasteforms corrosion. Innovations in Corrosion and Materials Science. 2014;**4**(2):90-95. DOI: 10.2174/2352094904666141126221626

[32] Saleh HM, Eskander SB. Long-term effect on the solidified degraded cellulose-based waste slurry in cement matrix. Acta Montanistica Slovaca. 2009;**14**(4):291-297

[33] Bayoumi TA, Reda SM, Saleh HM. Assessment study for multi-barrier system used in radioactive borate waste isolation based on Monte Carlo simulations. Applied Radiation and Isotopes. 2012;**70**(1):99-102

[34] Saleh HM. Stability of cemented dried water hyacinth used for biosorption of radionuclides under various circumstances. Journal of Nuclear Materials. 2014;**446**(1–3):124-133

Chapter 2

Nonlinear Calculations of the Strength of Cross-sections of Bending Reinforced Concrete Elements and Their Practical Realization

Kochkarev Dmitriy and Galinska Tatyana

Additional information is available at the end of the chapter

http://dx.doi.org/10.5772/intechopen.75122

Abstract

Calculation methodology of reinforced concrete elements based on the calculated resistance of reinforced concrete is presented. The basic depending which allows setting the strength of bending sections and elements is obtained. The reliability of the dependencies is experimentally confirmed. There are calculation examples of bending elements by the developed methodology. According to the given method, tables have been developed, which depending on the accepted parameters allow determining the resistance of the concrete, the stresses in the reinforced concrete and reinforcement, and the total relative deformation of the cross section. Using the calculated resistances of reinforced concrete allowed to reduce the calculation of reinforced concrete elements according to the nonlinear deformation model to the application of the formulas of the classical resistance of materials and to significantly simplifies the process of their calculation.

Keywords: bending, resistance, beam, deformation model, reinforced concrete

1. Introduction

Concrete is a composite material that is made of gravel, sand, cement, water, and various types of additives. Each of the components has its own characteristics, which together determine the physical and mechanical parameters of concrete. The current normative documents regulate to establish these parameters by testing the experimental samples of specified sizes—prisms or cylinders—the quality of the resulting concrete is controlled by cubes. The resistance of the concrete to the compression is determined by dividing the maximum

compressive load into the cross-sectional area of the experimental sample of the appropriate sizes [1, 2]. Considering the fact that for different sizes of samples, this ratio will have different meanings, it can be confirming that the term "calculated resistance of concrete" is relative. However, the introduction of this term allowed to have starting points when calculating the cross sections of concrete and reinforced concrete elements under the influence of various force factors.

A similar situation with the tension. Tension is a characteristic of a stress-strain state, which is determined by multiplying the corresponding deformations into a deformation module. Thus, it is not possible to determine the tension directly by experimental way. We determine deformations and then tension by using certain assumptions. Again, without lowering the values of the accepted terms, we have rather relative parameters. Based on these considerations, the introduction of the term calculated resistance of reinforced concrete should also take place. At first sight, this term is perceived quite difficult, especially in conditions of classical reinforced concrete. But at the same time its introduction reduces the calculation of cross sections of reinforced concrete elements to formulas of resistance of materials.

2. The term calculated resistance reinforced concrete

The basic idea of accepting calculated resistance is to separate the geometric parameters from the physical and mechanical ones. When we talk about elements from a single material, this does not cause any contradictions. In the case of composite materials, there are physical, mechanical, and geometric parameters of each material. In many cases geometric parameters can be selected in general from all physical and mechanical ones, but not individually. That is why the calculated resistance of composite materials will depend on the physical and mechanical parameters of all materials of which the cross section of the element is formed. In general, this can be expressed by the following equation:

$$f_i(a_1, \ldots, a_n) = \frac{F_{Ed}}{f(b_1, \ldots, b_n)}, \tag{1}$$

where $f_i(a_1, \ldots, a_n)$ is the calculated resistance of the cross section of the element of a composite material under the condition of destruction on the i material, MPa; F_{Ed} the external calculated force factor, which corresponds to the limiting state of the element; $f(b_1, \ldots, b_n)$ the corresponding geometric characteristic; $a_1, \ldots, a_n$ the physical and mechanical parameters of material's cross section of the composite element; and $b_1, \ldots, b_n$ the geometric parameters of the cross section of the composite element.

For a single cross-section of a composite element there may be a large number of calculated resistances due to the fact that the strength of the cross section is determined by the strength characteristics of all materials from which the composite element is formed. Therefore, the total calculated resistance of a composite material is determined by the minimum value of the calculated resistances under conditions of destruction on all materials from which the cross section of the element is formed:

$$f = \min\left(f_1(a_1, \ldots, a_n), \ldots, f_i(\ldots, a_n) \ldots, f_n(\ldots, a_n),\right. \tag{2}$$

where f is the calculated (total) resistance of the cross section of composite material.

The calculated resistance of composite materials can be obtained both theoretically and experimentally. To determine it theoretically, the necessary valid hypotheses and statics equations are adopted. The calculated resistance (obtained by this way) does not contain empirical coefficients, but is determined by generally accepted experimental and theoretically grounded hypotheses and prerequisites. In the case of the experimental setting of the calculated resistance, it is more appropriate to determine the calculated resistance separately for each condition of destruction. This allows balancing various experimental studies to the same conditions.

The feature of the use of calculated resistance is that they are determined for specific tabulated values of the corresponding classes or characteristics of the materials. In particular cases, these may be parameters that determine the characteristics of materials of a certain class. For concrete, this characteristic may be $K = 1.05(E_{cd}\varepsilon_{c1}/f_{cd})$ [3].

Introduction of the calculated resistance of composite materials allows the use of no less important term *tension in the cross-section of the composite material* σ_i. It is also a conditional hypothetical term by which it is possible to determine the parameters of a stress-strain state at different levels of load. These tensions are determined by a formula similar to expression (1):

$$\sigma_i(a_1, \ldots, a_n) = \frac{F_i}{f(b_1, \ldots, b_n)}, \tag{3}$$

where $\sigma_i(a_1,\ldots,a_n)$ is the tension in the cross section of an element of a composite material, MPa, and F_i the external force factor, which corresponds to a certain level of load.

The geometric characteristic in expressions (1) and (3) for the same type of deformation has the same meaning. To theoretically obtain these tensions it is necessary to consider systems of equations of equilibrium for a certain type of deformation and to lead them to dimensionless quantities. The parameters that are obtained this way are tabulated depending on the load level, the accepted parameters, the classes of materials, etc. Typically, the tension is determined on the condition that the material does not reach the limit values of the deformations in the operating stages of work of the cross section of the element, and therefore, unlike the calculated resistance, they will have a single value, so there is no need for the introduction of formulas of type (2).

Finally, it is worthwhile to note the features of using the method of calculated resistances:

1. The basics of calculation contain experimentally and theoretically grounded preconditions and hypotheses.
2. Establishment of geometric parameters allows to balance calculated systems of equations to the clear separation of geometrical, physical, and mechanical parameters of cross sections.
3. Diagrams of deformation of materials are established. It should be noted that the adopted diagrams do not play a significant role for this method. The calculated resistance for a certain type of deformation can be established for practically all existing diagrams.

4. By conducting preliminary calculations, the main calculated parameters are tabulated.

The advantages of this method should include:

1. The only methodology for calculating composite materials for nonlinear deformation of materials with classical material resistance.
2. Simplicity and convenience of the calculating process.
3. Ability to use different diagrams of deformation of materials.
4. Setting parameters of a stress-strain state at different load levels.
5. When obtaining new knowledge about the features of deformation of composite materials, it is enough to specify the value of the calculated resistance, and the method of calculation will remain unchanged, which greatly simplify the process of balance of norms [4].
6. Conducting comparative and estimating calculations of cross sections from different materials.

Regarding the disadvantages, then they primarily relate suitability of this method for some classes of materials, and some discomfort associated with using tables.

3. Calculation of bending reinforced concrete elements of a rectangular cross section

Consider the definition of the calculated resistance of reinforced concrete for bending reinforced concrete elements with single reinforcement. In order to show the universality of this method, regardless of the calculation method (force or deformation), first consider the term of the calculated resistance of the reinforced concrete for the force model laid down in the design standards SNiP 2.03.01-84* [5].

For the stress-strain state shown in **Figure 1**, the equilibrium equation is written when $\xi \le \xi_R$, taking the sum of the moments relative to the neutral line:

$$f_{yd}A_s - f_{cd}bx = 0. \tag{4}$$

$$f_{yd}A_s(d-x) + f_{cd}b\frac{x^2}{2} = M_{Ed}. \tag{5}$$

The value of x is determined from Eq. (4) and substituted by expression (5). As a result of simple transformations received:

$$f_{yd}\rho_f - \frac{f_{yd}^2\rho_f^2}{2f_c} = \frac{M_{Ed}}{bd^2}. \tag{6}$$

In formula (6) the left part is denoted by D_1; then $D_1 = M_{Ed}/bd^2$.

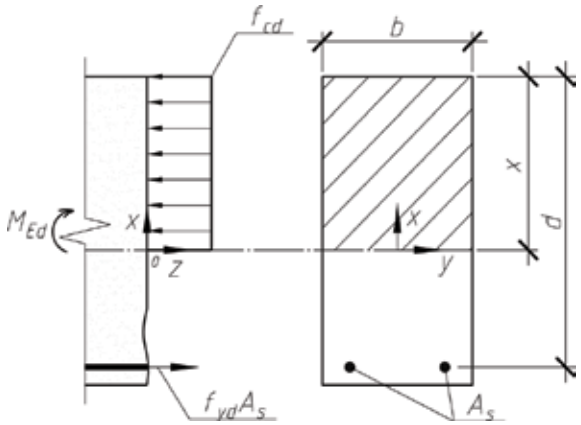

Figure 1. Scheme of forces in the cross section of bending reinforced concrete element for single reinforcement.

For the formula to take a familiar form, which is used in the resistance of materials in the calculations of metal, wooden, and stone structures, the left and right sides are multiplied by 6 and written like

$$6D_1 = \frac{6M_{Ed}}{bd^2} \quad or \quad 6D_1 = \frac{M_{Ed}}{W_c}. \tag{7}$$

In this formula W_c is the elastic moment of the resistance of the working cross section of concrete; $6D_1$ is nothing more than the calculated resistance of the reinforced concrete to the bend $f_{zM,1}$, namely:

$$f_{zM,1} = \frac{M_{Ed}}{W_c}. \tag{8}$$

Similarly, it is obtained with $\xi > \xi_R$:

$$\alpha_R f_c = \frac{M_{Ed}}{bd^2}. \tag{9}$$

The left part is denoted by D_2 and then $D_2 = M_{Ed}/bd^2$, finally receiving

$$f_{zM,2} = \frac{M_{Ed}}{W_c}. \tag{10}$$

The conditions are used (2) for the expression of the total calculated resistance:

$$f_{zM,SNiP} = \min \begin{cases} 6f_{yd}\rho_f - \dfrac{6f_{yd}^2\rho_f^2}{2f_c} \\ 6\alpha_R f_c \end{cases}. \tag{11}$$

Obtained by this way, calculated resistance of reinforced concrete for reinforcement A-400 and A-500 is shown in **Table 1**.

Similar expressions are obtained for nonlinear calculations. Write the value of the corresponding calculated resistances for different cases of destruction:

$$f_{zM,1dm} = 6\left(\frac{\int_0^{\varepsilon_c}\sigma_c\varepsilon_c d\varepsilon_c}{\left(\int_0^{\varepsilon_c}\sigma_c d\varepsilon_c\right)^2} - \frac{\varepsilon_c}{\int_0^{\varepsilon_c}\sigma_c d\varepsilon_c}\right)\rho_f{}^2 f_{yd}^2 + 6\rho_f f_{yd}, \tag{12}$$

$$f_{zM,2dm} = 6\left(\frac{\int_0^{\varepsilon_c}\sigma_c\varepsilon_c d\varepsilon_c}{\left(\int_0^{\varepsilon_c}\sigma_c d\varepsilon_c\right)^2} - \frac{\varepsilon_c}{\int_0^{\varepsilon_c}\sigma_c d\varepsilon_c}\right)\rho_f^2 E_s^2\varepsilon_c^2 + 6\rho_f E_s\varepsilon_c. \tag{13}$$

To determine the corresponding calculated resistance, it is necessary for expressions (12) and (13) to apply an extreme criterion in the form:

$$\frac{df_{zM,idm}}{d\varepsilon_c} = 0, \quad \varepsilon_c \ \epsilon[\varepsilon_{cl}, \varepsilon_{cu}]. \tag{14}$$

The total calculated resistance to bend in calculating by the deformation model will be determined by the condition.

$$f_{zM,dm} = \min\begin{cases} f_{zM,1\text{Д}M}, \ \dfrac{df_{zM,1dm}}{d\varepsilon_c} = 0, \quad \varepsilon_c \ \epsilon[\varepsilon_{cl}, \varepsilon_{cu}]; \\ f_{zM,2\text{Д}M}, \ \dfrac{df_{zM,2dm}}{d\varepsilon_c} = 0, \quad \varepsilon_c \ \epsilon[\varepsilon_{cl}, \varepsilon_{cu}]. \end{cases} \tag{15}$$

For the further use of the expression (15), it is necessary to adopt a concrete deformation diagram. Adopted function of the deformation diagram does not have essential value, but it must satisfy the conditions for deformation of concrete. Accepting for deformation diagram for concrete Eurocode-2 [3], expression (3.14), the tabulation is executed so that the maximum fault in interpolation will not be more than 5%. The value of the calculated resistance to bending for single reinforcement for all classes of concrete and reinforcement classes A-400 and A-500 are shown in **Table 2**.

Similarly, the calculated resistance for bend for double reinforcement is obtained. For this purpose, the calculated resistance for different conditions of destruction of bending reinforced concrete elements for double reinforcement are determined:

Class of concrete	Percentage of reinforcement ρ_f								
	0.05	**0.50**	**1.00**	**1.25**	**1.50**	**1.75**	**2.00**	**2.50**	**3.00**
	f_{yd} = 375 MPa (A400C)								
C8/10	1.11	9.49	15.47	15.66	15.66	15.66	15.66	15.66	15.66
C12/15	1.11	10.01	17.54	20.37	21.73	21.73	21.73	21.73	21.73
C16/20	1.12	10.33	18.83	22.39	25.50	28.14	28.61	28.61	28.61
C20/25	1.12	10.52	19.59	23.58	27.20	30.46	33.36	35.06	35.06
C25/30	1.12	10.63	20.02	24.25	28.17	31.78	35.07	40.08	40.08
C30/35	1.12	10.71	20.34	24.74	28.88	32.75	36.35	42.73	44.77
C32/40	1.12	10.77	20.58	25.13	29.44	33.50	37.33	44.26	49.13
C35/45	1.12	10.83	20.81	25.49	29.95	34.21	38.25	45.70	52.31
C40/50	1.12	10.87	20.97	25.73	30.30	34.68	38.86	46.66	53.69
C45/55	1.12	10.90	21.09	25.93	30.59	35.07	39.38	47.46	54.84
C50/60	1.12	10.93	21.22	26.13	30.87	35.46	39.89	48.26	55.99
	f_{yd} = 450 MPa (A500C)								
C8/10	1.32	10.97	15.33	15.33	15.33	15.33	15.33	15.33	15.33
C12/15	1.33	11.71	19.85	21.22	21.22	21.22	21.22	21.22	21.22
C16/20	1.34	12.18	21.72	25.50	27.87	27.87	27.87	27.87	27.87
C20/25	1.34	12.45	22.81	27.20	31.07	34.06	34.06	34.06	34.06
C25/30	1.34	12.61	23.43	28.17	32.46	36.31	38.85	38.85	38.85
C30/35	1.34	12.72	23.88	28.88	33.49	37.71	41.54	43.31	43.31
C32/40	1.34	12.81	24.24	29.44	34.29	38.79	42.95	47.42	47.42
C35/45	1.34	12.89	24.57	29.95	35.03	39.81	44.28	51.91	51.91
C40/50	1.34	12.95	24.79	30.30	35.53	40.48	45.16	53.69	55.27
C45/55	1.34	12.99	24.98	30.59	35.94	41.05	45.90	54.84	58.28
C50/60	1.35	13.04	25.16	30.87	36.36	41.61	46.64	55.99	61.44

Note: Intermediate values are determined by straight-line interpolation.

Table 1. Calculated resistance of reinforced concrete to bend for single reinforcement $f_{zM,SNiP}$, MPa.

$$f_{zM2,1dm} = 6\frac{\frac{\int_0^{\varepsilon_c}\sigma_c\varepsilon_c d\varepsilon}{\varepsilon_c^2} + \rho_{fc}f_{yc}\left(k - nk^2\right) + \varepsilon_c(k-1)^2 k\rho_f E_s}{k^2}. \tag{16}$$

$$f_{zM2,2dm} = 6\frac{\frac{\int_0^{\varepsilon_c}\sigma_c\varepsilon_c d\varepsilon}{\varepsilon_c^2} + \rho_{fc}f_{yc}\left(k - nk^2\right) + \rho_f f_{yd}\left(k^2 - k\right)}{k^2}. \tag{17}$$

Class of concrete	Percentage of reinforcement ρ_f								
	0.05	**0.50**	**1.00**	**1.25**	**1.50**	**1.75**	**2.00**	**2.50**	**3.00**
	f_{yd} = 375 MPa (A400C)								
C8/10	1.10	9.44	14.68	15.12	15.43	15.67	15.86	16.13	16.32
C12/15	1.11	9.97	17.38	20.09	20.85	21.27	21.60	22.10	22.45
C16/20	1.11	10.30	18.70	22.19	25.20	27.38	27.90	28.71	29.29
C20/25	1.11	10.49	19.48	23.40	26.95	30.11	32.88	34.82	35.65
C25/30	1.11	10.60	19.91	24.08	27.93	31.46	34.66	39.64	40.69
C30/35	1.12	10.68	20.24	24.59	28.66	32.45	35.96	42.12	45.45
C32/40	1.12	10.75	20.49	24.98	29.23	33.22	36.96	43.69	49.26
C35/45	1.12	10.81	20.72	25.35	29.76	33.94	37.90	45.16	51.52
C40/50	1.12	10.84	20.88	25.60	30.11	34.42	38.53	46.14	52.94
C45/55	1.12	10.87	21.01	25.80	30.40	34.82	39.05	46.95	54.10
C50/60	1.12	10.90	21.14	26.00	30.69	35.21	39.56	47.75	55.26
	f_{yd} = 450 MPa (A500C)								
C8/10	1.32	10.90	14.57	15.02	15.35	15.60	15.79	16.07	16.27
C12/15	1.33	11.66	19.40	20.15	20.70	21.13	21.48	21.99	22.35
C16/20	1.33	12.13	21.53	25.17	26.50	27.16	27.71	28.53	29.13
C20/25	1.33	12.41	22.65	26.95	30.69	32.67	33.42	34.57	35.43
C25/30	1.34	12.57	23.28	27.93	32.12	35.82	37.89	39.33	40.40
C30/35	1.34	12.69	23.74	28.66	33.18	37.28	40.93	43.80	45.10
C32/40	1.34	12.78	24.11	29.23	33.99	38.39	42.40	48.01	49.53
C35/45	1.34	12.86	24.44	29.76	34.75	39.42	43.78	51.43	54.52
C40/50	1.34	12.92	24.67	30.11	35.26	40.11	44.68	52.94	58.52
C45/55	1.34	12.96	24.86	30.40	35.68	40.69	45.43	54.10	61.40
C50/60	1.34	13.01	25.04	30.69	36.10	41.25	46.17	55.26	63.37

Note: Intermediate values are determined by straight-line interpolation.

Table 2. Calculated resistance of reinforced concrete to bend for single reinforcement $f_{zM,dm}$, MPa.

$$f_{zM2,3dm} = 6\varepsilon_c \frac{\frac{\int_0^{\varepsilon_c} \sigma_c \varepsilon_c d\varepsilon}{\varepsilon_c^3} + E_s \rho_{fc}(1-nk)^2 k + E_s \rho_f (k-1)^2 k}{k^2}. \tag{18}$$

$$f_{zM2,4dm} = 6\varepsilon_c \frac{\frac{\int_0^{\varepsilon_c} \sigma_c \varepsilon_c d\varepsilon}{\varepsilon_c^3} + E_s \rho_{fc}(1-nk)^2 k + \frac{f_{yd}}{\varepsilon_c} \rho_f (k-1) k}{k^2}. \tag{19}$$

http://dx.doi.org/10.5772/intechopen.75122

In the given expressions, k is determined from the first equation of equilibrium under the conditions of the destruction of the element.

The total calculated resistance to bend in double reinforcement according to the deformation model will be determined by the condition:

$$f_{zM2,\,dm} = \min\begin{cases} f_{zM2,\,1dm},\ \dfrac{df_{zM,\,1dm}}{d\varepsilon_c} = 0, \quad \varepsilon_c \ \epsilon[\varepsilon_{cl},\,\varepsilon_{cu}]; \\ f_{zM2,\,2dm},\ \dfrac{df_{zM,\,2dm}}{d\varepsilon_c} = 0, \quad \varepsilon_c \ \epsilon[\varepsilon_{cl},\,\varepsilon_{cu}]; \\ f_{zM2,\,3dm},\ \dfrac{df_{zM,\,3dm}}{d\varepsilon_c} = 0, \quad \varepsilon_c \ \epsilon[\varepsilon_{cl},\,\varepsilon_{cu}]; \\ f_{zM2,\,4dm},\ \dfrac{df_{zM,\,4dm}}{d\varepsilon_c} = 0, \quad \varepsilon_c \ \epsilon[\varepsilon_{cl},\,\varepsilon_{cu}]. \end{cases} \tag{20}$$

In **Table 3** the expression of the calculated resistance to bend for double reinforcement is derived taking the diagram of deformation of concrete in the form of the function Eurocode-2 [3].

As can be seen from **Tables 2** and **3** in some cases, double reinforcement significantly (more than three times) increases the calculated resistance of reinforced concrete of bending elements and accordingly increases their bearing capacity. In this way, the reinforcement can greatly enhance the compressed area of concrete of bending reinforced concrete elements. For comparison, the data of the calculated resistance to bend for double reinforcement are presented by methodology of SNiP 2.03.01–84* [5] (**Table 4**).

Compare the calculated resistance of reinforced concrete to bending defined by the force model and deformation method for single and double reinforcement. As can be seen from **Tables 5** and **6**, the calculated resistance of reinforced concrete to the bend differs within the limits of the calculated fault. This makes it possible to say that for heavy concrete classes C8/10÷C50/60 and ordinary reinforcement classes A-400 and A-500, calculations of the strength of the cross sections of bending reinforced concrete elements with single and double reinforcement can be performed on any of the mentioned methods. By these ways, the maximum difference will be within 8% and only for certain conditions.

One of the main advantages of the deformation model in comparison with the force one is the possibility of obtaining the parameters of the stress-strain state for the operational load. Let's show how this can be done using the method of calculated resistance of reinforced concrete. For this purpose, the tensions in the bending reinforced concrete element are determined $\sigma_{zM,\text{ДМ}}$ under operational loads, at which cross sections of the element can work without cracks at $M < M_W$, with cracks in the stretched zone at $M \geq M_W$, without cracks at $M \geq M_W$ (areas in the block between the cracks). In this case, it is proposed to determine the tension in the reinforced concrete for cross sections until formation of cracks.

$$\sigma_{WzM} = 6\varepsilon_{c,\,W} \times \frac{\dfrac{\int_0^{\varepsilon_{c,\,W}} \sigma_c \varepsilon_c d\varepsilon}{\varepsilon^3_{c,\,W}} + \dfrac{\int_0^{\varepsilon_{ctu}} \sigma_{ct} \varepsilon_{ct} d\varepsilon}{\varepsilon^3_{c,\,W}} + E_s \rho_{fc} (1 - nk_W)^2 k_W + E_s \rho_f (k_W - 1)^2 k_W}{k_W^2}. \tag{21}$$

Class of concrete	ρ_f = 0.01			ρ_f = 0.02			ρ_f = 0.03		
	ρ_{fc}/ρ_f								
	0.25	0.50	0.75	0.25	0.50	0.75	0.25	0.50	0.75
n = 0.06–0.1	f_{yd} = 375 MPa (A400C)								
C8/10	18.09	20.02	21.04	25.81	35.75	41.17	31.54	46.74	60.39
C12/15	19.28	20.55	21.16	31.33	38.53	41.70	37.42	52.38	61.58
C16/20	20.03	20.88	21.19	35.78	39.85	42.03	43.99	56.93	62.33
C20/25	20.46	21.07	21.23	37.52	40.63	42.22	50.11	58.67	62.76
C25/30	20.71	21.17	21.26	38.51	41.06	42.32	53.39	59.66	63.01
C30/35	20.89	21.22	21.29	39.24	41.39	42.35	55.04	60.39	63.19
C32/40	21.02	21.26	21.32	39.80	41.64	42.38	56.31	60.95	63.33
C35/45	21.14	21.31	21.36	40.33	41.87	42.41	57.50	61.48	63.44
C40/50	21.21	21.35	21.39	40.68	42.03	42.44	58.30	61.84	63.50
C45/55	21.28	21.39	21.43	40.98	42.14	42.46	58.95	62.13	63.53
C50/60	21.35	21.43	21.46	41.27	42.25	42.50	59.61	62.42	63.55
n = 0.06–0.1	f_{yd} = 450 MPa (A500C)								
C8/10	20.23	23.59	25.13	27.70	39.59	48.97	34.49	52.69	70.91
C12/15	22.45	24.35	25.25	33.11	44.76	49.73	40.27	58.17	73.21
C16/20	23.52	24.82	25.31	39.06	46.91	50.20	46.71	64.31	74.28
C20/25	24.14	25.08	25.36	43.38	48.03	50.45	52.71	68.76	74.90
C25/30	24.49	25.18	25.41	44.81	48.65	50.50	57.47	70.19	75.25
C30/35	24.74	25.26	25.45	45.87	49.11	50.55	61.98	71.25	75.50
C32/40	24.92	25.33	25.49	46.67	49.46	50.60	65.05	72.05	75.68
C35/45	25.08	25.40	25.53	47.42	49.78	50.65	66.84	72.80	75.74
C40/50	25.18	25.46	25.56	47.92	49.98	50.69	67.99	73.29	75.78
C45/55	25.27	25.50	25.60	48.32	50.13	50.73	68.92	73.70	75.82
C50/60	25.35	25.55	25.64	48.70	50.24	50.77	69.87	74.08	75.87

Note: Intermediate values are determined by straight-line interpolation.

Table 3. Calculated resistance of reinforced concrete to bend for double reinforcement $f_{zM2,dm}$, MPa.

It is noted that the tension σ_{WzM} also allows to determine the moment of formation of cracks, so depending on the tasks, it can also be called the calculated resistance of the reinforced concrete to the bend until formation of cracks.

Tension in a cross section with a crack in the stretched zone at $M \geq M_W$ is determined by the

$$\sigma_{2zM} = 6\frac{\int_0^{\varepsilon_c} \sigma_c \varepsilon_c d\varepsilon}{k^2\varepsilon_c^2} + \frac{\int_0^{\varepsilon_{ctu}} \sigma_{ct}\varepsilon_{ct} d\varepsilon}{k^2\varepsilon_c^2} + 6\varepsilon_c E_s \rho_{fc}\frac{(1-nk)^2}{k} + 6\varepsilon_c E_s \rho_f \frac{(k-1)^2}{k} + \frac{(k-1)}{k}\Delta\sigma_{s,x}\rho_f. \quad (22)$$

Class of concrete	ρ_f **= 0.01**			ρ_f **= 0.02**			ρ_f **= 0.03**		
	ρ_{fc}/ρ_f								
	0.25	**0.50**	**0.75**	**0.25**	**0.50**	**0.75**	**0.25**	**0.50**	**0.75**
n = 0.06–0.1	f_{yd} = 375 MPa (A400C)								
C8/10	18.20	20.06	21.04	26.23	36.61	41.20	31.51	47.37	60.48
C12/15	19.37	20.58	21.17	32.29	38.67	41.71	37.58	53.43	61.64
C16/20	20.10	20.90	21.25	36.06	39.97	42.04	44.47	57.20	62.37
C20/25	20.52	21.09	21.30	37.77	40.73	42.23	50.91	58.91	62.80
C25/30	20.76	21.20	21.32	38.73	41.15	42.33	53.91	59.87	63.04
C30/35	20.94	21.28	21.34	39.45	41.47	42.41	55.52	60.59	63.21
C32/40	21.08	21.34	21.36	40.00	41.72	42.48	56.77	61.14	63.35
C35/45	21.21	21.40	21.37	40.52	41.95	42.53	57.93	61.66	63.48
C40/50	21.30	21.43	21.38	40.87	42.10	42.57	58.71	62.00	63.57
C45/55	21.37	21.47	21.39	41.15	42.23	42.60	59.36	62.29	63.64
C50/60	21.44	21.50	21.40	41.44	42.36	42.63	60.01	62.58	63.71
n = 0.06–0.1	f_{yd} = 450 MPa (A500C)								
C8/10	20.51	23.15	24.78	26.60	37.87	47.32	32.24	49.15	66.05
C12/15	22.31	24.07	25.11	32.49	43.72	48.64	38.12	55.03	70.58
C16/20	23.44	24.64	25.32	39.14	46.02	49.47	44.78	61.69	72.44
C20/25	24.10	24.98	25.44	43.13	47.37	49.96	50.97	67.18	73.54
C25/30	24.47	25.17	25.51	44.63	48.13	50.23	55.76	68.89	74.15
C30/35	24.75	25.31	25.56	45.73	48.70	50.43	60.22	70.16	74.61
C32/40	24.97	25.42	25.60	46.59	49.14	50.59	64.33	71.15	74.97
C35/45	25.17	25.52	25.64	47.39	49.55	50.74	66.68	72.07	75.30
C40/50	25.30	25.59	25.66	47.93	49.82	50.84	67.88	72.68	75.52
C45/55	25.41	25.65	25.68	48.37	50.05	50.92	68.88	73.19	75.70
C50/60	25.52	25.70	25.70	48.82	50.27	51.00	69.89	73.70	75.89

Note: Intermediate values are determined by straight-line interpolation.

Table 4. Calculated resistance of reinforced concrete to bend for double reinforcement $f_{zM2,SNiP}$, MPa.

The tensions between the cracks are determined by

$$\sigma_{mzM} = 6\frac{E_s^2(k-1)^2\int_0^{\frac{\sigma_{s,m}}{E_s(k-1)}}\sigma_c\varepsilon d\varepsilon}{k^2\sigma_{s,m}^2} + 6\frac{(k-1)^2\int_0^{\varepsilon_{ctu}}\sigma_{ct}\varepsilon_{ct}d\varepsilon}{k^2\varepsilon_{ctu}^2} + 6\frac{k-1}{k}\sigma_{s,m}\rho_f + 6\frac{(1-kn)^2}{k(k-1)}\rho_{fc}\sigma_{s,m}. \quad (23)$$

All of the above tensions in concrete are determined by expression:

Class of concrete	Percentage of reinforcement ρ_f								
	0.05	**0.50**	**1.00**	**1.25**	**1.50**	**1.75**	**2.00**	**2.50**	**3.00**
	f_{yd} = 375 MPa (A400C)								
C8/10	0.997	0.995	0.949	0.965	0.985	1.001	1.013	1.030	1.042
C12/15	0.997	0.996	0.991	0.986	0.960	0.979	0.994	1.017	1.033
C16/20	0.996	0.997	0.993	0.991	0.988	0.973	0.975	1.003	1.024
C20/25	0.996	0.997	0.994	0.992	0.991	0.989	0.986	0.993	1.017
C25/30	0.996	0.998	0.995	0.993	0.992	0.990	0.988	0.989	1.015
C30/35	0.996	0.998	0.995	0.994	0.992	0.991	0.989	0.986	1.015
C32/40	0.996	0.998	0.996	0.994	0.993	0.992	0.990	0.987	1.003
C35/45	0.996	0.998	0.996	0.995	0.994	0.992	0.991	0.988	0.985
C40/50	0.996	0.998	0.996	0.995	0.994	0.993	0.991	0.989	0.986
C45/55	0.996	0.998	0.996	0.995	0.994	0.993	0.992	0.989	0.986
C50/60	0.996	0.997	0.996	0.995	0.994	0.993	0.992	0.990	0.987
	f_{yd} = 450 MPa (A500C)								
C8/10	0.998	0.993	0.951	0.980	1.001	1.018	1.030	1.049	1.061
C12/15	0.997	0.995	0.977	0.950	0.976	0.996	1.012	1.037	1.054
C16/20	0.997	0.996	0.991	0.987	0.951	0.975	0.994	1.024	1.045
C20/25	0.996	0.997	0.993	0.991	0.988	0.959	0.981	1.015	1.040
C25/30	0.996	0.997	0.994	0.992	0.990	0.987	0.975	1.012	1.040
C30/35	0.996	0.997	0.994	0.992	0.991	0.989	0.985	1.012	1.042
C32/40	0.996	0.997	0.995	0.993	0.991	0.990	0.987	1.012	1.044
C35/45	0.996	0.998	0.995	0.993	0.992	0.990	0.989	0.991	1.050
C40/50	0.996	0.998	0.995	0.994	0.992	0.991	0.989	0.986	1.059
C45/55	0.996	0.998	0.995	0.994	0.993	0.991	0.990	0.986	1.053
C50/60	0.996	0.998	0.995	0.994	0.993	0.991	0.990	0.987	1.031

Table 5. Comparison of the calculated resistance of reinforced concrete to bend for single reinforcement $f_{zM,dm}/f_{zM,SNiP}$.

$$\sigma_{izM} = \frac{M}{W_c}. \tag{24}$$

Parameters of the stress-strain state at the operating load levels are necessary for determining the deflection and width of the crack opening. Therefore, the basic parameters that are necessary for this will be: tension in the reinforcement and curvature.

The tension in the reinforcement until formation of cracks is determined by expression

$$\sigma_{s,W} = (k_W - 1)\varepsilon_{c,W}, \tag{25}$$

under certain values k_W, $\varepsilon_{c,W}$.

Class of concrete	ρ_f **= 0.01**			ρ_f **= 0.02**			ρ_f **= 0.03**		
	ρ_{fc}/ρ_f								
	0.25	**0.50**	**0.75**	**0.25**	**0.50**	**0.75**	**0.25**	**0.50**	**0.75**
1	2	3	4	5	6	7	8	9	10
n = 0.06–0.1	f_{yd} = 375 MPa (A400C)								
C8/10	0.994	0.998	1.000	0.984	0.977	0.999	1.001	0.987	0.999
C12/15	0.996	0.998	1.000	0.970	0.996	1.000	0.996	0.980	0.999
C16/20	0.997	0.999	0.997	0.992	0.997	1.000	0.989	0.995	0.999
C20/25	0.997	0.999	0.997	0.993	0.998	1.000	0.984	0.996	0.999
C25/30	0.997	0.999	0.997	0.994	0.998	1.000	0.990	0.996	1.000
C30/35	0.998	0.997	0.998	0.995	0.998	0.999	0.991	0.997	1.000
C32/40	0.997	0.996	0.998	0.995	0.998	0.998	0.992	0.997	1.000
C35/45	0.997	0.996	0.999	0.995	0.998	0.997	0.993	0.997	0.999
C40/50	0.996	0.996	1.001	0.996	0.998	0.997	0.993	0.997	0.999
C45/55	0.996	0.996	1.002	0.996	0.998	0.997	0.993	0.997	0.998
C50/60	0.996	0.997	1.003	0.996	0.997	0.997	0.993	0.997	0.998
n = 0.06–0.1	f_{yd} = 450 MPa (A500C)								
C8/10	0.986	1.019	1.014	1.041	1.045	1.035	1.070	1.072	1.074
C12/15	1.006	1.012	1.005	1.019	1.024	1.022	1.056	1.057	1.037
C16/20	1.003	1.007	0.999	0.998	1.019	1.015	1.043	1.042	1.025
C20/25	1.002	1.004	0.997	1.006	1.014	1.010	1.034	1.024	1.019
C25/30	1.000	1.000	0.996	1.004	1.011	1.005	1.031	1.019	1.015
C30/35	0.999	0.998	0.996	1.003	1.009	1.002	1.029	1.015	1.012
C32/40	0.998	0.996	0.995	1.002	1.007	1.000	1.011	1.013	1.010
C35/45	0.996	0.995	0.996	1.001	1.005	0.998	1.002	1.010	1.006
C40/50	0.995	0.995	0.996	1.000	1.003	0.997	1.002	1.008	1.004
C45/55	0.994	0.994	0.997	0.999	1.002	0.996	1.000	1.007	1.002
C50/60	0.993	0.994	0.997	0.998	0.999	0.995	1.000	1.005	1.000

Table 6. Comparison of the calculated resistance of reinforced concrete to bend for double reinforcement $f_{zM2,dm}/f_{zM2,SNiP}$.

The tension in the reinforcement in the cross section with the crack in the stretched zone are calculated at known values k, ε_c, $\Delta\sigma_{s,x}$. Average tensions in the reinforcement on the section in the block between the cracks $\sigma_{s,m}$ are defined as the arithmetic mean of the tensions that are determined by expressions (22) and (23).

The curvature of the cross sections of reinforced concrete elements, taking into account the hypothesis of plane cross sections, is determined by the expression

$$1/r = \sum \varepsilon/d, \tag{26}$$

where $\Sigma\varepsilon$ is the total deformation of fibrous concrete fibers and stretched reinforcement.

The total deformation of fibrous concrete fibers and stretched reinforcement must be determined by the following formulas:

- For cross sections without cracks at $M < M_W$:

$$\sum \varepsilon = \varepsilon_{c,W} + \varepsilon_{s,W} = \varepsilon_{c,W} + \sigma_{s,W}/E_s. \tag{27}$$

- For cross sections with a crack in the stretched zone:

$$\sum \varepsilon = \varepsilon_{c,2} + \varepsilon_{s,fic} = \varepsilon_{c,2} + (k_{W,2} - 1)\varepsilon_{c,2}. \tag{28}$$

- For cross sections without cracks at $M \geq M_W$

$$\sum \varepsilon = \varepsilon_{c,m} + \varepsilon_{s,m} = \frac{\sigma_{s,m}}{E_s(k-1)} + \frac{\sigma_{s,m}}{E_s}. \tag{29}$$

Deflections are determined by curvature by using numerical methods.

According to the given method, tables have been developed, which depending on the accepted parameters allow to determining the resistance of the concrete, the stresses in the reinforced concrete and reinforcement, and the total relative deformation of the cross section. For this purpose, the deformation diagram was adopted in the form of Eurocode-2 function [3]. These tables are given in [6].

The calculation of the strength of the cross sections of bending reinforced concrete elements and crack resistance is recommended to be performed according to the formula:

$$\frac{M_{Ed}}{W_c} \leq f_{zM}(f_{WzM}). \tag{30}$$

Calculation of tension limitation in the reinforcement is carried out as follows:

$$\sigma_{zM} = \frac{M_e}{W_c} \rightarrow \varepsilon_{si} \rightarrow \sigma_s \leq \sigma_{s,Table}, \tag{31}$$

where $\sigma_{s,Table}$ is the tension in the reinforcement, in which there is no need to determine the width of the cracks opening, which are determined by Table 2.5 [7].

The calculation of the width of the cracks opening is carried out in same scheme:

$$\sigma_{zM} = M_e/W_c \rightarrow \varepsilon_{si} \rightarrow \sigma_{si} \rightarrow S_r \rightarrow W_k. \tag{32}$$

Calculation of deflections is performed in the following order:

$$\sigma_{zM} = M_e/W_c \rightarrow \Sigma\varepsilon \rightarrow 1/r = \Sigma\varepsilon/d \rightarrow f. \tag{33}$$

A separate important issue in the theory of reinforced concrete is the consideration of regime loads and influences: long-term, quasi-constant, low cycle, temperature, humidity and others. Thus, taking into account the long-term load can be realized by introducing the creep coefficient to the curvature or by introducing into the calculation of the deformation diagrams with the corresponding parameters. The calculation of regime load under the first condition can be carried out according to the given method by using tables for short-term load. When performing calculations under the second condition, it is necessary to use the tables obtained for the corresponding parameters of the diagrams. Similar tables can be made for virtually all regime loads and influences, which greatly simplify the calculations of strength, crack resistance, stiffness and width of crack opening. This is an issue that needs to be studied in detail, but the use of the calculated resistance of reinforced concrete gives confidence in the successful solution of this problem.

4. Examples of calculation of bending reinforced concrete elements

Example 1. Reinforced concrete beam with working cross section $b \times d = 20 \times 45$ sm is made of concrete of class *C*25/30 and reinforced 4∅25 of steel of class A500C. Determine the carrying capacity of the beam.

Solution. The percentage of beam reinforcement with stretched reinforcement is calculated:

$$\rho_f = \frac{A_s}{bd} \times 100\% = \frac{19.63}{20 \times 45} = 2.181\%.$$

According to the tables the calculated resistance of the reinforced concrete to the bend is determined:

$$f_{zM} = 37.12 \text{ MPa}.$$

The carrying capacity of the beam is calculated by the formula:

$$M_{Ed} = W_c f_{zM} = \frac{bd^2}{6} f_{zM} = \frac{20 \times 45^2}{6} 37.12 \times 10^{-3} = 250.56 \text{ kNm}.$$

Example 2. Reinforced concrete beam with working cross section $b \times d = 30 \times 45$ sm is made of concrete of class C25/30 and steel of class A400C and should take an external moment $M_{Ed} = 266.46$ kNm. Determine element reinforcement.

Solution. The moment of resistance of the concrete cross section is determined:

$$W_c = \frac{bd^2}{6} = \frac{30 \times 45^2}{6} = 10125 \text{ sm}^3.$$

The required calculated resistance of the reinforced concrete to the bending is calculated:

$$f_{zM} = \frac{M_{Ed}}{W_c} = \frac{266.46 \times 10^3}{10125} = 26.32 \text{ MPa}.$$

According to the tables the required percentage of reinforcement is determined:

$$\rho_f = 1.453\%.$$

The area of the cross section of the working reinforcement is equal:

$$A_s = \rho_f \times b \times d = 0.01453 \times 30 \times 45 = 19.62 \text{ sm}^2.$$

By gage 4Ø25, A_s = 19.63 sm^2 is accepted.

Example 3. Determine the cross-sectional dimensions of the beam of concrete class C16/20 and the area of the cross section of the working reinforcement of steel of class A400C, if the beam perceives the bending moment M_{Ed} = *136* kNm, and the contents of the working armature are ρ_f = 1.25%.

Solution. According to the tables, the calculated resistance of the reinforced concrete to the bend is found: f_M = 21.60 MPa. The moment of resistance is determined:

$$W_c = \frac{bd^2}{6} = \frac{M_{Ed}}{f_{zM}} = \frac{136 \times 10^3}{21.60} = 6296 \text{ sm}^3.$$

Accepting the ratio b = *0.5d*, calculate

$$d = \sqrt[3]{12 \times W_c} = \sqrt[3]{12 \times 6296} = 42.27 \text{ sm}.$$

Accepting $b \times d$ = 20 × 42 sm, then the area of cross section of the working reinforcement will be $A_s = \rho_f \times b \times d$ = 0.0125 × 20 × 42 = 10.5 sm^2. By gage 2Ø20 + 2Ø18, A_s = 11.37 sm^2.

Example 4. Reinforced concrete beam with working cross section $b \times d$ = 30 × 55 sm has to perceive the bending moment M_{Ed} = 486 kNm. To define the conditions under which the bearing capacity of the beam will be provided and accept the reinforcement.

Solution. The required calculated resistance of the reinforced concrete to the bend is calculated:

$$f_{zM} = \frac{M_{Ed}}{W_c} = \frac{6M_{Ed}}{bd^2} = \frac{6 \times 486 \times 10^3}{30 \times 55^2} = 32.12 \text{ MPa}.$$

From the tables it is clear that such a calculated resistance can be provided for different classes of concrete, reinforcement, and the percentage of reinforcement, starting with the concrete of class C20/25 and percentage of reinforcement 1.5 and more. Following physical, economic, and technological considerations, the designer takes the option that best suits the customer, for example, concrete class C25/30 and reinforcement of class A500C with percentage of reinforcement ρ_f = 1.42%. Then the area of the cross section of the working reinforcement will be $A_s = \rho_f \times b \times d = 0.0142 \times 30 \times 55 = 23.43$ sm^2. By gage 3Ø28 + 2Ø20, A_s = 24.75 sm^2 is accepted.

5. Conclusions

Obtained parameters of the stress-strain state of bending reinforced concrete elements: the calculated resistance of reinforced concrete to bend and tension in the cross section of the bending reinforced concrete element, the above dependencies allow to solve a number of problems, namely:

1. Calculation of the strength of the cross section of the bending reinforced concrete element with known cross-sectional dimensions of the concrete and reinforcement area.
2. Determination of the required cross-sectional area of the reinforcement for a given load with known cross-sectional dimensions of concrete.
3. Foundation the dimensions of the cross section of concrete and reinforcement for a certain percentage of reinforcement and the given load.
4. Checking strength with known cross-sectional area of the reinforcement and given cross-sectional dimensions of the concrete.
5. Verification of the conditions for ensuring the strength of the cross section of reinforced concrete element.
6. Calculation of the moment of formation of cracks.
7. Calculation the width of the crack opening under operating load.
8. Determination of the deflections of the elements under the operational load.

Using the calculated resistances of reinforced concrete allowed to reduce the calculation of reinforced concrete elements according to the nonlinear deformation model to the application of the formulas of the classical resistance of materials and to significantly simplify the process of their calculation.

Author details

Kochkarev Dmitriy[1]* and Galinska Tatyana[2]

*Address all correspondence to: dim7@ukr.net

1 National University of Water and Environmental Engineering, Rivne, Ukraine

2 Poltava National Technical Yuri Kondratyuk University, Poltava, Ukraine

References

[1] GOST 10180-90. Concrete. Methods for Determining the Strength of Control Samples. Moscow: NIIJB Gosstroia SSSR; 1991. 31 p

[2] GOST 24452-80. Concrete. Methods for Determining the Prismatic Strength, Modulus of Elasticity, and Poisson's Coefficient. Moscow: NIIJB Gosstroia SSSR; 1980. 14 p

[3] EN 1992: Eurocode 2: Design of concrete structures—Part 1: General rules and rules for buildings. Brussels. 2002. 230 p

[4] Problems of harmonization of the developed national normative document "Concrete and reinforced concrete constructions. General provisions" with EN 1992-1-1:2004 (Eurocode 2). Bambura A, Davydenko O, Sliysarenko Yu, et al. Building Structures: Collection of Scientific Works. Vol. 67. Kyiv: NDIBK; 2007. pp. 9-20

[5] SNiP 2.03.01-84*. Concrete and Reinforced Concrete Constructions. Moskow: CITP Gosstroia SSSR; 1989. 80 p

[6] Kochkarev D. Nonlinear Resistance of Reinforced Concrete Elements and Structures to Force Influences: Monograph. Rivne: O. Zen; 2015. 384 p. Fig.139; Tables 48; literature: 326. ISBN: 978-617-601-125-5

[7] DSTU B V.2.6-156:2010. Concrete and reinforced concrete constructions. Design rules. Kyiv: Minregionbud; 2010. 166 p

Chapter 3

Fibre Reinforced Cement Composites

Wafa Abdelmajed Labib

Additional information is available at the end of the chapter

http://dx.doi.org/10.5772/intechopen.75102

Abstract

Progression in cement-based technology has driven the development of fibre reinforced concrete (FRC) materials; such as concrete technology. Steel fibre and synthetic fibre are fundamental fibre types, which include glass, carbon, polyvinyl, polyolefin, waste fibre materials and polypropylene. The mechanical properties of FRC members are affected from these fibres individually and in hybrid aspects. The type, content and geometry of fibres are relied to these mechanical properties. A significant improvement in mechanical and dynamic properties of reinforced concrete members is enabled due to additional fibres into cementitious composites. Most mechanical properties are enhanced through intercept micro-cracks. The level of enhancement accomplished relied on the type and dosage of fibre as compared to plain concrete. Effective tensile strength, energy dissipation capacity and toughness are explained through FRC. The shear, punching and flexure are significantly increased through the level of enhancement accomplished. These fibres include polyvinyl, glass, carbon, polyolefin and polypropylene that improve the mechanical properties of concrete. The historical use of fibres and types of fibres are reported in this chapter. Similarly, the curing of steel, structural synthetic fibres, the mechanical properties of cement, the addition, placing, finishing and mixing are based on waste fibres, hybrid fibres, steel and structural synthetic.

Keywords: cement, steel fibre, synthetic fibre, hybrid fibre, waste fibre, concrete

1. Introduction

Advancements in cement-based technology, such as concrete technology, have led to the development of fibre reinforced concrete (FRC) materials [1]. Considerable research efforts have been made contributing to theoretical and technological knowledge about properties and behaviour of FRC across the globe. Applications of FRC are very common in civil and structural engineering.

There are numerous fibre types, in various sizes and shapes, available for commercial and experimental use. The basic fibre types are steel fibre; synthetic fibres, such as polypropylene, glass, carbon, polyolefin and polyvinyl; and waste fibre materials. Using these fibres individually as well as on hybrid basis has an effect on the mechanical properties of FRC members. These mechanical properties depend on the type, geometry, and content of fibres [2, 3] as described below.

The addition of fibres into cementitious composites enables considerable improvement in mechanical and dynamic properties of reinforced concrete members. The delay and control of tensile cracking in the composite material are the most considerable outcome of fibre associated with concrete [4]. Most mechanical properties of composite are enhanced using intercept micro-cracks. ACIFC [5] stated the reliance of the level of enhancement accomplished on the type of fibre and the dosage rate as compared to plain concrete. Thus, FRC demonstrates excellent tensile strength, toughness and energy dissipation capacity [6, 7]. It also increases significantly the shear [8–10], flexural [9, 11, 12], punching [13, 14], resistance and durability ([15, 16]; Kunieda et al., 2014) of concrete structures as well as superb resistance to cracking [17].

Those attractive properties allow the direct application of fibres in concrete. However, each fibre type could enhance specific concrete properties. Accordingly, the aim of this chapter is to investigate into the potential of using various types of fibres which include steel fibre and synthetic fibres such as polypropylene, glass, carbon, polyolefin and polyvinyl in enhancing the mechanical properties of concrete.

Recent researches have shown that waste fibres can also be a valuable reinforcement system to decrease significantly the brittle behaviour of cement-based materials, by improving their toughness and post-cracking resistance [18]. It also has beneficial environmental and economic impacts [19, 20]. The effect of using waste fibre in enhancing concrete properties is also reported.

The use of two or more types of fibres in a suitable combination showed a great potential to optimise the properties of concrete material as well as to improve the mechanical performance of reinforced concrete members. This combining of fibres, often called hybridization is currently used as the inclusion of single fibre in concrete cannot attain an optimal performance. The use of hybrid is commonly limited to two types. These are a mix of steel and polypropylene fibres and a mix of steel fibres with different geometry, shape and size. A further description on different fibre combinations is shown in the below sections. This chapter reported on the historical use of fibres; types of fibres; the addition, mixing, placing, finishing and curing of steel, polypropylene and structural synthetic fibres and the mechanical properties of cement-based composites reinforced with steel, polypropylene, structural synthetic, water fibres and hybrid fibres.

2. Fibres: origin and history

Fibres were used at least 3500 years ago to build the 57 m high hill of Aqar Quf near Baghdad through brittle matrix materials and sun-baked bricks [21]. Additionally, masonry mortar and plaster were reinforced through horsehair [22]. Similarly, cement products were reinforced through asbestos fibres for about 100 years ago. In contrast, alternate fibre types were instigated within the 1960s and 70s due to health issues related to asbestos fibres.

In the nineteenth century, the use of reinforcing rods in the tensile zone of the concrete was imposed for the low tensile strength and brittle character of concrete [23]. In addition, the incorporation of discontinuous steel reinforcing elements including metal chips, nails and wire segments into concrete was attempted through patents recently.

Romualdi and Baston [24] have investigated the steel fibres potential for steel reinforcing rods in concrete during the early 1960s in the United States. Afterwards, steel fibre reinforced concrete has been advanced through assorted experimentation, industrial application and research development. Similarly, Goldfein [25] conducted experiments with and without reinforcement using plastic fibres in concrete. Structural synthetic fibres were used explicitly by Japanese construction companies since 1997 as an alternate of steel fibre reinforcement. The expansion of structural synthetic fibres is attempted in Europe, North America and Australia.

Most applications suggest the use of fibre reinforced concrete such as refractory materials, concrete products, and road and floor slabs over the past 40 years [23].

3. Types of fibres

Fibre types are accessible for experimental and commercial use in assorted sizes and shapes. The basic fibre categories are steel fibre; synthetic fibres, such as polypropylene, glass, carbon, polyolefin and polyvinyl; and waste fibre materials. However, in structural cement-based elements, steel, polypropylene and structural synthetic fibre reinforced concrete as well as waste fibres are the main types of fibre, which are used as a replacement for conventional steel fabric reinforcement. Using these fibres individually as well as on hybrid basis has an effect on the mechanical properties of FRC members. These mechanical properties depend on the type, geometry and content of fibres [2, 3] as described below.

3.1. Steel fibres

Many efforts have been made in recent years to optimise the shape of steel fibres to achieve improved fibre-matrix bond characteristics, and to enhance fibre dispersibility in the concrete mix [26]. The classification for four general types is provided by ASTM A 820 on the basis of manufacturing products [22]. These products include cut sheet, melt extracted, cold-drawn wire and other fibres.

Figure 1 has shown other common types of steel fibres. By cutting and chopping wire, rounded and straight steel fibres, having a diameter between 0.25 and 1.0 mm are produced. Furthermore, shearing sheet of flattening wire produces flat and straight steel fibres of 0.15–0.41 mm thickness by 0.25–1.14 mm width. The production of crimped and deformed steel fibres is based on the full-length crimpling or bent or enlarged at each side of the fibres. The bending or flattening process is used to deform fibres to expand bond and allow mixing and handling [28].

The handling and mixing process is facilitated through fibres being collated into bundles. The bundles are distributed into single fibres during the mixing process. Similarly, cold-drawn wire is used to produce fibres that are smooth for making steel wool. In addition, the melt extraction process is used to produce steel fibres [22].

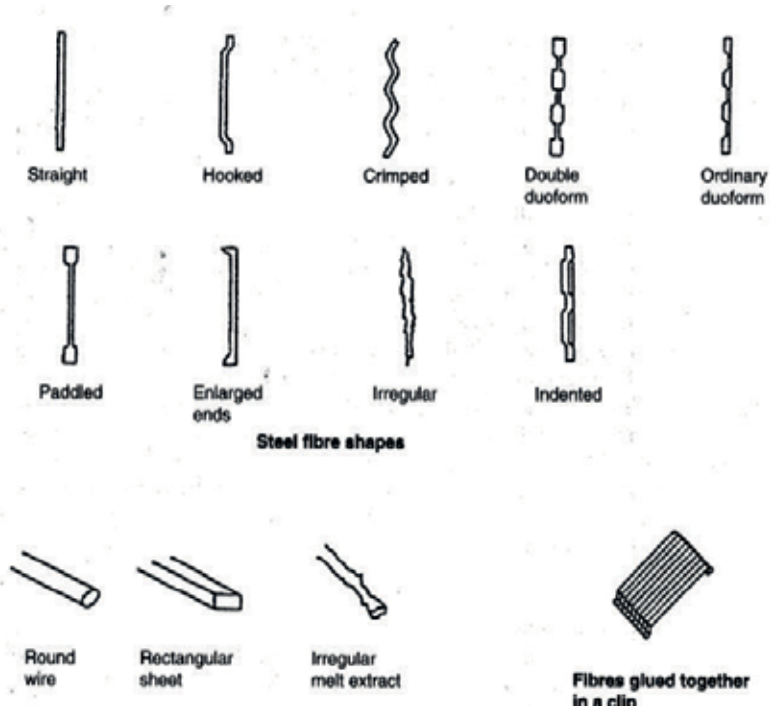

Figure 1. Different steel fibre types [27].

Young's modulus is 205 MPa, aspect ratio varies from 30 to 100, ultimate tensile strength of steel fibre varies from 345 to 1700 MPa, and length varies from 19 to 60 mm for respective fibres.

The largest fibre producers offer a statistical analysis to claim the sale of 67% fibre based on the hooked type. Katzer (2006) explained that crimped fibre (8%), straight fibre (9%) and fibre with deformed wire (9%) are other most popular fibre types.

3.2. Synthetic fibres

Research and development reflect the efforts of man-made fibres in the form of synthetic fibres specifically in the textile and petrochemical industries. Organic polymers derive fibres for synthetic fibre reinforced concrete based on available formulations [22]. Acrylic, polyethylene, polypropylene, nylon, polyester, carbon and aramid are the concrete-based matrices for synthetic fibre types in Portland cement. However, there is a dearth of these fibres, but other fibres are found extensively in commercial applications [22]. Low modulus of elasticity and high elongation properties are found in synthetic and organic fibres. In contrast, high modulus of elasticity is found in steel, glass, carbon and asbestos and fibres [29]. Similarly, structural and polypropylene are emerged as synthetic fibres and extensively found in concrete ground floor-slabs.

3.2.1. Polypropylene fibres (micro-synthetic fibres)

The significance of polypropylene fibres emerged due to their high alkaline resistance and low price of the raw polymer material [30, 31]. Their formation is based on fibrillated or monofilament manufactured in an enduring process through polypropylene homopolymer resin extrusion. Micro synthetic fibres are used for reducing, plastic settlement cracking and plastic shrinkage cracking in ground-supported slabs based on 100% polypropylene. According to Perry [32], micro-synthetic fibres are usually 12 mm long by 18 μm diameter.

3.2.2. Structural synthetic fibres (macro-synthetic fibres)

During the last 7 years, the development of micro-synthetic fibres has expanded comprehensively. The potential of these fibres is evident in providing concrete with significant ductility. These fibres have potential to control cracking resultant from lasting drying shrinkage and thermal movements in concrete floors and slabs [33]. These macro-synthetic fibres vary from polypropylene micro-fibres due to their large and higher polymers even though they typically comprise few polypropylenes [32]. A significant level of post-crack control is provided from synthetic structural fibres to accomplish steel fibres and fabrics [34].

Steel fibres and polypropylene fibres as well as structural synthetic fibres are the most common types of fibres used in structural members. Therefore, the following section discusses the addition, mixing, placing, finishing and curing of steel, polypropylene and structural synthetic fibres. Also, they present the effect of adding these fibre types on the properties of fresh and hardened concrete. However, using waste fibres is relatively a new practice and it is not limited to one type of wastes. Therefore, there is no clear guidance for the addition, mixing, placing, finishing and curing of such fibres. On the other hand, using hybrid fibres is limited to the use of steel and polypropylene as well as using different types of steel fibres. Thus, the below practices of adding single steel or polypropylene fibres are applicable.

4. Fibre reinforced concrete addition, mixing, placing, finishing and curing

4.1. Steel fibre

4.1.1. Composition and quality

Higher cement, smaller aggregates and fine contents are generally combined in the fibre reinforced concrete as compared to plain concrete. The fibre content increases to decrease the extent of the slump [21, 22]. Therefore, a steel wire manufacturer signifies the following specification for acquiring steel fibre reinforced concrete [35].

4.1.2. Addition and mixing of steel fibre

It is deemed that 20–40 kg/m^3 is usually the recommended dosage for steel fibres. According to Knapton, [27], the flexural strength of the concrete results in higher dosage rate. In general, the fresh concrete is combined with the fibres and; afterwards, these fibres are moved initially to the mixer. Newman and Choo [21] revealed that these fibres can be incorporated to the aggregated conveyor belt. The fibres might be dispensed directly regardless of any balling risk, when the aspect ratio of the fibre is less than 50. Particular packing techniques are employed by manufacturers for reducing the risk with higher aspect ratios [22]. On the contrary, the satisfactory outcome of visual inspection is evaluated for fibre distribution during pouring [27].

4.1.3. Placing finishing and curing

Approved mixing, quality control procedures, and finishing are required for good quality and economic construction of steel fibre reinforced concrete [22]. The placement of concrete through good concrete practice is affective in positioning during curing. The reduced flow characteristics allow positively the final placement of steel fibre reinforced concrete (Unwalla, 1982; [36]).

Placing, curing and finishing steel fibre reinforced concrete are satisfactorily used by traditional tools, procedure and equipment [36–39]. Antiwear products and cement are usually expanded on the concrete surface after levelling and compaction [27]. Same methods and techniques can be used for curing and protecting SFRC. Plastic and shrinkage cracking can be produced through insufficient curing methods in traditional concrete [36, 37, 39].

4.1.4. Mechanical properties of fresh steel fibre-reinforced concrete

The important problem produced during the steel fibre reinforced concrete is the accomplishment of sufficient workability. Fibres are included in the concrete mix with aspect ratio and fibre volume, which affect the workability [36, 40]. The steel fibres can mitigate the estimated

Element	**Quantity**
Cement	320–350 kg/m^3
Well-graded sharp sand	750–850 kg/m^3
Continuous aggregate grading	28 mm
Crushed stone	14 mm, 15–20%
Characteristic compressive strength	25 N/mm^2
Water/cement ratio	0.50–0.55

Table 1. Concrete mix design of steel fibre reinforced concrete.

composite slump as reported from the variations of volume fractions included in steel fibre reinforced concrete (0.25–1.5 vol%). Furthermore, the effects of vibration are suggested to assess workability of a SFRC mixture with the VB test because mechanical vibration is suggested in a number of SFRC applications as compared to traditional slump measurement. A good workability is maintained through the inclusion of superplasticiser. In contrast, the fibre balling should be ignored when considering above specifications.

4.2. Polypropylene fibre-reinforced concrete

4.2.1. Addition and mixing (polypropylene)

The addition of polypropylene fibres is at a recommended dosage of approximately 0.9 kg/m^3 (0.1% by volume) [27]; the fibre volume is so low that mixing techniques require little or no modification from normal practice [21]. The fibres may be added at either a conventional batching/mixing plant or by hand to the ready-mix truck on site [27].

4.2.2. Placing finishing and curing (polypropylene)

Polyproline fibres are comprised of concrete mixes that can be transformed by normal methods and; therefore, flow easily from the hopper outlet. The essential compaction might be used for providing traditional means of vibration and tamping. The traditional concrete can be considered strictly for curing procedures. The floating and trowelling of fibre-dosed mixes can be used for normal hand and poor tools [27].

4.2.3. Mechanical properties of fresh fibre-reinforced concrete

According to Ramakrishnan [4], proper design and application of fibre reinforced concrete mixes can be essentially considered on the basis of knowledge of the fresh concrete properties. The occurrence of polypropylene fibres is mechanically observed since a comprehensive impact is imparted on the concrete, cement hydration and delaying evaporation by holding water [27]. The polypropylene fibres did not affect the slump of fibre-dosed concrete. The properties of the fresh concrete are modified through the primary role of polypropylene. The movement of solid particles, the bleed of water chemicals and the homogeneity of the mix are stabilised, blocked and increased through polypropylene fibres. The bleed capacity of the concrete and plastic settlement is reduced, and decreases the rate of bleed through polypropylene fibres.

The plastic concrete is formed due to plastic cracking and drying shrinkage. The formation of plastic cracks took place in the first 24 h, when there is high evaporation rate and the concrete surface dries after the placement of the concrete [27]. The appearance of concrete along with its durability and physical and mechanical properties is affected through this high evaporation rate [41]. The width of plastic shrinkage cracks can be restricted due to the polypropylene fibres. In the initial phases, the post-cracking ductility of the concrete emerged from the fibres, increasing strain capacity and affecting plastic shrinkage cracking [21].

4.3. Structural synthetic fibres

For synthetic structural fibres, the dearth of available references and design guidelines are the considerable barriers for effective comprehension to add, mix, compact, finish, cure, and place within concrete properties. The information associated to these sources are mentioned in the following paragraph [32, 34, 42]. During the patching or mixing processes, the fibres can be incorporated to the concrete at any point.

The particular application and intended properties relied on the additional rate, which differs from 1.8 to 7 kg/m^3. Careful attention is required for their additional rate within both batching procedures and mix design to accomplish optimum consequences. The required workability is accomplished by ensuring the adjustments into the mix design. Afterwards, the fine aggregate contents include a slight increase for coating the fibres comprehensively. The concrete is assisted with efficient finishing and rapid placing. In contrast, medium to high level of workability is accomplished through the inclusion of a superplasticiser. It is evident that the position of structural synthetic fibres is appropriately similar according to the normal concrete. Moreover, concrete must be compacted adequately to assure the surface placement with the easy finishing. An easy float is typically transformed over the concrete for patching the surface after compaction. The fibre reinforced is enabled to cure effective concreting practice once it is levelled, floated and compacted. Structural synthetic fibre mostly relies on surface friction to achieve anchorage across a crack. It controls plastic shrinkage cracking and cracking due to drying shrinkage of the concrete. Moreover, it improves concrete properties including ductility, fracture toughness, impact and fatigue resistance.

5. Effect of using single type of fibres on concrete mechanical properties

5.1. Steel fibres

Steel fibre is becoming an important type of concrete reinforcement due to the numerous advantages that it offers for concrete. Compared to traditional fabric reinforcement, steel fibres have a tensile strength typically two to three times greater and a significant greater surface area to develop a bond with the concrete matrix [5]. Over the past three decades, the potential of using steel fibre reinforced concrete (SFRC) to improve the performance of structures has been investigated [43]. The available literature on the subject shows that steel fibre reinforcement can increase significantly the compression, tension, flexure, impact and toughness, shear and punching resistance, as well as the energy dissipation capacity and durability of concrete structures.

The occurrence of fibres affects the compressive strength as it varies from 0 to 15%. In contrast, the order of 30–40% fibres is increased with direct tension. There are little data dealing strictly with the torsion and shear even though they are usually increased [22, 44]. Moreover, steel fibre has a noteworthy effect on the residual tensile strength and flexural strength, with increase of more than 100% being reported [45, 46]. The most important part of the commercial use of steel fibre is the post-crack flexural performance, which is based on the steel fibre

concrete and sections subjected to point or flexure load. The flexural behaviour of concrete reinforced with straight and hooked end steel fibres was studied by Pajak and Ponikiewski [26]. It was found that the increase of fibre volume ratio increases the flexural tensile strength. The fracture energy increases with the increase of fibre dosage and is higher for hooked end steel fibres than for straight ones. Steel fibres continue to carry stresses after matrix failure. This is also confirmed by many researchers [9, 11, 12].

According to Hauwaert et al. [47], impact strength and toughness are significantly increased, which is defined as energy absorbed to failure. Under the load deflection curve, the toughness increases resulting in tension and flexure due to the increase in area [21]. A claim is usually made due to fatigue and increased resistance to dynamic load. The resistance of increased resistance to dynamic loading highly emerged as it is associated with the fibre distribution in concrete [48].

In studying the effect of steel fibres on the shear capacity of concrete, some investigations were carried out for evaluating the performance of beam–column sub assemblages. Susetyo et al. [10] undertaken experimental investigations on concrete panels based on pure-shear monotonic loading conditions for assessing the steel fibre effectiveness to meet minimal shear reinforcement requirements for concrete elements. Ductile behaviour, good crack control attributes and sufficient shear strength are exhibited through the test results. Minimum extent of traditional shear reinforcement is accomplished through the level of performance. The role of steel fibres in enhancing the shear strength of concrete was also confirmed by many researchers [8, 9, 49].

Labib (2008) conducted experimental investigations on concrete slab-column connections reinforced with hooked end steel fibres failing in punching; it was found that the inclusion of steel fibres significantly increases the load carrying capacity of tested specimens and is strongly dependent on the fibre dosage. Moreover, the crack opening restraint provided by the reinforcement mechanisms of steel fibres bridging the crack surfaces leads to a significant increase in terms of load carrying capacity and energy absorption capability of concrete structures. This was also confirmed by [13, 14].

In particular, steel fibre possesses a positive impact on the shrinkage behaviour of concrete that mitigates the extent and organises the cracks width, as compared to plain concrete [22, 28]. The fibres will corrode quickly in exposed situations, if the concrete compacts the fibre corrosion under the surface. The deterioration caused due to freeze-thaw cycling and the permeability of cracks can be reduced from the fibres [22, 50].

The role of fibres in bridging the crack opening and enhancing the load capacity and post-peak behaviour leads to better concrete durability and structural integrity ([15, 16]; Kunieda et al., 2014). This was also confirmed by the experimental results of Stephen (2001) which showed that the introduction of steel fibres into the concrete can arrest the early spalling of the concrete cover and increase the load capacity as well as the ductility of the columns over that of comparable non-fibre reinforced specimens. Similar observations were reported more recently by Lee et al. [49], Joao (2010), and Röhm and Arnold [51]. Steel fibres improve the ductility of concrete under all modes of loading.

5.2. Synthetic fibres

Synthetic organic fibres have low modulus of elasticity and high elongation properties [29]. Therefore, they have the potential to provide concrete with significant ductility. As a result, when added to concrete, these fibres are able to control cracking caused by thermal movements and long-term drying shrinkage [33] and improve the performance of concrete by negating its disadvantages such as low tensile strength, low ductility and low energy absorption capacity (Lakshmi et al., 2010; [52]; Mu et al., 2000; [53, 54]). Glass, polyvinyl, polypropylene, polyolefin and carbon are concrete-based matrices used in the synthetic fibre types in Portland cement.

Synthetic fibre types that have been tried in Portland cement concrete-based matrices are: polypropylene, glass, carbon, polyolefin and polyvinyl. For many of these fibres, there is little reported research or field experience, while others are found in commercial applications and have been the subject of extensive reporting [22]. Among these materials, polypropylene fibres are one of the most widely used for construction applications such as blast-resistant concrete and pavements (Mwangi, 2001).

Polypropylene fibres are gaining significance due to the low price of the raw polymer material and their high alkaline resistance [30, 31]. Their formation is based on fibrillated or monofilament manufactured in an enduring process through polypropylene homopolymer resin extrusion. Micro-synthetic fibres are used for reducing, plastic settlement cracking and plastic shrinkage cracking in ground-supported slabs as based on 100% polypropylene. Polypropylene fibres are used extensively in concrete for the purpose of reducing, plastic shrinkage cracking and plastic settlement cracking [32].

Mazaheripour et al. (2011) investigate the effect of polypropylene fibre inclusion on fresh and hardened properties of concrete. The results obtained have shown that the polypropylene fibres did not influence the compressive strength and elastic modulus; however, applying these fibres at their maximum percentage volume increased the tensile strength and the flexural strength of concrete.

Fire still remains one of the most serious risks for tunnels, buildings and other concrete structures. Thereby, the risks related with increased temperatures should be considered by engineers when designing concrete structures, including explosive spalling due to adverse concrete deterioration (Phan et al., 2002; Horiguchi et al., 2004).

It has been widely shown that polypropylene fibres are very effective in mitigating spalling in concrete exposed to elevated temperatures. Bangi et al. (2012) conducted an experimental study for investigating the fibre type effect and maximum pore pressure amount in fibre reinforced high-strength concrete. It uses different lengths of steel fibres, polyvinyl and polypropylene. The pore pressure reduction in heated concrete is contributed through pore pressure measurements based on organic fibres. The most effective maximum pore pressure development is polypropylene fibres as compared to polyvinyl alcohol fibres. On the contrary, there is a low effect found on the steel fibres. This result has been proved by studies from different researchers. These studies found that the complex mechanism of porosity variations in concrete at elevated temperatures, enriched with polypropylene fibres (Khoury, 2008; [55, 56]; Zeimi et al., 2006; Muzzucco et al., 2015).

On the other hand, polypropylene fibres can improve not only mechanical properties of concrete but also its durability due to reduced crack width by fibre bridging effect. Therefore, it could be considered as solution to extend lifecycle in terms of improvement of durability (Kunieda et al., 2014). The polypropylene fibres enhance the resistance to frost attack and the surface of abrasion resistance. The protection of the steel reinforcement is increased through these aspects alongside corrosion and mitigates the concrete water permeability. Knapton [27] states that the chemical resistance of concrete is not changed in this process. In particular, polypropylene fibres are usually more durable as compared to plain concrete [28].

As stated previously, while polypropylene is extensively used in concrete, other synthetic fibres such as glass, carbon, polyolefin and polyvinyl had little reported research or field experience. Barhum et al. (2012) studied the impact of the dispersed and short fibres of carbon and alkali resistance on the textile-reinforced concrete's fracture behaviour. The strength, fracture behaviour and deformation of the study are performed through a series of deformation-controlled and uniaxial tension tests. Pronounced enhancement of first-crack stress was achieved due to the addition of glass and carbon fibres. While more and finer cracks were observed on the specimens with short fibres added, a moderate improvement in tensile strength was recorded.

The formation of polyolefin fibre reinforced concrete is based on the employment of polyolefin fibres since they are lighter and possess a final lower cost and not chemically stable. They have been proved to be suitable for structural uses. Moreover, in some cases, they have substituted steel fibres (Behfarnia et al., 2014; Pujadas et al., 2014; Alberti et al., 2015). On the other hand, polyvinyl alcohol organic fibres and nylon are also effective in mitigating spalling, while others like polyethylene fibres are not so effective. Investigations from Laura et al. (2014) indicated that the use of synthetic fibre reinforced concrete can enhance the ductility and energy dissipation capacity of concrete.

5.3. Waste fibres

The use of waste fibres plays an important role in sustainable solid waste management. It helps to save natural resources, decreases the pollution of the environment and saves energy production processes. It has beneficial environmental and economic impacts; therefore, wastes and industrial by-products should be considered as potentially valuable resources merely awaiting appropriate treatment and application [19, 20]. Therefore, the addition of waste to concrete corresponds to a new perspective in research activities, integrating the areas of concrete technology and environmental technology.

Steel fibres originated from the industry of tyres and plastic wastes are among these wastes; their disposal has harmful effects on the environment due to their long biodegradation period, and therefore one of the logical methods for reduction of their negative effects is the application of these materials in other industries.

Recent research is showing that steel fibres originated from the industry of tyre recycling and can be a valuable reinforcement system to decrease significantly the brittle behaviour of cement-based materials, by improving their toughness and post-cracking resistance. Recycled steel fibre reinforced concrete is therefore becoming a promising candidate for both structural

and non-structural applications [18]. Zamanzadeh et al. [43] compared the characterisation of the post-cracking properties of recycled steel fibre reinforced concrete and industrial steel fibre reinforced concrete, on its use as shear reinforcement. Although the results indicated that the fibre reinforcement mechanisms for relatively small crack width levels were not as effective in the recycled steel fibres as the industrial steel fibres, it was verified that both fibres have similar trend in the post-cracking behaviour.

Much research effort has focused on reusing waste materials from plastic industries in concrete. Different works have analysed the effect of the addition of recycled polyethylene terephthalate (PET) to the properties of concrete (Choi et al., 2005; Jo et al., 2007; Robeiz, 1995). The reinforced concrete with PET bottles has been analysed by Foti (2011). The study has found that there is a great influence on post-cracking performance of simple concrete elements, when incorporating little amount of recycled fibres from PET bottle wastes. The sample's toughness and the concrete plasticity are enhanced and increased, respectively, through these fibres. Moreover, fibres are used from recycled PET bottles in reinforced mortar by De Oliveira et al. (2011). The findings have shown that a significant enhancement on compressive strength of mortars is shown from these PET fibres on their toughness and their flexural strength. The possibility of recycling PET fibres is explored by Foti (2013) as acquired from waste bodies with assorted shapes. The ductility of concrete is increased through these tests and PET fibres in a concrete mixture. At the end, as limited research has been carried out in this area, therefore, more studies could be carried out on the effect of using the previously mentioned wastes on the mechanical properties of concrete to prove the above results and to further examine different mechanical properties. In addition, the effect of using other types of wastes on the mechanical properties of concrete could be investigated.

6. Effect of using hybrid fibres

It is noteworthy to examine that the concrete failure is based on a multi-scale and a gradual process even though the research mentioned above have convinced us that remarkable improvement in mechanical performance can be achieved by using single fibre type in concrete. Therefore, significant attempts are made toward fibre combinations with different functions and constitutive responses and dimensions into cementitious composite. Potential advantages can be offered through hybrid combinations of steel and non-metallic fibres to enhance concrete properties and to reduce the entire cost of concrete production (Bentur and Mindess, 1990). Fibre fractions result in a uniform and a denser fibre distribution within the concrete as it enhances post-crack strength of concrete and reduces shrinkage cracks. This combination of low- and high-modulus fibres can arrest the micro- and macro-cracks, respectively, which could be also achieved by using a combination of long and short fibres as different lengths of fibres would control different scales of cracking.

A number of studies indicated the overall benefits of using combinations of steel fibres and polypropylene fibres (Xu et al., 2011; Sivakumar, 2011; Chi, 2014; Ding et al., 2010; Sahoo et al., 2015), while limited research was carried out on the effect of using steel fibres and other types of fibres such as glass and polyethylene (Banthia et al., 2014) or using a mix of short and long steel fibres [11].

Xu et al. (2011) found that the tensile strength of steel-polypropylene hybrid fibre reinforced concrete. The results indicated that the tensile strength of conventional concrete can be dramatically improved by mixing with hybrid steel-polypropylene fibres. The enhancing effect of hybrid fibre is better than that of single fibre, and the volume fraction of steel fibre is observed to have a great impact on the tensile strength. The same results were found by Sivakumar (2011) who studied the flexural strength, toughness, and ductility of concrete specimens containing individual steel fibres and hybrid combinations of steel and non-metallic fibres such as glass, polyester and polypropylene. He found that the ability of non-metallic fibres to bridge smaller micro-cracks was suggested as the reason for the enhancement in flexural properties compared to individual steel fibre.

The effect of inclusion hybrid steel-polypropylene fibre reinforced concrete on triaxial compression was developed by Chi (2014). The results showed that the steel fibres mainly contribute to the composite's triaxial strength that was observed to improve significantly when both the volume fractions and aspect ratios of steel fibre were increased. On the other hand, the polypropylene fibres were found to have considerable effect on improving the tensile meridian rather than compressive meridian.

Ding et al. (2010) analysed the influence of various fibre types, including steel macro-fibre and hybrid fibre (macro-steel fibre and macro-plastic fibre) on the shear strength and shear toughness of reinforced concrete beams. The results indicated that hybrid fibres can evidently enhance both the shear toughness and the ultimate shear bearing capacity.

Sahoo et al. (2015) studied the influence of using both high-modulus (steel) and low-modulus (polypropylene) fibres on the shear strength of reinforced concrete beams. A better post-peak residual strength response is noticed in the case of all FRC beam specimens due to multiple cracking associated with the fibre bridging action. The main parameters investigated are shear strength, failure mechanism and displacement ductility. The FRC specimens with combined steel and polypropylene fibres showed that the shear resistance and deformability values are improved significantly; multiple cracks of smaller crack width are noticed at the failure stage of the specimens indicating the better fibre bridging action of combined metallic and non-metallic fibres.

Banthia et al. (2014) used hybrid fibres by using two types of macro-steel fibres and a micro-cellulose fibre. Flexural and direct shear tests were performed, and the results were analysed to identify the degree of enhancement in the mechanical properties associated with various fibre combinations.

7. Conclusion

This chapter reported on the historical use of fibres; types of fibres; and the addition, mixing, placing, finishing and curing of steel, polypropylene and structural synthetic fibres. This chapter also discussed the potential of using various types of fibres in reinforced concrete to optimise the properties of concrete material as well as to improve the mechanical performance of reinforced concrete members. The reviewed literature highlighted the role of fibres

in enhancing the concrete tensile strength, flexure strength; shear strength, punching shear strength, toughness, energy dissipation capacity, resistance to cracking and durability. The reviewed literature also indicated that, in most cases FRC contains individual type of fibres, which includes steel, polypropylene, glass, carbon, polyolefin and polyvinyl. Although extensive research is conducted on the FRC, the reviewed literature showed a dearth of research conducted on waste fibre. The reviewed literature highlighted that the research conducted on the use of waste fibre in concrete is limited to the effect of waste fibre on toughness, flexural strength, compression strength and post-peak behaviour of concrete elements. In addition, this chapter reported on the use of two or more types of fibres in a suitable combination which has proved the potential to improve the mechanical properties of concrete. Numerous studies on hybrid fibre reinforced concrete have been performed. The reviewed literature showed that combination of fibres is commonly limited to two types of mixes, a mix of steel and polypropylene fibres and a mix of steel fibres with different geometry, shape and size. It is recommended that more mixes should be analysed to identify the degree of enhancement in the mechanical properties associated with various fibre combinations.

Author details

Wafa Abdelmajed Labib

Address all correspondence to: wlabib@psu.edu.sa

Prince Sultan University, PSU, Riyadh, Saudi Arabia

References

[1] Huang L, Xu L, Chi Y, Xu H. Experimental investigation on the seismic performance of steel–polypropylene hybrid fiber reinforced concrete columns. Construction and Building Materials. 2015;**87**:16-27

[2] Bentur A. Microstructure, interfacial effects, and micromechanics of cementitious composites. Ceramic Transactions. 1990;**16**:523-550

[3] Buratti N, Mazzotti C, Savoia M. Post-cracking behaviour of steel and macro-synthetic fibre-reinforced concretes. Construction and Building Materials. 2011;**25**(5):2713-2722

[4] Ramakrishnan V. Materials and Properties of Fibre Reinforced Concrete. London: Civil Engineering; 1988. pp. 29-40

[5] ACIFC. An Introduction Guide: Steel Fibre Reinforced Concrete Industrial Ground Floors. Warwickshire: ACIFC; 1999

[6] Brandt AM. Fibre reinforced cement-based (FRC) composites after over 40 years of development in building and civil engineering. Composite Structures. 2008;**86**(1-3):3-9

[7] Di Prisco M, Plizzari G, Vandewalle L. Fibre reinforced concrete: New design perspectives. Materials and Structures. 2009;**42**(9):1261-1281

[8] Aoude H, Belghiti M, Cook WD, Mitchell D. Response of steel fiber-reinforced concrete beams with and without stirrups. ACI Structural Journal. 2012;**109**(3):359

[9] Barros JA, Lourenço LA, Soltanzadeh F, Taheri M. Retracted article: Steel fibre reinforced concrete for elements failing in bending and in shear. European Journal of Environmental and Civil Engineering. 2014;**18**(1):33-65

[10] Susetyo J, Gauvreau P, Vecchio FJ. Steel fiber-reinforced concrete panels in shear: Analysis and modeling. ACI Structural Journal. 2013;**110**(2):285

[11] Caggiano V, Fogassi L, Rizzolatti G, Casile A, Giese MA, Thier P. Mirror neurons encode the subjective value of an observed action. Proceedings of the National Academy of Sciences. 2012;**109**(29):11848-11853

[12] de Montaignac R, Massicotte B, Charron JP, Nour A. Design of SFRC structural elements: Post-cracking tensile strength measurement. Materials and Structures. 2012;**45**(4):609-622

[13] Safeer-ul-Hassan M, Munir M, Mujahid MY, Kisana NS, Akram Z, Nazeer AW. Genetic analysis of some biometric characters in bread wheat (*Triticum aestivum* L.). Journal of Biological Sciences. 2004;**4**(4):480-485

[14] Ventura-Gouveia A. Constitutive models for the material nonlinear analysis of concrete structures including time dependent effects [PhD thesis]. Department of Civil Engineering; 2011

[15] Granju JL, Balouch SU. Corrosion of steel fibre reinforced concrete from the cracks. Cement and Concrete Research. 2005;**35**(3):572-577

[16] Jiang Z, Banthia N. Size effects in flexural toughness of fiber reinforced concrete. Journal of Testing and Evaluation. 2010;**38**(3):332-338

[17] Shi C, Qian J. High performance cementing materials from industrial slags—A review. Resources, Conservation and Recycling. 2000;**29**(3):195-207

[18] Aiello A, Lindlein N, Marquardt C, Leuchs G. Transverse angular momentum and geometric spin Hall effect of light. Physical Review Letters. 2009;**103**(10):100401

[19] Graeff C, Durante M, Bert C. Motion mitigation in intensity modulated particle therapy by internal target volumes covering range changes. Medical Physics. 2012;**39**(10):6004-6013

[20] Neocleous K, Tlemat H, Pilakoutas K. Design issues for concrete reinforced with steel fibers, including fibers recovered from used tires. Journal of Materials in Civil Engineering. 2006;**18**(5):677-685

[21] Newman J, Choo B. Advanced Concrete Technology (Processes). Oxford: Elsevier Ltd; 2003

[22] ACI Committee 544.1R. Fibre Reinforced Concrete. Michigan, USA: American Concrete Institute; 1996

[23] ACI Committee 544. State-of-art report on fibre reinforced concrete. In: ACI Manual of Concrete Practice, Part 5 – 1990. Michigan, USA: American Concrete Institute; 1986

[24] Romualdi J, Baston G. Mechanics of crack arrest in concrete. Proceedings ASCE. 1963; **89**(EM3):147-168

[25] Goldfein S. Plastic fibrous reinforcement for Portland Cement. Technical Report No. 1757-TR; Fort Belvoir: US Army Engineering Research and Development Laboratories; 1963

[26] Pająk M, Ponikiewski T. Flexural behavior of self-compacting concrete reinforced with different types of steel fibers. Construction and Building Materials. 2013;**47**:397-408

[27] Knapton J. Ground Bearing Concrete Slabs. London: Thomas Telford; 2003

[28] Concrete Society. Concrete Industrial Floors—A Guide to Their Design and Construction. Technical Report No. 34; Slough: The Concrete Society; 1994

[29] Manolis G, Gareis P, Tsonos A, Neal J. Dynamic properties of polypropylene fibre-reinforced concrete slabs. Cement and Concrete Composites. 1997;**19**:341-349

[30] Keer J. Fibre reinforced concrete. In: Swamy RN, editor. Concrete Technology and Design, Volume 2: New Reinforced Concretes. London: Surry University Press; 1984

[31] Maidl B. Steel Fibre Reinforced Concrete. Berlin: Bernhard R. Maidl in co-operation with Jorg Dietrich, Ernst & Sohn; 1995

[32] Perry B. Reinforcing external pavements with both large and small synthetic fibres. 2003;**37**(8):46-47

[33] Concrete Society. Concrete industrial floors—A guide to their design and construction; Technical Report No. 34; Slough: The Concrete Society; 2003

[34] Clements M. Synthetics as concrete reinforcement. Concrete. 2002;**36**(8):37-38

[35] Bekaert. Industrial Floors with Dramix Steel Wire Fibre Reinforced Concrete. Zwevegem, Belgium: NV Bekaert SA; 1990

[36] Swamy R. The technology of steel fibre-reinforced concrete for practical applications. Proceedings of the Institution of Civil Engineers, London. 1974, 1994;**56**(1):143-159

[37] ACI Committee 544. Guide for proportioning, mixing, placing and finishing steel fibre reinforced concrete. ACI Materials Journal. 1993;**90**(1):94-101

[38] Killen P, Dalgleish P. Practical applications of steel fibre reinforced concrete floor slabs for industrial projects. In: Australia, Proceedings of the Asia-Pacific Specialisty Conference on Fibre Reinforced Concrete; Singapore; August 28-29, 1997. pp. 137-144

[39] Knapton J. Single Pour Industrial Floors. London: Thomas Telford; 1999

[40] Hannat D. Fibre Cements and Fibre Concretes. New York: John Wiley & Sons; 1978

[41] Ma Y, Zhu B, Tan M, Wu K. Effect of Y type polypropylene fibre on plastic shrinkage cracking of cement mortar. Materials and Constructions. 2004;**37**:92-95

[42] Grace Construction Company. Nov. 2005. Available from: www.graceconstruction.com

[43] Zamanzadeh Z, Lourenço L, Barros J. Recycled steel fibre reinforced concrete failing in bending and in shear. Construction and Building Materials. 2015;**85**:195-207

[44] Amir A, Mirsayah, Banthia N. Shear strength of steel-fibre-reinforced concrete. ACI Materials Journal. 2002;**99**(5):273-279

[45] Johnston C. Steel fibre reinforced mortar and concrete: A review of mechanical properties. In: Fibre Reinforced Concrete, ACI SP – 44. Detroit: American Concrete Institute; 1974. pp. 127-142

[46] Khaloo R, Afshari M. Flexural behaviour of small fibre reinforced concrete slabs. 2005; **27**(1):141-149

[47] Hauwaert A, Delannay F, Thimus J. Cracking behaviour of steel fibre reinforced concrete revealed by means of acoustic emission and ultrasonic wave propagation. ACI Materials Journal. 1999;**96**(3):291-296

[48] Cachim P, Figueiras J, Pereira P. Fatigue behaviour of fibre-reinforced concrete in compression. Cement and Concrete Composites. 2002;**24**(2):211-217

[49] Lee H, Dellatore SM, Miller WM, Messersmith PB. Mussel-inspired surface chemistry for multifunctional coatings. Science. 2007;**318**(5849):426-430

[50] Rapoport J, Aldea C, Shah S, Ankenman B, Karr A. Permeability of cracked steel fibre-reinforced concrete; Technical Report Number 115; USA: National Institute of Statistical Sciences; January 2001

[51] Röhm D, Arnold A. Lattice Boltzmann simulations on gpus with espresso. The European Physical Journal Special Topics. 2012;**210**(1):89-100

[52] Chanvillard G, Banthia N, Aitcin PC. Normalized load-deflection curves for fibre reinforced concrete under flexure. Cement and Concrete Composites. 1990;**12**(1):41-45

[53] Banthia N, Mindess S. Impact resistance of steel fiber reinforced concrete. Materials Journal. 1996;**93**(5):472-479

[54] Bayasi MZ, Zeng J. Composite slab construction utilizing carbon fiber reinforced mortar. ACI Structural Journal. 1997;**94**(4):442-446

[55] Han CS, Gao H, Huang Y, Nix WD. Mechanism-based strain gradient crystal plasticity—II. Analysis. Journal of the Mechanics and Physics of Solids. 2005;**53**(5):1204-1222

[56] Kalifa P, Chene G, Galle C. High-temperature behaviour of HPC with polypropylene fibres: From spalling to microstructure. Cement and Concrete Research. 2001;**31**(10): 1487-1499

[57] Deacon C. Welded steel fabric in industrial ground floor construction. Concrete. 1991; **25**(7):41-44

[58] Elasto-Plastic Concrete. Dec 2005. Available from: www.elastoplastic.com

[59] Fujii N, Hayashi T, Hirshman MF, Smith JT, Habinowski SA, Kaijser L, et al. Exercise induces isoform-specific increase in 5′ AMP-activated protein kinase activity in human skeletal muscle. Biochemical and Biophysical Research Communications. 2000;**273** (3):1150-1155

[60] Kelly J. Fibres for floors. Concrete. 1990;**24**(4):19-20

[61] Meda A, Pizzari G. New design approach for steel fibre-reinforced concrete slabson-ground based on fracture mechanics. ACI Structural Journal. 2004;**101**(3):298-303

[62] Neal F. ICE Design and Practice Guide: Concrete Industrial Ground Floors. London: Thomas Telford; 2002

[63] Ramakrishnan V, Gollapudi S, Zellers R. Performance characteristics and fatigue strength of polypropylene fibre reinforced concrete. In: Fibre Reinforced Concrete Properties & Applications, SP-105. Detroit: American Concrete Institute; 1987. pp. 141-158

[64] Xotta G, Mazzucco G, Salomoni VA, Majorana CE, Willam KJ. Composite behavior of concrete materials under high temperatures. International Journal of Solids and Structures. 2015;**64**:86-99

Chapter 4

Cement Microstructure: Fostering Photocatalysis

Elena Cerro-Prada

Additional information is available at the end of the chapter

http://dx.doi.org/10.5772/intechopen.74365

Abstract

The singularities and the qualities of the hydrated cement microstructure have been identified by researchers as enhancers to promote photocatalytic processes, mediated by titanium dioxide, to create environment-friendly cement. In this chapter, we intend to expose the microstructural characteristics of cement and those aspects that make it possible for the promotion of photocatalytic activity. Within the inherent complexity of the cement microstructure, we describe a framework of two key elements in the microstructure of this material that affects the promotion of TiO_2 photocatalysis, to offer a more comprehensive view of the physical-chemical processes involved. These elements are: the porosity and the nanostructure of the C-S-H. This framework is also a starting point for future studies that seek to improve the photocatalytic response of titanium dioxide inserted in the cement matrix, as well as to provide implications for the application of photocatalytic cement technology in the construction materials industry.

Keywords: titanium dioxide, photocatalysis, cement porosity, calcium-silicate-hydrate (C-S-H), photodegradation, photocatalytic cement

1. Introduction

Cement develops its microstructure during its hydration process, which is, without any doubt, one of the most studied phenomena in materials science. Its high complexity is due to the number of actors involved in the process as well as the conditions in which it is being developed. Several physical-chemical processes take place in a perfectly coordinated manner, resulting in a material with exceptional properties. Cement clinker reacts with water giving insoluble hydration products which, in a cement paste (a mixture of cement powder and water) or concrete (a cement paste containing sand and aggregate filler), gradually replace the water in the

spaces between the cement grains and aggregate particles, and eventually provide a matrix that effectively binds the composite mass together. The reaction products, called hydrates, are responsible for strength development and they give cement its binding properties.

The hardening reaction in a cement paste is mainly associated with the hydration of the two calcium silicate compounds which occupy more than 80% by mass of the anhydrous clinker of ordinary Portland cement. These two phases produce the same products when they react with water: on the one hand, a colloidal calcium silicate hydrate, also known as a C-S-H gel, is formed together with a crystalline solid solution of calcium hydroxide, $Ca(OH)_2$ or CH, also called portlandite, which tends to form large crystals with a distinctive hexagonal-prism morphology. Within a few hours of mixing with water, cement paste starts to gain in stiffness and strength, going from a viscous fluid to a plastic solid, and finally, to a stiff solid. This change occurs because the hydration products have a lower density than the anhydrous phases and occupy more space, filling most of the space created by the consumption of water and increasing the solid volume. There are two main steps involved: the rapid initial formation of gelatinous hydrate coatings around the cement grains and, after a dormant period, the growth from these coatings of fibrillar C-S-H gel material into a reticulate network between the cement grains. **Figure 1A** and **B** show two scanning electron micrographs of Portland cement pastes. **Figure 1A** illustrates early hydration of the paste, where amorphous-looking gelatinous envelope of C-S-H gel bridges the cement grains at their points of contact. CH portlandite can also be observed among micro and macroporous structure of the hydrated material. **Figure 1B** corresponds to a mature paste, where C-S-H gel shows a fibrous morphology, which provides a reticular network within the system. C-S-H is then considered as responsible for the cement paste's internal skeleton, for the paste's adherence to the aggregates in the formation of mortar and concrete and for the strength and durability of cement-based materials.

This complex microuniverse has been explored by scientists for decades and even more since the recent developments of nanotechnology. The new and powerful tools for visualization, manipulation, and analysis of nanostructures have made it possible to host nanomaterials in the cement microstructure, providing the material with novel properties, or consolidating or improving its most characteristic behavior. In this sense, nanotechnology has allowed interesting developments which include the use of nanoparticles, carbon nanotubes, nanofibers and latest generation of additives to improve the strength and durability of cement-based materials

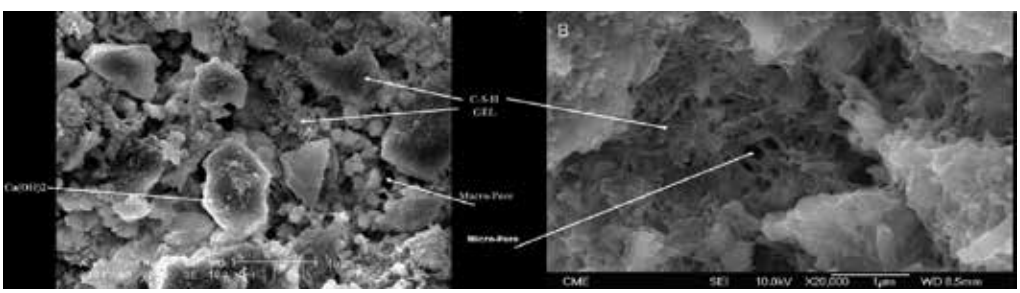

Figure 1. Scanning electron micrograph of hydrated Portland cement, (A) at early stage of hydration, and (B) fibrillar C-S-H gel in mature Portland cement paste.

[1–3]. Of special interest for building materials is nano-titanium dioxide. Its photocatalytic characteristics provide additional functionality mainly used to remove organic contaminants from surfaces exposed to ultraviolet radiation, such as road pavements and cement-based facade finishing products [4]. In addition, it has been proven that TiO_2 nanoparticles accelerate the hydration rate and increase the degree of hydration of the cement matrix [5].

This growing interest that has appeared in recent years by the nanoscale, is derived from the fact that the properties of the same material vary, and even new ones appear, depending on the size. This is the case with titanium dioxide, a semiconductor formed by covalent bond between titanium metal and oxygen. Titanium, the ninth most common element in the earth's crust, is a metal that is found in nature but not in a free form. Titanium interacts naturally with oxygen to form titanium oxides, which are commonly found in minerals, powders, sands and soils. The beginnings of the TiO_2 industry go back 30 years when paint manufacturers were looking for a substitute for white lead, which is considered toxic. It was then when it caught the attention of the entire scientific community, to verify the important positive characteristics that it has: it is chemically stable, non-toxic and inexpensive. On the other hand, the increase of the specific surface that occurs when this semiconductor is in the form of nanoparticles gives it greater functionality to promote reactions that take place on the surface, such as photocatalytic processes. Titanium dioxide as a nanomaterial can be found in several crystalline phases, the most common being anatase, brookite, and rutile. The first two are transformed to rutile with the increase in temperature, since the latter is the most thermodynamically stable under normal conditions. Anatase and rutile have an octahedral structure, while brookite has an orthorhombic system.

In this chapter, we intend to expose the microstructural aspects of hydrated cement that promote photocatalytic processes based on titanium dioxide. Initially, the physical mechanisms that give photocatalytic properties to TiO_2 in the form of nanoparticles will be detailed. Next, the microstructural characteristics of the cement-base materials modified with titanium dioxide nanoparticles will be described, analyzing their feasibility as new construction materials. Consequently, we describe a framework of two key elements in the microstructure of this material that affect the promotion of TiO_2 photocatalysis, to offer a more comprehensive view of the physical-chemical processes involved. These elements are: the porosity and the nanostructure of the C-S-H gel. At the end, several possible routes are suggested for future investigations in heterogeneous photocatalysis in cement.

2. TiO_2-driven heterogeneous photocatalysis

Heterogeneous photocatalysis is a physical-chemical process that occurs in certain semiconductors when they are excited by electromagnetic radiation of a certain wavelength. The photocatalytic reaction begins when an incident photon promotes an electron from the valence band (VB) to the conduction band (CB), provided that the energy absorbed from the photon is equal to or greater than the semiconductor gap, leaving behind a hole in the valence band. The electron-hole pair produced catalyzes oxidation reactions of certain organic compounds adsorbed on the surface of the semiconductor, such as the NOx pollutant, in the presence of

water molecules. Electrically, titanium dioxide is a wide-band-gap semiconductor (3 eV for rutile and 3.2 eV for anatase), requiring photons of wavelength less than 383 nm and greater than 403 nm respectively to promote valence band electrons.

Four chain reactions are fundamentally involved in the overall process: (1) photoexcitation: transfer of energy from a photon to an electron producing an electron–hole pair, (2) adsorption of organic species on the surface of the semiconductor, (3) capture and recombination of charge carriers and (4) interfacial load transfer. These four mechanisms compete with a possible electron–hole recombination. **Figure 2** illustrates the process of TiO_2-driven heterogeneous photocatalysis of NOx species.

The effectiveness of the photoinduced reactions is controlled by the light absorption characteristics of the semiconductor, which in turn depend on (1) the microstructural characteristics of the semiconductor itself, (2) the energy of the incident photons and (3) the substrate where the reactions take place. As for the semiconductor microstructure, it would be desirable for it to have a series of important properties:

- high specific surface;
- uniform distribution of particle size;
- spherical particles; and
- presence of superficial defects that promote the adsorption reactions of contaminating species.

In this regard, TiO_2 has been successfully nanostructured in the form of nanoparticles by a variety of techniques and a wide range of sources. Due to its greater surface area, porosity and number of defects and its photochemical reactivity, the catalytic performance obtained from TiO_2 nanoparticles is significantly improved compared to that obtained if the material was not nanostructured. On the other hand, it is necessary that the photocatalyst process is triggered

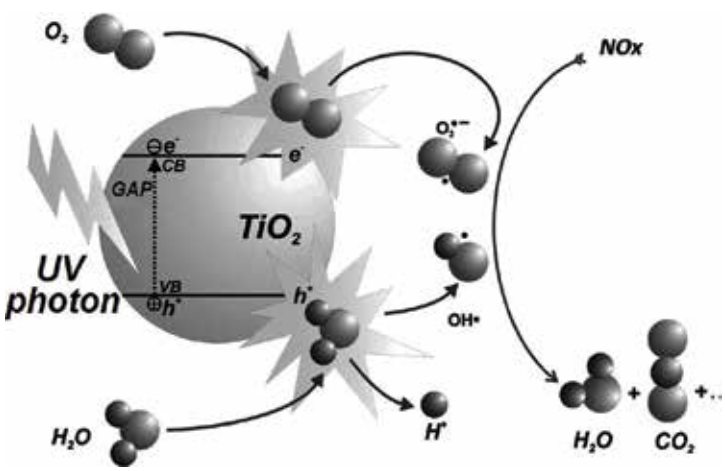

Figure 2. Heterogeneous photocatalysis of titanium dioxide for NOx degradation: photoexcitation of an electron from the semiconductor valence band to the conduction band, leaving a positive hole in the valence band.

by photons belonging to the spectrum of ultraviolet radiation, which can be obtained from solar radiation. This aspect, together with the excellent properties of TiO_2 as a photocatalyst, results in a clearly versatile and low-cost degradation technology for air pollutants.

Despite these proven functional characteristics, such as self-cleaning, antimicrobial properties as well as the degradation of a range of organic (e.g., volatile organic compounds) and inorganic pollutants (e.g., NOx and SO_2), technical aspects such as UV radiation acquiring, are still a limitation for the large-scale application of this light-driven technology [6]. In addition, the photocatalysis mechanism of TiO_2 has certain limitations that hinder the development of commercial applications, for example, the large band gap of TiO_2, the electron–hole recombination process and deactivation of TiO_2 by partially oxidized intermediate blocks that occupy active catalytic sites on the photocatalyst.

3. Influence of nanosized TiO_2 on cement hydration

The incorporation of nano-TiO_2 as a filler in a cementitious matrix presents distinctive microstructural characteristics. Research has shown that the photocatalytic activity is superior in nano-crystalline TiO_2 and that it exhibits maximum efficiency in anatase phase compared to rutile or brookite phase [7]. When added to Portland cement, it is considered to act as inert filler and has not been believed to take part in the hydraulic reaction of Portland cement. However, the modification of particle size distribution due to chemically inert filler addition changes the system porosity, providing additional sites for nucleation of cement hydration products; consequently, the kinetics reaction might be catalyzed. In this sense, Jayapalan et al. [8] reported an increasing effect in the rate of early age hydration proportional to the dosage of TiO_2, as well as found that smaller particles seem to accelerate the reaction more than larger particles. While in this and other reported studies TiO_2 particles were added as TiO_2 nanopowder and mixed with water prior to the addition of cement, researchers have recently being investigating the effects on the microstructure and photocatalytic activity of cement pastes doped with nanosized TiO_2 prepared by other techniques; as, for example, sol–gel method [9].

Consequently, relevant research on this topic concludes in the same consequences that come from housing TiO_2 nanoparticles on the cement microstructure. On the one hand, the nanoparticles are located in the porous structure of the cement and promote the formation of C-S-H gel around, forming microspheres that are interconnected by fibrillar structures of C-S-H (**Figure 3A** and **B**). On the other hand, the nanoparticles of TiO_2 present in the cement matrix decrease the pore size and promote the formation of hydration products through the consumption of capillary water displaced from the pores. As observed in **Figure 3**, the TiO_2 nanoparticles are covered with inner C-S-H gel. Most of the nanoparticles preferentially cluster at the entrance of the micropores, which may reasonably increase the overall density and promote the formation of C-S-H inside these micropores. These findings, widely confirmed by many researchers, point out that TiO_2 nanoparticles present in the cement matrix accelerate C-S-H gel formation and improve the microstructure of cementitious materials by shifting the distributed pores to finer ones.

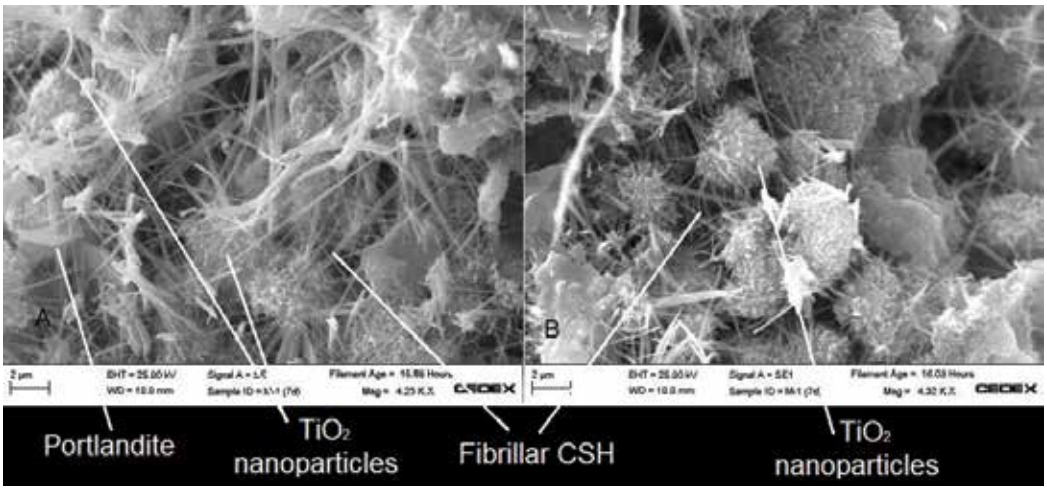

Figure 3. (A) Detail of SEM micrograph of TiO_2-doped cement paste after 7 days hydration time, showing shell microspheres of amorphous inner C-S-H gel formed around the TiO_2 nanoparticles. Fibrillar outer C-S-H bridges the spheres filling the inter-hydrate space. (B) Same TiO_2-cement paste after 14 days hydration displaying the same features.

4. Fostering photocatalysis through cement microstructure

In the previous section, we have exposed the most significant effects that nanoparticles of titanium dioxide, as filler, cause on the microstructure of the hydrated cement. Extensive research has been reported to show these clear modifications in the microstructure: decrease of porosity, increase of density in the C-S-H gel and increase of hydration products in the cement matrix. However, there exist not many works dedicated to the study of the cement microstructure as a valid support to favor the processes of photocatalysis. In this section, we try to explore the most relevant microstructural characteristics of hydrated cement for the promotion of the photocatalytic activity of nano-TiO_2.

The first view of the problem indicates that in order to obtain reasonable rates of photocatalytic activity, the substrate must be able to adsorb the pollutant particles and trap them in some way to expose them to the photocatalytic process. The adsorption of contaminants on the surface of the photocatalyst is, therefore, an important factor in achieving high rates of degradation. To promote adsorption, composite structures comprising inert domains coexisting with photocatalytic domains can be used. In this way, the pollutants are adsorbed first in the inert sites and then diffuse to the photocatalytic domains. This is the so-called "Adsorb and Shuttle" (A&S) effect [10]. In this sense, there are important benefits derived from the use of the microstructure of the cement matrix as a suitable substrate for the nano-TiO_2 photocatalyst. The TiO_2 nanoparticles are located in the porous microstructure of the cement, where surface and volume irregularities occur. This defects population also promotes the adsorption of inorganic species that are trapped on the surface. On the other hand, since the water molecules participate in the photocatalytic process both as adsorbents, as OH sources and as reaction products, it is obvious that the water content that naturally possesses the cementitious materials can have a significant effect on photocatalytic efficiency.

http://dx.doi.org/10.5772/intechopen.74365

It is evident then that the porosity and the presence of water of hydration in the microstructure of the cement are influential factors in the photocatalytic activity. With the aim to deeply analyze these factors, we propose a framework that helps identify the conditions for potential photocatalysis substrates in the cement material. Porosity and nanostructure of C-S-H gel are the two key elements in the microstructure of this material that affect the promotion of TiO_2 photocatalysis and will be studied in the following subsections.

4.1. Pore system of cement microstructure

When cement particles are dissolved and surrounded by water, they can react to produce solid reaction products (surface products) or spontaneously nucleate in the capillary water to produce crystals (pore products) [11]. The surface product is mainly the C-S-H gel and the major pore product is portlandite (CH). Yet, the surface product (C-S-H) is still porous media at nanoscale, forming gel pores, thus small molecules can diffuse through, and generally, its surfaces are negatively charged. In **Figure 4**, the presence of surface products (C-S-H, labeled as (1)) and pore products (portlandite crystals, labeled as (2)), can be observed in the microstructure, which occupy different spots, leaving spare room in between them. These voids are macropores (pore size larger than 50 μm), which are normally filled by water vapor. The capillary pores, however, are voids with average radius ranging from 5 to 5000 nm, where water persists even after hydration in completed, and that were previously available for pore products' nucleation.

This landscape draws a complex porous structure whose pore size distribution can vary from nanometers to thousands of microns, if macropores due to inadequate compaction are also

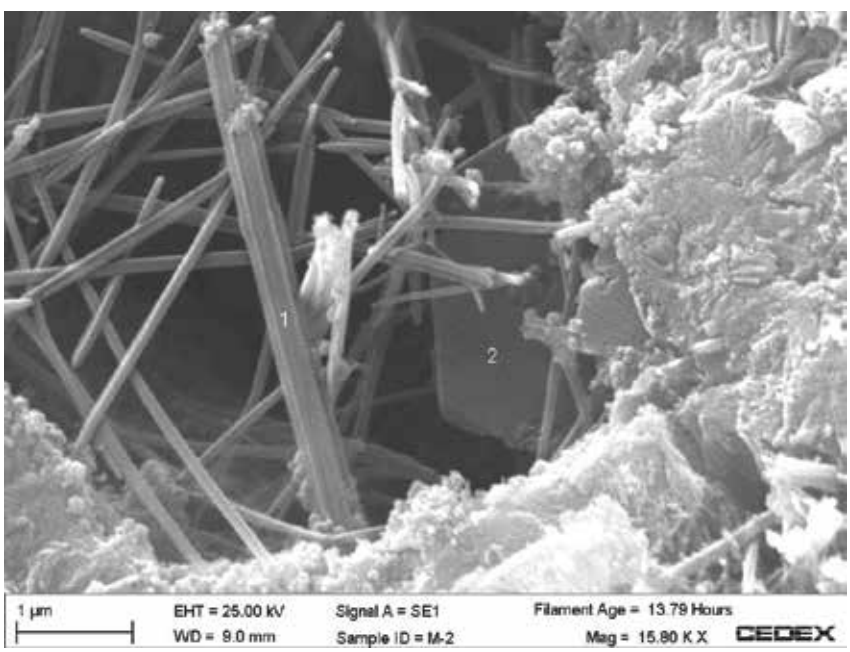

Figure 4. Scanning electron micrograph of cement paste displaying (1) C-S-H gel and (2) portlandite crystals as surface product and pore product respectively.

present. Moreover, large pores could be connected to gel pores through the fine capillary pores. Cement porosity is therefore directly related to the water present in the mix. The classification of the state of water in cement paste is generally based on the location where it is held and the nature of its bonding with the solid structure. Apart from the water vapor in the pores and the capillary water, it is suggested that water can also exist as adsorbed water (held by hydrogen bonds on the surface of the hydrated particles) and interlayer water [12]. Thus, the inherent availability of water in the vicinity of capillary pores leads to consider these porous structures as possible inert domains for hosting the photocatalytic nanoparticles.

4.2. Nanostructure of C-S-H gel

Since the C-S-H gel is the main solid reaction product that is formed during the hydration process, its presence must necessarily be compatible with the nanoparticle housing. As we have seen, nanoparticles not only do not interact negatively with the gel, but they are able to promote its development; therefore, the nanostructure of the C-S-H must be a clear reference in the photocatalytic capacity of TiO_2.

Hydrated cement is a continually evolving material: even after the hydration process has reached its end, the material keeps experimenting changes due to both increased hydration of the cement particles and changes in the microstructure of the products after they form. These changes include increases in the specific surface area, changes to the pore size distribution and a continued increase in stiffness. Likewise, the evolution of the C-S-H gel during hydration time implies changes in its density. Therefore, understanding the formation of the gel nanostructure is crucial to predict its mass/volume ratio.

Among the many different structural models suggested for C-S-H, the colloidal models proposed by Jennings [13] successfully explain various bulk properties of C-S-H found in hydrated cement pastes. The basic of these models is the existence of a 5-nm-diameter building block. These basic units pack together to form the microstructure of C-S-H. However, more recent studies [14] propose that the basic building block is a unit of C-S-H that is roughly spherical and approximately 2 nm across with a specific surface area of about 1000 m^2/g. These building blocks flocculate to form larger units. This model has been already validated by many experimental works [15], where spherical nanostructures of C-S-H gel have been found. According to this model, the density of the smallest unit that can be used to build the nanometer structure of C-S-H is taken as 2450 or 2800 kg/m^3, which are typical of the values for densities reported in the literature. Taking into account the high density of the C-S-H basic unit, the probability of a nanoparticle falling within a volume close to the gel is reasonable. Furthermore, according to this model, water fills the pore space starting with the finest, which impulses the idea of placing the TiO_2 nanoparticles in capillary pores that might be directly connected or closely near to fine deposits of water.

4.3. Cement as substrate-mediator for TiO_2 photocatalysis

Before discussing the validity of cement microstructure as support for photocatalysis of nano-TiO_2, let us expand the implications of the photoinduced reactions that take place during photocatalysis. Once the UV photon has promoted the electron to the conduction band, leaving a gap in the valence band, this electron–hole pair is "trapped" and should proceed with the interfacial charge transfer process to directly oxidize/reduce contaminants or generate reactive oxidants.

http://dx.doi.org/10.5772/intechopen.74365

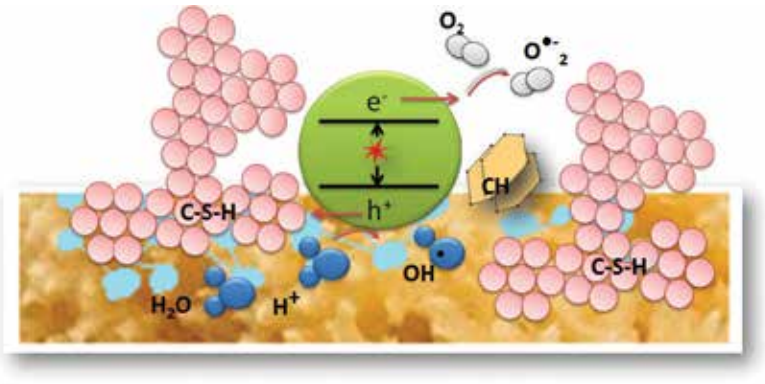

Figure 5. Illustration of cement-mediated charge recombination on nano-TiO_2 in the photocatalysis conversion process.

The transfers of trapped electrons and trapped holes should be fast enough to compete against electron-hole recombination, which is the main process that limits the overall photocatalysis performance. All this occurs on the surface of TiO_2; therefore, the charge transfer reactions are clearly limited by the photocatalyst surface conditions.

In the cement microstructure, the TiO_2 nanoparticles are naturally placed in the capillary pores, since these locations are surrounded by vapor water and are thermally stable. In this situation, the nanoparticles exhibit high surface specific area and have defects around them that act as traps for the adsorbents. Moreover, the capillary pores are connected to each other by capillary water, which ensures the provision of water molecules essential for the photocatalytic process to take place.

In this picture, we now add the presence of C-S-H gel nanostructures as nanosphere clusters, in addition to portlandite crystals that prefer to nucleate in the surface pores. We must remember that the density of the C-S-H gel is very high, and it is also surrounded by negative charge. On the other hand portlandite, namely calcium hydroxide, tends to react with oxygen and carbon dioxide to form calcite. These facts ensure the presence of molecular oxygen in the vicinity of nano-TiO_2. The situation is illustrated in **Figure 5**.

Owing to the negative charges of the C-S-H gel nanostructure framework, it is expected that the trapped electron feels the Coulomb repulsion force that pushes the electron away favoring its reaction with adsorbents. The overall effect results in providing charge reservoir sites which promote the interfacial charge transfer mechanism. Cement microstructure can therefore effectively mediate in TiO_2 photocatalytic performance.

5. Nano-TiO_2-cement composites preparation for photocatalytic applications

When preparing photocatalytic cement, it is crucial to take into account some key factors that will determine both the compound photodegradant capacity and its final performance as structural material. On the one hand, the choice of photocatalytic dosage and insertion method

usually depends upon the composition of the host cement-based composite. On the other hand, TiO_2 photocatalyst can be used either as freestanding particulate or as coating on a substrate. However, much more insight is needed from engineering design and modeling point of view, for successful application of the laboratory-scale techniques to large-scale operation. Questionless, there exist some beneficial effects on the environment derived from inclusion of TiO_2 nanoparticles to cement production. But on its own, cement is a highly efficient material in terms of energy consumption and welfare that generates; therefore we should aim to respect its identity in attempting to develop a more sustainable material.

5.1. Optimal content and inclusion method of nano-TiO_2 in cement

Initially, we focused on the optimum weight fraction of TiO_2 nanoparticles that should be added to the cement to develop a sufficiently efficient photocatalytic activity. Many works reported in literature ensure that the minimum fraction of nanoparticles to be added to cement in order to obtain a minimum photocatalytic activity must exceed 1% by mass of cement [16]. In fact, the photocatalytic properties begin to be significant from the eco-efficient point of view when the percentage of nanoparticles included in cement is close to 3%. This percentage not only provides photocatalytic activity to the material, but also favors the development of hydration products, leading to improvements of up to 62% in mechanical properties for long ages [17].

Regarding the preparation method, the TiO_2 nanoparticles can be synthesized by chemical-physical methods, such as sol-gel, using different precursors based on titanium oxides, such as titanium tetrabutoxide and titanium tetraisopropoxide (TTIP). These methods have proven to be suitable for the formation of spherical nanoparticles with controlled particle size. In addition, the so obtained nanostructured material features high specific area, which is an essential requirement to obtain adequate rates of photocatalysis.

At the end of the synthesis procedure, the nanoparticles can be kept in liquid medium or be subjected to a calcination process in order to increase their crystallinity and achieve a particulate system. Regardless, the most appropriate way to include the nanostructured TiO_2 in the cement matrix is found to be adding it directly to the hydration water. Thus, the nanoparticles will directly occupy the capillary pores that remain as the water is consumed due to the formation of products. In addition, the aqueous environment around the nanoparticles is guaranteed.

5.2. Suitable fabrication parameters of the cementitious matrix

Another key factor when preparing photocatalytic cement with adequate structural characteristics is the correct choice of manufacturing parameters for the cement mixture. Many researchers have used white cement to prepare their photocatalytic mixtures. The choice of white cement basically supports esthetic reasons, since from its preparation, it already seems a "clean" material and therefore more conducive to integration in a pollutant-free environment. In any case, other types of cement are also valid to form the cementitious matrix in which the nanoparticles are going to be housed. The requirement is so that the matrix must be properly hydrated and provide an adequate porous structure. In this sense, the water-cement ratio plays an extremely important factor.

The water-cement ratio directly influences the permeability properties of the material. Thus, a water-cement ratio of cement paste above 0.4 likely leads to having prohibitive sedimentation and bleeding. At the same time, the "Adsorb and Shuttle" (A&S) effect explained in previous sections implies that cement particles need to be kept in suspension before setting and hardening, in order to allow the adsorbents to be located in the microstructure. On the other hand, an excessive amount of cement would give rise to a material with significant hydration defects, since the available water would be almost entirety consumed, without leaving enough water molecules in the environment of the nanoparticles, in addition to a significant amount of clinker that would remain anhydrate.

Taking into account the previous comments as well as the experimental results reported in the literature, given that the water cement ratio is directly involved in the porosity of the resulting mixture, it seems essential to estimate what percentage of porosity will be in the cementitious matrix manufactured with a reasonable water-cement ratio. In this regard, 0.5 is the ratio most widely used in literature related to the manufacture of photocatalytic cements. Such water-cement ratio produces about 32.3% porosity in the cement matrix [18], along with a specific surface area of 134 m^2/g and bulk density of 1448 kg/m^3. These microstructural values have been used to predict the photocatalytic performance of nano-TiO_2-cement composites through a Monte Carlo approach [19], resulting in an increase of the amount and distribution of adsorbents within the exposed area. This likewise explains the effect of higher reaction rate constant obtained when 0.5 water-cement composite is present as the TiO_2 substrate.

6. Conclusions

This chapter concludes that the singularities and the qualities of the hydrated cement microstructure enhance the photocatalytic processes, driven by titanium dioxide, to create environment-friendly cement. We have exposed the microstructural characteristics of cement and those aspects that make possible the promotion of photocatalytic activity. The cement porosity and the nanostructure of the C-S-H have been identified as surface modificators of nano-TiO_2 providing charge reservoir sites which promote the interfacial charge transfer mechanism. Cement microstructure can therefore effectively mediate in TiO_2 photocatalytic performance. Suggested directions have been provided for the preparation of photocatalytic mixtures, taking into account both the suitable content of nano-TiO_2 as well as the formulation of the cementitious material, according to the most recent trends reported. This framework is also a starting point for future studies that seek to improve the photocatalytic response of titanium dioxide inserted in the cement matrix as well as to provide implications for the application of photocatalytic cement technology in the construction materials industry.

Conflict of interest

The author declares that there was no conflict of interest.

Author details

Elena Cerro-Prada

Address all correspondence to: elena.cerro@upm.es

Civil Engineering Department – Construction, Infrastructure and Transportation, Technical University of Madrid (UPM), Madrid, Spain

References

[1] Sobolev K, Gutiérrez MF. How nanotechnology can change the concrete world. American Ceramic Society Bulletin. 2005;**84**(11):16-19

[2] Lee J, Mahendra S, Alvarez PJJ. Nanomaterials in the construction industry: A review of their applications and environmental health and safety considerations. ACS Nano. 2010; **4**(7):3580-3590

[3] Sanchez F, Sobolev K. Nanotechnology in concrete—A review. Construction and Building Materials. 2010;**24**(11):2060-2071

[4] Xiong G, Deng M, Xu L, Tang M. Properties of cement-based composites by doping nano-TiO_2. Kuei Suan Jen Hsueh Pao. 2006;**34**(9):1158-1161

[5] Han B, Guan X, Ou J. Specific resistance and pressure-sensitivity of cement paste admixing with nano-TiO_2 and carbon fiber. Kuei Suan Jen Hsueh Pao. 2004;**32**(7):884-887

[6] Maury-Ramirez A, Demeestere K, De Belie N. Photocatalytic activity of titanium dioxide nanoparticle coatings applied on autoclaved aerated concrete: Effect of weathering on coating physical characteristics and gaseous toluene removal. Journal of Hazardous Materials. 2012;**211-212**:218-225

[7] Tanaka K, Capule MFV, Hisanaga T. Effect of crystallinity of TiO_2 on its photocatalytic action. Chemical Physics Letters. 1991;**187**(1-2):73-76

[8] Jayapalan AR, Lee BY, Fredrich SM, Kurtis KE. Influence of additions of anatase TiO_2 nanoparticles on early-age properties of cement-based materials. Transportation Research Record. 2010;**2141**:41-46

[9] Cerro-Prada E, Manso M, Torres V, Soriano J. Microstructural and photocatalytic characterization of cement-paste sol-gel synthesized titanium dioxide. Frontiers of Structural and Civil Engineering. 2016;**10**(2):189-197

[10] Paz Y. Preferential photodegradation—Why and how? Comptes Rendus Chimie. 2006; **9**(5-6):774-787

[11] Garboczi EJ, Bentz DP. Computer simulation of the diffusivity of cement-based materials. Journal of Materials Science. 1992;**27**(8):2083-2092

[12] Pellenq RJM, Lequeux N, van Damme H. Engineering the bonding scheme in C-S-H: The iono-covalent framework. Cement and Concrete Research. 2008;**38**(2):159-174

[13] Jennings HM. Refinements to colloid model of C-S-H in cement: CM-II. Cement and Concrete Research. 2008;**38**(3):275-289

[14] Jennings HM. Model for the microstructure of calcium silicate hydrate in cement paste. Cement and Concrete Research. 2000;**30**(1):101-116

[15] Cerro-Prada E, Costa VT, Fernández PH, Ceccone G, Manso Silván M. Interface between cement paste and thin TiN film for corrosion resistance enhancement; structural, morphological and electrochemical properties. Construction and Building Materials. 2015; **80**:48-55

[16] Cárdenas C, Tobón JI, García C, Vila J. Functionalized building materials: Photocatalytic abatement of NOx by cement pastes blended with TiO_2 nanoparticles. Construction and Building Materials. 2012 Nov 30;**36**:820-825

[17] Ma B, Li H, Mei J, Li X, Chen F. Effects of nano-TiO_2 on the toughness and durability of cement-based material. Advances in Materials Science and Engineering. 2015 Jul;**30**:2015

[18] Houst YF, Wittmann FH. Influence of porosity and water content on the diffusivity of CO_2 and O_2 through hydrated cement paste. Cement and Concrete Research. 1994 Jan 1; **24**(6):1165-1176

[19] Cerro-Prada E, Escolano F, Varela F. Computational nanotechnology to predict photocatalysis of titania nanoparticles in cement-based materials. In: 2017 IEEE 17th International Conference on Nanotechnology (IEEE-NANO); Pittsburgh, PA; 2017. pp. 208-213

Chapter 5

Water Sorption of Hardened Cement Pastes

Mohammad Hajmohammadian Baghban

Additional information is available at the end of the chapter

http://dx.doi.org/10.5772/intechopen.76378

Abstract

Hardened cement paste (hcp), binding the components in cementitious composites, usually controls most strength, transport, and durability properties of these materials. Water sorption in hcps can cause durability problems such as sulfate and chloride ingress, frost deterioration, and esthetic problems. Replacement of air by water in the pores can also increase the thermal conductivity of the material and affect the energy efficiency. Capillary suction test as a simple method for characterization of the material resistance to water sorption is described in this chapter. Different factors affecting water sorption of hcps such as changing water to cement ratio (w/c), using pozzolanic materials, and internal hydrophobation are also discussed. Furthermore, resistance number, capillary number, and pore protection factor as different criterions for characterizing the moisture transport in cement-based materials are described. Since cement-based materials modified for reducing water sorption have different behavior in capillary suction test compared to ordinary materials, the abovementioned criteria may become inapplicable for characterizing these materials. Thus, "effective moisture transport (*EMT*)" factor is introduced here which can be a more comparative measure for modified cementitious materials with denser or internally hydrophobed pore structure.

Keywords: cement paste, hcp, water sorption, pozzolanic materials, capillary suction, resistance number, hydrophobic agent, silane, silica

1. Introduction

Water sorption of hardened cement pastes (hcps) is one of the key factors that can affect particular properties of cement-based materials. Chloride and sulfate ingress as well as frost deterioration and esthetic appearance are some of durability problems that are caused by water transport in these materials. Thermal properties are also affected by changes in water

sorption of cementitious composites. Reducing moisture content can, for example, lower thermal conductivity and reduce heat exchange through the materials in the building envelope.

Water is mainly transported through the capillary pores in hcps. Since increasing water to cement ratio (w/c) increases capillary porosity, the first solution to reduce water permeability is usually reducing w/c [1]. Using pozzolanic materials such as silica fume, fly ash, and slag can also result in a denser pore structure and average pore size, which results in more resistance to water sorption. The other method to modify water permeability in cement-based materials is using hydrophobic agents. Both the material surface and the internal structure can be made water-repellant by using these agents [2–5]. While UV light of the sun can affect water repellence of the surface-treated material, internal hydrophobation does not have this drawback.

In this chapter, water sorption of hcps as the important factor in permeability of cement-based materials is described. Moreover, the resistance number and the capillary number [6], which are calculated based on capillary suction test, will be described here. These numbers are used for the characterization of the material resistance to water sorption. However, this method is not suitable for modified structure of hcps that have high resistance to water sorption. Thus, an alternative parameter "effective moisture transport (*EMT*)" factor is proposed in this chapter instead of the resistance number according to the experimental results.

2. Capillary suction test

Smeplass and Skjølsvold [6] improved the test for capillary suction by including information about the pore structure of hardened concrete. Martys and Ferraris [7] have also studied capillary transport in mortars and concrete. In order to perform the capillary suction test, the specimens are usually placed in a ventilated incubator at 105°C until reaching constant weight. Lower temperatures (e.g., at 50°C in an oven or at 20°C in a desiccator) with longer drying interval may also be chosen to reduce the effect of drying on pore structure and composition of the material components. After drying, the specimens are placed on a grating 1–2 mm below the water surface. The test is usually performed in the following order:

1. drying to a constant weight,
2. capillary suction for 4–5 days,
3. submersion in water for 3–4 days at 1 atm,
4. submersion in water for 1–3 day at 50–80 atm,
5. recording the specimen volume,
6. drying the specimen at 105°C to reach a constant weight.

The duration of each step may vary depending on the water resistance of the sample as well as its height. For ordinary materials, the standard test procedure in each country may be used; however, for modified materials, it may be necessary to adjust the test parameters such as duration and water pressure.

3. Specimen preparation for capillary suction test

In case of concrete samples casted in the laboratory, 20-mm slices from cylinders cured for 28 days are usually cut for the test. To avoid material spalling from edges due to cutting, epoxy or other hard-wearing coating can be applied on the cylinders. **Figure 1** illustrates an example of sample preparation from concrete cylinders.

A similar procedure may be used for preparing hcp samples. The size of these specimens is usually smaller than concrete samples. The mixing procedure for hcps may also be different from ordinary concrete. Using a high-speed kitchen blender to facilitate proper mixing

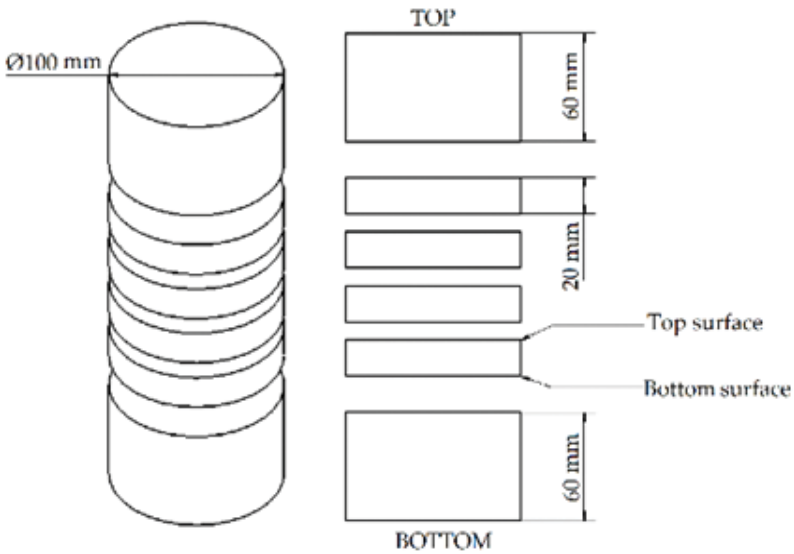

Figure 1. Cutting specimens from concrete cylinders for capillary suction test [4].

of water and cement is popular in this process. The following order may be carried out for mixing: a 1-min medium rate mixing; cleaning the mixer wall with a flexible plastic spatula; a 4-min fast rate mixing; cleaning the mixer wall with a spatula and finally a 1-min slow rate mixing. Moreover, the admixtures (such as hydrophobic agents, plasticizer air-detraining admixture) may be mixed with water for 1 min, before adding to the cement to assure proper dispersion in the cement paste. The specimens with high w/c that have risk of separation may be cured on a slow-rate rolling machine on the first day.

4. Parameters affecting water sorption of hcps

Changes in the pore structure by altering w/c or adding pozzolanic materials as well as incorporating hydrophobic agents are the main parameters affecting the water sorption of hcps. In this part, the effect of each parameter will be illustrated by presenting the results from experimental

Mix type		w/c	Alkyl alkoxysilane (% m_c)	Rapeseed oil (% m_c)	Silica fume (% m_c)	Plasticizer (% m_c)	Air-detraining admixture (g/l)
Ref		0.58	0	0	0	0.6	8
		0.44	0	0	0	0.6	8
		0.36	0	0	0	0.6	8
Si		0.58	1	0	0	0.6	8
		0.44	1	0	0	0.6	8
		0.36	1	0	0	0.6	8
Oil		0.58	0	1	0	0.6	8
		0.44	0	1	0	0.6	8
		0.36	0	1	0	0.6	8
SF	w/b = 0.48	0.58	0	0	20	0.72	8
	w/b = 0.40	0.44	0	0	10	0.66	8
	w/b = 0.37	0.44	0	0	20	0.72	8
	w/b = 0.34	0.44	0	0	30	0.78 *(SP)*	8
	w/b = 0.30	0.36	0	0	20	1.44 *(SP)*	8

Table 1. Mix proportions for reference (Ref) samples and the sample containing rapeseed oil (Oil), alkyl alkoxysilane (Si), and silica fume (SF).

investigations [5, 8]. **Table 1** presents mix proportions for four mix series of hcps. The effect of changes in w/c is investigated by considering three different ratios of 0.58, 0.44, and 0.36 in each series.

Portland cement (CEM I 45.5 R) with a specific area of 550 (m^2/kg) and a specific density of 3120 (kg/m^3) were used. The series include reference (Ref) which is plain hcp, two series containing hydrophobic agents, and one series containing silica fume (SF) as pozzolanic material.

One percent of cement mass (mc) of a silane-based product (100% alkyl alkoxysilane) which has a small molecular size of 5–10 Å was used in the "Si" series. This material is developed for surface hydrophobation but it was used here as an admixture to study its effect for internal hydrophobation. In addition, food quality rapeseed oil with 8% saturated, 62% monounsaturated, and 30% polyunsaturated fatty acids was used as the other hydrophobic admixture in the "Oil" series with a dosage of 1% mc. The oil was selected as an environmental friendly substitute for existing chemical hydrophobic agents [9, 10]. Today, there are different hydrophobic agents in the market as concrete admixture where the producer claims effective hydrophobicity and no negative effect on mechanical properties; the selected hydrophobic agents here are to show how these agents may affect the water sorption of hcps.

The "SF" series contain densified silica fume with a specific density of 2200 (kg/m^3) and a dosage of 20% mc. This high dosage was considered to see the effect of finer pore structure in water suction of hcps.

In order to reduce undesirable macro-air pores, an air-detraining admixture based on modified polysiloxanes with 0.5% dry matter was used in all of the mixes. In addition, a plasticizer based on ligno-sulfonates with 40% dry matter and a super plasticizer (SP) based on modified acrylic polymers with 30% dry matter were used in the cement paste mixes. The composition of the mixes is listed in **Table 1**. The water to binder ratio (w/b) is also given for the SF series in this table since pozzolanic materials work as a part of binder in cementitious composites.

The samples were cured in water for 12 weeks, and then dried in ventilated oven for 2 weeks at 50°C. Parameters obtained from capillary suction test are given in **Table 2**. Capillary suction porosity (ε_{csuc}), capillary submersion porosity (ε_{csub}), and pressure saturated porosity (ε_{ps}) are calculated from the mass gain after capillary suction, submersion in water at 1 (atm) and submersion in water at 50 (atm), respectively. Furthermore, **Figures 2–4** show the pore distribution of different mixes with the same w/c. Note that this test is not an accurate test for porosimetry and is intended for characterizing material behavior under water sorption. The results show that the total capillary porosities ($\varepsilon_{csuc} + \varepsilon_{csub}$) are decreased for the Oil samples due to reduction in water absorption by using hydrophobic agents. Unlike impregnating agent emulsion that was used by Haugan [4], alkyl alkoxysilane had a minor effect on internal hydrophobic treatment for all the three selected mixes with different w/c, showing that not all the hydrophobic agents developed for surface treatment are also effective in reducing water sorption when used as admixture.

Furthermore, using silica fume has decreased ε_{csuc} and increased ε_{csub} and it is more obvious in lower w/c. In fact, there is a minor reduction in the total capillary porosity of SF samples, but the reason and amount of this reduction is different from the Oil samples. Moreover, considering Ref and SF samples with w/b in the same range, we can see that although the total porosity has slightly increased for SF samples, ε_{csuc} has decreased, indicating more resistance to water transport in SF samples due to reduction in pore size and connectivity between the pores.

The oil shows the best effect on reducing absorption, with a large amount of pore space that can only be accessed by high water pressure. The performance of oil is probably due to some water repellency effect, whereas the performance of silica fume is due to a reduction in pore size and connectivity between the pores. In fact, changes in the pore structure by altering w/c have only changed the total porosity of the material and did not have a significant effect on reducing the capillary suction of hcps. Adding silica fume had a minor effect on reducing the total capillary water absorption ($\varepsilon_{csuc} + \varepsilon_{csub}$) but decreased the capillary suction by creating a denser pore structure. However, using a low amount of proper hydrophobic agent as admixture can reduce the water sorption of hcps significantly.

In addition to the results shown in **Table 2**, the degree of hydration was calculated from w/c and ε_{tot} shown in this table to calculate the dry sample density (ρ_d) according to Power's model [11] which agreed very well with measured ρ_d (mainly less than 2% difference). Thus, these hcps behave as they should in terms of Powers model.

"Pore protection factor" (PF) is a criterion for assessing frost resistance of concrete in Finnish Standard SFS 4475 [12]. It is defined as the air content as a percentage of the total porosity ($PF = \varepsilon_{air}/\varepsilon_{tot}$). It is worth noting that ε_{ps} is usually considered as ε_{air} for normal concrete, but the abovementioned hcps contain a low amount of air pores as judged from **Table 2** for the

Mix type		w/c	ε_{csuc} (vol%)	ε_{csub} (vol%)	ε_{ps} (vol%)	ε_{tot} (vol%)	ρ_s (kg/m^3)	ρ_d (kg/m^3)
Ref		0.58	49.2 ± 0.5	1.1 ± 0.6	0.4 ± 0.1	50.7 ± 0.2	2696 ± 2	1329 ± 4
		0.44	42.3 ± 0.1	0.4 ± 0.0	0.4 ± 0.0	43.1 ± 0.1	2712 ± 3	1543 ± 3
		0.36	35.8 ± 1.4	1.5 ± 1.4	0.6 ± 0.1	38.0 ± 1.4	2737 ± 10	1698 ± 6
Silane		0.58	46.6 ± 0.7	2.7 ± 0.5	1.7 ± 0.3	51.1 ± 0.1	2686 ± 2	1315 ± 3
		0.44	39.9 ± 0.4	1.7 ± 0.6	1.3 ± 0.5	43.0 ± 0.3	2675 ± 7	1526 ± 14
		0.36	33.4 ± 3.3	4.0 ± 3.2	1.0 ± 0.1	38.4 ± 0.1	2724 ± 3	1677 ± 2
Oil		0.58	29.8 ± 1.9	12.0 ± 1.4	7.4 ± 0.8	49.2 ± 0.1	2631 ± 5	1335 ± 2
		0.44	22.7 ± 1.8	6.5 ± 1.5	12.2 ± 1.0	41.1 ± 0.4	2642 ± 6	1548 ± 14
		0.36	19.6 ± 0.6	3.8 ± 1.6	13.3 ± 1.1	36.7 ± 0.1	2679 ± 2	1695 ± 4
Silica fume	w/b = 0.48	0.58	43.1 ± 0.8	2.3 ± 0.9	2.0 ± 0.3	47.4 ± 0.1	2687 ± 2	1413 ± 2
	w/b = 0.40	0.44	37.4 ± 0.5	1.9 ± 0.2	2.2 ± 0.4	41.5 ± 0.1	2704 ± 11	1582 ± 10
	w/b = 0.37	0.44	33.1 ± 2.4	4.8 ± 2.2	2.9 ± 0.1	40.8 ± 0.1	2716 ± 6	1607 ± 1
	w/b = 0.34	0.44	26.0 ± 2.0	10.7 ± 1.7	2.8 ± 0.5	39.5 ± 0.2	2699 ± 4	1632 ± 4
	w/b = 0.30	0.36	25.2 ± 0.8	7.9 ± 0.7	2.5 ± 0.3	35.6 ± 1.2	2719 ± 31	1751 ± 12

Table 2. Capillary suction porosity (ε_{csuc}), capillary submersion porosity (ε_{csub}), pressure saturated porosity (ε_{ps}), total porosity (ε_{tot}), average density of solids (ρ_s), and dry sample density (ρ_d), derived from capillary suction test.

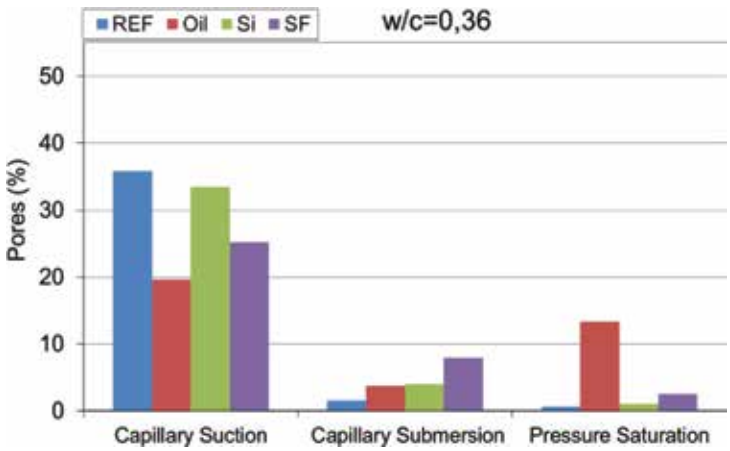

Figure 2. Pore distribution of different mixes with the w/c of 0.36 for reference (Ref) sample and the samples containing 1% rapeseed oil (Oil), 1% alkyl alkoxysilane (Si), and 20% silica fume (SF).

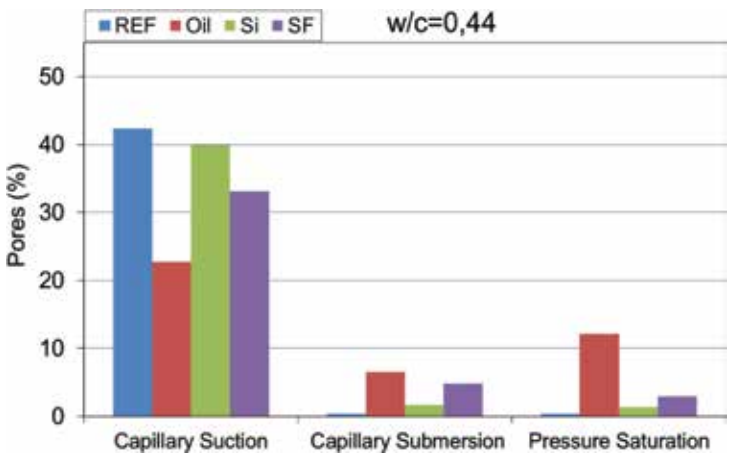

Figure 3. Pore distribution of different mixes with the w/c of 0.44 for reference (Ref) sample and the samples containing 1% rapeseed oil (Oil), 1% alkyl alkoxysilane (Si), and 20% silica fume (SF).

reference materials. On the other hand, in case of internal hydrophobation of these samples, a considerable amount of the capillary pores are not filled after 3 days of submersion in water at 1 atm but they fill at 50 atm. The apparent air voids may thus be a part of ε_{ps}. **Figure 5** shows PF values for different mixes by considering ε_{ps} as ε_{air}. According to this figure, it is concluded that although silica fume gives a denser pore structure, it has a minor effect on blocking the pores from the suction of water at atmospheric pressure. On the contrary, oil has been effective in increasing the PF value, indicating water repellency effect in the pores. This effect has been increased by a reduction in w/c where the overall pore size becomes smaller.

Eq. (1), La Places or Washburn's equation, shows the pressure that forces water with surface tension between air and water (σ) into a pore of radius (r). Since the contact angle for the

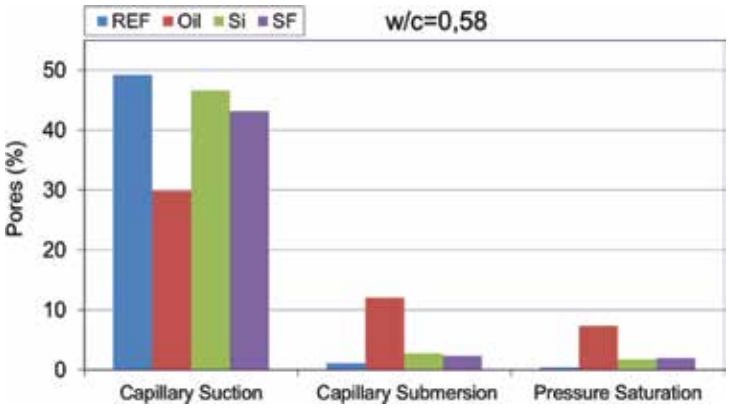

Figure 4. Pore distribution of different mixes with the w/c of 0.58 for reference (Ref) samples and the samples containing 1% rapeseed oil (Oil), 1% alkyl alkoxysilane (Si), and 20% silica fume (SF).

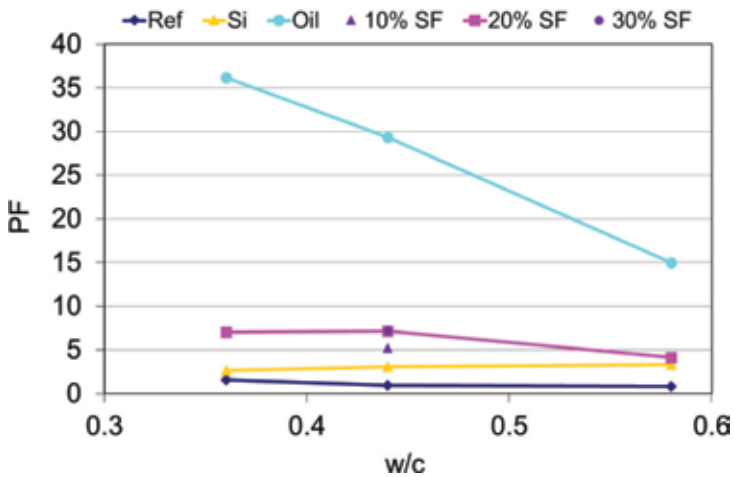

Figure 5. Pore protection factor (PF) for reference (Ref) sample and the samples containing rapeseed oil (Oil), alkyl alkoxysilane (Si), and silica fume (SF).

hydrophobed surface is more than 90°, the pressure sign will be positive, thus the smaller the pore radius, the larger the repellency effect if these small pores are hydrophobed. The pore structure of hcp is more complicated than a capillary tube with connections between the pores. In addition, the hydrophobic agents may not cover all the pore surface areas. One may generally assume that the pore structure of hcps with lower w/c is finer than the higher w/c, simply by comparing the volumetric fraction of gel pores. Consequently, it is expected that water-repellant admixtures will be more effective in lower w/c if these smaller pores are the main part of the pore system that is impregnated. This effect is observed in the current example as an increase in ε_{ps} by using hydrophobic agents (**Figure 6**).

$$P = \frac{(-2\sigma \cos\theta)}{r} \tag{1}$$

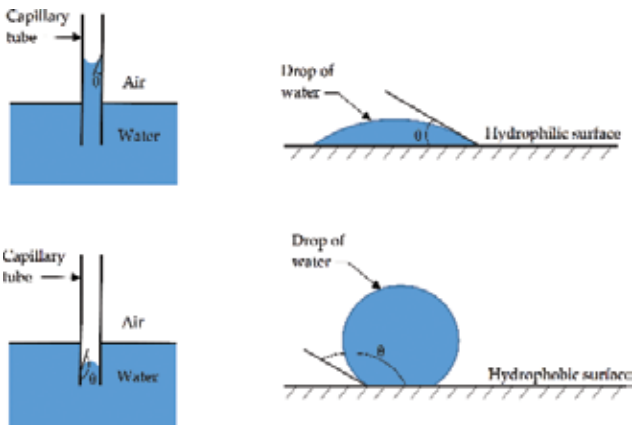

Figure 6. Hydrophobic and non-hydrophobic surfaces [13].

Note that the behavior of hcps to water sorption may have some differences with concrete specimens. Hardened cement paste gets some micro-cracks during drying period. Visual observations of micro-cracks on these pastes indicate that they cause faster water suction when placed on the water surface. These micro-cracks will, however, close after water absorption and are not expected to highly change the total porosity, but they may open some of the pores that were not accessible to capillary water and reduce pressure-saturated porosity. Since the effect of cracking can be more in higher w/c due to a higher amount of capillary water, the PF value may be less for higher w/c compared to lower w/c for Oil samples. On the other hand, the interfacial transition zone (ITZ) between the cement paste and aggregates in concrete that is the weak part of the concrete matrix can be the reason for different behavior of hydrophobic agents in hcp and concrete.

In addition, pore blocking by oil droplets and denser pore structure are the other possible reasons that have been mentioned by [3] for less PF values in some concrete samples. The effect of denser pore structure can be seen in **Figure 5** by comparing the PF value for Ref samples with w/c = 0.36 and SF samples with w/c = 0.44 which have a w/b of 0.37. The PF values for SF samples are higher than Ref samples due to denser and more discontinuous pore structure, but this effect is not comparable to the water repellency effect of rapeseed oil.

5. Effective moisture transport factor

In order to measure the resistance to capillary suction, Smeplass and Skjølsvold [6] have suggested calculating the time, t_{cap}, and the corresponding absorption value, Q_{cap}, that the water front reaches the top surface of the specimen with the height "h" (see **Figure 7**). The mass storage is usually registered in the following order during capillary suction test:

- 10 and 30 min,
- 1, 2, 3, 4, and 6 h,
- 1, 2, 3, 4 and alternatively 5 days.

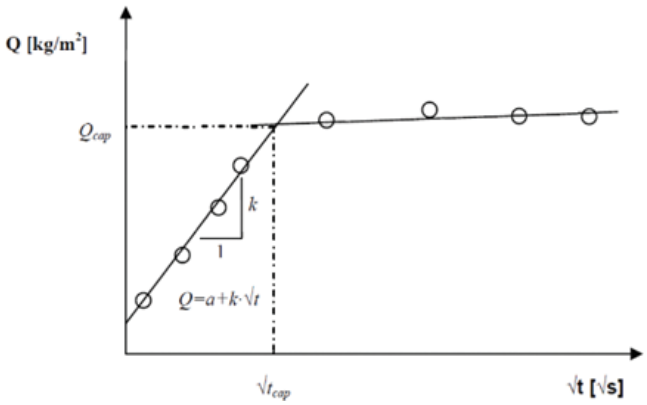

Figure 7. Regression analysis for calculating the resistance number (m) and the capillary number (k).

A regression analysis is then carried out based on the data points from 10 min to 6 h for the first/left linear part, and the rest of the points (from 1 to 4 days or alternatively 5 days) for the second/right linear part. Then, the resistance number, m, and the capillary number, k, will be calculated using the following equations:

$$m = \frac{t_{cap}}{h^2} \tag{2}$$

$$k = \frac{Q_{cap}}{\sqrt{t_{cap}}} \tag{3}$$

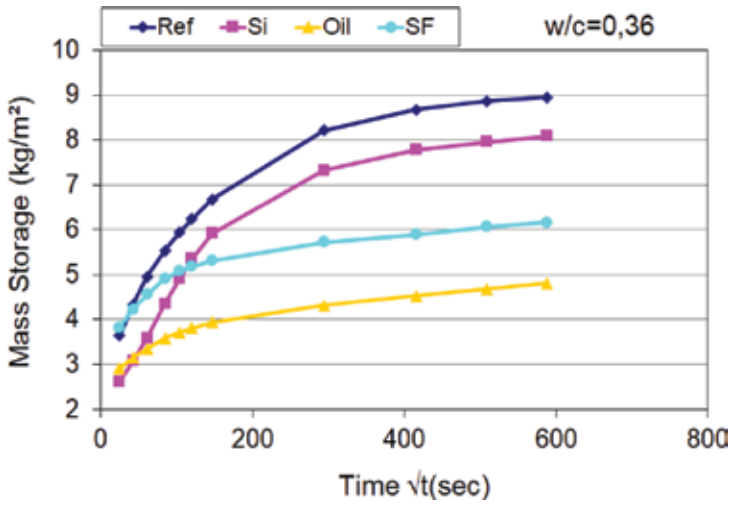

Figure 8. Water absorption versus the square root of time of different mixes with the w/c ratio of 0.36 for reference (Ref) samples and the sample containing 1% rapeseed oil (Oil), 1% alkyl alkoxysilane (Si), and 20% silica fume (SF) (w/b = 0.30).

The resistance number and the capillary number reflect the fineness of the pore system. In cementitious composites, the capillary number indicates the amount of the binder in the material by neglecting water sorption of the other composite components. However, these values cannot be properly calculated to give a good reflection of the material behavior under capillary suction in the current SF and Oil samples. The reason is high resistance of these specimens to water suction which does not give a clear nick point for calculating t_{cap} and Q_{cap}. Thus, another method for characterization of these samples is desired which can give a proper comparison between ordinary materials and the modified ones. *EMT* factor will be defined in this part for this purpose.

Figure 8 presents the water absorption versus the square root of time for specimens with w/c = 0.36. As seen in the figure, although silica fume does not have a high effect on PF, it reduces capillary suction compared to reference and silane samples. The reason can be described as the finer pore structure as well as less connection between the pores (less percolated), but since it does not repel water or block the pores, the pores will more easily be filled with water than hydrophobized samples in case of submersion. Moreover, the Ref samples have a higher absorption than the other samples since they have less resistance to water transport in the pores. On the other hand, although the rate of mass transport (the slope of the lines in **Figure 8**) in SF and Oil samples is similar in this case, but the absorption in SF samples is larger than Oil samples. This is probably due to the initial moisture content of SF samples. In other words, SF and Oil samples have shown similar resistance to water suction according to **Figure 8**, but since the SF samples had a higher moisture content after drying at 50°C, the moisture content is higher for SF samples after the water suction test. Since the samples have been dried in the oven for 2 weeks at 50°C, it can be judged that the moisture content after this drying period is not very active in water transport during capillary suction test. Therefore, by considering the initial moisture as mass content with low mobility, we can define the mobile capillary suction porosity (ε_{mcsuc}) as the weight gain after capillary suction excluding initial moisture (**Table 2**). This can be a more realistic estimation of the part of the pore structure which is involved in capillary suction compared to the value obtained after severe drying at 105°C which highly affects the pore structure of the material as well.

The slope of the line obtained from the first 6 h of suction curve, K'', can be an indication of the rate of mass transport in the material. Furthermore, the final mass storage after water suction test could be different for the samples with the same K'' due to different gradients in the curves after the first 6 h. In other words, ε_{mcsuc} can be different for the samples with the same K'' due to different pore structure or pore chemistry. Thus, both ε_{mcsuc} and K'' are indications of moisture transport in the material in the abovementioned capillary test. A general experience with capillary suction testing of cement-based materials is that the capillary nick points become less clear at reducing w/b, when adding pozzolana, increasing the initial moisture content and in hydrophobed samples. In such cases, the resistance number and the capillary number are not useful, and therefore a different parameter is proposed here: "effective moisture transport (*EMT*)" factor. *EMT* can be defined as a criterion for the effective mass transport in the material where we have problems of defining a nick point:

$$EMT = \sqrt{\varepsilon_{mcsuc} \times K''} \tag{4}$$

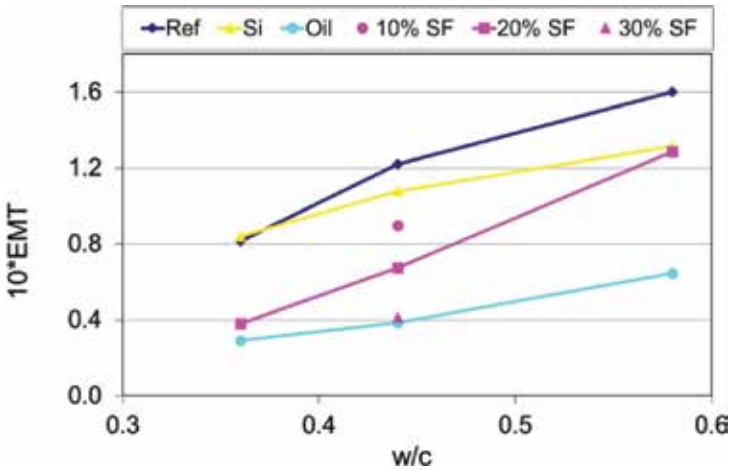

Figure 9. Effective moisture transport factor (*EMT*) for reference (Ref) samples and the sample containing 1% rapeseed oil (Oil), 1% alkyl alkoxysilane (Si), and silica fume (SF).

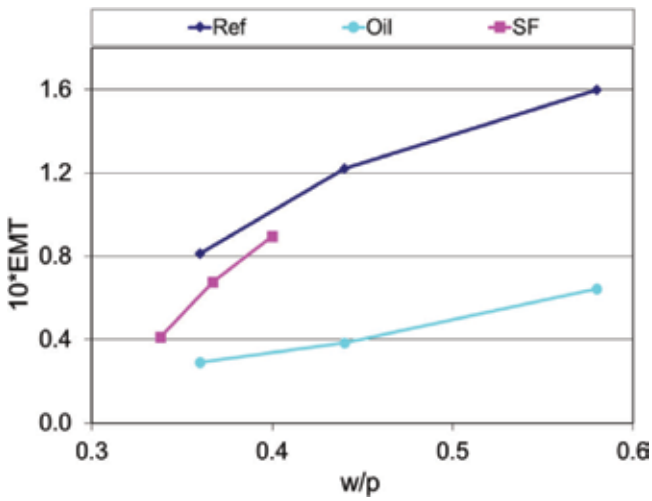

Figure 10. Effective moisture transport factor (*EMT*) for reference (Ref) samples and the sample containing 1% rapeseed oil (Oil) and 10, 20, and 30% silica fume(SF) as a function of water to binder (w/b) ratio.

where ε_{mcsuc} is the mobile capillary suction porosity and K'' is the slope of the line obtained from the first 6 h of suction curve. Both ε_{mcsuc} and K'' depend on the fineness, connectivity, chemistry, and volume of the mobile capillary suction pores in the material but from different perspectives; thus, a square root of multiplication of these two values can be a criterion for effective mass transport in the material.

Figure 9 shows *EMT* for different w/c ratios of the mixes. The effect of fine pore structure is shown for both adding the same amount of silica fume to different w/c ratios and increasing the dosage of silica fume for a constant w/c ratio. All correlation coefficients from the regression

analysis of the slopes were more than 0.93. Since the slopes of the lines for both SF and Oil have been similar during the first 6 h and the rest of the capillary suction test (**Figure 8**), a similar *EMT* value has been obtained for these samples. Furthermore, the difference between the resistance of SF to water suction compared to Si and Ref samples is clearer in **Figure 9**. Moreover, the figure shows that using 1% rapeseed oil has a reduced *EMT* of the hcp with w/c = 0.58 to a level even lower than the reference material with w/c = 0.36. Using 30% SF was as effective as using 1% rapeseed oil in samples with w/c = 0.44. It is worth noting that adding silica fume is more effective in resistance to mass transport than reducing w/c ratio. This is shown in **Figure 10** in which the effect of adding 10, 20, and 30% silica fume in reducing *EMT* is compared to the Ref and Oil samples as a function of water to binder ratio (w/b). However, 1% oil is found to be more effective than using SF.

6. Conclusions

Factors affecting the water sorption of hcps such as w/c, pozzolanic materials, and internal hydrophobation were described in this chapter. The hcps with lower w/c have a less total porosity which results in a less water sorption. The amount of pores filled with water under capillary suction (ε_{csuc}) was near to total porosity (ε_{tot}) for plain hcps (Ref samples). In addition, silica fume as pozzolanic material increases resistance to water transport in hcps due to a reduction in the pore size and the connectivity between the pores, but it is not effective in reducing the total water suction of hcps.

A minor effect on water sorption was observed using alkyl alkoxysilane showing that this agent which is developed for surface treatment is not suitable for internal hydrophobation. However, rapeseed oil as a hydrophobic agent resulted in an obvious reduction in the water suction of hcps. Pore blocking by oil droplets and denser pore structure can be the other possible reasons for less PF values in some samples. However, the effect of a denser pore structure is not comparable to the water repellency effect of the oil. The behavior of hcps under water suction can be different from cement-based composites due to the effect of ITZ in the composite materials and the formation of micro-cracks in hcps during drying.

Due to the lack of clear capillary nick points, for the determination of resistance number and capillary number, an alternative parameter "effective moisture transport (*EMT*)" factor was proposed instead in this chapter. The *EMT* factor can be a more comparative measure for denser or hydrophobed samples, especially when the samples are dried at lower temperatures to reduce the effect of drying on pore structure and composition of the material components.

Acknowledgements

The author gratefully appreciates the Norwegian University of Science and Technology (NTNU) for project funding, professor emeritus Per Jostein Hovde, professor Stefan Jacobsen, and adjunct professor Roar Myrdal at NTNU for their advices as well as the help given by engineer Ove Edvard Loraas in the NTNU laboratory.

Author details

Mohammad Hajmohammadian Baghban

Address all correspondence to: mohammad.baghban@ntnu.no

Department of Manufacturing and Civil Engineering, Norwegian University of Science and Technology (NTNU), Gjøvik, Norway

References

[1] NS-EN 206-1. Concrete. Part 1: Specification, Performance, Production and Conformity (Amendment prA1:2003 Incorporated). Oslo: Norwegian Standardization Board; 2001

[2] Årskog V, Guofei L, Ferreira M, Gjørv O. Effect of surface hydrophobation on chloride ingress into concrete harbour structures. In: 4th International Conference on Concrete under Severe Conditions (CONSEC'04); Seoul, Korea; 27 June 1; 2004

[3] Justnes H. Low Water Permeability through Hydrophobicity, SINTEF Building and Infrastructure, COIN Project Report 1. Oslo; 2008

[4] Haugan L. Internal hydrophobation of concrete—Short and long term effects, SINTEF Building and Infrastructure, Project No. 3D006051. Trondheim; 2010

[5] Hajmohammadian Baghban M, Hovde PJ, Jacobsen S. Effect of internal hydrophobation, silica fume and w/c on water sorption of hardened cement pastes. In: International Conference on Durability of Building Materials and Components (XII DBMC); Porto, Portugal; April 2011:**2011**;12-15

[6] Smeplass S, Skjølsvold O. Concrete Testing. Capillary Suction and Porosity, SINTEF Internal Procedure KS 70 110 (in Norwegian). Trondheim; 1996

[7] Martys NS, Ferraris CF. Capillary transport in mortars and concrete. Cement and Concrete Research. 1997;**27**(5):747-760

[8] Hajmohammadian Baghban M, Hovde PJ, Jacobsen S. An experimental investigation on factors affecting water sorption of hardened cement pastes. In: 5th International Building Physics Conference (IBPC); Kyoto, Japan; May 28-31; 2012

[9] Justnes H, Østnor TA, Barnils Vila N. Vegetable oils as water repellents for mortars. In: Proc. 1st International Conference of Asian Concrete Federation; Chiang Mai, Thailand; 28-29 October 2004. Vol. 2. pp. 689-698

[10] Chandra S, Xu A. Influence of vegetable oils addition on portland cement mortars. In: Proc. 7th International Congress on Polymers in Concrete (ICPIC); Oostende, Belgium; 3-5 July 1995. pp. 187-192

[11] Sellevold EJ, Farstad T. The PF-method—A simple way to estimate the w/c-ratio and air content of hardened concrete. In: Proceedings of Con. Mat'05 and Mindess Symposium; UBC, Vancouver; 2005

[12] SFS 4475. Concrete. Frost Resistance. Protective Pore Ratio; Finland; Soumen Standardoimisliitto SFS; 1988

[13] Bertolini L, Elsener B, Pedeferri P, Polder RB. Corrosion of Steel in Concrete. Prevention, Diagnosis, Repair. Weinheim, Germany: Wiley-VCH; 2004

Chapter 6

Morphogenesis of Cement Hydrate: From Natural C-S-H to Synthetic C-S-H

Rouzbeh Shahsavari and Sung Hoon Hwang

Additional information is available at the end of the chapter

http://dx.doi.org/10.5772/intechopen.77723

Abstract

Triggered by the recent advance in materials synthesis and characterization techniques, there has been an increasing interest in manipulating properties of calcium silicate hydrates (C-S-H), which constitute the fundamental, strength-responsible building blocks of concretes. Concretes are the indispensable constituents of today's modern infrastructures and simultaneously the most widely used synthetic material on the planet. Despite the widespread impact and high societal values, the production of their major binder component, Portland cement (PC), is the major culprit for global warming since it contributes to 5–10% carbon dioxide emission worldwide. Consequently, enhancing the ultimate strength and durability of concretes by tuning structural, compositional and mechanical properties of their basic building units and assembling them via bottom-up engineering is one of the key strategies to mitigate the aforesaid concerns. This is simply because the longer the concretes last, the less production of PC would incur. Furthermore, the current role of C-S-H in industry is not only confined to the context of construction materials but to diverse sectors of industry including drug delivery, CO_2 sorbent and materials for bone replacement. This wide scope of potential applications can be ascribed to the high versatility regarding tunable structural properties such as porosity, size and morphology, all of which can be fine-tuned during the synthetic procedure. Among the listed properties, understanding and gaining control over morphological factors of C-S-H is particularly important since they are directly associated with their functional roles. C-S-H with various morphologies can be produced by altering key experimental conditions, which encompass types of synthetic procedure, precursor types such as different calcium and silicate sources and types of additives. This chapter discusses a variety of morphologies of C-S-H acquired in multiple environments. The latter include the hydration of PC or PC-blends containing supplementary materials such as slag, synthetic C-S-H produced using silica-lime reactions and crystalline CSH synthesized using hydrothermal treatment. At the end, the chapter will provide a complete review on the current range of morphologies for calcium silicate hydrate.

Keywords: cement hydrate, shape-controlled synthesis, cubic cement, calcium silicate hydrate

1. Morphology of C-S-H observed during the hydration of PC or PC-based blend

Before reviewing the morphology of naturally formed, semicrystalline C-S-H acquired during the hydration of PC, it is necessary to review its nucleation and growth mechanism during the hydration process. Despite the decadelong efforts, the complete picture for the mechanism of C-S-H formation during the hydration of cement is yet to be acquired, and several nucleation, growth and structural models have been proposed [1, 2]. The consensus is that the initial stage is comprised of dissolution of cement phases such as tricalcium silicate (C_3S) and dicalcium silicate (C_2S), releasing calcium, hydroxide, and silicate ions [3, 4]. Jennings et al. studied morphological development of hydrating C_3S, one of the major phases of cement, using the combination of multiple electron microscopic techniques, transmission electron microscopy (TEM), scanning transmission electron microscopy (STEM), and scanning electron microscopy (SEM) [5]. The authors herein found that the morphology of C-S-H formed during the hydration of C_3S varies between the early, middle and the late stages of the cement hydration. At the early stages of the hydration, fibrous products were observed on the surface of the grains. During the middle stages, where the rapid exothermic reaction takes place, a mixture of different morphologies was observed. The complete layer of amorphous gel product along the boundaries of the C_3S particle was found while needles with the lengths of 0.75–1.0 μm radiating from the grain and tapered fibers with the length of 0.25–0.5 μm were also observed. In the late stages, the authors found that crumpled foils and dense inner products dominate.

The amorphous, gel-like layer found on the grain at the middle stage of C_3S in Jenning's study above support that the initial reaction products form via heterogenous nucleation and grow outward into water-filled pore solutions. Herein, the rates of nucleation and growth of C-S-H are heavily influenced by the degree of supersaturation of the constituent ions encompassing calcium and silicate ions [4]. It was later found via multiple studies that natural C-S-H found during the PC hydration can be divided into two types showing distinct morphologies. C-S-H gel that occupies the boundary region of the anhydrous cement grain is called an "inner product" and that forms in the originally water-filled pore spaces is called an "outer product." Those two types form at different stages of hydration and exhibit distinct morphologies [6, 7]. Richardson et al. found via TEM analysis that the outer product C-S-H has a fibrillar morphology and that the aspect ratio of the corresponding fibrils depends on the amount of available space in pore spaces [8, 9]. Coarse fibrils with the high aspect ratio were present in larger pore spaces and vice versa. On the other hand, the inner product exhibited a dense, homogeneous morphology with the significantly decreased porosity compared to the outer product (**Figure 1**). Furthermore, within each of the inner and outer type of C-S-H, the size of the anhydrous cement grain also affected the final morphological features [8]. The inner product formed within the smaller cement grains, with each grain being less than around 5 μm, exhibited less density and higher porosity compared to that

http://dx.doi.org/10.5772/intechopen.77723

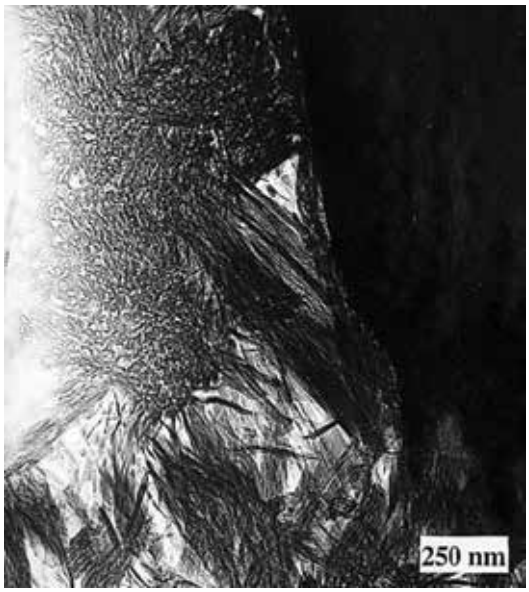

Figure 1. TEM image showing fine, dense morphology of the inner C-S-H and less dense, fibrillary morphology of the outer C-S-H formed during the hydration of C_3S [9].

formed within the larger grains. Richardson et al. further divided the outer product into two morphologically distinct types exhibiting different Ca/Si ratios. The higher Ca/Si ratio corresponded to the fibrillar, directional morphology, while the lower Ca/Si ratio corresponded to the foil-like morphology.

Taylor et al. also found that the age of the sample also significantly affects the morphology of C-S-H found in PC and PC-slag blends [10]. The authors compared the morphology of C-S-H existing in 20-year-old neat PC and PC-slag blend samples with those found in similar samples, which are only 14 months old [10]. The authors found that the outer product found in the 20-year-old neat PC sample is finer, showing little variation in morphology between the inner and the outer product in contrast to the samples, which are 14 months old. Furthermore, the morphology of the outer product C-S-H was different for the PC-slag samples containing different amounts of slag. As the amount of slag was increased from 0 to 90%, the fibrillar morphology was gradually transformed to foil-like morphology and only the crumpled foil was observed for the slag-only paste at the end.

Alkali-silica reaction, which is the common reaction between reactive silica species and alkalis found in cementitious materials, also produces C-S-H with the unique "sheaf of wheat" morphology [11]. Zampini et al. studied the evolution of the wet cement paste-aggregate interface from 5 minutes to 10 days using environmental scanning electron microscopy (ESEM) and found that the C-S-H with a "sheaf of wheat" morphology was formed from the alkali-silica reaction [12]. The authors concluded that formation of this specific morphology is favored at water-to-cement ratio of 0.5, and also facilitated by the inclusion of silica fume. This in turn implies that the presence of silicate ions in a supersaturated solution of hydrated lime is critical in inducing the aforesaid "sheaf of wheat" morphology.

2. Morphology of synthetic C-S-H

Synthetic C-S-H exhibits varying morphologies depending on types of synthesis techniques and experimental factors encompassing the initial Ca/Si ratio and the types of precursors [13, 14]. Common reaction pathways encompass silica-lime reactions, where lime or hydrated lime is reacted with pozzolans such as silica fume and double decomposition technique, where both calcium nitrate and sodium silicate become decomposed into their constituent ions, the ionic building blocks for C-S-H [14–16].

Silica-lime reaction can be performed via either mechanochemical synthesis, where the mixture of silica and lime are reacted in solid state under the assistance of mechanical milling, or solution-based synthesis, where the precursors are reacted in the form of solutions [17–19]. Rodriguez et al. performed the mechanochemical synthesis using lime and fumed silica at different starting Ca/Si ratios, and also carried out the solution-based synthesis using preprepared slurries containing lime and fused silica separately [19]. The authors found that both mechanochemical and solution-based synthesis lead to the formation of foil-like C-S-H regardless of the initial Ca/Si ratio. In contrast, when the authors performed the controlled hydration of pure C_3S at a constant lime concentration, the initial Ca/Si ratio exerted a greater effect on the final morphology. As the Ca/Si ratio was increased from the value below 1.58 to the value above 1.58, the morphology transformed from a foil-like morphology to fiber-like status.

Kurtis et al. synthesized C-S-H via the alkali-silica reaction, where silica sources in the form of the alkali-silicate gel acquired from dam, silica fume and silica gel were reacted with saturated solution of calcium hydroxide. In case of the silica gel, another reaction was performed where it was also exposed to a separate solution of sodium hydroxide and calcium chloride [20]. The authors studied each reaction using high-resolution transmission soft X-ray microscopy and observed

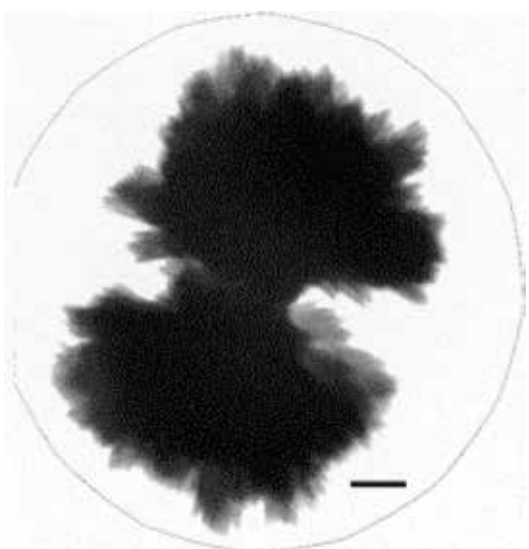

Figure 2. X-ray image showing the "sheaf-of-wheat" morphology for C-S-H acquired from the alkali-silica reaction. Scale bar is 1 μm [36].

the "sheaf of wheat" morphology for the reaction between the alkali-silicate gel and supersaturated solution of calcium hydroxide (**Figure 2**). This implies that the unique "sheaf of wheat" morphology can be materialized by mimicking the natural alkali-silica reaction described above.

3. Formation of crystalline CSH

Hydrothermal synthesis is a common technique used to grow crystalline calcium silicate hydrate phase such as tobermorite $Ca_5Si_6O_{16}(OH)_2 \cdot 4H_2O$, jennite $Ca_9Si_6O_{18}(OH)_6 \cdot 8H_2O$ and xonotlite $Ca_6Si_6O_{17}(OH)_2$, the mineral analogues of amorphous C-S-H from cement hydration. Hara et al. synthesized lath-shaped crystals of jennite, with the width of around 1 μm elongated along b-axis based on hydrothermal reactions of fumed silica and lime at 80°C [13].

During the hydrothermal treatment, addition of metal ions such as sodium and aluminum ions, which are commonly present in supplementary cementitious materials including slag and fly ash, also influences the final type and morphology of crystalline calcium silicate hydrate [21]. Nocuń-Wczelik et al. performed the hydrothermal synthesis using the mixture of metal hydroxide, various powder forms of silica and hydrated lime at the temperature range of 160–240°C. It was shown that sodium and silica content exceeding 20 and 50 wt%, respectively, favor the formation of pectrolyte, the sodium-bearing crystalline product, with broom-like morphology. The addition of aluminum ions to the initial mixture comprising calcium hydroxide, silica and sodium hydroxide facilitated the transformation of amorphous C-S-H to crystalline tobermorite, accompanying the morphological change from the interlocked fibers to plate-like morphology. Furthermore, needle-like xonotlite crystals were formed when the initial Ca/Si ratio was set close to 1 during the hydrothermal synthesis.

Tobermorite, the most commonly referred material for the crystalline analogue of amorphous C-S-H, typically has a basal spacing of 1.1 and 1.4 nm. It can be readily synthesized via the hydrothermal treatment of the ternary $CaO\text{-}SiO_2\text{-}H_2O$ system. 1.1 nm tobermorite is also often observed in hydrothermally cured concretes (tobermorite synthesis under hydrothermal conditions) [22]. Bell et al. performed the hydrothermal treatment of the mixture containing lime and high-purity quartz at the Ca/Si ratio of 0.83 and the pH of 12.6 at 150°C [22]. The reaction led to the formation of two distinct morphologies for tobermorite, platelets and fibers, with the former possibly induced by the heterogenous nucleation and the latter stemming from the homogenous nucleation.

Galvánková et al. studied the effect of different experimental conditions on the formation of tobermorite [23]. Hydrothermal synthesis was performed using the mixture of silica source and grounded limestone, which had been preheated, at the temperature range between 170 and 190°C. Acicular crystals of tobermorite were observed when silica sand was used as the precursor and the reaction temperature beyond 180°C favored the conversion of tobermorite to xonolite.

Hartmann et al. also investigated the effect of the additive Ca-formate on the morphology of crystalline CSH during the hydrothermal reactions [24]. The authors hydrothermally treated the mixture of quartz, lime and calcium formate at 200°C for 40.5 hours and investigated the effect of varying amounts of calcium formate on final morphology of the resultant CSH. The calcium-bearing additive, even with the lowest amount added, induced the morphological

change of tobermorite crystals from typical acicular shape to bent needle-like morphology. This morphological change is likely to have arisen from the adsorption of formate ions on growing (001) faces during the synthesis, thereby impeding the normal growth process of tobermorite. This switches the major growth direction from [001] axis to [010] axis, leading to the observed morphological change.

4. Synthesis of cubic C-S-H and morphology-induced improvement in mechanical properties

The aforesaid control over the morphology of calcium silicate hydrate is somewhat limited to crystalline CSH grown in hydrothermal conditions or amorphous C-S-H with the restricted scope of final shapes encompassing fibrils, plates and foil. Therefore, the extensive control over a wide range of morphologies for gel-like C-S-H had not been accomplished and the range of experimental techniques somewhat lacked diversity. Considering that the surfactant-assisted, template-based synthesis had been widely applied to generate compositionally similar calcium-silicate glass particles with well-defined shapes, the similar techniques could be applied to synthesize C-S-H with a wider range of morphologies than described above [25, 26].

Moghaddam et al. accomplished for the first time the well-defined rhombohedral and cubic morphology for C-S-H, concomitantly proving beneficial properties arising from the specific morphology in the context of construction industry [27]. Herein, the authors employed the surfactant assisted, seed-mediated technique to materialize various well-defined morphologies for C-S-H, where the naturally formed calcium carbonate particles were exploited as seed particles for C-S-H nucleation and growth.

When the silicate source, sodium silicate and calcium source, calcium nitrate were dissolved in water solution under sonication, atmospheric carbon dioxide was also dissolved in the reaction mixture, releasing carbonate ions. The authors hypothesized based on the free energy of formation that in the presence of two types of anions, the silicate and the carbonate ions, calcium ions combine selectively with carbonate ions, thereby forming calcium carbonate seeds [28]. The cationic surfactant, cetyltrimethylammonium bromide (CTAB) stabilized the nano-sized seeds, promoting their combination and growth in [104] directions to form microsized seeds with cubic/rhombohedral shapes. Owing to the formation of the seeds described above, the amount of available CO_3^{2-} ions naturally decreased, thereby prompting the subsequent reaction between calcium and silicate ions to form C-S-H. The formation of C-S-H started with the heterogenous nucleation on the microsized $CaCO_3$ seeds as the seed-mediated nucleation is more energetically favorable than homogenous nucleation. The subsequent growth led to the formation of C-S-H with well-defined cubic and rhombohedral morphologies.

Experimental factors such as the initial Ca/Si ratio, temperature of the reaction medium and the types of surfactants all exerted the significant influence on final morphology of the as-formed C-S-H.

Selecting the appropriate type of surfactant was the critical factor for achieving the final well-defined morphology. Cationic surfactants including cetylammonium bromide (CTAB)

could undergo electrostatic interactions with silicate ions and stabilize them, directing the reaction pathway toward the formation of cubic particles. Similarly, tetra(decyl)ammonium bromide (TDAB) ultimately induced a greater variety of morphologies ranging from cubic to rods. In contrast, anionic surfactants such as sodium dodecylsulfate, owing the inherent negative charges, repel the silicate ions and thus could play the stabilizing role similar to CTAB. It is likely that they exerted the undesired electrostatic attraction with calcium ions, disrupting the formation of cubic calcite seeds. Consequently, this led to the formation of highly aggregated, irregularly shaped C-S-H. Also, it was found that using nitrate ions as counterions was the most favorable for the formation of cubic and rhombohedral morphologies, while chloride or hydroxide ions resulted in irregular particles and sheets, respectively.

Aside from the types of surfactants, the final morphology was also influenced by various reaction conditions such as precursor concentration and temperature. An increase in the precursor concentration prompted the formation of larger particles due to the greater availability of ionic building blocks to participate in growth of C-S-H. This also resulted in a greater proportion of twins, triplet and multiplet particles with poorly defined morphologies. On the other hand, when the precursor concentration was low, the as-formed C-S-H seed particles assembled to form dendritic structures instead of serving as the cubic seeds for nucleation and semiepitaxial growth of C-S-H. This hypothesis was verified by the observable cubic subunits, which constitute tails and edges of the dendritic structures under SEM.

The types of counterions within the calcium source also affected the final morphology of C-S-H. The use of calcium nitrate yielded the best results in terms of the cubic/rhombohedral morphology. However, the use of calcium chloride and calcium oxide resulted in C-S-H with poorly defined irregular shapes and crumpled sheets, respectively.

Overall, this sonication-assisted, in situ seed-mediated pathway mapped out the complex, morphology-oriented synthesis of semicrystalline C-S-H using four reaction parameters, encompassing the initial Ca/Si ratio, types of counterions within a calcium source, types of surfactants and the mixing method (**Figure 3**).

The authors then verified the morphology-induced enhancement in mechanical properties based on the combination of nanoindentation technique and compressive testing. Although mechanical properties of synthetic C-S-H have been linked to its final Ca/Si molar ratio or silicate polymerization before, the authors herein proved for the first time the shape-dependent mechanics from the scale of a single particle to assembled states [29, 30]. Compared to the previous reports, where the mechanics of C-S-H had been often evaluated using compacted samples, the authors devised a de novo matrix-based strategy to probe the mechanics of individual C-S-H particles first. The results showed that the individual cubic particles exhibit approximately 650 and 300% increase in hardness and stiffness, respectively, compared to the control C-S-H with irregular morphology. Nanoindentation was also performed on a pressure-induced sample using a (10 × 10) grid, thereby exhibiting ~83 and ~30% increase in the average values of hardness and elastic modulus for cubic samples compared to the control samples, which consisted of irregular C-S-H compacted under external pressure. Furthermore, the compressive toughness and ductility of the cubic samples were ~300 and 77% higher compared to the control samples.

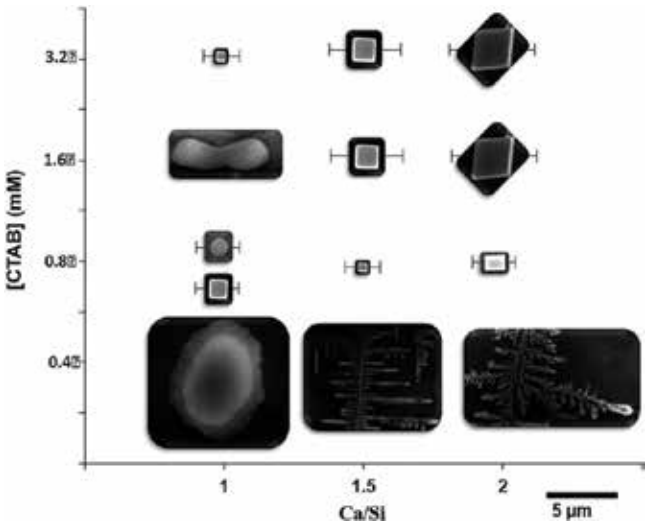

Figure 3. Morphology map as a function of surfactant concentration and the initial Ca/Si molar ratio [27].

5. Morphology of C-S-H for drug delivery

Outside the framework of construction industry, C-S-H also offers numerous benefits as drug carriers, such as high bioactivity and the enhanced affinity toward certain organic drug molecules owing to the presence of calcium ions on the surface [31–33]. Wu et al. synthesized near-spherical, mesoporous C-S-H particles using the surfactant-free, sonochemical method with tetraethylorthosilicate (TEOS) and calcium nitrate as the silicate and calcium source, respectively [33]. Each particle exhibited a 3D-network produced by the assembly of nanosheets, leading to the presence of meso- and macropores (**Figure 4**). The resultant large surface area later facilitated the subsequent loading and unloading of Ibuprofen, utilized as the model drug. Zhang et al. applied the similar sonochemical technique but along with CTAB to produce hollow CSH microspheres [34]. The authors sonicated the mixture of sodium silicate and calcium hydroxide or calcium nitrate, thereby investigating the effect of two distinct calcium-bearing precursors on the final morphology, and also tried two separate mixing techniques, simple stirring and sonication. It was found that well-defined spherical shapes were only produced under sonication while stirring induced the formation of irregular agglomerated nanosheets. Furthermore, calcium hydroxide was found to be a more effective calcium source in inducing hollow spherical morphology than calcium nitrate, owing to the higher dissociation speed of the latter. The fast release of calcium and nitrate ions led to the increased combination rate of calcium and silicate ions prior to the attachment of silicate ions onto the CTAB micelle, thereby resulting in a greater proportion of nonspherical particles. Wu et al. also synthesized ultrathin calcium silicate nanosheets for use as adsorbents for drugs and metal ions [35]. The solvothermal treatment using the as-synthesized nanosheets at 180°C for 24 hours increased crystallinity of the products and induced the nanobelt-like morphology with the thickness of around 5 nm. Further extending this reaction time to 120 hours produced the similar nanobelt-like C-S-H with the enhanced width.

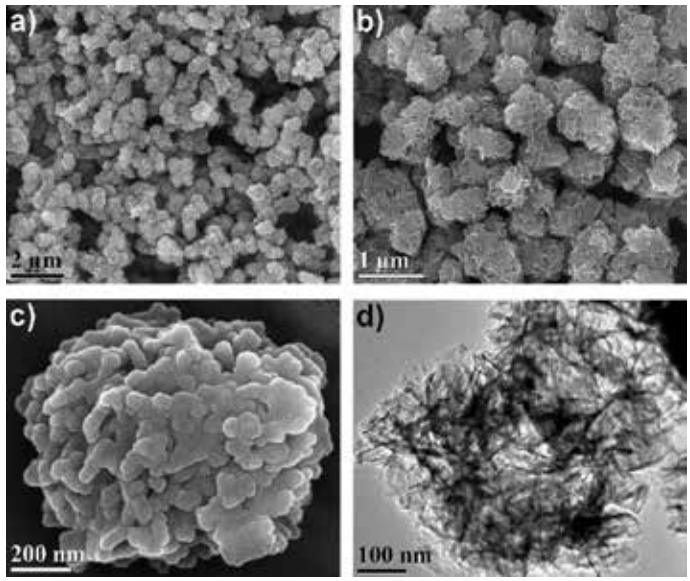

Figure 4. Hierarchically structured, mesoporous C-S-H spheres for drug delivery [33].

6. Conclusion

Calcium silicate hydrate, the most commonly renowned as the glue of concretes, has now found widespread potential applications encompassing cementitious and insulation materials, drug delivery, water treatment and bone-tissue engineering. In addition to the inherent benefits including high strength, high bioactivity and high biodegradability, a long list of various C-S-H members accompanying different stoichiometric ratios implies that there exists a room for the attainment of diverse morphologies. Consequently, a large number of efforts have been directed toward achieving specific, well-defined morphologies, which can optimize the functions. For example, enhanced mechanical properties of cementitious materials arising from cubic building blocks and large drug-loading capacity stemming from the large surface area of mesoporous spherical shapes have been achieved. Based on the rapidly advancing nanofabrication techniques, greater diversity regarding the shapes of C-S-H will be accomplished in future.

Author details

Rouzbeh Shahsavari[1,2,3]* and Sung Hoon Hwang[1]

*Address all correspondence to: rs28@rice.edu

1 Department of Material Science and Nano Engineering, Rice University, Houston, TX, USA

2 Department of Civil and Environmental Engineering, Rice University, Houston, TX, USA

3 The Smalley-Curl Institute, Rice University, Houston, TX, USA

References

[1] Pellenq RJM, Kushima A, Shahsavari R, Van Vliet KJ, Buehler MJ, Yip S, Ulm FJ. A realistic molecular model of cement hydrates. Proceedings of the National Academy of Sciences of the United States. 2009;**106**:16102-16107

[2] Livingston RA. Fractal nucleation and growth model for the hydration of tricalcium silicate. Cement and Concrete Research. 2000;**30**:1853-1860

[3] Thomas JJ. A new approach to modeling the nucleation and growth kinetics of tricalcium silicate hydration. Journal of the American Ceramic Society. 2007;**90**:3282-3288

[4] Valentini L, Favero M, Dalconi MC, Russo V, Ferrari G, Artioli G. Kinetic model of calcium-silicate hydrate nucleation and growth in the presence of PCE superplasticizers. Crystal Growth & Design. 2016;**16**:646-654

[5] Jennings HM, Dalgleish BJ, Pratt PL. Morphological development of hydrating tricalcium silicate as examined by electron-microscopy techniques. Journal of the American Ceramic Society. 1981;**64**:567-572

[6] Diamond S. The microstructure of cement paste and concrete-A visual primer. Cement and Concrete Composites. 2004;**26**:919-933

[7] Taylor HFW. Cement Chemistry. 2nd ed. Thomas Telford; 1997

[8] Richardson IG. The nature of C-S-H in hardened cements. Cement and Concrete Research. 1999;**29**:1131-1147

[9] Richardson IG. The nature of the hydration products in hardened cement pastes. Cement and Concrete Composites. 2000;**22**:97-113

[10] Taylor R, Richardson IG, Brydson RMD. Composition and microstructure of 20-year-old ordinary Portland cement-ground granulated blast-furnace slag blends containing 0 to 100% slag. Cement and Concrete Research. 2010;**40**:971-983

[11] Wang H, Gillott JE. Mechanism of alkali-silica reaction and the significance of calcium hydroxide. Cement and Concrete Research. 1991;**21**:647-654

[12] Zampini D, Shah SP, Jennings HM. Early age microstructure of the paste-aggregate interface and its evolution. Journal of Materials Research. 1998;**13**:1888-1898

[13] Hara N, Inoue N. Formation of jennite from fumed silica. Cement and Concrete Research. 1980;**10**:677-682

[14] Chen JJ, Thomas JJ, Taylor HFW, Jennings HM. Solubility and structure of calcium silicate hydrate. Cement and Concrete Research. 2004;**34**:1499-1519

[15] Shi CJ, Day RL. Pozzolanic reaction in the presence of chemical activators-Part I. Reaction kinetics. Cement and Concrete Research. 2000;**30**:51-58

[16] Shi CJ, Day RL. Pozzolanic reaction in the presence of chemical activators-Part II. Reaction products and mechanism. Cement and Concrete Research. 2000;**30**:607-613

[17] Saito F, Mi GM, Hanada M. Mechanochemical synthesis of hydrated calcium silicates by room temperature grinding. Solid State Ionics. 1997;**101**:37-43

[18] Sasaki K, Masuda T, Ishida H, Mitsuda T. Synthesis of calcium silicate hydrate with Ca/Si=2 by mechanochemical treatment. Journal of the American Ceramic Society. 1997;**80**: 472-476

[19] Rodriguez ET, Richardson IG, Black L, Boehm-Courjault E, Nonat A, Skibsted J. Composition, silicate anion structure and morphology of calcium silicate hydrates (C-S-H) synthesised by silica-lime reaction and by controlled hydration of tricalcium silicate (C3S). Advances in Applied Ceramics. 2015;**114**:362-371

[20] Kurtis KE, Monteiro PJM, Brown JT, Meyer-Ilse W. High resolution transmission soft X-ray microscopy of deterioration products developed in large concrete dams. Journal of Microscopy (Oxford). 1999;**196**:288-298

[21] Nocun-Wczelik W. Effect of Na and Al on the phase composition and morphology of autoclaved calcium silicate hydrates. Cement and Concrete Research. 1999;**29**:1759-1767

[22] Bell NS, Venigalla S, Gill PM, Adair JH. Morphological forms of tobermorite in hydrothermally treated calcium silicate hydrate gels. Journal of the American Ceramic Society. 1996;**79**:2175-2178

[23] Galvánková L, Másilko J, Solný T, Štěpánková E. Tobermorite synthesis under hydrothermal conditions. Procedia Engineering. 2016;**151**:100-107

[24] Hartmann A, Khakhutov M, Buhl JC. Hydrothermal synthesis of CSH-phases (tobermorite) under influence of Ca-formate. Materials Research Bulletin. 2014;**51**:389-396

[25] Hwang SH, Miller JB, Shahsavari R. Biomimetic, strong, tough, and self-healing composites using universal sealant-loaded, porous building blocks. ACS Applied Materials & Interfaces. 2017;**9**:37055-37063

[26] Li X, Zhang LX, Dong XP, Liang J, Shi JL. Preparation of mesoporous calcium doped silica spheres with narrow size dispersion and their drug loading and degradation behavior. Microporous and Mesoporous Materials. 2007;**102**:151-158

[27] Moghaddam SE, Hejazi V, Hwang SH, Sreenivasan S, Miller J, Shi BH, Zhao S, Rusakova I, Alizadeh AR, Whitmire KH, Shahsavari R. Morphogenesis of cement hydrate. Journal of Materials Chemistry A. 2017;**5**:3798-3811

[28] Rog G, Kozlowskarog A. Determination of the standard Gibbs free-energies of formation of the calcium silicates by Emf-measurements. The Journal of Chemical Thermodynamics. 1983;**15**:107-110

[29] Kim JJ, Foley EM, Taha MMR. Nano-mechanical characterization of synthetic calcium-silicate-hydrate (C-S-H) with varying CaO/SiO_2 mixture ratios. Cement and Concrete Composites. 2013;**36**:65-70

[30] Pelisser F, Gleize PJP, Mikowski A. Effect of the Ca/Si molar ratio on the micro/nano-mechanical properties of synthetic C-S-H measured by nanoindentation. Journal of Physical Chemistry C. 2012;**116**:17219-17227

[31] Hench LL. Bioceramics. Journal of the American Ceramic Society. 1998;**81**:1705-1728

[32] Coleman NJ, Bellantone M, Nicholson JW, Mendham AP. Textural and structural properties of bioactive glasses in the system CaO-SiO_2. Ceramics-Silikáty. 2007;**51**:1-8

[33] Wu J, Zhu YJ, Cao SW, Chen F. Hierachically nanostructured mesoporous spheres of calcium silicate hydrate: Surfactant-free sonochemical synthesis and drug-delivery system with ultrahigh drug-loading capacity. Advanced Materials. 2010;**22**:749

[34] Zhang ML, Chang J. Surfactant-assisted sonochemical synthesis of hollow calcium silicate hydrate (CSH) microspheres for drug delivery. Ultrasonics Sonochemistry. 2010;**17**: 789-792

[35] Wu J, Zhu YJ, Chen F. Ultrathin calcium silicate hydrate nanosheets with large specific surface areas: Synthesis, crystallization, layered self-assembly and applications as excellent adsorbents for drug, protein, and metal ions. Small. 2013;**9**:2911-2925

[36] Gartner EM, Kurtis KE, Monteiro PJM. Proposed mechanism of C-S-H growth tested by soft X-ray microscopy. Cement and Concrete Research. 2000;**30**:817-822

Green Cements

Chapter 7

Heat Integration in a Cement Production

Stanislav Boldyryev

Additional information is available at the end of the chapter

http://dx.doi.org/10.5772/intechopen.75820

Abstract

The cement industry sector is an energy-intensive industrial sector; cement is the most widely used material for construction and modern infrastructure needs. The cement industry is one of the largest consumers of carbon-containing primary energy sources and one of the primary polluters of the environment. Energy consumption represents the largest part of the production cost for cement factories and has a significant influence on product prices. The potential of waste heat utilization of cement production was determined and a recovery potential accounting site wide in demand is defined by the process integration technique. The author has analyzed the energy consumption of a cement factory to obtain minimum energy needs of production and proposed the options to improve energy efficiency by the process integration approach. The authors conclude that the energy consumption of the cement factory can be reduced by 30%. The results help to the cement plant's profitability and reduce environmental impact of the cement industry as well as sustainability. Given that it is realized in modern society that infrastructural projects lead to a higher level of economy and sustainability for countries, reducing the production cost in the cement industry is a very important problem.

Keywords: process integration, pinch analysis, energy efficiency, cement production, energy targets, heat exchangers

1. Introduction

Nowadays, cement manufacturing is an energy-intensive industry. The energy costs of cement industry are about 40% of the product cost that indicates that this sector is one of the biggest CO_2 emitter. The global anthropogenic CO_2 emission of cement industry is approximately 5% [1].

The International Energy Agency reported in 2011 that the world cement production was 3635 Mt. with a forecast rising up to 4556 Mt. in 2020, 4991 Mt. in 2030 and 5549 Mt. in 2050 according to scenarios with high demands. In case of the same scenarios, by 2050, the cement manufacturers have to reduce the CO_2 emissions by 15%, with a direct decrease of up to 913 Mt. [2].

Hence, cement manufacturing has to implement more energy reduction to be more environmentally friendly. However, as there is a large amount of CO_2 coming from the existing technology, it is important to estimate a renewable energy potential use in the cement production industry or even switch from conventional fuel to a new one with low CO_2 emissions.

Due to great significance of the cement industrial sector and high environmental perception [3] last time, a lot of researches worldwide have shown the energy efficiency improvement of cement factories and pollution reduction. Most of the published researchers investigated the improvement of the cement technology and different varieties for CO_2 emission reduction. Pardo et al. [4] are trying to define the potential of energy efficiency improvement of the EU's cement sector and CO_2 gaseous emission reduction by 2030. Liu et al. [5] have presented the retrofit and building of new cement factories in China, accounting different technologies. Chen [6] had defined the advantages of the clinkering process by compact internal burning of carbon inside a cement shaft kiln. This research demonstrated the competitiveness of the proposed measure with the existing one that uses the precalciner kiln process. The work published by Hasanbeigi et al. [7] points out the CO_2 cost curves for the Thailand cement sector. An estimated potential and expenses of CO_2 abatement were investigated taking into account the expenses and CO_2 abatement for a variety of applications. As presented by Worrell et al. [8], an in-depth analysis of a US cement industry considering a potential for energy cost and CO_2 emission decreasing by the national technologies database was done. It was found that one of the most effective pyro-processing cement manufacturing systems composed of a calciner, several preheaters and the rotary kiln. The data of observed factory for the analysis of the parameters influencing the energy usage of a rotary kiln were utilized in the research by Atmaca and Yumrutas. Their work highlighted that high-energy savings may be obtained by reduction of heat losses with use of insulation, decreasing the outlet gas temperature and heat transfer enhancement. Sheinbaum and Ozawa [9] have presented the energy demands and CO_2 emissions of the cement sector of Mexico, summarizing, that the measures of a fossil fuel, CO_2 and other pollutants reduction have to be focused on the use of environmentally friendly energy sources. These assumptions were also concluded by Mikulčić et al. [10]. With the use of real industrial data and combination of kinds and flow rates of alternative energy sources, the work [11] estimated the ecological impact of cement manufacturing process. It is concluded that the environmental impact of the cement manufacturing process could be lowered if a more energy-saving process of cement manufacturing is utilized along with alternative fuels.

Stefanović et al. [12] estimated the potential of CO_2 emission reduction that may be lowered partly by use of cement with fly ash in the concrete. The research showed that the properties and quality of the new kind of concrete remain the same. Another work by Zervaki et al. [13] investigated the properties of the cement mortars manufactured by use of sludge water. It was examined that the sludge water, as well as a dry or wet sludge, may be employed in

a mortar manufacturing process without remaining its physical properties. As presented by Wang et al. [14], the exergy approach combining with an organic Rankine cycle (ORC) and Kalina cycle were made to estimate of cogeneration opportunities of a cement factory as well as the calculation of optimal conditions and maximum efficiency. Process integration methods may be used as well to decrease energy use and emissions as were summarized in the work of Professor Seferlis et al. [15]. Presented approaches are based on thermodynamics laws and have different applications in different processing sectors; this issue was reported by Boldyryev and Varbanov [16]. In order to employ the industrial low potential heat and improve a heat utility system of different users and suppliers, a total site integration (TSI) may be employed as shown by Klemeš et al. [17]. Later, a similar approach was developed by different authors. As an example, Chew et al. [18] expanded the content of a pinch approach of individual process changes to improve a TSI and adapted the plus-minus principle for process modification options to improve process efficiency. Grip et al. [19] used the mixed-integer linear programming (MILP) approach, exergy analysis and pinch analysis (PA). Experience and results of a multiple approach were presented and considered in literature by many authors. For instance, Baniassadi et al. [20] represented a technique for an industrial energy system analysis with the use of modified R-curve approach. This methodology estimates the use of the most efficient fuel type for the industrial utility system. Mian et al. [21] employed the pinch analysis and the process integration approaches for energy optimization of cement manufacturing with primary energy demands of 3600 MJ/t. Authors calculated the thermodynamically and exergy available amount of heat that can be utilized and summarized that the potential of thermal energy reduction is 30%. However, the authors did not propose the retrofit project design nor was the definition of a feasible temperature approach provided. Summarizing the abovementioned, the recent works were rarely supplemented with proper industrial applications of the methodology, especially for the new heat exchanger network (HEN) design and retrofit of existing ones. The analysis and application of different methodologies are usually faced with process features of different industries. In addition, there is a lack of industrial applications of process integration techniques in the cement manufacturing processes owing to its specific process features and process limitations, such as solid particles of process streams, solid-gas and solid-air heat exchange and fast cooling of gaseous streams. Such approaches can be analyzed and subsequently used in appropriate case studies to achieve a real efficiency of the cement manufacturing processes. Thus, this chapter is dedicated to energy efficiency and pathways toward maximization of feasible heat recovery and the concept design of heat exchange system at the particular cement factory.

The energy efficiency potential of a cement factory is estimated. The total energy consumption of the particular cement manufacturing was compared with the benchmark value. Nowadays, considering a best available technology (BAT), the one with the lowest energy consumption of cement production is the rotary kiln use, many cyclone preheaters and the calciner. This technology has energy demands of a cement factory at about 2.93 GJ/t. The same amount is now used for benchmarking point [22]. Present technologies that use the kiln process have total energy consumption at about 3.65 GJ/t of cement. As mentioned, there are still opportunities to reduce the energy consumption of the particular cement factory.

The main goal of this chapter is to identify the potential of feasible energy recovery and to suggest pathways for a new concept design of heat exchange system avoiding the process traps and limitations. The maximum heat recovery of the particular cement manufacturing was obtained, and the updated heat exchange system was proposed. The author concluded that the energy consumption of the particular cement plant may be lowered by 30%. Thus, the features of the cement production process forced a methodology update to suggest feasible retrofit pathways with the objective of achieving the optimal temperature approach of the heat exchange system. There are different streams and processes that contain solid particles, gaseous phase and fast cooling down; these facts make a solution more complicated by the special construction of the process equipment, which causes impossible a heat transfer between some process streams.

2. Description of process flow diagram

Quarrying is the first step of the cement manufacturing (see **Figure 1**). Inside the quarry that is close to the cement factory, low- and high-grade marl and limestone are mined by blasting. Further, the raw material with granulation of up to 800 mm has to be transported via dump trucks to the hammer crusher, where it is crushed to the granulation of 0–80 mm for marl and 0–50 mm for limestone.

The low-grade and high-grade marl and quartz (silica corrective material) are then stored separately. From the depository the raw materials are transferred to the vertical roller mill

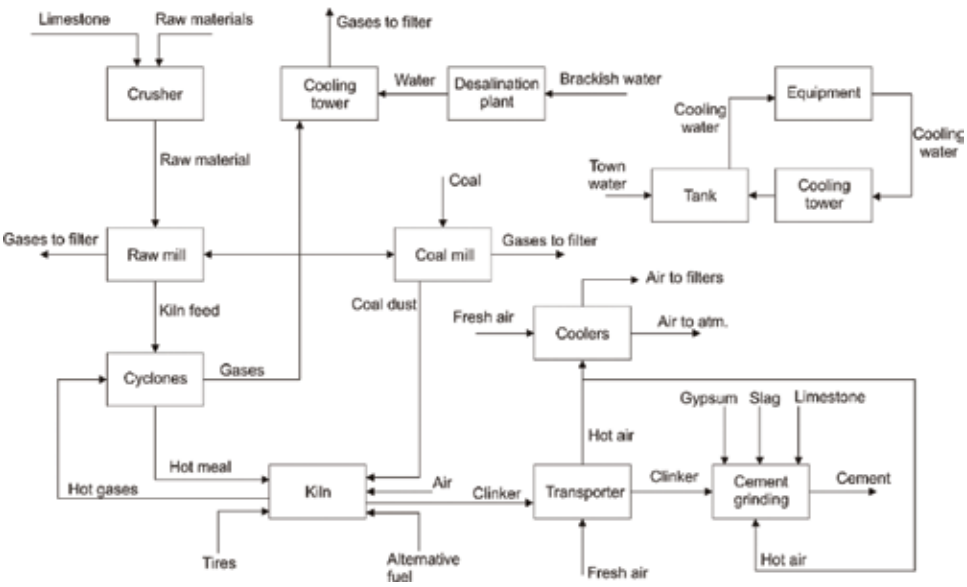

Figure 1. Principal flowsheet of the cement manufacturing process.

http://dx.doi.org/10.5772/intechopen.75820

with a capacity of 170 t/h and appropriate raw meal is produced. The storage of current raw meal has two silos with a capacity of 2200 t each.

The prepared raw meal from the silos is supplied to the kiln. The kiln has an operation capacity of 90 t/h and upper bound of 110 t/h. A total of 57 t/h of the clinker is produced inside the kiln. For the heating of the raw mill, kiln raw meal, and a coal mill, hot flue gases from the kiln are deployed. Gases exit from a preheating tower with a temperature at about 370°C. Flue gases have be cooled down at the cooling tower because the filter bags cannot operate at the temperature higher than 140°C. The flue gases at the cooling tower are cooled to a temperature of 175°C by 10.5 m^3 of cooling water. To further reduce the flue gas temperature from 175 to 105°C, fans are used to pump the ambient air. Flue gases go to the stack after filtration, and further, they are discharged into the environment.

At the kiln outlet side the temperature of the clinker is approximately 1450°C. At this stage, to preserve the clinker mineral structure, that is, its quality, the clinker has to be cooled very quickly to a temperature of approximately 150°C. A large amount of ambient air is introduced through seven clinker cooler fans to achieve the target temperature outlet. The ambient air is heated up to 290°C. After that, a small amount of this air is employed as an additional oxygen source in the kiln and a bigger part is supplied for cement mill heating if it is under operation. The operation mode with disabled cement mill envisages air cooling down before the filter bags. The gas has to be cooled to 105°C prior to the clinker cooler filter bags, after the gas is eliminated to the stack by four rows of four blowers.

The hot gases are needed for the cement grinding process. The hot air is taken to the separator where materials (clinker, limestone/slag and gypsum), pre-grinded on the roller press, are heated to extract moisture and prepare the resulting material for filter bags. They can be delivered from the clinker cooler or, in the case when the kiln does not operate, generated by a hot gas generator (HGG) with use of light oil as a fuel. It is the expensive option but it is used only in several weeks when the kiln overhauls. The consumption of the light oil is about 200 l/h.

A material mixture is kept in a bin with a capacity of 70 t that is supplied by a cement ball mill. Dust and fly ash are supplemented after the ball mill depending on the required kind of cement. The cement is then transferred through a bucket elevator to the next separator. Particles comprise the final product that is supplied to the cement silo.

3. Process integration in cement production

The methodology is grounded on the thermodynamic analysis of the heat energy system by composite curves of process streams. The general issues are based on process integration aspects. The pinch analysis (PA) for optimal process structure synthesis is well illustrated by Klemeš et al. [23]. It provides a solution that is very close to the global optimum in a simply and understandable way. The methodology produces the result of potential savings, capital cost and payback period prior to the flow-sheet design. Often, a super targeting procedure is employed to obtain the optimal temperature approach (ΔT_{min}) of the heat exchanger

network, but in this case, it is difficult due to manufacturing issues. The existing process design presumes a hot meal heating inside the kiln by flue gases that cannot be executed by another stream owing to the technology. Another problem is a hot clinker, which is from the kiln. The clinker must be cooled down rapidly, and that is done by fresh ambient air. The level of technology that is used now has several restrictions for process changes. They have to be taken into account when the retrofit of HEN is made. The methodology stages were updated and are presented later to obtain the more feasible solution of an efficient heat exchanger network design.

3.1. Data extraction by energy expertise execution

An audit expertise of a particular cement factory was conducted to verify energy and mass balances. A measurement of temperatures, flow rates and fuel burning efficiency is accomplished. The composite curves approach and balanced grand composite are employed for the estimation of energy targets, heat recovery and the operation condition of heat transfer equipment, taking into account the cross-pinch heat exchange. Inefficient heat transfer is identified, and process restrictions and forbidden matches between heat transfer equipment are determined.

3.2. Targeting

Considering the next step, the composite curves of cement production are constructed to obtain the energy target and pinch point position of the existing and improved process. At this step, process restrictions are not considered, and only thermodynamically available heat recovery is obtained.

3.3. New concept of heat exchanger network

Based on the previous stages, the heat exchanger network is built taking into account the process restrictions. It is shown that the cross-pinch heat transfer still exists and it cannot be avoided in this production process due to features. Process streams with limitations are not excluded from the considerations to show the actual heat recovery and the real energy efficiency potential of cement manufacturing. The heat exchanger network was built for the range of ΔT_{min} from 1 to 300°C with step 1°.

3.4. Heat recovery improvement

Based on the previous step, energy targets and pinch point location are defined for different $\Delta T_{min,}$ and maximum heat recovery was found. This procedure determines the heat exchanger network temperature approach, cross-pinch heat transfer and topology heat matches in the heat network.

3.5. Economic analysis

All topologies of heat exchanger network are compared with the base case taking into account operation cost, investment for new networks, operation time, tax rate and other economic prerequisites. Economic results of retrofit execution are defined based on the determination

of the reduced total cost of the new design with the use of reduced operating and investment cost [23].

3.6. Utilization of waste heat in cement production

The next step is performed by the analysis of the waste heat potential in the retrofitted cement production. As was identified by grand composite, there is waste heat utilization potential, and its possibility should be analyzed additionally. The appropriate integration and efficient placement of heat engines is used by grand composite, which shows the available energy, the supply and demand temperatures of heat engines and a heat source. The waste heat utilization that is discarded by cooling capacity, along with attempts to derive energy from low-potential heat sources, has motivated the use of heat engines, for example, by the organic Rankine cycle (ORC) [24] or utilization of wide site cooling and heating demands [16].

An additional intermediate stream may utilize the heat from process streams to site heating capacities. This may be steam of different pressure, hot water, thermal oil and so on. The selection of the intermediate utility stream is mainly dependent from its start and target temperatures. The T-H diagram represents a total site sink and source profiles by employing individual ΔT_{min} specifications of heat transfer between process streams to show the real stream temperatures [25]. Total site targets of heating and cooling, heat engine capacity and produced emissions are considered by Sun et al. [26]. The use of multiple intermediate utilities of heat recovery and modified total site targets is represented by Boldyryev [27] and methodology advances are discussed. All computations were performed by the HILECT software [28] applying integrated process design with technological restrictions mentioned earlier.

4. Representative case study

4.1. Data collection and reconciliation

This case study was previously introduced by Boldyryev et al. [29, 30]. The energy expertise of the cement factory was conducted during the summer operation mode. The steady-state devices and portable equipment were used. The historical data of process monitoring were collected and analyzed. There are two operation modes of the particular cement factory. The first one is when the raw mill is under operation and, in this case, the cooling water flowrate at the cooling tower is 3 t/h. A hot gas from the kiln is fed into the raw mill and a raw material is heated. The second operation mode presumes that the raw mill is out of operation. In this case, the cooling water flowrate greatly increases and it is 11 t/h. At the same time, the waste heat with hot gases from the kiln is also increased. There are 18 process streams, which may be included to the heat integration of a particular cement factory. There is a heat recovery of an inspected cement plant and a necessary process heat is provided by the fuel combustion while a cooling capacity is delivered by ambient air that is pumped by air fans. **Table 1** has all necessary thermophysical parameters of process streams under analysis.

№	Name of the stream	Type	Supply temperature (°C)	Target temperature (°C)	Heat capacity flowrate (kW/K)	Heat load (kW)
1	Gases to raw mill	Hot	370	105	13.35	3537.42
2	Gases from the kiln	Hot	860	380	40.97	19,663.31
3	Hot gases to cooling	Hot	370	175	11.68	2276.67
4	Gases to coal mill	Hot	370	90	0.73	204.75
5	Clinker from the kiln	Hot	1450	60	15.00	20,850.00
6	Air after clinker cooling	Hot	290	100	70.28	13,352.75
7	Air to cement grinding	Hot	270	105	8.86	1461.60
8	Raw material in a raw mill	Cold	25	110	41.62	−3537.42
9	Kiln raw material	Cold	105	810	21.44	−15,114.42
10	Hot meal	Cold	810	1450	21.19	−13,559.47
11	Coal/petcoke to coal mill	Cold	25	90	3.15	−204.75
12	Coal dust to kiln	Cold	55	170	1.75	−201.25
13	Air to the kiln	Cold	25	170	38.13	−5528.29
14	Tires to the kiln	Cold	25	170	0.14	−20.30
15	Used oil to kiln	Cold	25	170	0.28	−40.48
16	Ambient air for clinker cooling	Cold	25	290	78.68	−20,850.00
17	Clinker to cement grinding	Cold	25	105	15.00	−1200.00
18	Mineral components grinding	Cold	25	105	3.27	−261.60

Table 1. Extracted data of inspected cement factory: raw meal under operation.

Economic data of utilities were also extracted to be able to execute the economic calculation of the retrofit solution. There are two types of fuel supplied to the kiln: coal and petcoke. Cooling water cools down the exhaust gases before the filter bags; the water is fed by the desalination plant. Another cold utility is electricity, and it is used by the hot air coolers, which emerges from the clinker cooling. Cleaned and cooled air from air filter bags is ejected to the environment. A total of 15.6 MW of low-grade heat is ejected to the atmosphere during raw mill operation; this amount is increased up to 19.4 MW if the raw mill is turned off. All fans and pumps of the cooling tower use the electricity.

The primary fuel that is used for this particular cement factory is coal and petcoke. The coal/petcoke ratio is 40/60%, and the caloric values of the fuel are 25.5 and 33 GJ/t, respectively, for coal and petcoke. The average power supply of the cement plant is 5.8 MW, whereas the minimum power consumption is 1.1 MW and the peak load reaches 10 MW. The reduced price of the hot utility is 75.9 EUR/kWy, and the cold utility is 82.0 EUR/kWy.

http://dx.doi.org/10.5772/intechopen.75820

4.2. Results and discussion

4.2.1. Existing process analysis

Based on the energy expertise, heat balances and stream table data, the composites of the existing cement factory were constructed considering different operation modes of the raw mill. The composite curves of the existing process are presented in **Figure 2**.

The composite curves in **Figure 2** present the energy requirements of the existing cement factory. The operation mode with the raw mill has a heat recovery of 41,125 kW, whereas the process requires extra heating of 19,397 kW and extra cooling of 20,225 kW. For the operation regime without raw mill it is necessary to have larger utility load as presented in **Figure 2**. The energy demands increase to 22,923 kW and 24,006 kW for heating and cooling, respectively. At the same time, the heat recovery decreases to 37,599 kW during raw mill operation mode. The minimum temperature approach of the heat exchanger network of the existing process with the raw mill operation is 247°C; without the raw mill operation, it goes up to 308°C. Both these temperature differences are calculated by energy expertise, mass and heat balances and data reconciliation. It should be noted that the minimum temperature approach of the particular process is 1°C due to direct heat transfer in a raw mill or at cement grinding. The raw mill operation mode is under further consideration to get low bound of energy-saving potential. It has to be extended in future by development of the factory operation modes taking into account fluctuations of process parameters and to develop a tool for operators. The significant difference between the thermodynamically grounded (see **Figure 2**) and real minimum temperature approaches may be additionally explained by cross-pinch heat transfer in the existing heat exchanger network. This is well presented in **Figure 3** by composite curves. Arrows show that the heat transfer from hot to cold streams and cross-pinch lines is absent as well as cold utilities are used above the pinch in E-108 (**Figure 4**).

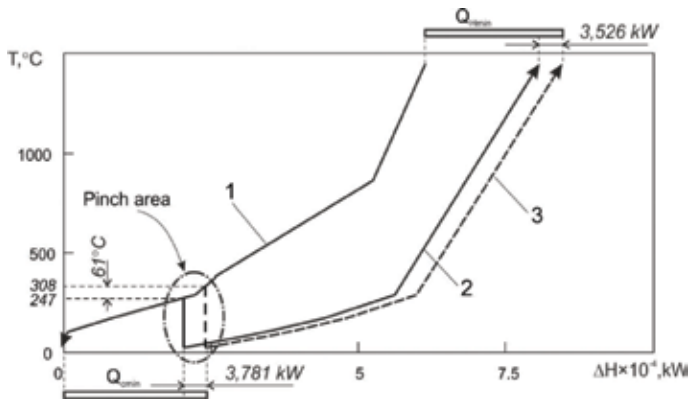

Figure 2. Temperature profiles of a particular cement factory. 1—Hot composite; 2—cold composite raw mill operation mode; 3—cold composite no raw mill operation; Q_{Cmin} = 24,006 kW—cold utility demands (cooling water, air); Q_{Hmin} = 22,923 kW—hot utility demands (fuel) (developed after [30]).

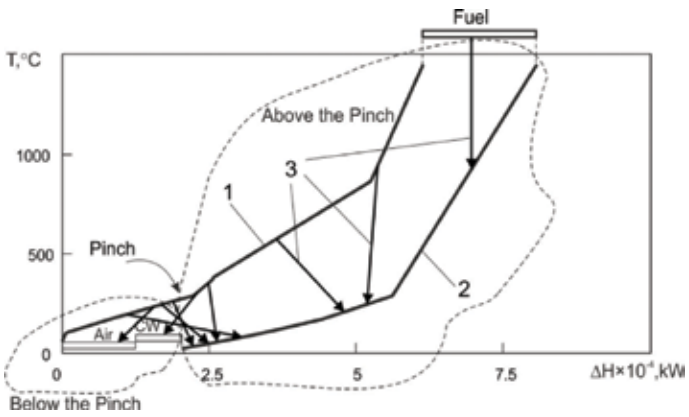

Figure 3. Heat transfer in cement production with raw mill considering the minimum temperature difference. 1—Hot composite curve; 2—cold composite curve, 3—heat exchangers (developed after [30]).

Grid diagram shown in **Figure 4** illustrates the initial heat exchanger network representing the heat transfer between the hot and cold process streams and utilities. The grid diagram illustrates cross-pinch heat transfer; it is a reason of increased utility consumption and lowered efficiency. It is a result of concept design, which was done without the use of optimal heat exchanger network methods and mostly oriented proper product quality.

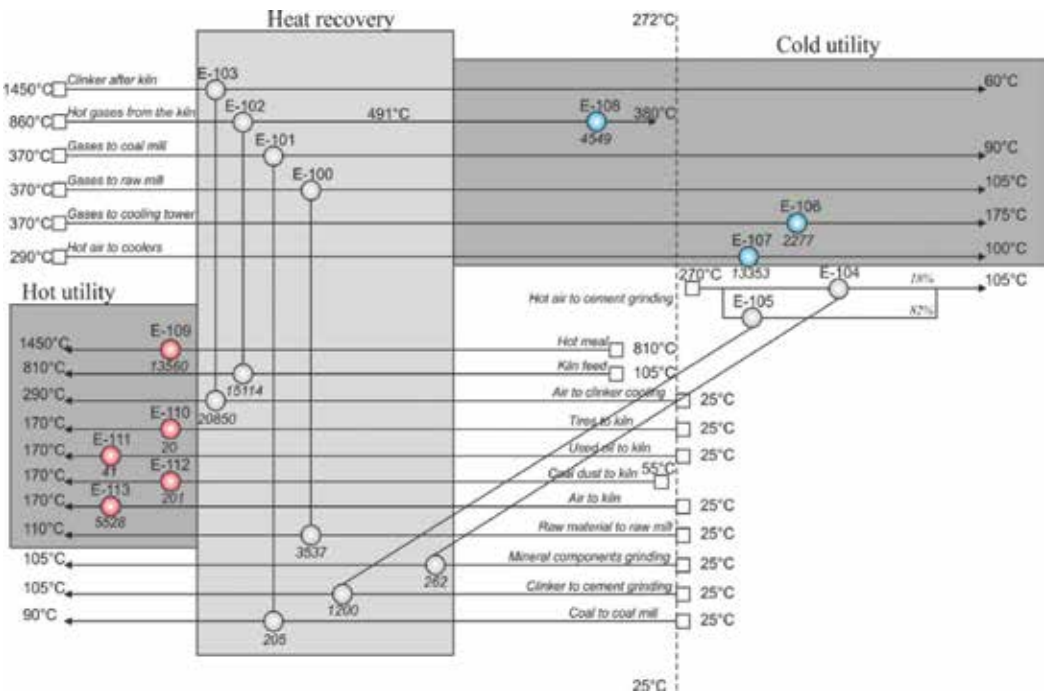

Figure 4. Grid diagram of existing cement production (developed after [30]).

Heat exchanger label	Cross-Pinch heat transfer (kW)
E-100	2229.0
E-101	133.1
E-102	0.0
E-103	3180.0
E-104	261.6
E-105	1200.0
E-106	1132.0
E-107	12,088.5
E-108–E-113	0.0
Network cross-pinch load	20,224.2

Table 2. Analysis result of heat exchanger placement.

The process design, which was oriented to obtain a product rather than energy efficiency, reduces opportunities for overall efficiency of plant operation as highlighted in [31]. The overview of heat exchangers placement of the initial plant design is shown in **Table 2**. The initial cross-pinch transfer is now greater than 20 MW that confirms the low efficiency of the initial design of the heat exchanger network.

4.2.2. Maximization of heat recovery considering process limitations

By providing pinch analysis, it is possible to get thermodynamically available energy targets for particular cement production that shows a large energy-saving potential. Eliminating the cross-pinch heat transfer and cold utility use above the pinch, it is possible to decrease energy consumption and heat recovery improvement. Additionally, the minimum temperature approach may be lowered to minimize the energy targets. This is well illustrated in **Figure 5** by composite curves position for ΔT_{min} = 20°C. Energy targets for hot and cold utilities are 4076 and 4904 kW, respectively; the heat recovery is enlarged up to 56,446 kW; the heat recovery improvement in case of maximum saving is 15,321 kW.

However, the cement manufacturing process has different features previously mentioned in Part 3 of this chapter, such as process streams with a mixture of solid-gas and others. These issues make the feasibility of the heat exchanger network retrofit with maximum heat recovery as impossible. Based on this, the heat exchanger network of the cement factory has huge energy efficiency potential, but it is not easy to achieve a profitable solution owing to the process limitation connected to heating and cooling process streams No 5 and No 10.

It is impossible to avoid process restrictions when implementing an integrated solution. There are some process streams that have such technological limits. First one is a hot meal that has to be heated from 810 to 1450°C inside the kiln. It is not possible to heat it in another with particular technology. Another issue that should be analyzed additionally is clinker from the

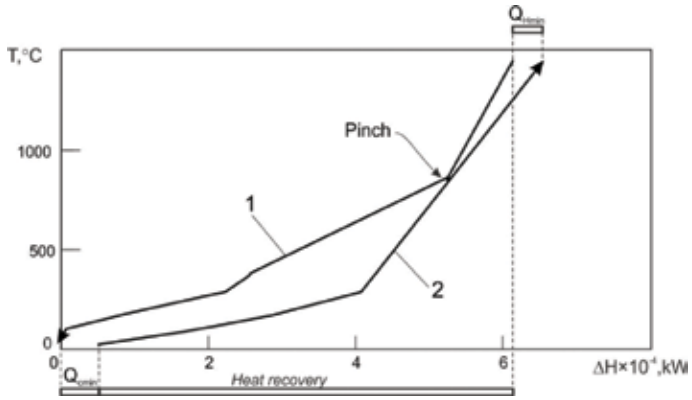

Figure 5. Composite curves of cement production with maximum heat integration. 1—Hot composite curve; 2—cold composite curve with raw mill operation; Q_{Hmin} = 4076 kW—hot utility demands; Q_{Cmin} = 4904 kW—cold utility demands (developed after [30]).

kiln; it has to be cooled down rapidly to 60°C. This is done in the existing process by big fan coolers, and the heat of air is ejected to the environment.

The maximum possible heat recovery of the cement factory taking into account the process restrictions was previously discussed in this chapter. There is an energy target (see right Y-axis, **Figure 6**) and pinch temperatures (left Y-axis, **Figure 6**); these indexes depend from the minimum temperature approach of the heat exchanger network. **Figure 6** shows energy targets (lines 1 and 2 in **Figure 6**, right axis Y) of the cement factory, which may be lowered to a process limit that is 50°C. The reduction of ΔT_{min} below 50°C is useless, as shown in **Figure 6**, due to its increases in the cross-pinch heat transfer and heat transfer area while the energy consumption remains unchanged. This issue also influences the heat exchanger network topology and reduces the cross-pinch heat transfer. The traditional super targeting

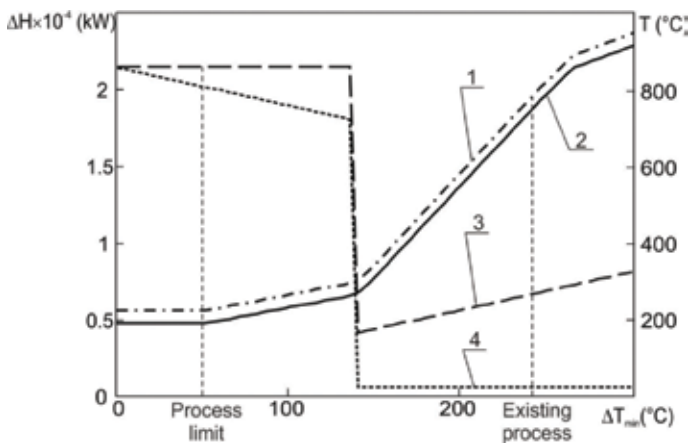

Figure 6. The definition of maximum heat recovery taking into account process restrictions. 1—Cold utility target; 2—hot utility target; 3—hot pinch temperature; 4—cold pinch temperature (developed after [30]).

procedure [23] does not take into account the technological restrictions, for example, as for particular cement manufacturing, and does not have a feasible solution. In our case, the minimum of total reduced cost corresponds to ΔT_{min} = 29°C (see **Figure 7**). Nonetheless, the design of the retrofit for ΔT_{min} = 29°C has the same energy targets as one with ΔT_{min} = 50°C but the heat transfer area is much higher (see **Figure 6**).

4.2.3. New concept of retrofit design

Based on results presented in **Figure 6**, the targets of the retrofit design of cement production are taken, including the minimum temperature approach, energy requirements and pinch point position.

The grid diagram shown in **Figure 8** is the base concept of a new heat exchanger network of a cement factory with minimized energy consumption. It has additionally installed four heat exchangers with an estimated heat transfer area of 1555.1 m^2 and total recovered heat energy of 5790.08 kW. The basic parameters of the new heat exchangers are illustrated in **Table 3**. The new heat exchanger network is presented in **Figure 8**, and it is shown that there is still a large cross-pinch transfer of 8850 kW. This issue may be additionally investigated in the future research of new efficient technologies of cement manufacturing. The cross-pinch heat transfer of the proposed heat exchanger network is illustrated in **Table 4**; there is only one cross-pinch heat exchanger.

The estimated total investment for new heat exchanger network implementation is 256,079 EUR, accounting the installation cost of E-114 and E-115 as 5000 and 10,000 EUR and 30,000 EUR for E-116 and E-117, respectively. The price of the heat transfer area is 800 EUR per 1 m^2, and the nonlinearity price coefficient is 0.87. A new concept design allows reduction of operation cost of 914,401 EUR/year assuming 8200 operation hours per annum. The simple payback period of investments is 3.4 months. By applying the process integration approach, the energy consumption is lowered by 2.56 GJ/t of produced cement, which is 14% less than the existing

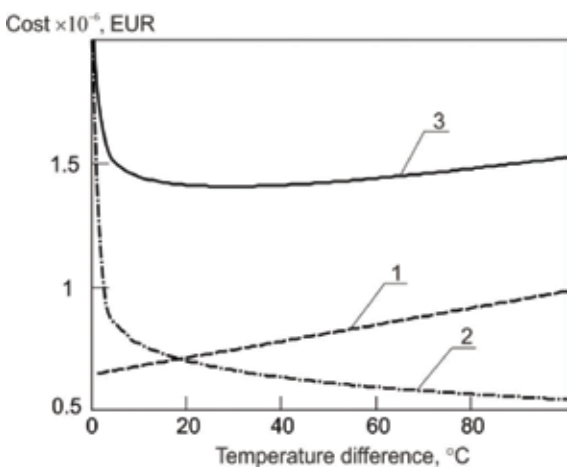

Figure 7. Super targets of cement production. 1—Operation cost; 2—investments; 3—total cost (developed after [30]).

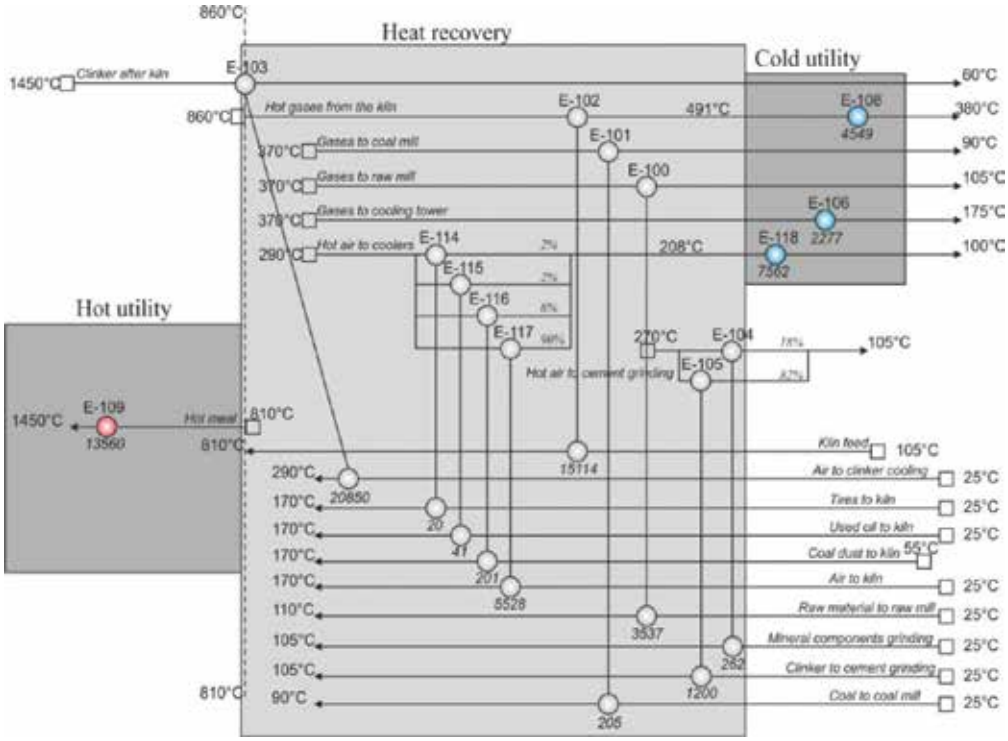

Figure 8. A grid diagram of a retrofit concept design of cement factory (developed after [30]).

Heat exchanger	Cold stream			Hot stream			Load (kW)	Area (m^2)
	Name	T_{in} (°C)	T_{out} (°C)	Name	T_{in} (°C)	T_{out} (°C)		
E-114	Tires to the kiln	25	170	Hot air to coolers	290	275.6	20.30	3.4
E-115	Used oil to the kiln	25	170	Hot air to coolers	290	261.2	40.48	6.7
E-116	Coal dust to the kiln	55	170	Hot air to coolers	290	242.3	201.30	39.9
E-117	Air to the kiln	25	170	Hot air to coolers	290	202.6	5528.00	1505.1
Total							5790.08	1555.1

Table 3. Calculated parameters of new additional heat exchangers of cement factory.

benchmark level. The developed new concept design of energy-efficient cement manufacturing demonstrates the feasible and profitable solution that could be potentially used for retrofit as well as new factory design.

Heat exchanger	Cross-pinch heat transfer (kW)
E-100–E-102	0.0
E-103	8850.0
E-104–E-118	0.0
Network cross-pinch load	8850.0

Table 4. Cross-pinch heat load of retrofitted heat exchanger network.

Making an additional analysis with taking into account site-heating needs and power demands of a cement factory other solutions were also proposed in this chapter. The waste heat potential may be used, for example, for electricity generation with use of Organic Rankine Cycle, which is shown in **Figure 9a**. The heat sources, in this particular case, are process streams 3 and 6 (for more details see **Table 1**), and the calculated power generation is 2482 kW.

The estimated investment cost of power generation design is about 3.4 million EUR. The analysis of site demands in winter operation mode identified the other option of waste heat utilization, which is a district heating system. The low-grade heat potential of existing cement factory is given in **Figure 9b** (see curve 3) and due to this measure it is possible eliminating cold utility while the hot utility remains. In a particular case, the primary cold utility is power for air fans (680 kW), and from the other side, 20,225 kW of site heating demands may be covered by low-grade waste heat. The implementation of winter mode retrofit measures requires an estimated investment cost of 20.3 million EUR. The total saving of both retrofit designs during winter and summer operation modes is 7.648 million EUR. The payback time of combined retrofit for winter and summer operation modes is 3.01 per year assuming the total investment cost of 23.7 million EUR.

4.2.4. Impact and future work

An additional analysis of the energy-saving heat exchange system for cement factory presents a room for improvement in terms of efficient energy use. The grid diagram of the proposed

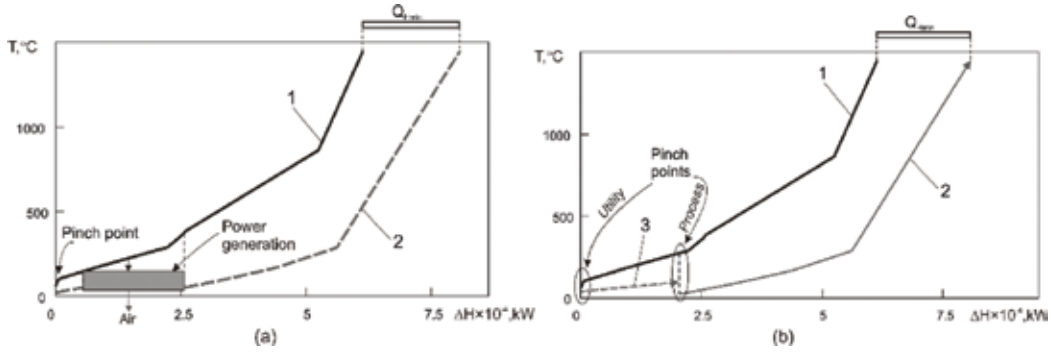

Figure 9. Composite curves of cement manufacturing for low-potential heat utilization; a—summer operation mode; b—winter operation mode; 1—hot composite curve; 2—cold composite curve with raw mill operation; 3—site heating demands; Q_{Hmin}—hot utility demands (developed after [29]).

heat exchanger network of the cement plant (**Figure 8**) has illustrated the ways to use waste heat. The potential of waste heat may be used for power generation by heat engines' application as demonstrated by Quoilin and Lemort [32]. The heat duty of waste gas is 14,338 kW and the temperature is 200°C or higher (see **Figure 8**). However, if the plant is operated in the mode without a raw mill, the power generation increases as well. Important points that have to be additionally discussed are the fluctuations of plant operation parameters, solid–gas source streams and installation features of power generator.

Another option of waste heat utilization from integrated cement production is the covering of site heating demands. The district heating system may be potentially supplied by waste heat to fulfill energy demands. The maximum capacity of waste heat that may be used is 14,338 kW as illustrated earlier. However, the technical implementation, including the heat losses and pressure drops, has to be additionally analyzed in details along with the economic issues of the retrofit design as well as energy planning. The results presented in this chapter have a cross-disciplinary impact and additional potential for future development of new cement manufacturing processes. A new design of a heat exchanger network could be a part of an energy-efficient environmentally friendly cement manufacturing process. It reduces fossil fuel consumption, CO_2 emission and operation cost of cement factories.

The utilization of low-grade heat for district heating systems could help for planning energy systems. The cement manufacturing process may be also considered as an energy source of district heating systems, additional power generation and so on. Nevertheless, the locations of cement factories have to be additionally analyzed with use of other systematic techniques, for example, based on total site analysis [33] to find a solution really close to the optimum.

5. Conclusion

This chapter provides results of research, which identified large energy-saving potential in the cement manufacturing process. Main results may be achieved by improvement of heat recovery, and potential of utility reduction is 30% and 29% for heating and cooling capacity, respectively, which translates to lower primary energy sources. These results were achieved by an updated process integration technique and update of a heat exchanger network. The case study of a particular cement factory was considered and feasible solutions were described that require an investment cost of 256,079 EUR with a payback period of 3.4 months. Besides, the improvement of energy efficiency may be additionally reached by improving the existing process of heat transfer equipment. Low-potential heat utilization covering 43% of power demands of the factory during summer operation mode and utilization of 20,225 kW of waste heat to site-district heating during winter operation are determined.

The use of excess heat may provide a way to reduce the primary energy sources and contribute to global CO_2 mitigation. This chapter shows a pathway for energy efficiency, main process restrictions and most feasible solutions for a new concept design of the cement industry. Nevertheless, the technical issues have to be additionally discussed for successful implementation.

Acknowledgements

This work was supported by the EC and Croatian Ministry of Science Education and Sports project "CARBEN" (NEWFELPRO Grant Agreement No. 39). The author acknowledges Holcim Company for provided data and personally Zoran Mohorovic for help in data extraction and reconciliation. The author acknowledges a SDEWES Centre and the Department of Energy, Power Engineering and Environment, Faculty of Mechanical Engineering and Naval Architecture, University of Zagreb, for administrative support.

Author details

Stanislav Boldyryev

Address all correspondence to: stas.boldyryev@fsb.hr

The Centre for Sustainable Development of Energy, Water and Environment Systems (SDEWES Centre), Zagreb, Croatia

References

[1] Mikulčić H, Vujanović M, Duić N. Improving the sustainability of cement production by using numerical simulation of limestone thermal degradation and pulverized coal combustion in a cement calciner. Journal of Cleaner Production. 2015;**88**:262-271. DOI: 10.1016/j.jclepro.2014.04.011

[2] IEA (International Energy Agency). Cement Technology Roadmap 2009: Carbon Emissions Reductions up to 2050. 2009. Available from: www.iea.org/publications/freepublications/publication/Cement_Roadmap_Foldout_WEB.pdf [Accessed: November 05, 2016]

[3] Mikulčić H, von Berg E, Vujanović M, Duić N. Numerical study of co-firing pulverized coal and biomass inside a cement calciner. Waste Management & Research. 2014;**32**:661-669. DOI: 10.1177/0734242X14538309

[4] Pardo N, Moya JA, Mercier A. Prospective on the energy efficiency and CO_2 emissions in the EU cement industry. Energy. 2011;**36**:3244-3254. DOI: 10.1016/j.energy.2011.03.016

[5] Liu F, Ross M, Wang S. Energy efficiency of China's cement industry. Energy. 1995;**20**(7):669-689. DOI: 10.1016/0360-5442(95)00002-X

[6] Chen H. Technical benefit and risk analysis on cement clinkering process with compact internal burning of carbon. Applied Thermal Engineering. 2015;**75**:239-247. DOI: 10.1016/j.applthermaleng.2014.08.051

[7] Hasanbeigi A, Menke C, Price L. The CO_2 abatement cost curve for Thailand cement industry. Journal of Cleaner Production. 2010;**18**:1509-1518. DOI: 10.1016/j.jclepro.2010.06.005

[8] Worrell E, Martin N, Price L. Potentials for energy efficiency improvement in the US cement industry. Energy. 2000;**25**:1189-1214. DOI: 10.1016/S0360-5442(00)00042-6

[9] Sheinbaum C, Ozawa L. Energy use and CO_2 emissions for Mexico's cement industry. Energy. 1998;**23**(9):725-732. DOI: 10.1016/S0360-5442(98)00022-X

[10] Mikulčić H, Cabezaas H, Vujanović M, Duić N. Environmental assessment of different cement manufacturing processes based on emergy and ecological footprint analysis. Journal of Cleaner Production. 2016;**130**:213-221. DOI: 10.1016/j.jclepro.2016.01.087

[11] Atmaca A, Yumrutas R. Analysis of the parameters affecting energy consumption of a rotary kiln in cement industry. Applied Thermal Engineering. 2014;**66**:435-444. DOI: 10.1016/j.applthermaleng.2014.02.038

[12] Stefanović G, Vučković G, Stojiljković M, Trifunović M. CO_2 reduction options in cement industry—The Novi Popovac case. Thermal Science. 2010;**4**:671-679. DOI: 10.2298/TSCI091211014S

[13] Zervaki M, Leptokaridis C, Tsimas S. Reuse of by-products from ready-mixed concrete plants for the production of cement mortars. Journal of Sustainable Development of Energy, Water and Environment Systems. 2013;**14**(2):152-162. DOI: 10.13044/j.sdewes.2013.01.0011

[14] Wang J, Dai Y, Gao L. Exergy analyses and parametric optimizations for different cogeneration power plants in cement industry. Applied Energy. 2009;**86**:941-948. DOI: 10.1016/j.apenergy.2008.09.001

[15] Seferlis P, Varbanov PS, Klemeš JJ. Applied thermal engineering solutions through process integration, modelling and optimisation. Applied Thermal Engineering. 2015;**89**:1001-1005. DOI: 10.1016/j.applthermaleng.2015.07.060

[16] Boldyryev S, Varbanov PS. Low potential heat utilization of bromine plant via integration on process and total site levels. Energy. 2015;**90**(1):47-55. DOI: 10.1016/j.energy.2015.05.071

[17] Klemeš J, Dhole VR, Raissi K, Perry S, Puigjaner L. Targeting and design methodology for reduction of fuel, power and CO_2 on total sites. Applied Thermal Engineering. 1997;**17**(8-10):993 1003. DOI: 10.1016/S1359-4311(96)00087-7

[18] Chew KH, Klemeš JJ, Wan Alwi SR, Manan ZA. Process modifications to maximise energy savings in total site heat integration. Applied Thermal Engineering. 2015;**78**:731-739. DOI: 10.1016/j.applthermaleng.2014.04.044

[19] Grip C-E, Larsson M, Harvey S, Nilsson L. Process integration. Tests and application of different tools on an integrated steelmaking site. Applied Thermal Engineering. 2013;**53**(2):366-372. DOI: 10.1016/j.applthermaleng.2012.03.040

[20] Baniassadi A, Momen M, Shirinbakhsh M, Amidpour M. Application of R-curve analysis in evaluating the effect of integrating renewable energies in cogeneration systems. Applied Thermal Engineering. 2016;**93**:297-307. DOI: 10.1016/j.applthermaleng.2015.09.101

[21] Mian A, Bendig M, Piazzesi G, Manente G, Lazzaretto A, Marechal F. Energy integration in the cement industry. Proceedings of 23rd European Symposium on Computer Aided Process Engineering. 2013;**32**:349-354. DOI: 10.1016/B978-0-444-63234-0.50059-2

[22] Mikulčić H, Vujanović M, Duić N. Reducing the CO_2 emissions in Croatian cement industry. Applied Energy. 2013;**101**:41-48. DOI: 10.1016/j.apenergy.2012.02.083

[23] Klemeš JJ, Varbanov PS, Wan Alwi SRW, Manan ZA. Process Integration and Intensification Saving Energy, Water and Resources. Berlin, Germany: De Gruyter; 2014. p. 252. DOI: 978-3-11-030685-9

[24] Pu W, Yue C, Han D, He W, Liu X, Zhang Q, Chen Y. Experimental study on organic Rankine cycle for low grade thermal energy recovery. Applied Thermal Engineering. 2016;**94**:221-227. DOI: 10.1016/j.egypro.2017.03.531

[25] Nemet A, Varbanov PS, Kapustenko P, Boldyryev S, Klemeš JJ. Capital cost targeting of total site heat recovery. Chemical Engineering Transactions. 2012;**29**:1447-1452. DOI: 10.3303/CET1229242

[26] Sun L, Doyle S, Smith R. Heat recovery and power targeting in utility systems. Energy. 2015;**84**:196-206. DOI: 10.1016/j.energy.2015.02.087

[27] Boldyryev S, Varbanov PS, Nemet A, Klemeš JJ, Kapustenko P. Minimum heat transfer area for total site heat recovery. Energy Conversion and Management. 2014;**87**:1093-1097. DOI: 10.3303/CET1229242

[28] HILECT Software [Internet]. 2015. Available from: powerlab.fsb.hr/sboldyryev/pinch/ [Accessed: December 09, 2017]

[29] Boldyryev S, Mikulčić H, Krajačić G, Duić N. Waste heat utilisation of Croatian cement industry accounting total site demands. Computer Aided Chemical Engineering. 2016;**38**:2223-2228. DOI: 10.1016/B978-0-444-63428-3.50375-1

[30] Boldyryev S, Mikulčić H, Mohorović Z, Vujanović M, Krajačić G, Duić N. The improved heat integration of cement production under limited process conditions: A case study for Croatia. Applied Thermal Engineering. 2016;**105**:839-848. DOI: 10.1016/j.applthermaleng.2016.05.139

[31] Yang Y, Shi L. Integrating environmental impact minimization into conceptual chemical process design—A process systems engineering review. Computers and Chemical Engineering. 2000;**24**:1409-1419. DOI: 10.1016/S0098-1354(00)00384-7

[32] Quoilin S, Lemort V. Technological and economical survey of organic Rankine cycle systems. In: 5th European Conference Economic and Management of Energy in Industry [Internet]; 2009. Available from: hdl.handle.net/2268/14609 [Accessed: December 09, 2017]

[33] Oluleye G, Jobson M, Smith R, Perry SJ. Evaluating the potential of process sites for waste heat recovery. Applied Energy. 2016;**161**:627-646. DOI: 10.1016/j.apenergy.2015.07.011

Chapter 8

Utilization of By-Product Materials in Ultra High-Performance Fiber Reinforced Cementitious Composites

Majed A. A. Aldahdooh

Additional information is available at the end of the chapter

http://dx.doi.org/10.5772/intechopen.74376

Abstract

This chapter presents a review on the use of various industrial wastes, by-products in the development of green ultra-high performance fiber-reinforced cementitious composites (UHPFRCCs), and their effects on mechanical properties of UHPFRCC, such as metakaolin, rejected fly ash, glass powder, and palm oil fuel ash. The outcomes of this chapter would encourage the use of by-product as a supplementary cementitious material. This could be useful in protecting the environment by minimizing the volume of waste disposed on the wasteland and minimizing the emission of greenhouse gases that are released during cement production, besides contributing to cost–saving, which could somehow contribute toward the sustainability of the concrete industry.

Keywords: waste materials, green concrete, cement, concrete technology, by-product materials

1. Introduction

Ultra-high performance fiber-reinforced cementitious composites (UHPFRCCs) are defined as a concrete matrix that are characterized with a high compression strength of 150–200 MPa, a uniaxial tension strength of 7–15 MPa, and a bending strength of 25–40 MPa [1–3]. UHPFRCC is characterized with a large binder content (cement and silica fume), a large volume of steel fiber, a low water/binder ratio (W/B), and a high microsilica [4]. Accordingly, UHPFRCCs compared with normal concrete (NC) and high-performance concrete (HPC) have become popular in practical applications [5, 6]. UHPFRCCs are more efficient in producing smaller, lighter, and thinner sections due to its superior properties [5, 7].

On the other hand, an increase in the cement content implies an increase in the overall demand for cement [8, 9], which could be translated into a greater cement production, which correspondingly increases the emission of certain greenhouse gases (CO_2, etc.), in addition to increasing the concrete cost as well as the electrical energy consumption [9]. Therefore, UHPFRCC products can be considered as uneconomical construction materials and pose a threat to the environment.

Aldahdooh et al. [10] stated that there are several methods that can be employed to reduce the binder content (cement and silica fume) in UHPFRCCs. For example, (i) optimizing the mix design of concrete using mathematical or statistical methods, such as response surface methodology, and so on [11, 12], (ii) utilizing industrial solid wastes and by-products as a supplementary cementitious materials (SCMs) in producing green UHPFRCCs, such as crushed quartz (CQ) [13], fly ash (FA) [14–16], palm oil fuel ash (POFA) [10, 17], recycled glass powder (RGP) [15], activated metakaolin (AM), and ground granulated blast-furnace slag (GBFS) [15, 18, 19].

Nowadays, the utilization of solid wastes is the challenge for engineers to use friendly SCMs produced at a reasonable cost with a low environmental impact. The addition of cost-saving materials by the replacement of a considerable amount of cement reduces CO_2 emission during the manufacturer of Portland cement. Moreover, SCMs can improve the majority of fresh and hardened properties of concrete [12, 20].

Based on the above, this review focused on the second method that is particularly dependent on the utilization of wastes and by-products in developing green UHPFRCCs, including their influence on the mechanical properties of UHPFRCCs.

2. Significance of review

This review focused on the utilization of industrial wastes and by-products in UHPFRCCs. This could lead to the greater utilization of SCMs in concrete. Subsequently, it could be useful in protecting the environment by minimizing the volume of waste disposed on the wasteland and minimizing the emission of greenhouse gases. Furthermore, it contributes to cost-saving, which contributes to the sustainability of the concrete industry.

3. UHPFRCCs

UHPFRCC is an advanced reinforced cementitious material and is one of the high-strength ductile concrete (HSDC) [1, 21]. In this review, the product is generally called UHPFRCC according to [22]. In the case of mechanical performance, UHPFRCC is characterized with a super-compressive strength, tensile strength, bending tensile strength, elastic modulus, energy absorption capacity, and elastic post-cracking bending strength. In terms of durability, UHPFRCC shows an extremely dense microstructure (negligible water adsorption, water and gas permeability, and porosity) and an extremely low diffusion coefficient [1–3, 23–25].

http://dx.doi.org/10.5772/intechopen.74376

Meanwhile, in the case of sustainability, this type of concrete still needs to be evaluated with regard to their high binder content (especially the cement content) relative to the regularly used mixtures [25].

3.1. Principles of UHPFRCC composition

The principles applied in UHPFRCC matrix development can be detailed based on previous studies:

1. Removal of coarse aggregate to enhance concrete homogeneity [3]; the recommended mean aggregate size used in producing UHPFRCCs is less than 1 mm and the aggregate-cement ratio can be up to 1.4 [21, 26].
2. Optimization of granular mixture [1, 3, 27]; ultrafine powder is added for the composition of fine-grained mixture, such as silica fume, fly ash, and so on. **Figure 1** shows the physical effect of ultrafine powder (e.g., silica fume), as
   - Filler between the cement particles,
   - Lubricant,
   - Psozzolanic materials because this substance reacts chemically with calcium hydroxide ($Ca(OH)_2$) that is also written as (CH). These substances produce compounds with cementitious properties (calcium silicate hydrates (C-S-H)/"cement gels"). This finding is reflected automatically by the decrease of porosity in the bulk and particularly in the interfacial zone. These materials improve the mechanical properties of the cement paste by reacting with CH.
3. Decreasing the W/C ratio using high-range water-reducing admixture; this maintains the small spacing of the cement grains, which decreases the space for the interfacial zone formation [1].
4. Optionally, post-setting heat treatment to enhance mechanical properties of the microstructure [1, 28].
5. Optionally, the application of pre-setting pressure for better compaction [1, 28].

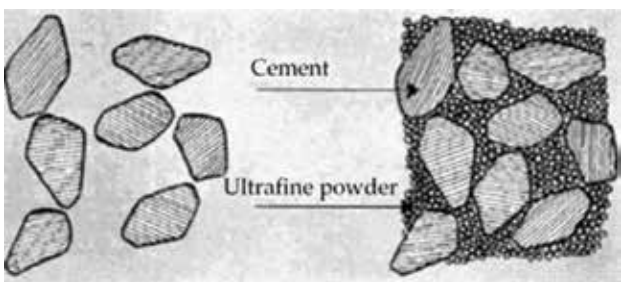

Figure 1. Ultrafine powder acting as "filler" between the cement particles [1].

3.2. Constituent materials and mix proportions of UHPFRCCs

In general, UHPFRCC is characterized as a composite that has a large content of cement and silica fume, a large volume of steel fiber, a high dosage of superplasticizer (SP), a low water/binder ratio, and the absence of coarse aggregates that are larger than 4 mm [4]. **Table 1** shows a summary of the ranges of UHPFRCC compositions and the average material properties. One example of UHPFRCCs is known under the trade name, CARDIFRC [22, 29, 30].

More details about the function of each ingredient in the UHPFRCC mix are presented in the following subsection.

3.2.1. Cement

Normally, ordinary Portland cement (OPC) can be used to produce UHPFRCCs [13, 35, 36]. UHPFRCC is characterized with a high cement content, which can be as high as 1000 kg/m^3 (**Table 1**). Vernet [37] stated that in the matrix of UHPFRCCs, not all of the cement contents become hydrated because of a low water content.

For a given W/C, the strength of concrete is largely dependent on cement content. Increasing the cement content does not improve the strength, after the required content is reached [38, 39]. A high cement content both increases air permeability and chloride penetration and may cause shrinkage-related-cracking problems [40–42], which will shorten the longevity of concrete, thus decreasing its performance (durability and strength). To prevent these problems,

		UHPFRCCs (kg/m^3)	**CARDIFRC [2, 22, 29, 30]**
Matrix composition	Portland cement	(700–1000) [1, 31]	744–855
	Coarse aggregate	(0–200) [1, 31]	0
	Fine aggregate	(1000–2000) [1, 31]	940–1173
	Silica fume	(200–300) [1, 31]	178–214
	Water	(110–200) [1, 31]	149–188
	Superplasticizer	(9–71) [32]	28–55
	Reinforcement/fibers	(>150) [1, 31]	468
	Water/cement ratio	(<0.24) [1, 31]	0.20–0.22
	Water/binder ratio	(<0.22) [1, 31]	0.16–0.18
	Superplasticizer/cement ratio	(0.018–0.051) [32]	0.033–0.074
	Silica fume/cement ratio	(>0.25) [1, 31]	0.24–0.25
Properties	Compressive strength (MPa)	(>150) [1, 31]	>185
	Tensile strength (MPa)	(>7) [33]	12–13.5
	Modulus of elasticity (GPa)	(50–70) [1, 31]	>48
	Splitting tensile strength (MPa)	(>18) [34]	24–25
	Flexural strength (MPa)	(>25) [1, 3]	>30

Table 1. The range of UHPFRCC compositions and average mechanical properties.

appropriate cement content should be used [39]. On the other hand, for a given W/C, decreasing cement content reportedly decreases permeability [38, 39, 41].

Yurdakul [39] stated that workability is a function of W/C and cement content; increasing W/C or cement content improves workability. The workability is affected by paste volume, because the paste lubricates the aggregates [39, 41]. For a given water content, decreasing the cement content increases the stiffness of concrete having poor workability [39, 43]. Although workability is increased by an increasing cement content, it causes higher internal temperatures in the concrete during the finishing and curing processes [39]. In addition, the workability increases as the cement content (paste content) increases for a given W/C ratio and aggregate content because there is more paste to lubricate the aggregates in the mixtures [38, 39].

Aldahdooh [12] stated that no special standard is published for UHPFRCC mix design. Therefore, an ideal strategy is needed for improving the mechanical properties of UHPFRCC relative to the binder contents. This finding can be realized by optimizing the mix design of concrete using mathematical or statistical methods or by utilizing SCMs.

In the case of using the mathematical or statistical methods, the mix design of UHPFRCC is still based on trial mix; therefore, no standard has been adopted yet and no rigorous mathematical approach is available. De Larrard and Sedran [44] already optimized the ultra-high performance concrete (UHPC) mix proportion using density-packing model (solid suspension model). The optimal mix was characterized with a cement content up to 1080 kg/m^3 and silica fume was up to 334 kg/m^3. Furthermore, the mix proportion of reactive powder concrete can be optimized using the group method of data handling and genetic programming [45]. They concluded that the optimum cement amount must be approximately from 1400 to 1600 kg/m^3, and the amount of silica fume might be 20 or 25% cement content. Yu, et al. [46] recently used the modified Andreasen & Andersen particle-packing model to achieve a densely compacted cementitious matrix. They concluded that by applying this modified model, producing dense UHPFRCCs using a relatively low binder content is possible as outlined in **Table 2**. They also stated that a large amount of unhydrated cement in the matrix has been observed, which can be further replaced by fillers to improve workability and cost efficiency of UHPFRCCs.

Recently, an advanced optimization method called as a response surface methodology (RSM) has been used for optimizing the binder contents by Aldahdooh et al. [11]. They concluded that although the results indicate that the prediction by RSM was satisfactory in adjusting the amount of binders in the production of UHPFRCCs materials, these values still need to be reduced further, meaning that another method could be used to reduce the cement and silica fume contents through partial replacement of cement by external ultrafine (or by-product) materials, such as crushed quartz [13], fly ash [14–16], recycled glass powder [15], and ground granulated blast-furnace slag [15, 18, 19], palm oil fuel ash [51], as outlined in **Table 2**.

3.2.2. Silica fume

Silica fume is considered as one of the main components in producing UHPFRCCs [1, 13]. Silica fume is an extremely fine non-crystalline silica produced by electric arc furnaces as a by-product of smelting process in the metallic silicon or ferrosilicon alloy production as outlined

References		Binder (kg/m^3)					W/B	St.F. (Vol. %)	Comp. 28 d (MPa)
		C	GGBS	SF	L.S.	POFA			
[47]	Without SCMs	950	0	238	0	0	0.2	2	190
[2, 22, 29, 30]		855	0	214	0	0	0.18	6	207
[2, 22, 29, 30]		744	0	178	0	0	0.16	6	185
[48]		860	0	215	0	0	0.2	2	198
[46]		875	0	44	0	0	0.19	2.5	156
[25]		1011	0	58	0	0	0.15	2	160
[49]		960	0	240	0	0	0.16	2.5	155
[50]		1050	0	275	0	0	0.14	6	160
[5]	With SCMs	657	418	119	0	0	0.15	2	150
[46]		612	0	44	263	0	0.19	2.5	142
[46]		700	0	44	175	0	0.19	2.5	149
[51, 52]		360	0	214	0	290	0.19	6	158

SCM refers to supplementary cementitious materials; C refers to cement content; GGBS refers to ground granulated blast-furnace slag; SFrefers to silica fume; L.S. refers to limestone; W/B refers to water-binder ratio; St.F. refers to steel fiber; Comp. 28 d refers to compressive strength at day 28.

Table 2. Examples on the binder content and compressive strength of optimized UHPFRCCs.

in **Table 2**. Silica fume is a highly reactive pozzolanic material. This substance has spherical-shaped particle and is characterized with an average particle size between 0.1 and 0.2 μm. Moreover, the SiO_2 content ranges from 58 to 98% [53]. Silica fume is observed to be much finer and have a higher SiO_2 content compared with the other by-products. For a given water content, addition of silica fume more than the limited value will degrade the workability of the mix, which results from the larger surface area of silica fume [54, 55].

The main functions of silica fume in UHPFRCCs are (i) acting as a filler between cement particles, (ii) for a given water-binder ratio (W/B), improving mixture lubrication caused by particle shape (sphericity), and (iii) producing hydration products by pozzolanic activity [3, 13, 35] as presented in **Figure 2**.

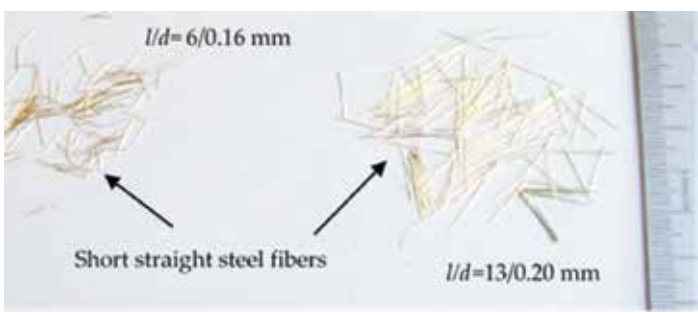

Figure 2. An example of steel fiber types used in UHPFRC [56].

The utilization of silica fume in microfiber-reinforced concrete can improve the degree of fiber dispersion, matrix interface, and interfacial zone [57], which results from the fineness of silica fume particles when compared with cement [55, 57, 58]. Furthermore, the bonding between steel fibers and matrix of steel fiber-reinforced concrete is significantly improved by utilizing silica fume. In addition, silica fume can enhance the properties of the materials used as filler [55, 58].

The theoretical amount of silica fume required for the reaction with cement product is 18% cement content [59]. The silica fume content must be practically increased from 25 to 30% cement content to obtain the densest mixture and to achieve the greatest compressive strength [1, 31, 59]. Chan and Chu [60] concluded that the highest interfacial bond strength and pullout energy between the steel fiber and concrete matrix can be obtained at a silica fume dosage of as high as 30%. The interfacial-toughening effect in the bond strength decreases when the silica fume content increases to 40%.

3.2.3. Fiber reinforcement

UHPFRCCs without reinforcement with fibers may exhibit high strength but are extremely brittle. The additional function of fibers in UHPFRCCs is enhancing ductility in tension and improving its tensile capacity [1, 13, 26].

UHPFRCC mix is generally characterized with a steel fiber content that is more than 2.5% of its volume as outlined in **Tables 1** and **2**. The dimensions range from 0.1 to 0.25 mm in diameter and from 6 to 20 mm in length with a tensile strength of more than 2000 MPa [21, 34]. For example, a large amount (up to 6% by volume) of brass-coated short straight steel fibers (6 and 13 mm) with 0.16 mm diameter has been used in CARDIFRC materials [22, 29]. The short fiber was used to enhance flexural and tensile strength, whereas the long fiber was used to increase toughness. Generally, the long steel fiber enhances the roughness of matrix by enhancing the tensile strength and strain capacity at the breakage stage at the same time, while the short steel fiber improves the tensile strength of matrix more than strain capacity at the breakage stage [22, 29].

Vande Voort et al. [13] stated that fiber size and aggregate size in any concrete mix are considered as the main factors that influence mix workability. Hence, in the absence of coarse aggregates, fiber size is considered as the primary factor influencing concrete flow (e.g., UHPFRCCs). Moreover, UHPFRCC workability tends to decrease with an increasing fiber content [13, 61].

The steel fiber-reinforced concrete with a high workability has a high probability of experiencing steel fiber segregation, which automatically reflects mechanical properties and concrete performance [62].

3.2.4. Superplasticizer

W/C ratios used in producing UHPFRCCs are generally less than 0.20, which lead to a notable reduction in the porosity of UHPFRCC matrix; this reduction in porosity increases

impermeability. Thus, significant improvement on the strength and durability of UHPFRCC matrix is observed; however, special SPs should be used to have adequate flowability [63].

SPs are chemical admixtures used for reducing water demand. They are also known as high-range water reducers (HRWR) [64]. Ultra-high-range polycarboxylic ether-based (PCE-based) SPs are commonly used to have adequate concrete UHPFRCC flowability. Thus, UHPFRCC behaves similar to self-compacting concrete. Therefore, UHPFRCC can be used for casting very slender elements [34, 36, 63].

Alsadey [65] concluded that compressive strength decreases if the applied SP dosage is beyond the optimum dosage because segregation and bleeding phenomena will occur. This finding can affect concrete uniformity and cohesiveness.

3.2.5. Sand

The fine aggregate (sand) functions by confining the cement matrix to add strength [13, 66]. Yurdakul [39] and Shilstone and Shilstone [67] revealed that an insufficient amount of sand induces the segregation of mixture and increases mix flow. By contrast, increasing sand content causes stiff mixture because the sand has a high water requirement due to its high specific surface area. Moreover, workability decreased as the cement content decreased for a given W/C and aggregate content because of inadequate amount of paste that lubricates the aggregate [38, 39, 68, 69].

Quartz sand is usually used for UHPFRCC production. This sand type is not chemically active in the cement hydration reaction [13, 66]. As outlined earlier, UHPFRCC is characterized as a composite that has a large volume of steel fiber and lacks coarse aggregates that are larger than 4 mm [4].

The recommended mean aggregate size used in producing UHPFRCCs is less than 1 mm, and the aggregate-cement ratio can be up to 1.4 [21].

3.2.6. Water

Generally, decreasing the W/C will decrease the permeability, the porosity of the paste decreases and concrete becomes less permeable thus reducing the passage of water and aggressive compounds such as chlorides and sulfates, thus the durability and strength increased [39, 41, 70]. Increasing W/C will increase workability [70]. Strength is considered to be a function of W/C [38, 39, 41]. To increase strength, thus, the W/C should be reduced; it is more efficient to reduce the water content than to use more cement [39].

Improving the relative density of concrete is the main goal in producing UHPFRCCs and not water content reduction. Several researchers optimized the water-binder ratio (W/B) for UHPFRCCs. Wen-yu et al. [71] reported an optimum W/B ration of 0.16 based from their experimental work. **Table 3** summarizes the mean and range for the W/C ratios and W/B ratios used in UHPFRCCs. The used W/B ration in producing UHPFRCC was in the range of 0.10–0.25, while for W/C it was found to be in the range of 0.13–0.37.

Properties	Low	Mean	High
W/B	0.10	0.17	0.25
W/C	0.13	0.22	0.37

Table 3. Classification of W/B and W/C ratios for UHPFRCCs summarized by Vande Voort et al. [13].

4. Utilization of by-products in UHPFRCC

Based on the earlier sections, there are several types of by-products or industrial wastes other than SF that can be used as an SCM or as an additive material in UHPFRCC products. Some of these wastes are metakaolin (MK), rejected fly ash, ground-granulated blast furnace slag, rice husk ash, recycled glass powder, palm oil fuel ash, and so on. The general chemical and physical properties of some of these SCMs and ordinary Portland cement (OPC) are summarized in **Table 4**. The influence of some of these SCMs on mechanical properties of UHPFRCC is described in the following subsections.

4.1. Metakaolin

Metakaolin (MK) is considered as a by-product material that is manufactured from kaolin clay. MK is a very fine-white clay mineral that has been traditionally used in porcelain production.

	OPC	FA	r-FA	GGBS	SF	MK	GP	RHA	UPOFA
SiO_2	20.44	35–60	47.23	34.4	91.4	53.87	71.4	88.32	65.01
Al_2O_3	2.84	10–30	24.54	9.0	0.09	38.57	1.4	0.46	5.72
Fe_2O_3	4.64	4–20	8.42	2.58	0.04	1.4	0.2	0.67	4.41
CaO	67.73	1–35	8.28	44.8	0.93	0.04	10.6	0.67	8.19
MgO	1.43	1.98	1.62	4.43	0.78	0.96	2.5	0.44	4.58
SO_3	2.20	0.35	0. 39	2.26	0.01	—	0.1	—	0.33
Na_2O	0.02	0.48	—	0.62	0.39	0.04	12.7	0.12	0.07
K_2O	0.26	0.4	—	0.5	2.41	2.68	0.5	2.91	6.48
MnO	0.16	—	—	—	0.05	0.01	—	—	0.11
TiO_2	0.17	—	0.99	—	0.0	0.95	—	—	0.25
Specific gravity	3.05	2.2–2.8	2.19	2.79	2.6–3.8	2.5	2.48	2.11	2.55
Particle size (μm)	10–40	≤45	>45	—	0.1	0.5–20	<45	11.5–31.3	2.06
Specific surface (m^2/g)	1.75	5–9	0.119	0.4–0.599	16.455	12.174	0.756	30.4–27.4	1.77

OPC, refers to ordinary Portland cement; GGBS, refers to ground-granulated blast-furnace slag; SF, refers to silica fume; FA, refers to fly ash; r-FA, refers to rejected fly ash; GP, refers to glass powder; RHA, refers to rice husk ash; MK, refers to metakaolin; POFA, refers to palm oil fuel ash.

Table 4. Chemical and physical properties of OPC and mineral admixtures (%) [12, 72–74].

MK is considered as highly pozzolanic materials, where major constituents of MK are SiO_2 and Al_2O_3, as tabulated in **Table 4** [75].

Table 4 shows that MK is characterized with the highest alumina content compared with other mineral admixtures and OPC, showing the capability to produce strengthening gel, that is, calcium aluminates hydrate (CAH) by reacting with the primary hydrate of cement. Moreover, MK has a considerable silica content which produce calcium silicate hydrate (CSH), by reacting with calcium hydroxide [72].

Nuruddin et al. [72] studied the effect of MK and the aspect ratio (l/d) of fibers on the mechanical properties of high-strength ductile concrete (HSDC) with constant slump (50 ± 10) as shown in **Figure 3**.

Nuruddin et al. [72] concluded that as the MK content increases the mechanical properties improved as shown in **Figure 3**. Among all the mix, the highest strengths have been observed with 10% MK and 2% volume fraction.

MK develops a high pozzolanic activity, however, degrading workability. Moreover, MK is its high embodied CO_2 generated for the production of one ton of MK, which is about 330 kg/ton compared with silica fume and fly ash 14 and 4 kg/ton, respectively. On the other hand, MK is characterized with a faster strength development along with a lower drying shrinkage compared with plain cement and silica fume [76].

4.2. Rejected fly ash

Kou and Xing [15] stated that more than 1 million tons of fly ash is produced annually in Hong Kong, as a by-product of electricity generation, where the finer fraction (f-FA) produced by passing the raw materials of ash via a classifying process is routinely used in the production of blended cements for construction. f-FA has a fineness requirement of not more than 12% by mass retained on the 45-μm test sieve. However, the remaining proportion is rejected due to its large particle size. In Hong Kong, this rejected fly ash (r-FA) has to be disposed of in large lagoons, creating an ever-increasing environmental hazard. Effect of r-FA and steam curing on mechanical properties of UHPFRC is shown in **Figure 4**. The chemical and physical properties of r-FA are tabulated in **Table 4**.

Kou and Xing [15] concluded that as the r-FA replacement level with silica sand increases, the mechanical strengths of UHPRCC tend to increase compared with the control mix. This increase in strength due to the replacement of fine aggregate with r-FA is attributed to (1) the improvement of packing density with r-FA and (2) the pozzolanic action of r-FA. However, the rate strength development decreases with the increase in r-FA content. This is due to the fact that r-FA reacts very slowly with calcium hydroxide liberated during the hydration of cement and does not contribute significantly to the densification of the concrete matrix at early ages. The highest replacement level is reached up to 50%.

4.3. Glass powder

Jin et al. [77] stated that the recycling process of glass is considered as a major problem in urban areas of developed countries.

http://dx.doi.org/10.5772/intechopen.74376

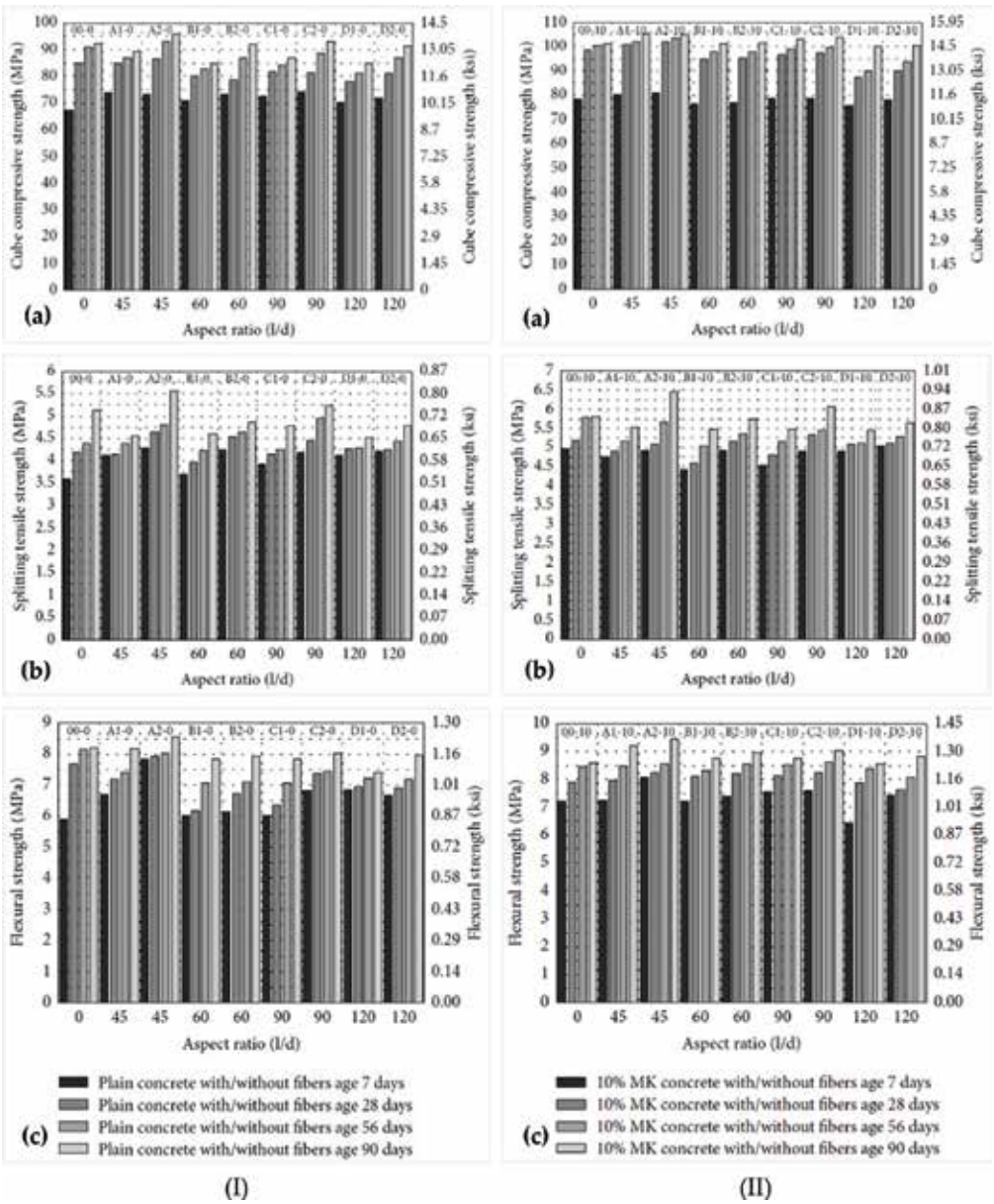

Figure 3. Influence of MK and fibers on mechanical properties of HSDC: (I) Plain concrete and (II) MK concrete: (a) Compressive Strength, (b) Splitting Strength, and (c) Flexural Strength [72].

Glass has been used in the concrete production as a crushed glass, as a raw siliceous material in the production of Portland cement [78], and as a hydration-enhancing filler [78].

Jin et al. [77] stated that glass powder (GP) is considered as amorphous and characterized with a high silica content. A particle size of 45 μm or less is reported to be favorable for pozzolanic reaction [15, 79].

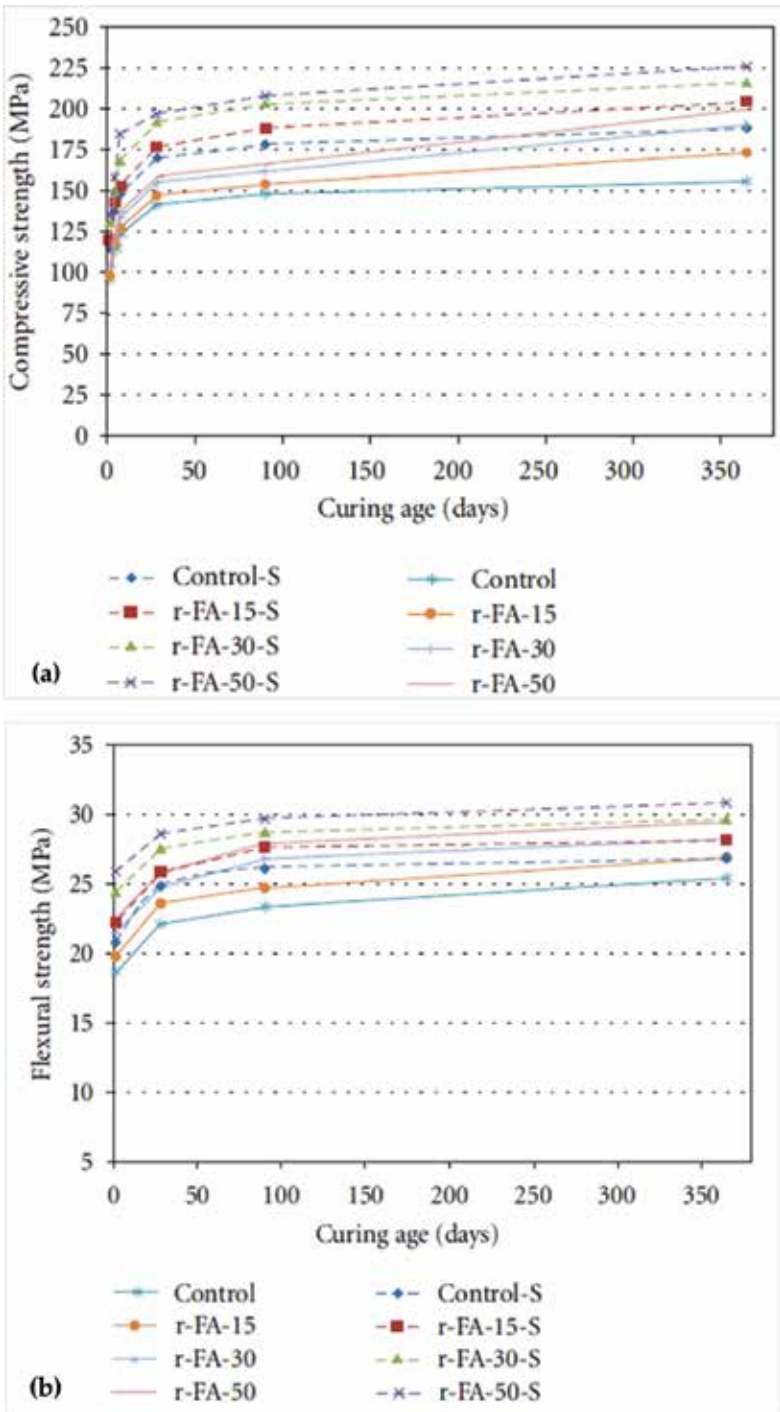

Figure 4. Influence of r-FA and steam curing (S) on mechanical properties of UHPFRC: (a) Compressive strength and (II) Flexural strength [15].

Several studies [80, 81] have showed that a cement replacement between 10 and 20% yields the highest strength, while fine aggregate replacement of up to 40% has little effect on compressive strength.

Kou and Xing [15] utilized the GP as supplementary cementitious materials in UHPFRC. The effect of GP and steam curing on mechanical properties of UHPFRC is shown in **Figure 5**. The results showed that the replacement of cement by glass powder decreased the early (before 7 days), but increased the later (after 28 days) strengths of UHPFRC, at all ages. The highest replacement level reached up to 30%.

4.4. Palm oil fuel ash

Palm oil fuel ash (POFA) is a by-product of burning: empty fruit bunches, kernel shells, and fibers, which are used in generating electricity for the boiler of palm oil mills [82, 83].

Palm oil industry is one of the major agro-industries in countries, such as Malaysia, Indonesia, and Thailand [84]. Most of the POFAs are disposed as waste in landfills, which may contribute to environmental problems in the future [85]. Therefore, a lot of research works have been conducted to find a suitable solution for proper POFA disposal.

Many researchers have found that POFA has pozzolanic qualities and properties in concrete. In fact, POFA can be considered as a pozzolanic material [86–88].

Awal and Hussin [84] showed that POFA can be utilized as supplementary cementitious materials, and POFA has a high potential in suppressing expansion associated with alkali-silica reaction in concrete.

POFA has been utilized in high-performance concrete (HPC) production, the highest compressive strength was found in the range of 60–86 MPa, which was obtained at POFA (with a median particle size of approximately 10 μm) replacement level of 20% at day 28 with 550–560 kg/m^3 total binder [87, 89, 90].

Megat Johari et al. [88] modified the treatment and grinding process of POFA by heat treatment to remove the excess carbon content and to decrease the POFA median particle size to approximately 2.06 μm as tabulated in **Table 4**. A highly efficient pozzolan was obtained through their treatment processes. The modified ultrafine POFA (UPOFA) was utilized for improving the properties of high-strength green concrete (HSGC). They concluded that the compressive strength could exceed 95 MPa with a replacement level of up to 60% OPC with UPOFA.

Recently, Aldahdooh et al. [10] reduced the binder content by replacing greater portions of the cement and silica fume in UHPFRCCs with UPOFA as supplementary cementitious materials while generally maintaining its mechanical properties as shown in **Figure 6**. The results showed that the ultimate flexural and uniaxial tensile strengths increased when the replacement levels of OPC by UPOFA increased and decreased when the replacement levels of densified silica fume (DSF) by UPOFA increased. Moreover, the optimal result was the production of a green UHPFRCCs (GUSMRC) with a low cement content of 360.25 kg/m^3 and

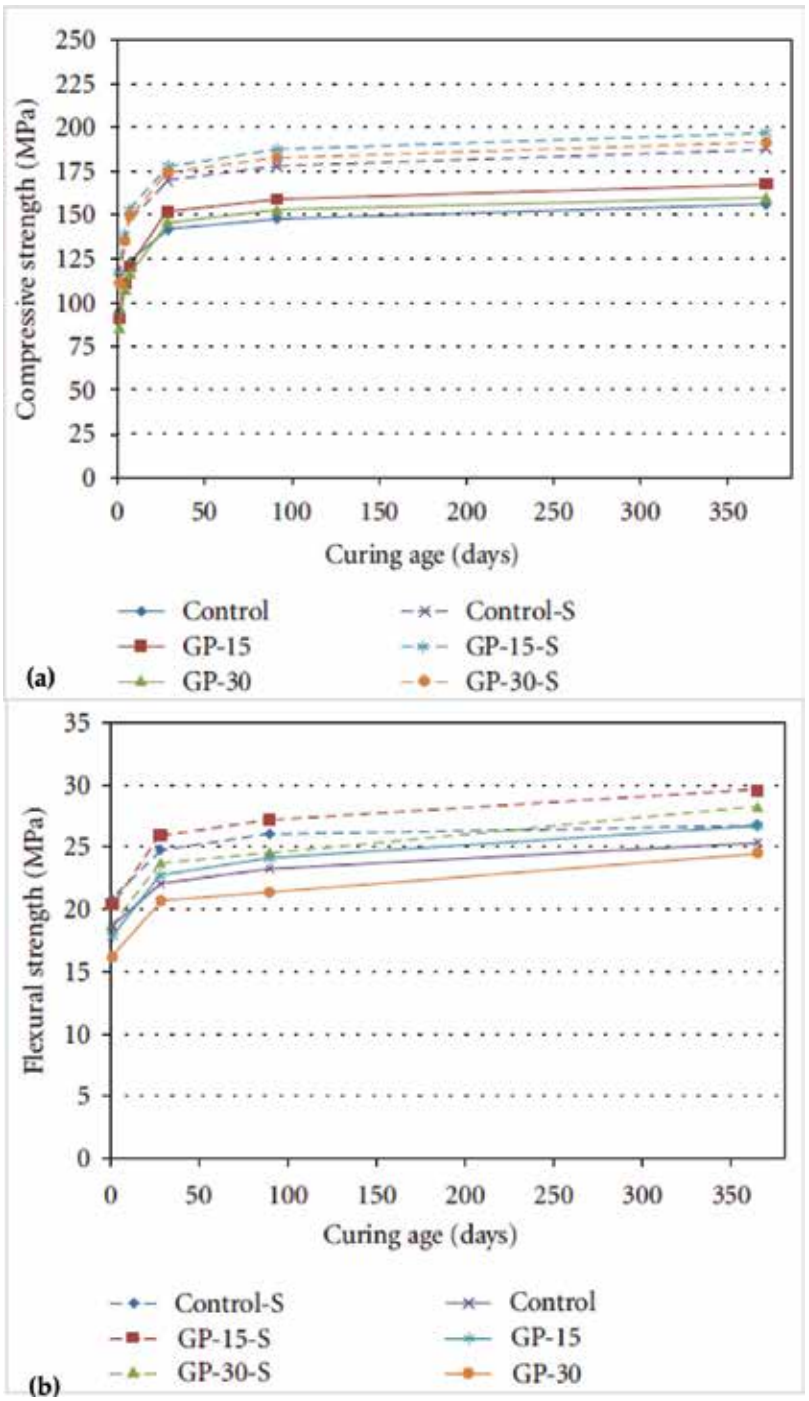

Figure 5. Influence of GP and steam curing (S) on mechanical properties of UHPFRC: (a) compressive strength and (II) flexural strength [15].

http://dx.doi.org/10.5772/intechopen.74376

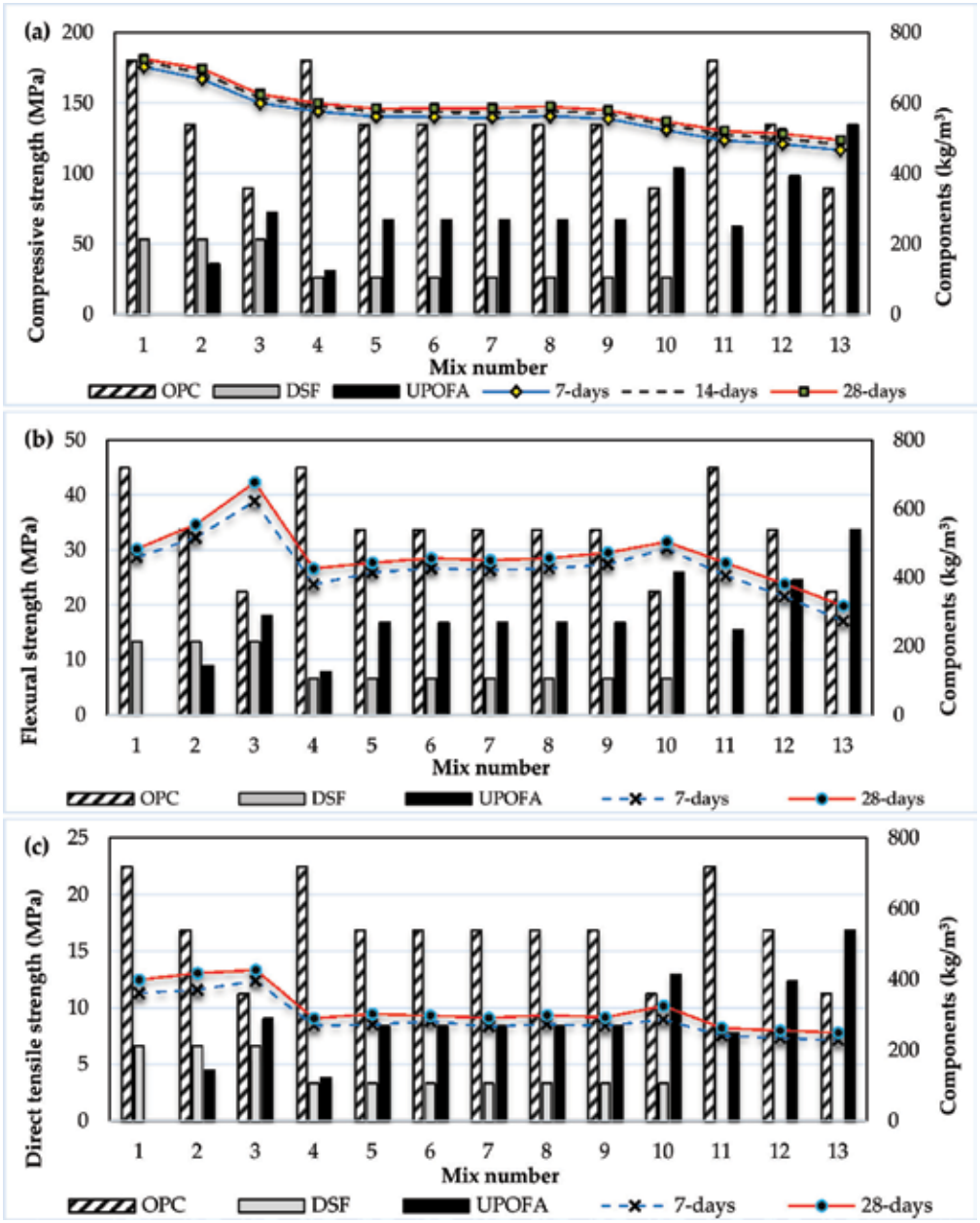

Figure 6. Effect of UPOFA on the mechanical strength of UHPFRCCs at 7 and 28 days: (a) compressive strength, (b) flexural strength, and (c) tensile strength [10, 17].

with a ultra-high compressive strength of 158.28 MPa as given in **Table 5**. Furthermore, the use of UPOFA (particularly in high volume) can contribute to a healthier and more sustainable environment, which increases green concrete products and may reduce concrete cost.

Components		(kg/m^3)
Cement		360.25
Microsilica		214.25
UPOFA		290.52
Mining sand		1057.3
Water		168.30
Superplasticizer		50.43
Steel fibers	$l_1 = 6$ mm	390
	$l_2 = 13$ mm	78
Water/binder		0.195
Microsilica/binder		0.247
Mechanical properties (28 days)	Compressive strength (MPa)	156.72
	Direct tensile strength (MPa)	13.35
	Flexural strength (MPa)	42.38
	Splitting tensile strength (MPa)	20.46
	Modulus of elasticity (GPa)	46.72

Table 5. Optimum GUSMRC mix constituents and properties [10, 17, 51].

Author details

Majed A. A. Aldahdooh

Address all correspondence to: maged.1987@live.com

Civil and Environmental Engineering Program, West Virginia University (WVU) - Bahrain Campus, Riffa, Kingdom of Bahrain

References

[1] Spasojević A. Structural implications of ultra-high performance fibre-reinforced concrete in bridge design. Ph.D thesis. EPFL; 2008

[2] Benson S, Karihaloo B. CARDIFRC®-development and mechanical properties. Part III: Uniaxial tensile response and other mechanical properties. Magazine of Concrete Research. 2005;**57**(8):433-443

[3] Richard P, Cheyrezy M. Composition of reactive powder concretes. Cement and Concrete Research. 1995;**25**(7):1501-1511

[4] Wille K, Naaman AE, Parra-Montesinos GJ. Ultra-high performance concrete with compressive strength exceeding 150 MPa (22 ksi): a simpler way. ACI Materials Journal. 2011; **108**(1):46-54

[5] Brühwiler E, Denarié E. Rehabilitation of concrete structures using Ultra-High Performance Fibre Reinforced Concrete. In: Proceedings, the Second International Symposium on Ultra-High Performance Concrete; 2008

[6] Iskhakov I et al. High performance repairing of reinforced concrete structures. Materials & Design. 2013;**44**:216-222

[7] Yang S, Diao B. Influence of curing regime on the ductility of ultra-high performance fiber reinforced concrete (UHPFRC). In: ICCTP 2009@ Critical Issues In Transportation Systems Planning, Development, and Management; ASCE; 2009

[8] Worrell E et al. Carbon dioxide emissions from the global cement industry 1. Annual Review of Energy and the Environment. 2001;**26**(1):303-329

[9] Arshad MF. Influence of multiple blended binders on engineering properties and durability of concrete, Ph.D. thesis, in Civil Engineering. Malaysia: Universiti Sains Malaysia; 2010

[10] Aldahdooh MAA, Bunnori NM, Megat JMA. Development of green ultra-high performance fiber reinforced concrete containing ultrafine palm oil fuel ash. Construction and Building Materials. 2013;**48**:379-389

[11] Aldahdooh MAA, Bunnori NM, Megat Johari MA. Evaluation of ultra-high-performance-fiber reinforced concrete binder content using the response surface method. Materials & Design. 2013;**52**:957-965

[12] Aldahdooh MAA. Development of Pofa-based Green Ultra-high Performance Fiber Reinforced Cementitious Composites as Retrofitting Material. Malaysia: Universiti Sains Malaysia; 2014

[13] Vande Voort T, Suleiman M, Sritharan S. Design and Performance Verification of UHPC Piles for Deep Foundations (Final report of project entitled Use of Ultra-High Performance Concrete in Geotechnical and Substructure Applications). Lincoln Way: Ames; 2008

[14] Mehta PK. High-performance, high-volume fly ash concrete for sustainable development. In: International Workshop on Sustainable Development and Concrete Technology. California, Berkeley, USA: Kejin Wang Beijing; 2004

[15] Kou SC, Xing F. The effect of recycled glass powder and reject fly ash on the mechanical properties of fibre-reinforced ultrahigh performance concrete. Advances in Materials Science and Engineering. 2012;**2012**:8

[16] Xie Y et al. Optimum mix parameters of high-strength self-compacting concrete with ultrapulverized fly ash. Cement and Concrete Research. 2002;**32**(3):477-480

[17] Aldahdooh MAA, Bunnori NM, Megat Johari MA. Influence of palm oil fuel ash on ultimate flexural and uniaxial tensile strength of green ultra-high performance fiber reinforced cementitious composites. Materials & Design. 2014;**54**:694-701

[18] Bayramov F, Taşdemir C, Taşdemir M. Optimisation of steel fibre reinforced concretes by means of statistical response surface method. Cement and Concrete Composites. 2004;**26**(6): 665-675

[19] Yazici H. The effect of curing conditions on compressive strength of ultra high strength concrete with high volume mineral admixtures. Building and Environment. 2007;**42**(5):2083-2089

[20] Badur S, Chaudhary R. Utilization of hazardous wastes and by-products as a green concrete material through S/S process: A review. Reviews on Advanced Materials Science. 2008;**17**(1–2):42-61

[21] Russell HG, Graybeal BA. Ultra-High Performance Concrete: A State-of-the-Art Report for the Bridge Community. Georgetown Pike, McLean, VA. 22101–2296: Federal Highway Administration; 2013

[22] Alaee F, Karihaloo B. Retrofitting of reinforced concrete beams with CARDIFRC. Journal of Composites for Construction. 2003;**7**(3):174-186

[23] Perry VH, Seibert PJ. The use of UHPFRC (Ductal®) for bridges in North America: The technology, applications and challenges facing commercialization. In: Proceedings of the Second International Symposium on Ultra High Performance Concrete, Kassel; 2008

[24] Park SH et al. Tensile behavior of ultra high performance hybrid fiber reinforced concrete. Cement and Concrete Composites. 2012;**34**(2):172-184

[25] Toledo Filho RD et al. Performance assessment of ultra high performance fiber reinforced cementitious composites in view of sustainability. Materials & Design. 2012;**36**:880-888

[26] Tayeh BA et al. Mechanical and permeability properties of the interface between normal concrete substrate and ultra high performance fiber concrete overlay. Construction and Building Materials. 2012;**36**:538-548

[27] Grabowski E, Gillott JE. Effect of replacement of silica flour with silica fume on engineering properties of oilwell cements at normal and elevated temperatures and pressures. Cement and Concrete Research. 1989;**19**(3):333-344

[28] Reda MM, Shrive NG, Gillott JE. Microstructural investigation of innovative UHPC. Cement and Concrete Research. 1999;**29**(3):323-329

[29] Benson S, Karihaloo B. CARDIFRC®-development and mechanical properties. Part I: Development and workability. Magazine of Concrete Research. 2005;**57**(6):347-352

[30] Karihaloo BL. CARDIFRC – From concept to industrial application. In: Parra-Montesinos G, Reinhardt H, Naaman AE, editors. High Performance Fiber Reinforced Cement Composites 6. Netherlands: Springer; 2012. pp. 397-404

[31] de Larrard F, Sedran T. Mixture-proportioning of high-performance concrete. Cement and Concrete Research. 2002;**32**(11):1699-1704

[32] Graybea BA. Characterization of the behavior of ultra-high performance concrete. Ph.D. thesis, in U.S. Department of Transportation, McLean University: Georgetown Pike, McLean, VA 22101–2296; 2006

[33] Toutlemonde F et al. Designing and Building with UHPFRC2010, John Wiley & Sons, Inc. New York: Wiley Online Library

[34] Nematollahi B et al. A review on ultra high performance 'ductile' concrete (UHPdC) technology. International Journal of Civil and Structural Engineering. 2012;**2**(3)

[35] Tayeh BA et al. The role of silica fume in the adhesion of concrete restoration systems. Advanced Materials Research. 2013;**626**:265-269

[36] Tayeh BA, Abu Bakar B, Megat Johari M. Characterization of the interfacial bond between old concrete substrate and ultra high performance fiber concrete repair composite. Materials and Structures. 2012:1-11

[37] Vernet CP. Ultra-durable concretes: structure at the micro-and nanoscale. MRS Bulletin. 2004;**29**(05):324-327

[38] Wassermann R, Katz A, Bentur A. Minimum cement content requirements: a must or a myth? Materials and Structures. 2009;**42**(7):973-982

[39] Yurdakul E. Optimizing concrete mixtures with minimum cement content for performance and sustainability. Ph.D thesis. United State of America: Iowa State University; 2010

[40] Kapelko A. Possibilities of cement content reduction in concretes with admixture of superplasticiser SNF. Journal of Civil Engineering and Management. 2006;**12**(2):117-126

[41] Dhir R et al. Role of cement content in specifications for concrete durability: aggregate type influences. Proceedings of the ICE-Structures and Buildings. 2004;**159**(4): 229-242

[42] Su N, Miao B. A new method for the mix design of medium strength flowing concrete with low cement content. Cement and Concrete Composites. 2003;**25**(2):215-222

[43] Klieger P, Lamond JF. Significance of tests and properties of concrete and concrete-making materials. Vol. 169. West Conshohocken, U.S.A: ASTM International; 1994

[44] De Larrard F, Sedran T. Optimization of ultra-high-performance concrete by the use of a packing model. Cement and Concrete Research. 1994;**24**(6):997-1009

[45] Haghighi A, Koohkan MR, Shekarchizadeh M. Optimizing mix proportions of reactive powder concrete using group method of data handling and genetic programming. In: 32nd Conference on our World in Concrete & Structures. Singapore: CI-Premier PTE LTD; 2007

[46] Yu R, Spiesz P, Brouwers H. Mix design and properties assessment of ultra-high performance fibre reinforced concrete (UHPFRC). Cement and Concrete Research. 2014;**56**: 29-39

[47] Hassan AMT, Jones SW, Mahmud GH. Experimental test methods to determine the uniaxial tensile and compressive behaviour of ultra high performance fibre reinforced concrete(UHPFRC). Construction and Building Materials. 2012;**37**:874-882

[48] Yang SL et al. Influence of aggregate and curing regime on the mechanical properties of ultra-high performance fibre reinforced concrete (UHPFRC). Construction and Building Materials. 2009;**23**(6):2291-2298

[49] Corinaldesi V, Moriconi G. Mechanical and thermal evaluation of ultra high performance fiber reinforced concretes for engineering applications. Construction and Building Materials. 2012;**26**(1):289-294

[50] Habel K et al. Development of the mechanical properties of an ultra-high performance fiber reinforced concrete (UHPFRC). Cement and Concrete Research. 2006;**36**(7):1362-1370

[51] Aldahdooh M et al. GUSMRC - From concept to structural application. In: Davim JP, editor. Green Composites. Germany: DE Gruyter; 2017

[52] Aldahdooh M et al. Retrofitting of damaged reinforced concrete beams with a new green cementitious composites material. Composite Structures. 2016;**142**:27-34

[53] Chung D. Review: improving cement-based materials by using silica fume. Journal of Materials Science. 2002;**37**(4):673-682

[54] Jolicoeur C, Simard MA. Chemical admixture-cement interactions: phenomenology and physico-chemical concepts. Cement and Concrete Composites. 1998;**20**(2):87-101

[55] Chung DDL. Review: improving cement-based materials by using silica fume. Journal of Materials Science. 2002;**37**(4):673-682

[56] Markovic I. High-performance hybrid-fibre concrete: development and utilisation. Ph.D. thesis. The Netherlands: Delft University Press; 2006

[57] Bhanja S, Sengupta B. Influence of silica fume on the tensile strength of concrete. Cement and Concrete Research. 2005;**35**(4):743-747

[58] Panjehpour M, Abang Ali AA, Demirboga R. A review for characterization of silica fume and its effects on concrete properties. International Journal of Sustainable Construction Engineering and Technology. 2011;**2**(2)

[59] Ma J, Dietz J, Dehn F. Ultra high performance self compacting concrete. Lacer. 2002;**7**:33-42

[60] Chan Y, Chu S. Effect of silica fume on steel fiber bond characteristics in reactive powder concrete. Cement and Concrete Research. 2004;**34**(7):1167-1172

[61] Tayeh BA. Interfacial bonding characteristics between normal concrete substrate and Ultra high performance fiber concrete repaired material. Ph.D thesis, in Civil Engineering. Malaysia: Universiti Sains Malaysia; 2013

[62] Schnütgen B, Vandewalle L. PRO 31: International RILEM Workshop on Test and Design Methods for Steel Fibre Reinforced Concrete-Background and Experiences. Vol. 31. Germany: RILEM Publications; 2003

[63] Voo YL, Foster SJ. Characteristics of ultra-high performance 'ductile'concrete and its impact on sustainable construction. The IES Journal Part A: Civil & Structural Engineering. 2010;**3**(3):168-187

[64] Zeyad AMA. Influence of steam curing on engineering and fluid transportation properties of high strength green concrete containing palm oil fuel ash. Ph.D thesis. Malaysia: Universiti sains Malaysia, 2013

[65] Alsadey S. Influence of superplasticizer on strength of concrete. International Journal of Research in Engineering and Technology. 2012:**1**(3)

[66] Porteneuve C et al. Structure-texture correlation in ultra-high-performance concrete: A nuclear magnetic resonance study. Cement and Concrete Research. 2002;**32**(1):97-101

[67] Shilstone JM, Shilstone J. Performance-based concrete mixtures and specifications for today. Concrete International. 2002;**24**(2):80-83

[68] Popovics S. Analysis of concrete strength versus water-cement ratio relationship. ACI Materials Journal. 1990;**87**(5)

[69] Schulze J. Influence of water-cement ratio and cement content on the properties of polymer-modified mortars. Cement and Concrete Research. 1999;**29**(6):909-915

[70] Kosmatka SH, Kerkhoff B, Panarese WC. Design and Control of Concrete Mixtures. 14th edition. USA: Portland Cement Association; 2002

[71] Wen-yu J, et al. Study on reactive powder concrete used in the sidewalk system of the Qinghai-Tibet railway bridge. In: Proceedings of International Workshop on Sustainable Development and Concrete Technology, Beijing; 2004

[72] Nuruddin MF et al. Strength development of high-strength ductile concrete incorporating Metakaolin and PVA fibers. The Scientific World Journal. 2014:11

[73] Kou SC, Xing F. The effect of recycled glass powder and reject fly ash on the mechanical properties of fibre-reinforced ultrahigh performance concrete. Advances in Materials Science and Engineering. 2012;**2012**

[74] Xiu-Chen Q, Chisun P, Zong-Shou L. Activation of rejected fly ash using flue gas desulphurization (FGD) sludge. Journal of Wuhan University of Technology-Materials Science Edition. 2003;**18**(4):84-88

[75] Krishna V, Sabnis G. Utilization of waste products and by-products in concrete: The key to a sustainable construction. In: International Conference on Civil and Architecture Engineering (ICCAE'2013), Kuala Lumpur, Malaysia; 2013

[76] Ferdosian I, Camões A, Ribeiro M. High-volume fly ash paste for developing ultra-high performance concrete (UHPC). Ciência & Tecnologia dos Materiais. 2017;**29**(1): e157-e161

[77] Jin W, Meyer C, Baxter S. "Glascrete"-Concrete with Glass Aggregate. ACI Materials Journal. 2000;**97**(2):208-213

[78] Chen G et al. Glass recycling in cement production—An innovative approach. Waste Management. 2002;**22**(7):747-753

[79] Meyer C, Baxter S, Jin W. Potential of waste glass for concrete masonry blocks. In: Materials for the New Millennium. USA: ASCE; 1996

[80] Shao Y et al. Studies on concrete containing ground waste glass. Cement and Concrete Research. 2000;**30**(1):91-100

[81] Meyer C, Egosi N, Andela C. Concrete with waste glass as aggregate. In: Proceedings of the International Symposium Concrete Technology unit of ASCE and University of Dundee, Dundee; 2001

[82] Chindaprasirt P, Homwuttiwong S, Jaturapitakkul C. Strength and water permeability of concrete containing palm oil fuel ash and rice husk-bark ash. Construction and Building Materials. 2007;**21**(7):1492-1499

[83] Jaturapitakkul C et al. Evaluation of the sulfate resistance of concrete containing palm oil fuel ash. Construction and Building Materials. 2007;**21**(7):1399-1405

[84] Awal A, Hussin MW. The effectiveness of palm oil fuel ash in preventing expansion due to alkali-silica reaction. Cement and Concrete Composites. 1997;**19**(4):367-372

[85] Tangchirapat W et al. Use of waste ash from palm oil industry in concrete. Waste Management. 2007;**27**(1):81-88

[86] Rukzon S, Chindaprasirt P. An experimental investigation of the carbonation of blended portland cement palm oil fuel ash mortar in an indoor environment. Indoor and Built Environment. 2009;**18**(4):313-318

[87] Tangchirapat W, Jaturapitakkul C, Chindaprasirt P. Use of palm oil fuel ash as a supplementary cementitious material for producing high-strength concrete. Construction and Building Materials. 2009;**23**(7):2641-2646

[88] Megat Johari MA et al. Engineering and transport properties of high-strength green concrete containing high volume of ultrafine palm oil fuel ash. Construction and Building Materials. 2012;**30**:281-288

[89] Sata V, Jaturapitakkul C, Kiattikomol K. Utilization of palm oil fuel ash in high-strength concrete. Journal of Materials in Civil Engineering. 2004;**16**(6):623-628

[90] Sata V, Jaturapitakkul C, Kiattikomol K. Influence of pozzolan from various by-product materials on mechanical properties of high-strength concrete. Construction and Building Materials. 2007;**21**(7):1589-1598

Chapter 9

Tire-Derived Aggregate Cementitious Materials: A Review of Mechanical Properties

Fariborz M. Tehrani and Nathan M. Miller

Additional information is available at the end of the chapter

http://dx.doi.org/10.5772/intechopen.74313

Abstract

This chapter presents an overview of tire-derived aggregate concrete, also known as rubberized concrete, a cementitious-based material with some or all of its mineral aggregates replaced with rubber particles. Typical source of rubber materials is scrap tire. Tire-derived aggregate concrete has practical applications as safety barriers, sound barriers, and architectural features among others. General observed trends include a decrease in compression strength, a decrease in flexural strength, and an increase in energy absorption and damping capacities with an increase of rubber content. These characteristics are modifiable by application of lightweight aggregates, fiber-reinforcement, admixtures, and other common techniques. The chapter also includes discussions on handling, design, and analysis of tire-derived aggregate concrete.

Keywords: tire-derived aggregate (TDA), rubberized concrete (RuC), mixture proportioning (mix design), strength, modulus of elasticity, toughness, lightweight aggregate (LWA)

1. Introduction

Investigation of rubberized concrete has received considerable attention since late twentieth century, when exploration of the idea of adding rubber particles to the concrete matrix began. The intriguing idea for many has been the combination of an ultra-flexible material to an ultra-rigid material to enhance ductile performance of the composite material. In addition, the idea of incorporating a waste material that may otherwise end up in a landfill is attractive for sustainable development. The main constituent of rubberized concrete is tire-derived aggregate (TDA), incorporated in a cementitious matrix through replacement of fine

or coarse aggregate as a percentage of volume or weight. This application redirects a significant amount of waste rubber from landfills to infrastructure industries.

The idea of repurposing a waste material for use in concrete has roots in concerns regarding the amount of waste tires in landfills. The United States alone generates 289 million scrap tires on an annual basis as of 2006 [1]. The Environmental Protection Agency (EPA) identifies stockpiled tires as an "ideal incubator for mosquito larvae" and connects this to the spread of the West Nile Virus from 1999 to 2005 [1]. As of 2012, tires were being recycled at a rate of 44.6% with rubber and leather contributing 6.18 million tons of waste after accounting for recycling and recovery [2]. The idea of reducing the number of waste tires that accumulate in landfills through recycling rubber for use in concrete has continued to attract the attention of researchers.

The general focus of research on rubberized concrete is the evaluation of mechanical properties of the concrete. The basic properties include compressive, tensile, and flexural strengths. The performance of TDA concrete subject to dynamic loading is another essential property of TDA concrete. In addition, application of supplementary cementitious materials and admixtures, such as silica fume and fly ash, has potentials to enhance various characteristics of TDA concrete. Research seems to be in support of the fact that the lower strength and enhanced dynamic properties of the TDA concrete mixtures are valuable in certain practical applications such as traffic barriers and other impact-resistant systems.

2. An overview of constituent materials

Other than the inclusion of the rubber particles, the rubberized concrete mix is virtually the same as most other concrete including cement, fine aggregates, coarse aggregates, and water. Some researchers have incorporated super plasticizers, in order to achieve better workability. Others have experimented with the use of silica fume and fly ash in order to achieve enhanced strengths. Further, researchers have experimented with pretreating the rubber particles using chemical washes in attempts to develop better bonds between the rubber particles and the cementitious matrix. Following sections discuss individual components making up the rubberized concrete matrix.

2.1. Tire-derived aggregate materials

TDA refers to the rubber particles, processed from multiple types of tires differing in composition and fiber type, used for replacing the mineral or rotary kiln expanded lightweight aggregates in many mixtures (**Figure 1**). Descriptive classification of rubber particles relies on the size and manufacturing processes of materials [3]. The first and largest classification of TDA is shredded tire chips, which are typically results of mechanical shredding. Resulting tire chips may be as large as 460 mm long by 230 mm wide to as small as 150 mm long. A combination of both primary and secondary shredding processes is also common to produce smaller shredded chips. The next classification is ground rubber; with a typical range of 19–0.1 mm in size. Ground rubber is subject to two stages of magnetic separation and

http://dx.doi.org/10.5772/intechopen.74313

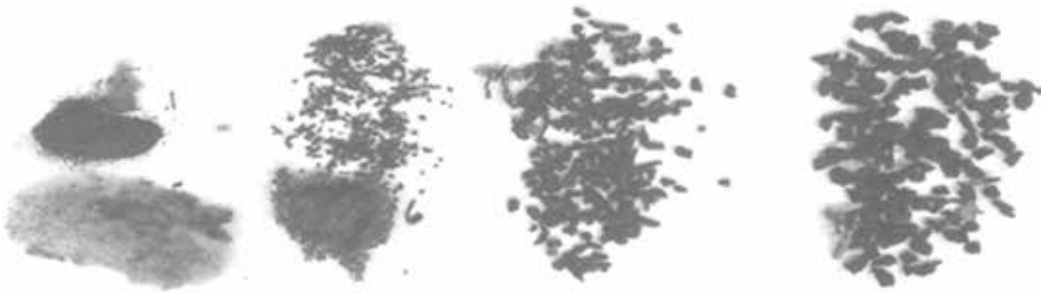

Figure 1. Crumb rubber manufactured through mechanical shredding of recycled tires.

screening to remove the steel fibers from the rubber particles. The smallest classification of TDA is crumb rubber, obtained through micro-milling, cracker-milling, and granular processes. Crumb rubber particle sizes range from 4.75 to 0.075 mm. Another method is a cryogenic method, in which the rubber is frozen using nitrogen and then shattered [3].

2.2. Mix design constituents

The common fine aggregate used in most research studies on rubberized concrete is natural sand with a gravel coarse aggregate. The cement used is either Type 1 or Type 2 cement, with no significant evidence suggesting one type of cement performing better. Other admixtures incorporated into rubberized concrete include the addition of silica fume and fly ash by replacement of cement. This enhances the strength of rubberized concrete and bond between the rubber and cement. Further, rubber particles may also replace lightweight aggregates (LWA), such as rotary kiln expanded shale, clay, and slate, in various lightweight concrete materials, where, the similarity between the volume weights of TDA and LWA enhances the ease of mixing and placing operations [4].

3. Mechanical properties

3.1. Compressive strength

Table 1 lists selected research projects and their characteristics. Existing literature indicates that an increase in rubber content results in a systematic decrease in the compression strength of the concrete material (**Figure 2**). The substitution of mineral aggregates with TDA is generally between 0 and 100% of the total aggregate volume in increments of 20%. The relationship between the compressive strength and rubber content in the mix is not linear [22]. Further, the size of the particles has an impact on this relationship. While, inclusion of 100% crumb rubber may reduce the compressive strength by more than 90% [8], substitution of fine aggregates by less than 25% appears to have no significant impact on this strength [13]. In particular, research has shown that application of fine crump rubbers has less negative impact on the compressive strength of the mix [5, 6, 15, 20]. A comparison between applications of coarse rubber particles

Reference	Rubber aggregate	Replaced conventional aggregate	Specimen type/ size
Aiello and Leuzzi [5]	Tire shreds 20 mm w/ Steel Fibers Included	Coarse aggregate 12.5–20 mm	Cube 150 mm Beams 250 × 250 × 900 mm
Al-Tayeb et al. [6]	Crumb rubber 1 mm	Sand fine aggregate	Cylinder 100Ø × 200 mm Beams 100 × 50 × 400 mm
Atahan and Sevim [7]	Shredded tire chips 11–22 mm	Crushed limestone coarse aggregate 4–16 mm	Cylinder 150Ø × 300 mm Full Scale Barriers 1000 × 450 × 250 mm
Atahan and Yucel [8]	Large rubber 13 mm and crumb rubber #10-20	Crushed Stone 19 mm and Sand	Cylinder 100Ø × 200 mm
Bignozzi and Sandrolini [9]	Scrap and crumb tires 0.05–2 mm	Fine aggregate sand 0–4 mm	Cube 150 mm
Ganjian et al. [10]	Chipped rubber 25 mm	Crushed siliceous coarse aggregate	Cube 150 mm Beams 100 × 100 × 500 mm
Guneyisi et al. [11]	Crumb rubber similarly graded to sand and tire chips 10–40 mm	Natural sand 4 mm and crushed limestone 20 mm replaced equally	Cube 150 mm Cylinder 150Ø × 300 mm (90-day strength)
Hernandez-Olivares et al. [12]	Rubber strip fibers 8.5–21.5 mm	No material removed	Cylinder 150Ø × 300 mm Beams 150 × 150 × 600 mm
Issa and Salem [13]	Crumb rubber (similar to sand used)	Crushed sand	Cylinder 150Ø × 300 mm
Khaloo et al. [14]	Coarse tire chips	Crushed stone gravel 20 mm	Cylinder (50-day strength)
Khatib and Bayomy [15]	Tire chips from mechanical shredding 10–50 mm	Coarse aggregate gravel	Cylinder 150Ø × 300 mm Beams 152 × 152 × 50 mm
Li et al. [16]	Truck & car tire chips and fibers with and w/o steel belt 25–51 mm	Coarse aggregate gravel	Cylinder 150Ø × 300 mm
Liu et al. [17]	Crumb tire rubber 0.178 mm	River sand fine aggregate 5 mm	Cubes 150 mm Cylinders 35Ø × 70 mm (SHPB Impact)
Miller and Tehrani [4]	Crumb rubber	Coarse lightweight expanded shale aggregate	Cylinder 150Ø × 300 mm Beams 152 × 152 × 50 mm

Reference	Rubber aggregate	Replaced conventional aggregate	Specimen type/ size
Mohammed et al. [18]	Crumb rubber 600 μm	River sand fine aggregate	Cube 100 mm
Son et al. [19]	Crumb rubber particles 1 mm	Total aggregate weight (coarse & fine)	Cylinder 100Ø × 200 mm
Topcu [20]	Rubber particles from mechanical grinding 6 mm	Crushed limestone coarse aggregate 4–16 mm	Cylinder 150Ø × 300 mm
Topcu and Avcular [21]	Large rubber particles 2.2 mm	Limestone coarse aggregate	Cylinder 150Ø × 300 mm
Toutanji [22]	Tire chips 12.7 mm	Crushed stone coarse aggregate 19 mm	Cylinder 100Ø × 200 mm Beams 100 × 100 × 350 mm
Xue and Shinozuka [23]	Crumb Rubber 6 mm	Gravel coarse aggregate 12 mm	Cylinder 100Ø × 200 mm Lumped Mass Columns
Zheng et al. [24]	Crushed rubber with steel belt wires 4–15 mm	Crushed stone coarse aggregate 31.5 mm	Cube 150 mm 60-day Beams 100 × 160 × 1000 mm
Zheng et al. [25]	Ground rubber 2.6 mm and crushed rubber with steel belt wires 4–15 mm	Crushed stone coarse aggregate 31.5 mm	Cylinder 150Ø × 300 mm

Table 1. Summary of selected research on rubberized concrete.

versus fine rubber particles indicate that coarse and fine rubber particles are more effective at substitution ratios of less and more than 25%, respectively [14]. Using larger sizes of TDA, also known as tire chips, provides an opportunity to keep the steel belt wires after shredding in order to lower the costs, even though, they may not provide any specific advantage for the mix [25]. On the same line, application of fiber reinforcement by adding polypropylene fibers has shown to be effective in reducing crack propagation due to shrinkage [12].

Similar to conventional concrete, application of supplementary cementitious materials such as silica fumes has shown to be effective on increasing the compressive strength of TDA concrete containing high water-to-cement ratios [11]. Replacing 7% of cement with silica fume has shown to increase the compressive strength between 3 and 7 MPa [23]. Tire-derived aggregates are also applicable to self-compacting concrete, which utilizes fine filler materials, admixtures such as superplasticizers, and viscosity modifying agents. Combination of shredded tire and crumb rubber has the potential to replace nearly 20–30% of the sand with a similar grain size [9]. Further, it is also possible to replace cement with ground rubber. Substitution of 5% of cement has shown to reduce the compressive strength by 5% [10]. Tire-derived aggregate concrete with enhanced characteristics due to admixtures and supplementary cementitious materials has

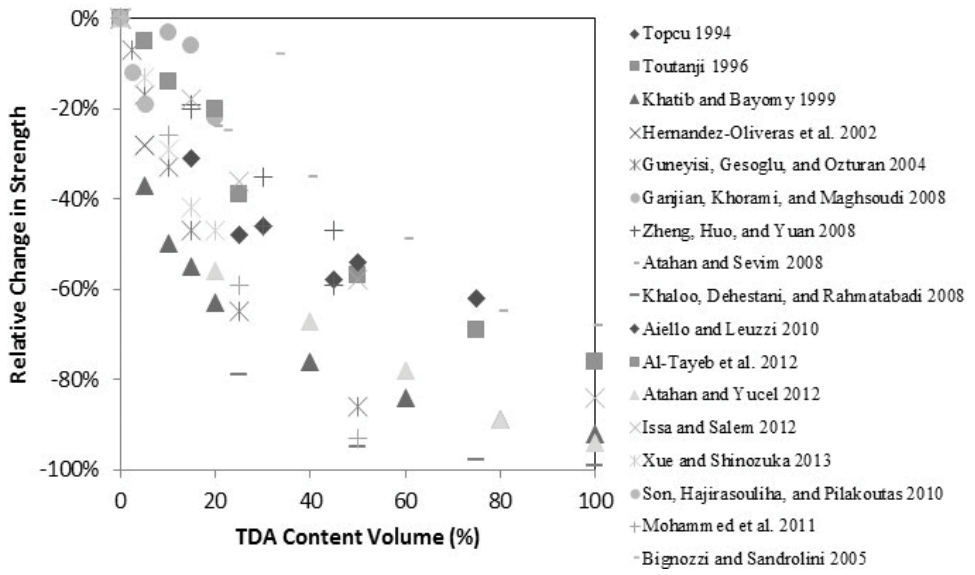

Figure 2. Selected reported relative changes in the compressive strength of rubberized concrete.

applications in hollow concrete blocks. The recommended rubber contents for loadbearing and non-loadbearing systems are 6.5 and 40.7%, respectively [18].

3.2. Modulus of elasticity - static

Research shows that increasing the rubber content in concrete decreases the static modulus of elasticity [6–8, 19]. However, there is not much agreement on the amount of reduction at high rubber contents (**Figure 3**). Generally, Tire-derived aggregates influence the stress-strain relationship and enhance the ductility of the concrete [14]. Some comparative studies on the size of

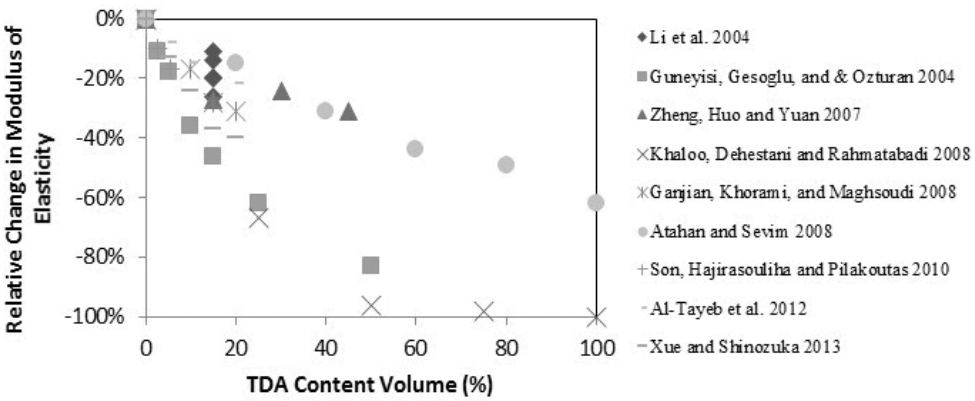

Figure 3. Selected reported relative changes in the static modulus of elasticity of rubberized concrete.

rubber aggregates suggest that using tire chips have more impact on the reduction of elastic modulus than using waste tire fibers do [16]. However, there are also evidences that the reduction of modulus of elasticity is only a function of the rubber content [10].

Further, using tire chips containing steel belts increases the stiffness of TDA concrete [16, 24, 25]. In addition, application of fly ash and silica fume can also enhance the modulus of elasticity [11, 23].

3.3. Split-tensile strength

Figure 4 indicates how increasing the rubber content reduces the splitting tensile strength. However, existing research agrees that capacity of rubber in absorbing energy enhances the toughness of the TDA concrete [6, 16, 20]. Application of fiber reinforcement using polypropylene fibers has shown to improve the toughness further [12]. Comparison of results for compressive and tensile strengths suggests that the rate of reduction for split-tensile strength is less than the same rate for compressive strength [11]. Further, there are reports indicating that specimens with ground tires perform better in tension than specimens containing large tire chips [10].

3.4. Flexural strength

The relationship between flexural strength and TDA content is similar to other mechanical properties (**Figure 5**). However, there are variations in this relationship. Studies generally indicate that reduction of flexural strength parallels an increase in the ductility of specimens [22]. Some research indicates that the rate of reduction for the flexural strength is much steeper than other mechanical properties, particularly at lower rubber contents [15]. Application of smaller rubber particles improves the observed flexural strength [5, 10]. Adding polypropylene fibers has also shown to be effective in crack control, but not necessarily in enhancement of the strength [12].

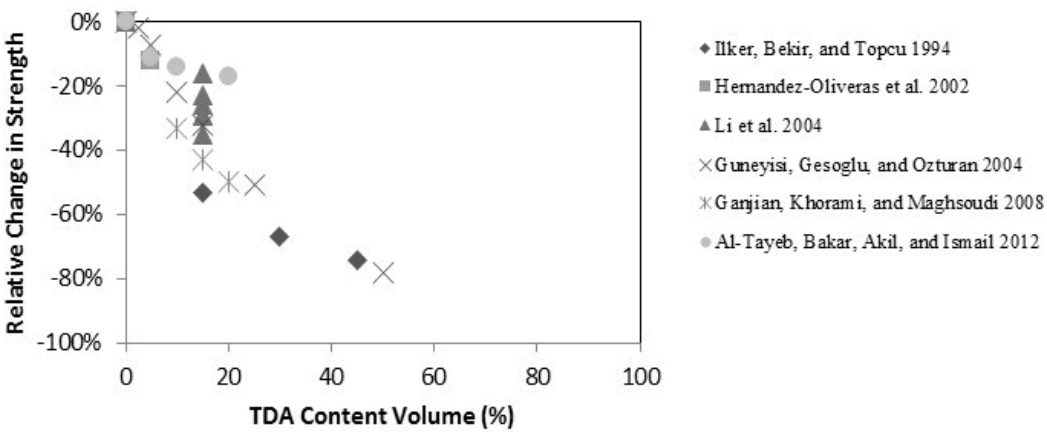

Figure 4. Selected reported relative changes in the split-tensile strength of rubberized concrete.

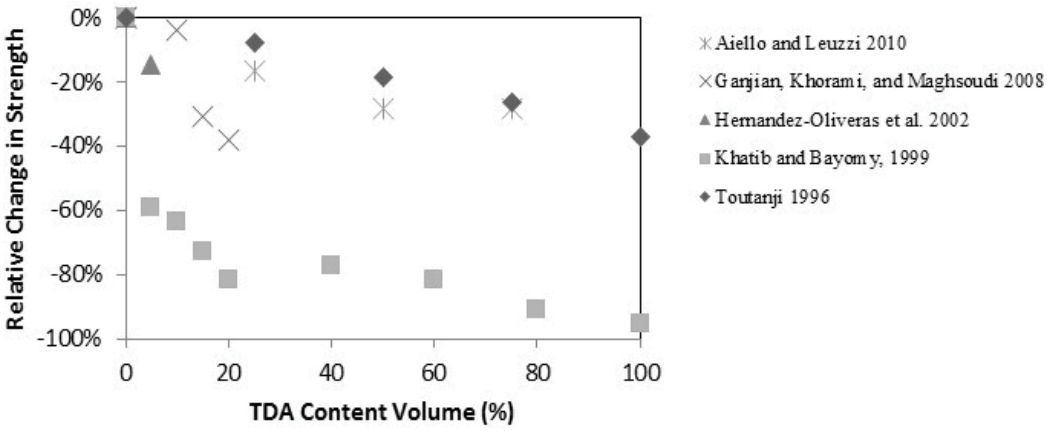

Figure 5. Selected reported relative changes in the flexural strength of rubberized concrete.

Rubberized concrete has also applications in composite floors. Research shows that floors with 10% rubber content have smaller failure load due to flexure in large spans, but nearly the same failure load caused by shear in short spans. The capability of TDA composite floors in withstanding larger deformations has a significant impact on the ductility of the system [26].

3.5. Toughness

Figure 6 contains selected reported data on the relationship between toughness and rubber content in TDA concrete. Toughness is generally a measure based on the area covered by the load-deflection diagrams, thus, it relates to both ductility and strength. As a result, reported data points on toughness are scattered, as rubber contents increases the ductility,

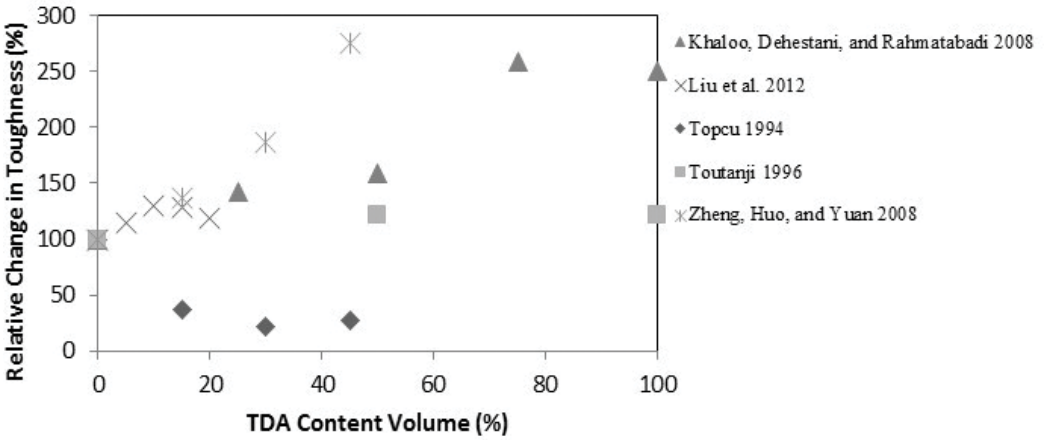

Figure 6. Selected reported relative changes in the toughness of rubberized concrete.

but reduces the strength. This explains how some studies have shown a reduction of toughness because of increasing the rubber content, even though subjected specimens have shown significant increase in ductility [20]. Nevertheless, most reported data show a general increase in toughness with the increase in rubber content [5, 22]. Some research studies have also suggested that a maximum toughness value exist for the optimum rubber content and proper TDA gradation [14]. Measuring toughness from the brittleness index using the stress-strain hysteresis loops also confirms the positive effect of rubber on the toughness [25]. In addition, the toughness of TDA concrete subject to impact load also increases with the increase in strain rate [17]. Furthermore, application of fibers, particularly in tensile specimens, significantly enhances the toughness [16].

3.6. Dynamic properties

Some of the most beneficial properties of rubberized concrete include its behavior under dynamic loading, making the enhancement of these properties desirable in comparison with the brittle and rigid behavior of plain concrete. Research suggests that rubberized concrete may have practical applications as traffic barriers, vibration mitigation, and seismic force mitigation among others. There are various techniques for investigation of these behaviors. **Figures 7** and **8** show two significant parameters, energy absorption and damping, respectively, measured for TDA concrete at different rubber contents. As shown in these figures, there are limited studies as the basis for each of these relationships.

The full-scale New Jersey-shaped safety barriers subject to non-severe impact loads indicate a gradual increase in the energy absorption when rubber content changes from 0 to 100% by volume [7]. These results are qualitatively comparable with similar collision testing studies [21]. However, impact testing on hybrid beams, containing a layer of TDA concrete on top of plain concrete has resulted in significant increase in energy absorption for only 20% rubber content [6]. Similar tests using falling weights confirms the effectiveness of TDA concrete in reducing the severity of the impact at only 20–40% rubber contents, even though, the pest performance is achieved at rubber contents larger than 60–80% [8].

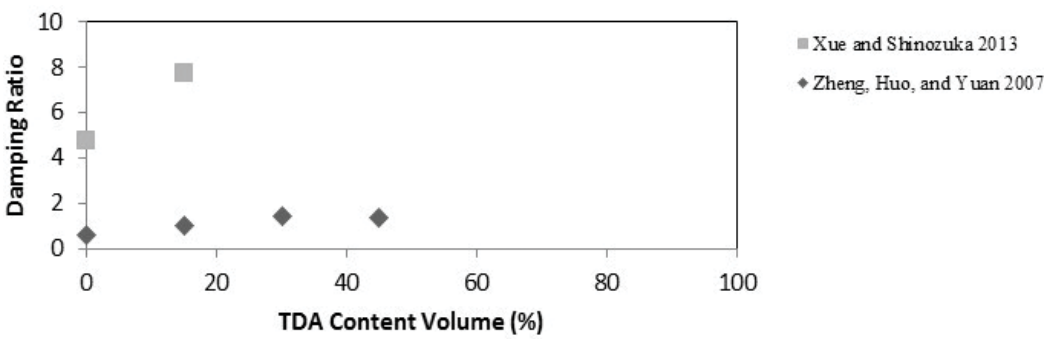

Figure 7. Selected reported relative changes in the damping ratio of rubberized concrete.

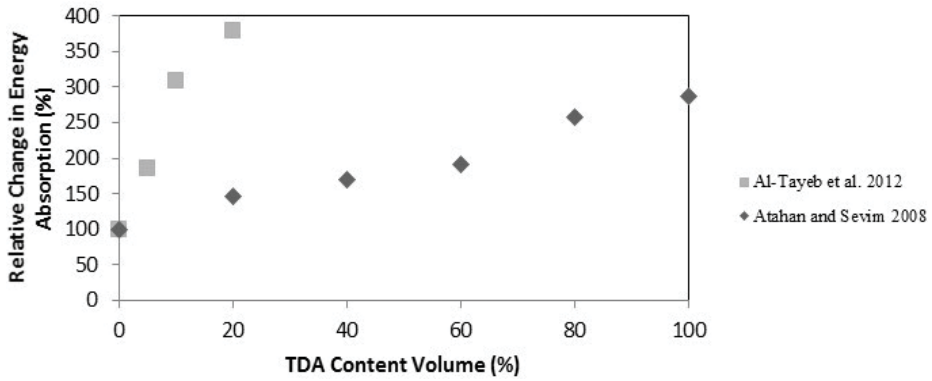

Figure 8. Selected reported relative changes in the absorbed energy of rubberized concrete.

Similarly, the damping ratio of TDA concrete measured by elastic wave method showed a moderate increase because of the increase in the rubber content in concrete [24]. However, the shake-table studies on TDA concrete columns indicated much higher damping ratios [23]. These comparisons indicate how TDA becomes more effective in post-peak performance of concrete specimens. Further, same shake table studies have shown that increasing rubber content in the TDA concrete reduces the natural frequencies and the response acceleration by 28 and 27%, respectively [23].

Non-destructive tests using ultrasonic pulses confirm that rubber reduces the velocity of waves, which is in correlation with lower dynamic modulus of elasticity [14]. Dynamic compression tests confirm the capability of TDA concrete in dissipating energy and show that increasing the load frequency or strain rate increases the dynamic modulus of elasticity [12, 17]. However, the age of the specimens has an adverse impact on the energy dissipation [12].

3.7. Thermal conductivity, electrical conductivity and sound absorption

Nonstructural mechanical properties of TDA concrete have been subject to studies for specific applications. Non-loadbearing wall elements often require proper thermal and electrical insulation as well as sound absorption. Studies indicate that TDA improves the sound absorption of concrete, reduces the thermal conductivity coefficient, and increases the electrical resistivity [13, 18, 27].

4. Design guidelines

4.1. Theoretical modeling and numerical simulation of rubberized concrete

A typical model for the behavior of TDA concrete is a modification of Holmquist-Johnson-Cook (H-J-C) constitutive model. The original H-J-C model contains 21 modifiable parameters

to present characteristics of TDA concrete, which was simplified to ten parameters in the modified form [17].

Numerical simulations using finite element analysis are also available to model mechanical properties of TDA concrete. The basis for these simulations is generally an elastoplastic model for the behavior of materials. Successful modeling of beam specimens has been reported using hexahedron elements with standard shape functions [6]. Using a two-phase composite material helps to define the dispersion of TDA in the cementitious matrix. This model utilized three-node triangular elements to simulate split-tensile tests [16].

4.2. Suggested strength reduction factors

Figure 9 shows a comparative view of the relationships between mechanical properties of TDA concrete and the TDA content volume. This figure suggests that developing a simple model for practical design of TDA concrete elements may be possible, as various strengths follow similar trends in respect to TDA content.

Eq. (1) presents a proposed model to find the strength reduction factor [15]:

$$SRF = a + b(1 - R)^m \tag{1}$$

In this model, SRF is the "strength reduction factor"; R is the rubber content as a volumetric ratio by the total volume of aggregates; and a, b, and m are modeling parameters. This equation is equal to unity at a rubber content of 0% and reaches an asymptote at higher rubber content values. The m parameter indicates the degree of curvature of the reduction and is a function of the particle size. In addition, parameters a and b must satisfy the relationship $a + b = 1$. **Table 2** contains suggested modeling parameters from past studies.

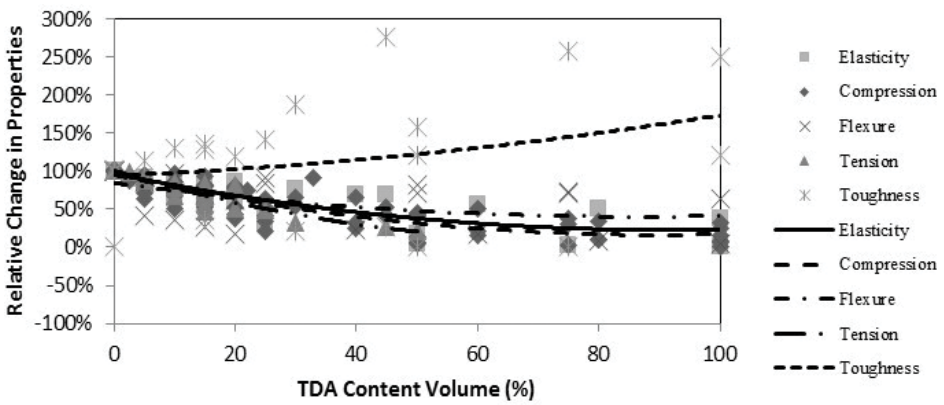

Figure 9. Selected reported relative changes in the dynamic properties of rubberized concrete (marked data) and their general trends (trend-lines).

Reference	a	b	m	Mechanical properties
Khatib and Bayomy [15]	0.1	0.9	3	Compression
	0.1	0.9	2	Split-tension
Khaloo et al. [14]	0.02	0.98	12	Compression
	0.01	0.99	11	Modulus of elasticity

Table 2. Summary of selected modeling parameters.

4.3. Handling procedures

Another important aspect of concrete design is the handling procedures used when placing the concrete while in the workable state. Care needs to be taken to ensure that segregation of materials does not occur and the mix remains as homogenous as possible while being placed and cured. An uneven distribution of rubber particles has been observed in concrete mixes, particularly when specimens are vibrated during placement causing light TDA to surface [10, 23].

5. Conclusions and recommendations

The state of the research on TDA concrete warrants further studies on analytical, experimental, and practical areas. On material properties, the environmental impacts on durability of rubber and long-term properties of TDA concrete is an area of interest for future research. Further, investigating the micromechanical characteristics of the bond between rubber particles and the cement paste is essential to understand the mechanical properties of TDA concrete, including toughness and tensile strength, better. Constitutive modeling and numerical simulation of the behavior of rubberized concrete are other areas of interest that can benefit from recent advancements in computational engineering and mechanics.

Application of TDA concrete requires development of design guidelines and specifications. Defining strength reduction factors is an area that requires further development. Current research studies are scattered in respect to parametric modeling and can benefit from additional experimental results. Further, these parametric analyses are essential for optimization of TDA concrete mix design to obtain proper rubber content for specific objectives. In addition, practical issues in mixing and placing concrete require development of proper specifications for handling TDA materials in concrete.

Mechanical properties of TDA concrete have shown to be desirable for many applications, such as traffic and sound barriers. Toughness and ductility of TDA concrete can be also effective in concrete elements subject to dynamic loads caused by earthquake and wind. Large-scale experimental studies are required for investigating these applications.

There has been limited studies on alternative TDA concrete products with application of fiber reinforcement, lightweight aggregate, fiber-reinforced polymers, admixtures, and supplementary

cementitious materials. Enhancing the properties of TDA concrete using these methods require further research.

Acknowledgements

The California State University, Fresno Foundation has partially supported this work.

Conflict of interest

The authors declare that there is no conflict of interest regarding the publication of this work.

Author details

Fariborz M. Tehrani* and Nathan M. Miller

*Address all correspondence to: ftehrani@csufresno.edu

California State University, Fresno, USA

References

[1] Environmental Protection Agency (EPA). Why are scrap tires an issue? Scrap Tire Management Forum; Rapid City, SD: EPA; 2006

[2] Environmental Protection Agency (EPA). Municipal Solid Waste Generation, Recycling, and Disposal in the United States: Facts and Figures for 2012. Annual Report. Washington DC: EPA; 2012

[3] Siddique R, Naik TR. Properties of concrete containing scrap-tire rubber - An overview. Waste Management. 2004;**24**:563-569

[4] Miller NM, Tehrani FM. Mechanical properties of rubberized lightweight aggregate concrete. Construction and Building Materials. 2017;**147**:264-271

[5] Aiello MA, Leuzzi F. Waste tire rubberized concrete: Properties at fresh and hardened state. Waste Management. 2010;**30**:1696-1704

[6] Al-Tayeb MM, Abu Bakar BH, Akil HM, Ismail H. Performance of rubberized and hybrid rubberized concrete structures under static and impact load conditions. Experimental Mechanics. 2012;**53**:377-384

[7] Atahan AO, Sevim UK. Testing and comparison of concrete barriers containing shredded waste tire chips. Materials Letters. 2008;**62**:3754-3377

[8] Atahan AO, Yucel AO. Crumb rubber in concrete: Static and dynamic evaluation. Construction and Building Materials. 2012;**36**:617-622

[9] Bignozzi MC, Sandrolini F. Tyre rubber waste recycling in self-compacting concrete. Cement and Concrete Research. 2005;**36**:735-739

[10] Ganjian E, Khorami M, Maghsoudi AA. Scrap-tyre-rubber replacement for aggregate and filler in concrete. Construction and Building Materials. 2008;**23**:1828-1836

[11] Guneyisi E, Gesoglu M, Ozturan T. Properties of rubberized concretes containing silica fume. Cement and Concrete Research. 2004;**34**:2309-2317

[12] Hernandez-Olivares F, Barluenga G, Bollau M, Witoszek B. Static and dynamic behaviour of recycled tire rubber-filled concrete. Cement and Concrete Research. 2002;**32**:1587-1596

[13] Issa CA, Salem G. Utilization of recycled crumb rubber as fine aggregates in concrete mix design. Construction and Building Materials. 2013;**42**:48-52

[14] Khaloo AR, Dehestani M, Rahmatabadi P. Mechanical properties of concrete containing a high volume of tire-rubber particles. Waste Management. 2008;**28**:2472-2482

[15] Khatib ZK, Bayomy FM. Rubberized Portland cement concrete. Materials in Civil Engineering. 1999;**11**:206-213

[16] Li G, Garrick G, Eggers J, Abadic C, Stubblefield M, Pang SS. Waste tire fiber modified concrete. Composites Part B: Engineering. 2004;**35**:305-312

[17] Liu F, Chen G, Li L, Guo Y. Study of impact performance of rubber reinforced concrete. Construction and Building Materials. 2012;**36**:604-616

[18] Mohammed BS, Anwar Hossain KM, Swee JTE, Wong G, Abdullahi M. Properties of crumb rubber hollow concrete block. Cleaner Production. 2011;**23**:57-67

[19] Son KS, Hajirasouliha I, Pilakoutas K. Strength and deformability of waste tyre rubber-filled reinforced concrete columns. Construction and Building Materials. 2010;**25**:218-226

[20] Topcu IB. The properties of rubberized concretes. Cement and Concrete Research. 1994; **25**:304-310

[21] Topcu IB, Avcular N. Collision behaviours of rubberized concrete. Cement and Concrete Research. 1997;**27**:1893-1898

[22] Toutanji HA. The use of rubber tire particles in concrete to replace mineral aggregate. Cement and Concrete Composites. 1996;**18**:135-139

[23] Xue J, Shinozuka M. Rubberized concrete: A green structural material with enhanced energy-dissipation capability. Construction and Building Materials. 2013;**42**:196-204

[24] Zheng L, Huo XS, Yuan Y. Experimental investigation on dynamic properties of rubberized concrete. Construction and Building Materials. 2007;**22**:939-947

[25] Zheng L, Huo XS, Yuan Y. Strength, modulus of elasticity, and brittleness index of rubberized concrete. ASCE Journal of Materials in Civil Engineering. 2008;**20**:692-699

[26] Mohammed BS. Structural behavior and m-k value of composite slab utilizing concrete containing crumb rubber. Construction and Building Materials. 2009;**24**:1214-1221

[27] Sukontasukkul P. Use of crumb rubber to improve thermal and sound properties of precast concrete panels. Construction and Building Materials. 2008;**23**:1084-1092

Chapter 10

Alternative Stabilizer for Mud Concrete

Chameera Udawattha and Rangika Halwatura

Additional information is available at the end of the chapter

http://dx.doi.org/10.5772/intechopen.76065

Abstract

Cement is one of the key stabilizers for earth constructions since Roman civilization. The invention of cement was one step in the human civilization. However, cement has many issues especially when it comes to the environmental conservation. The production of cement creates a lot of carbon dioxide and destroys the natural setting to some extent due to the high consumption of clay and lime. Therefore, this study was conducted to alter the cement in mud concrete block. The study started with an inventory of alternative stabilizers that can be found in nature as well as in the human production. And then, the chemical patterns of those stabilizers were carefully identified to alter the typical Portland cement. Several mix proportions were tested and developed to alter the cement and found that the following materials can be developed to alter cement. A natural stabilizer such as tree resins, latex rubber stabilizer, waste ash, rice husk ash and many other ashes can be developed to chemically stabilize the earth blocks. However, out of the invented stabilizers, fly ash and rice husk ash have the high potential to replace cement.

Keywords: mud, cement, alternative stabilizers, natural polymers, industrial waste

1. Introduction

Cement as stabilizer had a vital role in the human civilization. The earliest civilizations such as Egyptians habituated calcined gypsum; Greeks and Romans used heated limestone powders made by volcanic explosions to make mortar. Finally, Romans built continental scale civilizations by using cement to build bonds. It was Romans who found and named cement 'pozzolanic' cement after the village Pozzuoli near Vesuvius, a giant volcano found in Italy.

However, not all civilization had the fortune of using volcanic ash. Britain learnt the technology from Romans and developed the technology to produce cement by crushing clay tile and

systematically burned with lime to produce cement. It was Joseph Aspdin from the UK who got the first patent for the Portland cement in 1824. Since then, Portland cement was developed into many variations to optimize and customize the stabilizing capacity (see **Table 1**).

The idea of stabilizing is to create a bond between two particles. Cement is such a stabilizer used widely on earth due to the availability of raw materials and production method. However, the cement as a stabilizer has much weakness including a high carbon footprint.

1.1. Mud concrete block

Mud concrete block is a building material invented by the University of Moratuwa, Department of Civil Engineering. The concept is to use available soil and mix them with 6% of cement and used alternative to the brick and cement blocks, mostly available in the market [1–5]. The concept is to aggregate 'Concrete' made using earth/soil. Concrete is a typical composite construction material made out of cement, sand, metal and water. Here, metal (coarse aggregate) controls the enduringness, cement acts as the binder and sand (fine aggregate) reduces the porosity and water acts as the reactor to cement. In mud concrete, the designated parts of sand and metal of concrete are replaced by a fraction of the soil. The precise gravel percentage governs the strength of mud concrete. The production method of mud concrete block is shown in **Figure 1**.

Description	SLS 107	SLS 1247	SLS 1257
Chemical composition			
Magnesium oxide (MgO) %	2	2.5	2.5
Sulfur trioxide (SO_3) %	2.25	2.3	2.3
		0.01	0.01
Chloride (Cl) %	0.01	1.5	1.5
Lime saturation factor (LSF) %	0.94		
Tri calcium aluminate (C_3A) %	7.5	275	275
Loss on ignition %	1.4	320	320
Insoluble residue %	1.4		
Physical properties		3350	3350
Fines (blaine) cm^2g	3200	1	1
Expansion soundness mm	0.9	0.04	0.04
Autoclave %	0.04	130	130
Time of setting	140	19	19
Compressive strength (N/mm^2)	45.5	50.5	50.5
2 Days	22.5	0.005	0.005
28 Days	55.6	0.046	0.046

Table 1. Chemical and physical properties of cement.

http://dx.doi.org/10.5772/intechopen.76065

The cement in this concrete is also used as a stabilizer in very low quantities. The quality of the cement is shown in **Table 1**. In this research, a fraction of soil has been classified as follows [5]:
Gravel—sieve size 4.25 mm ≤ gravel≤20 mm
Sand—sieve size 0.425 mm ≤ sand ≤4.25 mm
Fine (silt and clay)— ≤ sieve size 4.25 mm

In achieving the concept of sustainability, green buildings are which provide environmentally suitable and friendly aspects of the building construction. In relation to material conservation, Mud Concrete Block (MCB) invented by the University of Moratuwa is a novel experience today in combining ancient technology with the modern [6]. Issues related to modern technology that needed to predict towards MCB were non-sustainability and higher cost [7–9]. Therefore, the invention of MCB has become a major companion in answering these two issues due to the facts that it is sustainable in the sense that it gains no harm to the environment and it is abundantly available [10]. Apart from that, MCB has 92% of reusability and concrete has only 70% [7]. This supports to reduce even waste generation due to the demolition of buildings. However, mud concrete has a weakness of having little higher carbon footprint due to the use of cement as a soil stabilizer. The use of cement as soil stabilizer creates other practical issues including the initial cost of the production of mud concrete blocks. Therefore, this research was conducted to alter the cement and explore possible alternative stabilizer for cement.

1.2. Soil stabilization

Soil stabilization is the alteration of soils to enhance their physical properties. Stabilization can increase the shear strength of a soil and/or control the shrink-swell properties of a soil, thus improving the load-bearing capacity of a sub-grade to support construction technology.

- **Mechanical**—This involves physically changing the property of the soil somehow, in order to affect its gradation, solidity and other characteristics. Dynamic compaction is one of the major types of mechanical stabilization; in this procedure, a heavyweight/force is dropped repeatedly onto the walling block at regular intervals and create the block, for example, cement-stabilized earth blocks (CSEB).
- **Chemical**—Chemical solutions are another of the major types of soil stabilization. All of these techniques rely on adding an additional material to the soil that will physically interact with it and change its properties. There are a number of different types of soil stabilization that rely on chemical additives of one sort or another; you will frequently encounter compounds that utilize cement, lime, fly ash (FA) or kiln dust. Most of the reactions sought are either cementitious or pozzolanic in nature, depending on the nature of the soil present at the particular site you are investigating.
- **Polymer/Alternative**—Both of the previous types of soil stabilization have been around for hundreds of years, if not more; only in the past several decades have technology opened up new types of soil stabilization. Most of the newer discoveries and techniques developed thus far are polymer based in nature, such as rubber. These new polymers and substances have a number of significant advantages over traditional mechanical and chemical

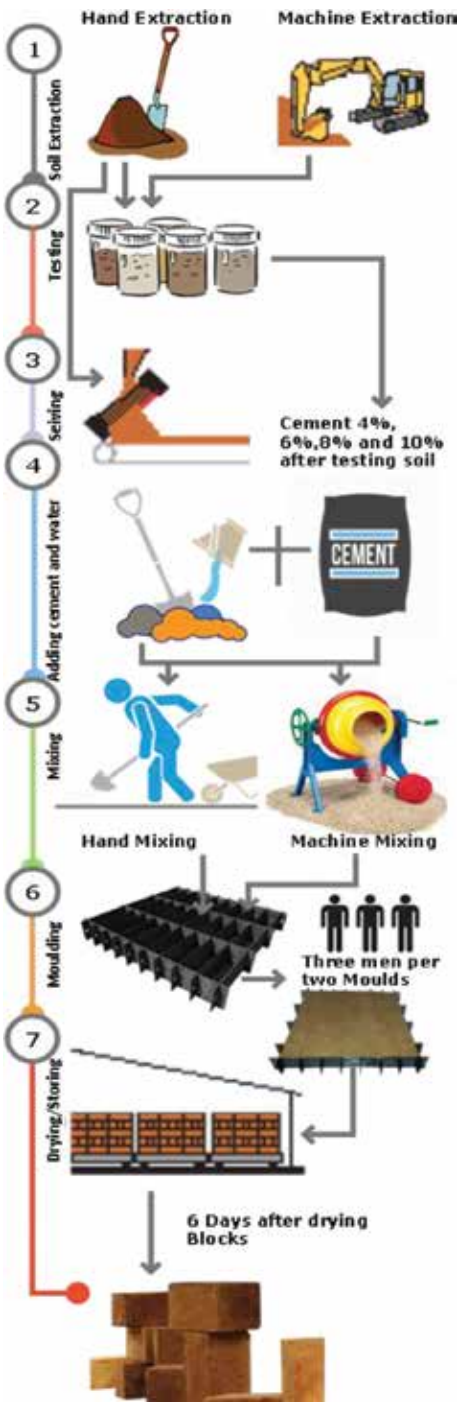

Figure 1. Manufacturing framework mud concrete block.

solutions; they are cheaper and more effective in general than mechanical solutions and significantly less dangerous for the environment than many chemical solutions tend to be.

1.3. Compares and alternatives for cement

The objective of this study is to alter cement in mud concrete technology. And the study was started with an inventory of alternative stabilizers found in nature. Nature is a grand material engineer. First, the study came up with an inventory natural polymer shown in **Table 2**. And then, the study was conducted to understand other waste from the human world. Therefore, the inventory was based on two types of stabilizers such as natural and artificial, polymers and non-polymers.

1.4. Polymeric substance-based stabilizers

Meanwhile, many types of research have been conducted on avoiding the use of cement or concrete in walling materials as its effect on the thermal comfort of the occupants due to the gypsum content [20]. The inclusion of polymeric substances has been one of the prominent recommendations for enhancing the general performance of concrete, especially cement and asphalt concretes [21]. Therefore, many effective polymeric latex substances have attracted the focus in order to develop and use them in respect of cement concrete in the construction industry [11]. There has been an active research development in polymer-modified mortar and concrete in various countries around the world for the past 70 years. As a result of these research and developments, polymer mortar and concrete became the dominant materials in the construction industry in the 1970s in Japan and in the 1980s in the United States. Now, they are competitively employed as popular construction materials [22]. The inclusion of polymeric substances into hydraulic cement concrete has made a tremendous effect on improving its performance properties. However, it should be included in concrete and should not cause damage to its mechanical capacities or to its durability characteristics [23]. Results have shown that the performance of latex-modified concrete is depending largely upon the techniques involved in the mixing procedure, water/cement ratio, latex content and curing regime [24]. Various bio-polymeric construction materials for soil treatment or enhancement have been introduced in several studies, to replace the use of conventional materials that have high environmental impacts, as efforts to develop environmentally friendly construction engineering approach [25].

Polymers are being increasingly used in civil engineering applications as concrete materials modifiers, especially for the purpose of improving workability, drying shrinkage, strength properties and durability characteristic [26]. Apparently, among several polymeric substances used in practice, elastomeric latexes are the most frequently applied [24]. Currently, elastomeric latexes, which mainly consist of hydrocarbon substances, are being used increasingly in civil engineering applications as modifiers for the purpose of performance improvement of hydraulic cement concrete [24].

	Name of stabilizer	Chemical formula	Available sources	Uses and properties	Production method
Natural Polymers	Rubber Latex [11]	Polyisoprene	Can be collected from rubber plants	Used in many applications and products in combination with other materials	Can be used with sulfur to stable and create longer bonds between the rubber materials
	Pines Gum	Pinene	Obtained from pines	Used as stabilized in many civilizations	Pines resins are generally produced as stem secretions
	Lignin	Carboxymethyl lignin	Sugarcane bagasse	Stabilizing agent in aqueous ceramic suspensions	Using ethanol-water as the solvent and sulfuric acid with 70c for 30 min
	Molasses	$C_6H_{12}NNaO_3S$	Sugarcane bagasse	Soil stabilization	Molasses made from sugar beets differ from sugarcane molasses. Only the syrup left from the final crystallization stage is called molasses
	Hydrophilic polymer		*Aegle marmelos*	(a complex mixture of vitamins, polyphenols, esters, aldehydes, sugars, mineral salts, organic acids and amino acids)	Concentrations used in the formulation were 2, 4, 6 and 8% w/w of cordial fruit gum
Industrial Waste	Fly ash [12–14]	Pulverized fuel ash	Any coal combustion plant	Land fill, dump	Coal combustion process produces tons of fly ash per day even in Sri Lanka
	Bottom ash [15, 16]	SiO_2 Al_2O_3 Fe_2O_3 CaO K_2O TiO_2 MgO SO_3-Na_2O P_2O_5 BaO	Ash that falls in the bottom of the boiler is called bottom ash. In modern coal-fired power plants	Bottom ash is part of the non-combustible residue of combustion in a furnace or an incinerator	Stuck in the furnace and taken out more than four lorries per day in Lakvijaya power plant
	Rice husk ash [17–19]	Crystalline silica		Increases the electrochemical stability of the film	
	Lime			stabilizer	

The inventory has produced to develop the experimental criteria. The most suitable stabilizers experimented with soil in order to test the strength development. The whole idea of developing alternative stabilizer to stable soil and mortar. Therefore, the main experiment is to develop the strength development.

Table 2. Inventory of alternative stabilizers for cement.

If this technology can be used in relation to soil, the product will be a sustainable one since that avoids the cement usage and lessens the energy usage. As soil is an environmentally friendly source and it provides a sufficient forum for energy conservation, the inclusion of soil into the newest technology of polymeric stabilizing will be an attractive turning point in civil engineering constructions.

1.5. Waste ash substance stabilizers

There are so many wastes generated and abundant in the natural setting without proper methods. The study shows that ashes like fly ash, bottom ash and rice husk ash have the similar cementitious properties such as color, particle size distribution, and so on. In addition, there have been many studies to develop those ashes into cementitious materials and stabilized earth. Geopolymerization is a similar concept where the ashes are activated by using alkaline solution to improve the bonding capacity of the ashes. First, ashes were combined with an alkaline solution and then make with soil and build earth blocks. This was invented in 2007 by Professor Joseph Davidovits. He has developed a series of geopolymerization techniques to develop the cementitious properties of the ashes to alter cement in the earth construction. Since after his innovation, there have been many attempts to develop the idea of geopolymerization. But for the first time, this study was conducted to geopolymerize mud concrete.

2. Effect of alternative natural and industrial waste for mud concrete construction

2.1. Latex (rubber)

Latex (rubber) got the attention due to many reasons. It is the best natural polymer in Sri Lanka. It is mass-produced and can be found in large scale if in case of a mass production of earth blocks. On the other hand, earth blocks have the compressive strength but not the tensile strength. Latex (rubber) has this capacity to bend if in case of a force and absorb tensile force. Hence, the idea of experimenting with rubber was optimized by various mix proportions as shown in **Figure 2**; it was to identify the best mix proportion for mud concrete block shown in **Table 3**. The ammonium hydroxide and sulfur were used as add mixtures to develop the workability and the strength of the mixture.

Since cement and rubber do not show any strength improvement, the study was extended to improve the quality of rubber soil mixture with altering cement with sulfur (see **Table 4**). The experimental programme is shown in **Table 4**. In this experiment, only the rubber was used in

Figure 2. Mix preparation for testing.

Soil (%)	Latex (%)	Dry rubber (%)	Cement	Admixture NH_4OH (%)
96	6.90	4	3.36	5
94	10.30	6	3.36	10
92	13.80	8	3.36	15
90	17.20	10	3.36	20
95	6.90	4	3.36	1
92	10.30	6	3.36	2
89	13.80	8	3.36	3
86	17.20	10	3.36	4
95	6.90	4	3.36	5
92	10.30	6	3.36	10
89	13.80	8	3.36	15
86	17.20	10	3.36	20

Table 3. Experimental compositions of rubber and soil mixes.

Rubber + NH4OH					Rubber +Sulphur				
		Area (mm^2)	N/mm^2	Average			Area (mm^2)	N/mm^2	Average
R 4%	A	8556	2.04	2.20	S 2%	A1	8188	0.83	0.82
	B	8556	2.43			B1	8418	0.89	
	C	8742	2.14			C1	8099	0.73	
R 6%	A	8417.5	2.33	2.29	S 4%	A1	8789	0.86	0.87
	B	8554	2.40			B1	9025	0.85	
	C	8742	2.12			C1	8554	0.89	
R 8%	A	8281	2.74	**2.79**	S 6%	A1	8648	0.83	0.80
	B	8281	2.67			B1	8836	0.80	
	C	8326.5	2.97			C1	8930	0.77	
R 10%	A	8418	2.67	2.61	S 8%	A1	8648	1.01	**0.99**
	B	8096	2.65			B1	8740	1.06	
	C	8280	2.49			C1	8930	0.90	

Table 4. Experimental composition with latex and sulfur to improve the dry strength.

order to improve the quality of rubber-stabilized earth block mixture. And the experimental criteria are as follows.

Table 5 shows the experiments done with sulfur and rubber mix design with soil in order to gain the strength. In addition, the upper corner of **Figure 3** shows the sun-drying process of

Mix design	Soil (g)	Cement(g)	Rubber		
			Rubber milk(g)	Water(g)	Sulfur(g)
0.5S2R4C	4675	200	100	50	25
1S2R4C	4650	200	100	50	50
1.5S2R4C	4625	200	100	50	75
2S2R4C	4600	200	100	50	100
4S2R4C	4500	200	100	50	200

Extended experiments with pure rubber-composed soil brick.

Table 5. Extended study with 100% rubber soil mixture altering cement with small amount of sulfur.

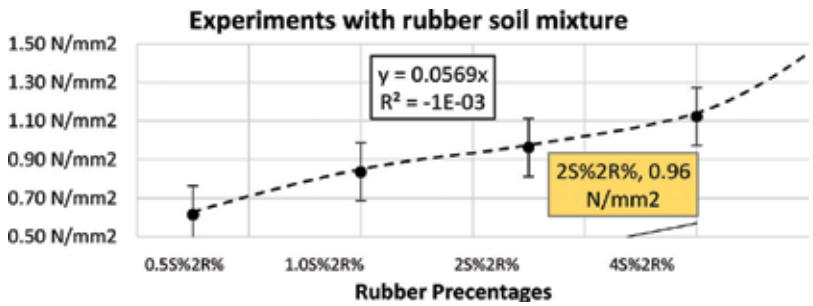

Figure 3. Improving the rubber soil mixture with the addition of sulfur.

the same bricks produced by the rubber and soil mixture. The results are astonishing to alter cement with 100% natural materials to use as a brick. The results are as follows.

2.2. The effect of rubber ratio into the constant sulfur combinations

The next study was conducted to understand the strength development due to an increase of rubber while maintaining the soil and sulfur ratios constant as shown in **Table 6**. This experiment was conducted to understand the optimum rubber content to be used to build rubber-stabilized earth blocks. And the previous experiments were observed where the rubber blocks may cause to shrink during the curing process. Therefore, alternatively, 100 × 100 mm blocks were used to understand the strength of the new mixture. The experimental schedule is shown in **Table 6**.

This study was to understand the optimum rubber content to develop the rubber-stabilized earth block. The optimum sulfur content was recognized as 2%. The sulfur is not natural materials and cannot be found in the natural form. The increase of carbon footprint may occur due to the use of sulfur. However, the sulfur itself helps to improve the compressive quality of the RSEB block. Therefore, the combination of rubber and sulfur may create a better bond between particles of the blocks. In addition, the results are as follows.

Experiments with latex-stabilized mud concrete block gave senior results with a high tensile capacity as shown in **Figure 4**. However, rubber-stabilized mud concrete blocks had many weaknesses including dry shrinkage. The dry shrinkage and the cost of latex rubber motivated

Mix design	Soil	Cement	Rubber		
			Rubber milk	Water	Sulfur
2S2R	92%	4%	2%	1%	2.00%
	4600 g	**200 g**	**100 g**	**50 g**	**100 g**
2S4R	90%	4%	4%	1%	2.00%
	4500 g	**200 g**	**200 g**	**50 g**	**100 g**
2S6R	88%	4%	6%	1%	2.00%
	4400 g	**200 g**	**300 g**	**50 g**	**100 g**
2S10R	84%	4%	10%	1%	2.00%
	4200 g	**200 g**	**500 g**	**50 g**	**100 g**

Table 6. Extended study with admixtures to develop the dry strength.

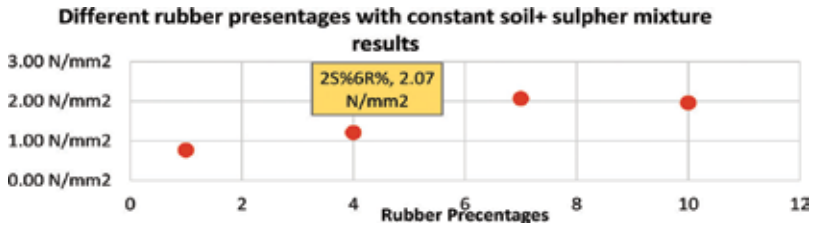

Figure 4. Different rubber percentages with constant soil+ sulfur mixture results.

to perform experiments with other natural polymers, assuming that there will be a better bonding to alter cement in mud concrete. The most common assumption for experimenting with natural polymers is the ability to develop a bond between two or three particles. And the own ancestors have used this for a long time in the past.

2.3. Tree resins and natural polymers

This experiment has gone too far corners of the historical methods of stabilizing earth into mortars and blocks. Ancient Sinhalese civilization in the fourth century builds the fortress Sigiriya by using tree resins and lime [27]. The study referred to the same technology and identified that natural polymers can make a bond between two materials and create a cementitious effect. Therefore, following the ancient inscription, cashew juice, Neolitsea cassia juice and pine resins were subjected to this study to alter cement in mud concrete technology (see **Figure 5**). The objective of this study is to study the possibility of developing mineralogy of natural polymers into suitable construction materials. The use of selected natural polymers to stabilize geotechnical properties of soil into engineering property consisting of masonry unit with a load-bearing capacity has been studied. The strength development and suitable mix development for such a masonry unit made out of earth stabilized by using natural polymers has also been studied.

http://dx.doi.org/10.5772/intechopen.76065

Figure 5. Experiments with natural polymers as alternative for cement.

The idea is not to use the raw polymers and resins, but to extrapolate the compounds that are developed into the proper mix. The results show that pines resins and cashew juice are vulnerable to make mud concrete blocks shown in **Figures 6–8**. The archived strength is more

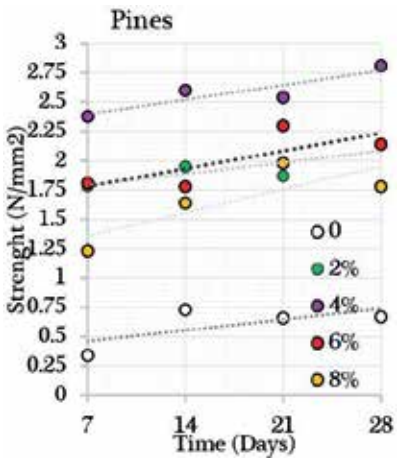

Figure 6. Pines.

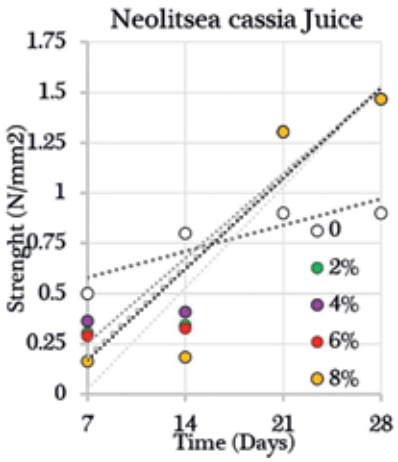

Figure 7. Neolitsea cassia juice.

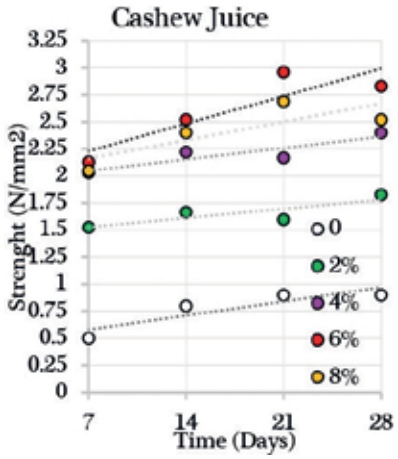

Figure 8. Cashew resin.

than 2 N/mm^2. In addition to the strength, pines-stabilized mud concrete gives a courteous smell and a reddish color. This can lead to developing architectural block. Therefore, these polymers can be developed to make earth blocks. But the issue was the mass production, and there are so many other alternative uses of these polymers and resins.

3. Experiments with industrial waste as stabilizers for mud concrete

The initial experiment was conducted to replace cement with raw fly ash, bottom ash and rice husk ash as shown in **Figure 9** as it is and found that those materials cannot improve the strength. The obtained results show that rather than stabilizing the soil, these materials unbound the clay and reduce the strength lower than 2 N/mm^2 [14, 16, 28].

The initial mix raw ash experiment was a failure without achieving any strength shown in **Figures 10–12**. But then, further study showed that the alkaline activation of ash can build a much better mixture than using it in raw. Therefore, a new experiment was conducted to develop alkaline-activated ash to develop a much stronger mud concrete block. This was invented in 2007 to describe the alumino silicate binders, which is formed by the alkali activation of a source material that is rich in content of aluminum and silicon [29]. These binders have superior properties that promote them as cement replacement materials. Geopolymer can utilize precursors

Figure 9. Fly ash, bottom ash, and rice husk ash.

http://dx.doi.org/10.5772/intechopen.76065

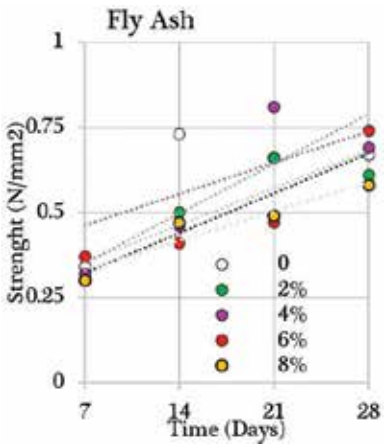

Figure 10. Fly ash.

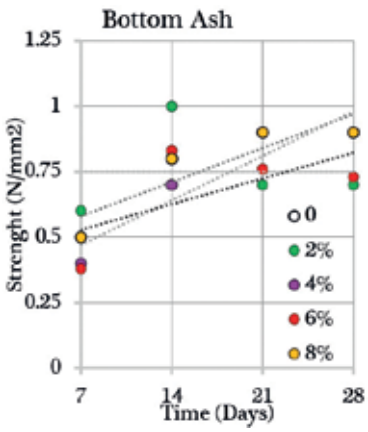

Figure 11. Bottom ash.

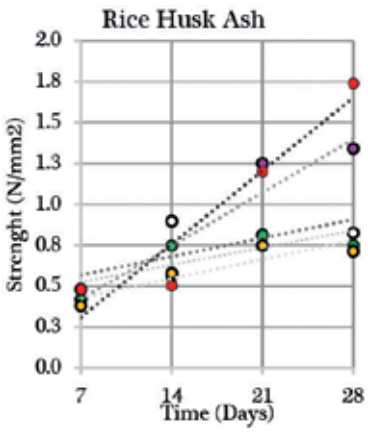

Figure 12. Rice husk ash.

from many industrial by-products fly ash (FA), bottom ash and rice husk ash. These by-products are usually disposed in landfills, which create serious environmental concerns.

4. Alkaline activation of fly ash

The further study about ashes found that they are having similar properties like cement and close brothers of cement (see **Figure 13**). And many studies show that alkaline activation of ashes can make a stronger material to stabilize earth to build the road. By studying the same concept, this experimental programme came up with new experimental criteria to build non-cement but fly ash-stabilized earth blocks. The experimental criteria are as follows.

4.1. The experimental criteria to alkaline activate the fly ash

The study shows that the concept of geopolymer can be applied to replace the cement in the mud concrete technology.

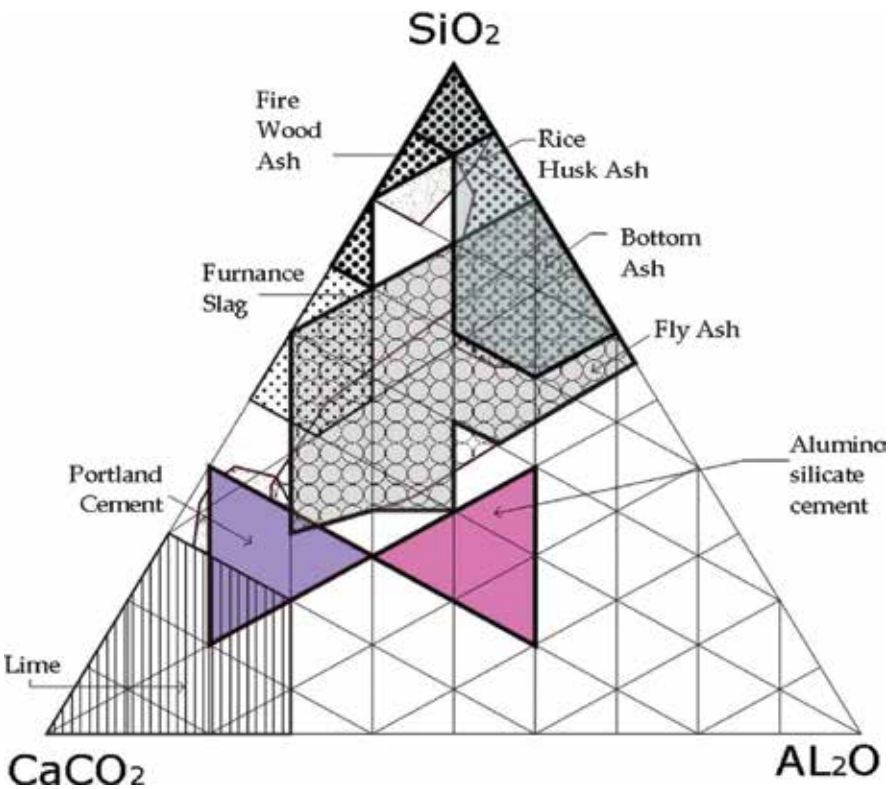

Figure 13. Comrades of cement.

The study shows the use of NaOH, and salt combination can activate the fly ash into the cementitious property. The process of geopolymerization is shown in **Figure 14**. Also known as polycondensation of alumina silicate bonds into jelly particle, they finally create the bond. This is not a novel concept; see Section "Introduction". However, this is the first time geopolymerization is an experiment with mud. The idea of stabilizing mud and developing mud-based mixture is to develop quick flow self-compacting mixture to alter a traditional compressed earth block technology. It was the mother research of this study which has found that utilizing mud can develop self-compacting mixture to alter compressed earth blocks [30].

The experimental programme started with a varying activator to identify the optimum alkaline solution to stable the mud concrete block as shown in **Table 7**. This is due to the different alumina silicate composition in the soil. However, after that, the salt content to dissolve the activator was identified. The results show that the optimum of 2% of the dry weight of the mixture can get the optimum strength for mud concrete block. And then, a profound mix was developed to test the required moisture content to make the mixture. For the mud concrete, the moisture ratio is critical to making a self-compacting mixture. The idea of self-compacting is to reduce the energy consumption of the mixture.

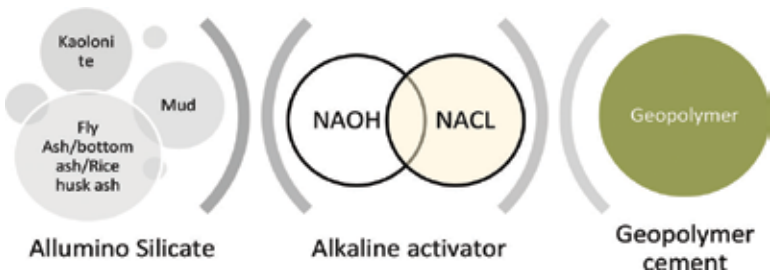

Figure 14. Experimenting with polymerizing mud concrete.

Soil	Fly ash		Activator		Salt		Water	Number of test blocks	
27,300 g	20%	7000 g	0.00%	0 g	2.00%	700 g	20.00%	6sundry	3ovendry
26,950 g	20%	7000 g	1.00%	350 g	2.00%	700 g	20.00%	6sundry	3ovendry
26,600 g	20%	7000 g	2.00%	700 g	2.00%	700 g	20.00%	6sundry	3ovendry
26,250 g	20%	7000 g	3.00%	1050 g	2.00%	700 g	20.00%	6sundry	3ovendry
25,900 g	20%	7000 g	4.00%	1400 g	2.00%	700 g	20.00%	6sundry	3ovendry
25,550 g	20%	7000 g	5.00%	1750 g	2.00%	700 g	20.00%	6sundry	3ovendry

Table 7. Experimental mix design for geopolymerizing fly ash-based mud mixture.

There are more than enough literature as well as the optimum mole content can be calculated. But since this is a practical product, it is better to establish the optimum caustic soda content to build mud concrete blocks out of fly ash and caustic soda [31–34]. The study shows that the required water mole content to produce the reaction is 20%. It is the required moisture content to produce the fly ash block. The moisture content is very important to develop the workability of the block mixture. The quick flow mixture shall help to improve the self-compacting capacity of the mixture. And the water in mud concrete block helps to improve the porosity and porosity helps to improve the thermal property of the block. The next step is the water content analysis, which was to find out the most suitable mix proportions to build fly ash-stabilized earth blocks. As per the results indicated in the previous experiment, the best compressive strength was shown when the moisture content was in between 15 and 20%. The

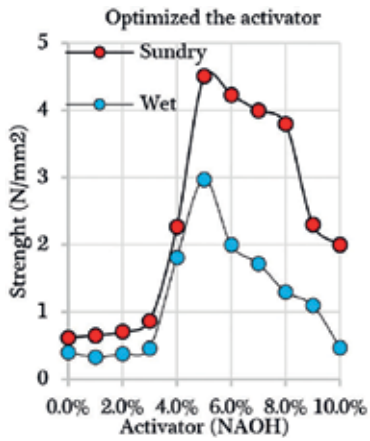

Figure 15. Optimizing NAOH.

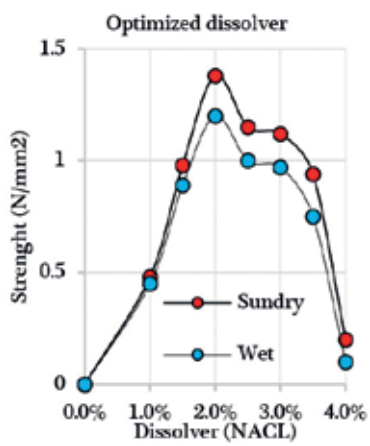

Figure 16. Optimizing NACL.

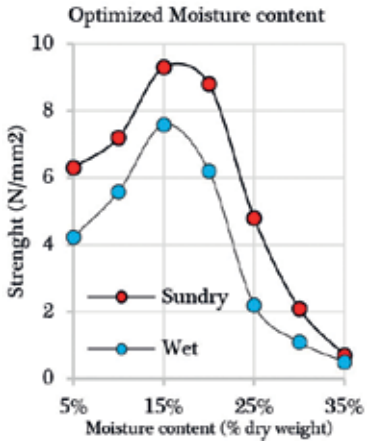

Figure 17. Optimizing moisture content.

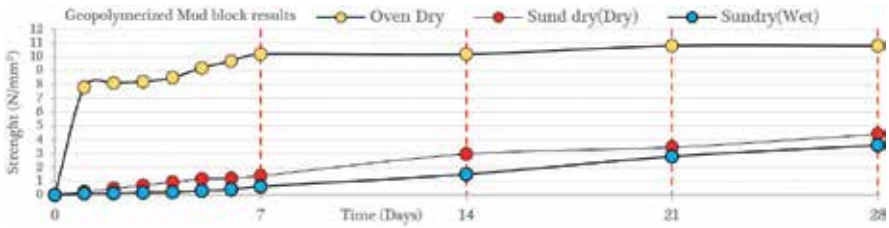

Figure 18. Geopolymerized mud concrete block final results.

results obtained are shown in **Figures 15–17**. After the confirmation of water content, the mix proportion was started varying the sand and gravel combinations as shown in **Figure 18**.

5. Application in construction

The use of invented stabilizers was tested upon different soil combinations to see the strength development. And then, they were employed to build a walling sample width of 1 m and a height of 1 m. Out of the entire study, the most vulnerable and practical stabilizers were selected to develop this walling samples test. A 1-m wide 1-m tall building wall sample was made at the University premises to check the practicality of this new mix as shown in **Figure 19**. The practical use and mass scale production were studied in this process and found that natural rubber should be avoided as alternative stabilizers. Geopolymerization of waste ashes such as fly ash, bottom ash and especially the rice husk ash has the quality of replacing the cement and build a novel walling material.

Figure 19. Fly ash geopolymerized mud concrete masonry unit wall.

6. Conclusion

This study was conducted to alter cement in mud concrete technology. Mud concrete is a novel walling material discovered to alter compressed earth blocks. The concept of mud concrete block is to build concrete by soil. Sand and metal of concrete are replaced by a fraction of the soil. The precise gravel percentage governs the strength of mud concrete. The cement in this concrete is also used as a stabilizer. But the cement has this weakness of initial cost and the heavy carbon footprint. If cement in mud concrete can be replaced with a much greener stabilizer, mud concrete can be recommended as a greener walling material.

The study was conducted after a series of nature studies and literature studies. In addition, the folk knowledge also has been considered prior to the experimenting with stabilizers. Then, the study builds an inventory of possible stabilizer which may replace the cement and act as a stabilizer for soil. At the very beginning, the study was focused to develop natural polymer-based stabilizer because ancient Sri Lankan ancestors used natural polymers to stabilize the earth and build gigantic structures and plastered them with frescos. However, the utilization of natural polymers was an utter failure due to the availability of materials. The experiment with natural latex rubber and mud concrete

achieved the required strength but there were many practical issues when it comes to the physical use of rubber-stabilized earth blocks. Then, a study was done with a series of natural polymers taken from other plants such as pines, chews, and so on. The results are good enough but practically cannot be applied in the real world where the mass production of earth blocks is required.

Then, the study was focused to utilize industrial waste into cementitious materials for mud concrete block. Fly ash, bottom ash and rice husk ash were subjected to this study and found astonishing results. The initial results with a raw form of waste were failure and they did not produce the required strength. And then, the developed mixture with alkaline solution creates much better strength with mud concrete block. After finalizing the mix and all, a sample wall area of 1 m × 1 m was built to check the practical application of this block to produce affordable walling. And it was noticed that highly alkaline solutions make the mixture somewhat difficult. The expanded study was conducted to rank the alternative stabilizers discovered in this study. The developed stabilizer was ranked according to their workability availability and the initial cost. And then, the extensive study was conducted with life cycle cost and carbon footprint analysis to understand the long-term use and the environmental impact of those stabilizers.

Acknowledgements

This material is based on the work supported by the NSF (National Science Foundation of Sri Lanka) grant number under RG/2017/EA & ICT /02. Any options, findings and conclusions or recommendation expressed in this material are those of the authors.

Author details

Chameera Udawattha* and Rangika Halwatura

*Address all correspondence to: udawatthe@gmail.com

University of Moratuwa, Sri Lanka

References

[1] Udawattha C, Halwatura R. Thermal performance and structural cooling analysis of br-ick, cement block, and mud concrete block. Advances in Building Energy Research. 2016:1-14

[2] Udawattha C, Halwatura R. Embodied energy of mud concrete block (MCB) versus brick and cement blocks. Energy and Buildings. 2016 Aug;**126**(0):28-35

[3] Udawattha C, Galabada H, Halwatura R. Mud concrete paving block for pedestrian pavements. Case studies in construction materials. 2017 Dec:249-262

[4] Nanayakkara NHVTN, Udawattha C, Halwatura RU. Investigation on Elements and their Fraction of Housing Construction Cost. Moratuwa Engineering Research Conference (MERCon). 2017:277-282

[5] Udawattha C, Arooz R, Halwatura R. New Earth Walling Material: Integrating Modern Technology into Ancient Mud Wall. In: 7th International Conference on Sustainable Built Environment 2016, Kandy, Sri Lanka, 16th to 18th December 2016; 2016, December

[6] Udawattha C, Arooz R, Halwatura R. Manufacturing framework and cost optimization for building mud concrete blocks (MCB). In: Mobilization modern technologies for sustainable development in Asia, Science council of Asia; 2016. p. 112

[7] Udawattha C, Halwatura R. Life cycle cost of different walling material used to build affordable housing in tropics. Case Studies in ConstructionMaterials. 2017;**7**:15-29

[8] Udawattha C, Halwatura R. Comparative Study of Embodied Energy in Different Walling Materials. In: Proceedings of the International Forestry and Environment Symposium 2016, Department of Forestry and Environmental Science, University of Sri Jayewardenepura, Sri Lanka; 2016, no. 224. p. 2016

[9] Udawattha C, Arooz R, Halwatura R. Energy content of walling materials—a comparison of mud concrete blocks, bricks cabook and cement blocks in tropics. In: International Conference on Sustainable Built Environment 2016; 2016 December

[10] Ren KB, Kagi DA. Upgrading the durability of mud bricks by impregnation. Building and Environment. 1995;**30**(3):433-440

[11] Muhammad B, Ismail M. Performance of natural rubber latex modified concrete in acidic and sulfated environments. Construction and Building Materials. 2012;**31**:129-134

[12] Nalbantoğlu Z. Effectiveness of class C fly ash as an expansive soil stabilizer. Construction and Building Materials. 2004;**18**(6):377-381

[13] Kaniraj SR, Havanagi VG. Compressive strength of cement stabilized fly ash-soil mixtures. Cement and Concrete Research. 1999;**29**(5):673-677

[14] Udawattha C, Dilshan P, Halwatura R. Use of fly ash as alternative stabilizer for mud concrete block. In: The annual International Research Conference of KDU; 2017. pp. 8-12

[15] Güllü H. Factorial experimental approach for effective dosage rate of stabilizer: Application for fine-grained soil treated with bottom ash. Soils and Foundations. 2014; **54**(3):462-477

[16] Udawattha C, Jayasinghe D, Halwatura R. Investigation of bottom ash as alternative stabilizer for mud concrete block. In: The annual International Research Conference of KDU; 2017. pp. 3-7

[17] Basha EA, Hashim R, Mahmud HB, Muntohar AS. Stabilization of residual soil with rice husk ash and cement. Construction and Building Materials. 2005;**19**(6):448-453

[18] Nagrale SD, Hajare H, Modak PR. Utilization Of rice husk ash. International Journal of Engineering Research and Applications. 2012;**2**(4):1-5

[19] Rahman MA. Properties of clay-sand-rice husk ash mixed bricks. International Journal of Cement Composites and Lightweight Concrete. 1987;**9**(2):105-108

[20] Ashour T, Korjenic A, Korjenic S, Wu W. Thermal conductivity of unfired earth bricks reinforced by agricultural wastes with cement and gypsum. Energy and Buildings. 2015;**104**:139-146

[21] Haggam RA, Ibrahim IM, El-Shafie M, Abd El Rhman AMM, El-Kholy SA. Improvements of properties of asphalt by poly(methyl methacrylate) additives. Russian Journal of Applied Chemistry. 2014;**87**(5):664-670

[22] Ohama Y. Recent progress in concrete-polymer composites. Advanced Cement Based Materials. 1997;**5**(2):31-40

[23] Muhammad B, Ismail M, Bhutta MAR, Abdul-Majid Z. Influence of non-hydrocarbon substances on the compressive strength of natural rubber latex-modified concrete. Construction and Building Materials. 2012;**27**(1):241-246

[24] Muhammad B, Saand A. Performance optimization of elastomeric latexes in cement concrete production. Science, Technology and Development. 2015;**34**(4):232-241

[25] Chang I, Prasidhi AK, Im J, Cho GC. Soil strengthening using thermo-gelation biopolymers. Construction and Building Materials. 2015;**77**:430-438

[26] Muhammad B, Mohammad I, Haron Z, Yussuf AA. Elastomeric effect of natural rubber latex on compressive strength of concrete at high temperatures. Journal of Materials in Civil Engineering. 2016 October;**25**:864-870

[27] Dhanapala DB. A short note on the technique of seegiriya Pictures. Universityof Ceylon Review. 1944;**3**:1-3

[28] Udawattha C, Halwatura R. Character of lime as an alternative stabilizer to improve the long term strength of mud concrete block. In: 8th International Conference on Structural Engineering and Construction Management ICSECM2017; 2017December

[29] Provis JL, Van Deventer JSJ. Geopolymers: Structure, processing, properties and industrial applications. Woodhead; 2009

[30] Halwathura R. AN-II_PATENT-MCB (1).pdf; 2016

[31] Rattanasak U, Chindaprasirt P. Influence of NaOH solution on the synthesis of fly ash geopolymer. Minerals Engineering. 2009;**22**(12):1073-1078

[32] Choo H, Lim S, Lee W, Lee C. Compressive strength of one-part alkali activated fly ash using red mud as alkali supplier. Construction and Building Materials. 2016;**125**:21-28

[33] Annie Paul S, Boudenne A, Ibos L, Candau Y, Joseph K, Thomas S. Effect of fiber loading and chemical treatments on thermophysical properties of banana fiber/polypropylene commingled composite materials. Composites. Part A, Applied Science and Manufacturing. Sep. 2008;**39**(9):1582-1588

[34] Chindaprasirt P, Chareerat T, Sirivivatnanon V. Workability and strength of coarse high calcium fly ash geopolymer. Cement and Concrete Composites. 2007;**29**(3):224-229

Chapter 11

Sorel Cements from Tunisian Natural Brines

Halim Hammi, Amal Brichni, Salima Aggoun and Adel Mnif

Additional information is available at the end of the chapter

http://dx.doi.org/10.5772/intechopen.74315

Abstract

In this chapter, the experimental design methodology is applied to optimize the formation conditions of magnesium chloride cement. A factorial design to model and to optimize the operating parameters that govern the formation was used. The studied factors were mass ratio of $MgCl_2.6H_2O/MgO$, mixing time and stirring speed. The considered responses were compressive strength and setting time. The optimum operating conditions were quite efficient to have a good compressive strength and suitable setting time. The phases' compositions of the magnesium oxychloride cement were evaluated by X-ray diffraction, the morphological properties were examined by scanning electron microscopy (SEM) method and their thermal behavior was analyzed by differential thermal analysis/thermogravimetric analysis (DTA/TGA). The raw materials used in the study were magnesium oxide and magnesium chloride hexahydrate obtained from natural brines in the south of Tunisia.

Keywords: magnesium oxychloride cement, experimental design methodology, optimization

1. Introduction

Magnesium chloride cement (MOC) has superior properties as compared to ordinary Portland cement such as high compressive strength [1], good resistance to abrasion, rapid hardening rate, good cohesiveness and high fire resistance [2], and it can be used with all kinds of aggregates [3]. The main used applications are architectural applications such as the construction of industrial floors, construction of thermal and acoustical insulating panels [4] and other prefabricated building boards [5]. The basic chemical reaction system of the MOC system is $MgO–MgCl_2–H_2O$ [6, 7]. The main bonding phases found in hardened MOC is $5Mg(OH)_2$.

$MgCl_2.8H_2O$ (phase5) and $3Mg(OH)_2.MgCl_2.8H_2O$ (phase 3) which are obtained by the following chemical reactions [7]:

$$5MgO + MgCl_2 + 13H_2O = 5Mg(OH)_2.MgCl_2 + 8H_2O \quad (1)$$

$$3MgO + MgCl_2 + 11H_2O = 3Mg(OH)_2.MgCl_2 + 8H_2O \quad (2)$$

They are the only stable phases in the system $MgO\text{-}MgCl_2\text{-}H_2O$. Due to the presence of excess water, a parallel or competitive reaction, corresponding to magnesium oxide hydration, can take place:

$$MgO + H_2O = Mg(OH)_2 \quad (3)$$

The presence of $Mg(OH)_2$ indicates the low quality of magnesium oxychloride cement.

Furthermore, the widespread use of magnesium oxychloride cement has been limited because of loss of strength on prolonged excessive exposure to water [8]. Much research has long been processed to improve the water resistance of magnesium oxychloride based on the ability to it binding to various organic and inorganic aggregates such as high active SiO_2 [9, 10], active aluminates [11] sulfates and phosphoric acid or phosphate [12].

In this chapter, the influence of three factors (mass ratio of $MgCl_2/MgO$, mixing time and stirring speed) on compressive strength and setting time of MOC was carried out. The application of the experimental design methodology was used in order to maximize synthesis yield by searching for optimum experimental conditions in a less number of experiments.

2. Raw materials from natural brines

The Tunisian territory contains a great number of sebkhas and chotts, especially in the South. The more important ones are Chott El Jerid, Sebkha El Melah of Zarzis, Sebkha Oum el Khialate, Sebkha El Briga and Sebkha El Adhibate (**Figure 1**) [13]. Previous geological, hydrogeological and geochemical studies proved that these deposits contain considerable reserves of natural brines (**Table 1**).

The meteorological conditions in the South of Tunisia and particularly at Sebkha El Melah of Zarzis (**Figure 2**) are favorable for the recovery of the existing salts by solar evaporation. The raw material is taken from Aïn Serab, located at the Northern border of Sebkha El Melah of Zarzis. This choice is justified by the advantages present in this mineral resource and the influence on the economic sector for possible industrial exploitation [14].

These salt lakes which are considered as important material resources useful for industry and agriculture. They are called sebkha or chott, and they cover a large part of Tunisian land. The liquid raw material enclosed in these deposits is named brine and always assimilated to the quinary system: Na^+, K^+, Mg^{2+}/Cl^-, SO_4^{2-}/H_2O. These solutions are valuable and expected to play an important role in the economic sector. To take advantage of this raw material, several works

http://dx.doi.org/10.5772/intechopen.74315

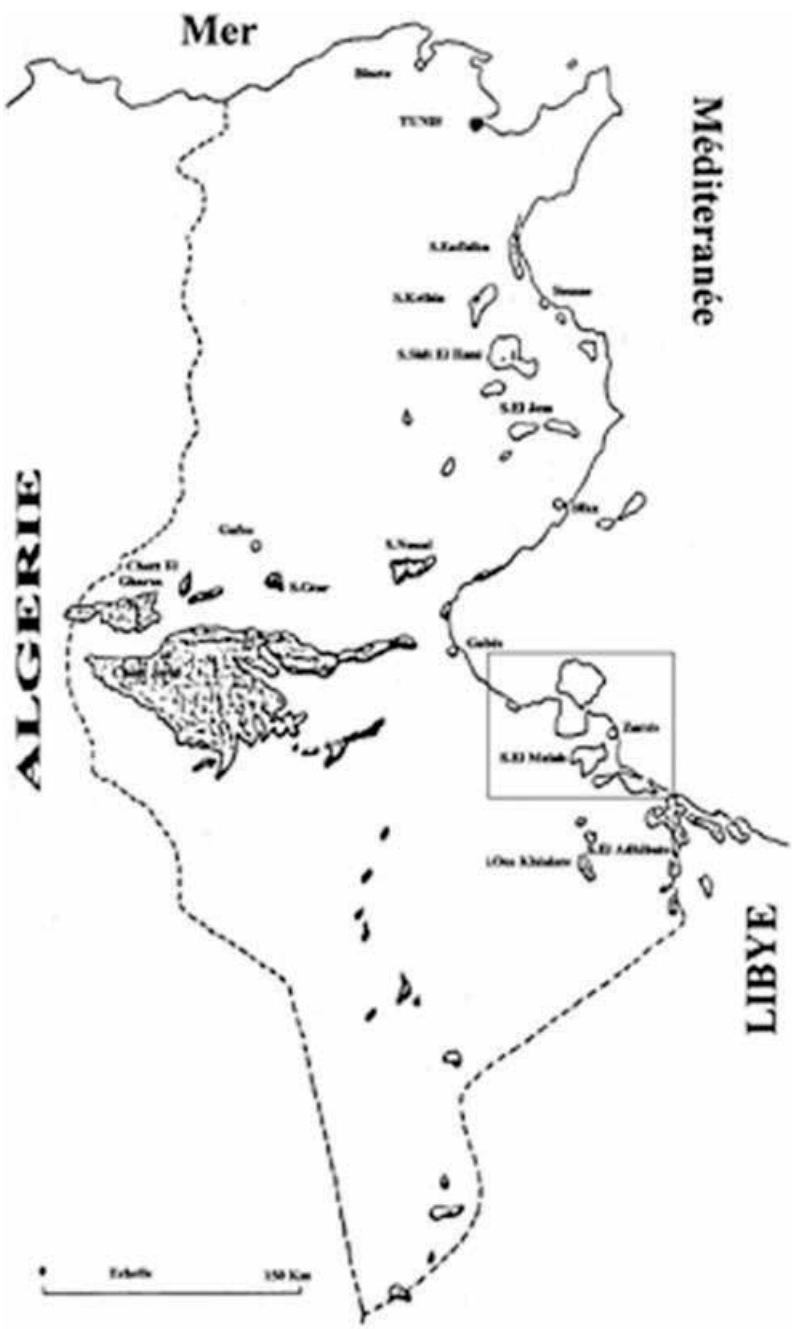

Figure 1. Location of Tunisian sebkhas and chotts.

were developed. Besides the study of geological aspects and phase diagrams of the system representing the brines, investigations were extended to the modeling of phase diagrams and extraction of interesting salts.

Sites	Geographic location	Surface, km^2	Total reserves, 10^6 m^3	Recoverable reserves, 10^6, m^3	Total salinity, g/L
Chott Jerid	Tozeur	5000	5000	600	330
S. El Melah	Zarzis	150	600	160	335
S. oum El Khialate	Tataouine	75	50	17	150
S. El Adhibate	Tunisian Libyan border	125	245	100	260
S. El Briga	Tunisian Libyan border	22	78	18	330

Table 1. Characteristics of south Tunisian sebkhas and chotts.

2.1. Magnesium oxide

Exceptional proprieties of MgO as a catalytic material [15, 16] or as an additive in building supplies (Sorel cement, lightweight building panels) and superconductor products have attracted both fundamental and application studies [17–22].

Magnesium oxide (MgO or periclase) is one among the most industrially important magnesium compounds. Approximately 20% of worldwide production came from seawater, brines and desalination reject brine [15]. Magnesium oxide is used as an exceptionally important material in catalysis [15, 16], toxic waste remediation [18] or as additives in refractories, paints, in the manufacture of fertilizers, animal feedstuffs, building materials (Sorel cement, lightweight building panels) and superconductor products [19–21]. A panel of fundamental and applied studies is encountered in literature [21–25]. It shows particularly that magnesium hydroxide production from seawater or brine precipitates by adding a strong base and after separation is calcined to produce MgO. Furthermore, magnesia qualities may differ depending upon the physicochemical conditions of preparation and the precursor type.

In the literature, MgO was prepared mainly by calcination of $Mg(OH)_2$ obtained either by precipitation [21, 22] or by MgO hydration [21, 23–25]. In our case, magnesium oxide was produced from magnesium sulfate ($MgSO_4.7H_2O$) by precipitation into $Mg(OH)_2$ using a strong base (NH_4OH) in the first step and then calcined in a programmable furnace under controllable conditions to produce MgO in the second step.

The sensitivity of the present reactions to several parameters was carried out. These considerations altogether led to applying the experimental design methodology in order to maximize synthesis yield by searching for the optimum experimental conditions in a smaller number of experiments.

2.2. Magnesium chloride

Magnesium chloride is industrially useful in some agricultural applications. It is mainly used for magnesium metal production and Sorel cement manufacturing (Büchel et al., 2000). Frequently, natural raw material is complex and must be treated to recover solid magnesium chloride. Various procedures (Boyum et al., 1973; Burke and Smith, 1949; Fezei et al., 2009; Smith, 1970) have been developed in order to produce this salt from natural brines. The

Figure 2. Sebkha El Melah of Zarzis [14].

present work is devoted to magnesium chloride hexahydrate recovery from a mixed salt solution. 1.4-Dioxan was chosen to achieve this aim. The action of this organic solvent on magnesium chloride has been often studied in the case of pure magnesium chloride solutions (Gaska, 1967; Weissenberg, 1969).

As shown in **Figure 3**, the investigated process is mainly composed of six stages. The adopted flow sheet is principally supported by the previous works on natural brines (Janecké, 1907; Berthon, 1962; Cohen-Adad et al., 2002; M'nif and Rokbani, 2004; Hammi, 2004) usually described using the oceanic quinary diagram Na^+, K^+, Mg^{2+}/Cl^-, SO_4^{2-}/H_2O. This useful graphic-tool is helpful in natural brines exploitation or valorization. In fact, it defines, during the system's evolution, the number, the nature, the composition and the relative quantity of different condensed phases that crystallize or disappear. The first treatment step consists in evaporating at 35°C the raw brine to precipitate the maximum of sodium chloride (halite).

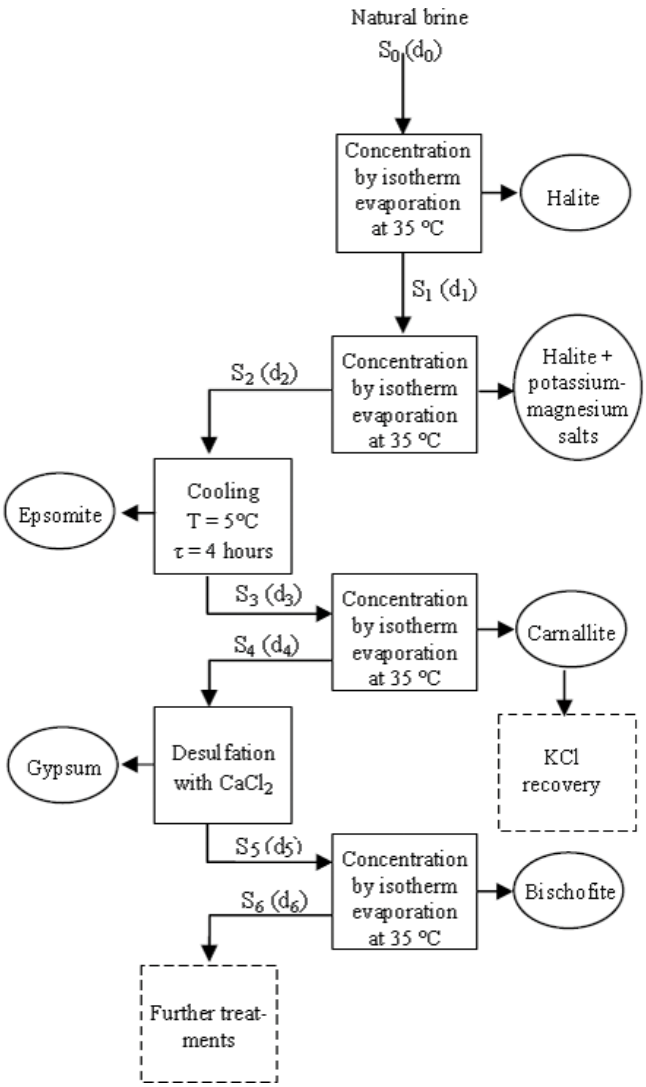

Figure 3. Flow sheet of the process for the bischofite salt recovery from Sebkha El Melah natural brine.

In the second step, The precipitated salts consist of sodium chloride and small amounts of magnesium-potassium double salt. The third stage consists in maintaining the obtained magnesium salts saturated solution under stirring during four hours at 5°C and to recover the precipitated salt. The fourth step consists in precipitating the potassium- magnesium double salt, carnallite ($KCl.MgCl_2.6H_2O$) to eliminate potassium ions; in order to avoid interference with the production of an end product having good quality. In the two last stages of the process the solution is desulphated by reaction with calcium chloride solution. After removing the calcium sulfate precipitate, the resulting brine; consisted of magnesium chloride together with residual potassium and sodium chloride; is concentrated by evaporation at 35°C to precipitate the magnesium chloride salt.

3. Results and discussion

3.1. Experimental procedure

Magnesium oxide powder was mixed with magnesium chloride solution mechanically to form homogenous MOC pastes. The weight of MgO is fixed and the weight of $MgCl_2.6H_2O$ has been varied. Mixtures were cast in cylindrical molds (26 mm in diameter, 50 mm high) and stored for 24 h, then unmolded and air-cured for 28 days.

The X-ray diffraction (XRD) analysis was carried out on the powdered sample using X-ray powder diffractometer (XRD PHILIPS) with Cu K radiation (λ K = 1.54 Å).

Differential thermograms were obtained using the Netzsch 449 STA F1 Jupiter thermal analysis system. The rate of heating was 15°C/min.

The microstructure of the samples was examined using scanning electron microscope, the Carl ZEIIS LEICA S430i model.

Measurement of thermal conductivity was performed in dry state using the photothermal deflection technique. Setting time was determined by using the Vicat Apparatus.

Porosity accessible to water of MOC is determined according to EN 12390-7 norm. The measurement of porosity in water under a vacuum of 0.1 bar quantifies the volume of open pores (accessible to water) using the following protocol:

Cement samples are placed in sealed desiccators and kept under vacuum of 0.1 bar for 12 h.

Previously degassed water is introduced progressively in desiccators to fill all the pores of samples, without introducing air bubbles.

Once the samples are saturated, they are kept immersed in water for 24 h, and finally we determined hydrostatic mass m_{sss}^{imm} and saturated dry surface mass mss.

The porosity is calculated by Eq. (4):

$$\frac{m_{sss}-m_{dry}}{m_{sss}-m_{sss}^{imm}} \quad (4)$$

where

msss: the saturated dry surface mass of the sample;

mdry: the mass of sample before saturation; and.

m_{sss}^{imm}: mass of sample measured in water.

3.2. Studied factors and experimental domains

According to the preparation of MOC, three quantitative factors are chosen: mass ratio of $MgCl_2$/MgO, stirring speed and mixing time. The corresponding variables and their levels (set according to the data of preliminary experiments and the equipment abilities) are given in **Table 2**. The two experimental responses tracked were compressive strength (Y_1) and the setting time (Y_2).

To test the direct influence of the three studied factors as well as their possible interaction effects on the measured experimental responses, we have realized a two-level complete factorial design 2^3 which is expected to provide excellent information concerning not only the main effects but also the double interaction effects.

The experimental design and the measured responses are summarized in **Table 2**.

Comparing MOC and Portland cement (setting time between 2 and 3 h), it is found that MOC has a faster setting. It also has better mechanical strength.

For a very short setting time (6 min), MOC has a high strength (75.48 MPa): in this case the cement is recommended for applications that require fast setting (decoration use, restoration of monuments, damaged marble, etc.).

For a longer setting time (64 min), it has a good mechanical strength (46.59 MPa): in this case the cement is recommended for applications which require a longer setting time (floor covering).

Considering that the interaction effects between three or more factors are negligible, the factor effect estimation is computed by Mathieu et al. [26]; according to Goupy [27]:

$$b_i = \frac{\sum_j^N \pm Y_j}{N} \quad (5)$$

where bi is the effect estimation of the factor i, Yj is the response j, and N is the number of experiences.

The pooled variance estimation used to determine the significant factors is computed as

$$S_a^2 = \frac{\sum_i^n \nu_i S_i^2}{n} \quad (6)$$

No. exp.	Mass ratio of $MgCl_2$/MgO	Mixing time (min)	Stirring speed (rpm)	Compressive strength (MPa)	Setting time (min)
1	1.42	5	650	49.47	20
2	2.22	5	650	46.59	64
3	1.42	15	650	4.55	17
4	2.22	15	650	21.20	37
5	1.42	5	1600	41.38	14
6	2.22	5	1600	76.40	41
7	1.42	15	1600	75.48	6
8	2.22	15	1600	20.50	32
9	1.82	10	1125	67.00	30
10	1.82	10	1125	60.54	31
11	1.82	10	1125	59.00	28

Table 2. Factorial matrix 2^3.

where S_a^2 is the pooled experimental variance, S_i^2 is the experimental variance estimation i, ν_i is the degree of freedom i, and $n = \sum \nu_i$ is the degree of freedom of the pooled experimental variance.

4. Identification of the influential factors

Based on check student for an error risk $\alpha = 5\%$, it was found that tabulated = 4.303. **Table 3** summarizes the factor effects estimation for the two responses: compressive strength (Y_1) and setting time (Y_2).

Coefficient	Y_1				Y_2			
	Value	SD	t.exp	P	Value	SD	t.exp	P
b0	47.464	1.279	37.087	0.000726	29.090	0.460	63.1634	0.000251
b1	−0.773	1.500	−0.515	0.657478	14.625	0.540	27.0802	0.001361
b2	−11.513	1.500	7.672	0.016568	−5.875	0.540	−10.878	0.008345
b3	11.493	1.500	7.658	0.016624	−5.625	0.540	−10.415	0.009093
b12	−8.808	1.500	−5.869	0.027819	−3.125	0.540	−5.7864	0.028592
b13	−4.216	1.500	−2.809	0.106780	−1.375	0.540	−2.5460	0.125809
b23	6.063	1.500	4.040	0.056143	1.625	0.540	3.0089	0.094979
b123	−13.691	1.500	−9.123	0.011802	2.875	0.540	5.3235	0.033522

Table 3. Factor signification for the two responses Y_1 and Y_2.

The two models are represented by the equations given below:

Compressive strength:

$$Ycal_1 = 47.464 - 11.51\,3X_2 + 11.49\,3X_3 - 8.808\,X_1X_2 - 13.6913\,X_1X_2X_3 \quad (7)$$

Setting time:

$$Ycal_2 = 29.090 + 14.62\,5X_1 - 5.87\,5X_2 - 5.625\,X_3 - 3.12\,5X_1X_2 + 2.875\,X_1X_2X_3 \quad (8)$$

4.1. Analysis of residue

Figure 4 reveals the distribution of the calculated values versus experimental values for the two responses (Y_1 and Y_2). The points are almost randomly distributed about the line representing exact agreement, providing good agreements between experimental values and those calculated using the model.

4.2. Analysis of variance

Table 4 summarizes the variance analysis of the chosen responses Y_1 and Y_2.

The main results for Y1 and Y2 are, respectively, 333.601 and 12.539, as lack of fit mean squares and 18.017 and 2.333 as the estimation of experimental variance. Thus, the values of the ratio between the lack of fit mean square and the estimation of experimental variance 18.51568 and 5.3739 for the responses Y1 and Y2 are inferior to tabled $F^{0.05}_{4,2}$ and $F^{0.05}_{3,2}$, respectively. Consequently, it is possible to confirm the validity of the two elaborated models. In addition, the ratios between the regression mean square and the residual mean square for the three responses Y1 and Y2 (4.638 and 5.3739) are superior to the tabled $F^{0.05}_{4,6}$ and $F^{0.05}_{5,5}$, respectively. Thus, the significant variables, applied to elaborate the three models, have a large significance on their responses.

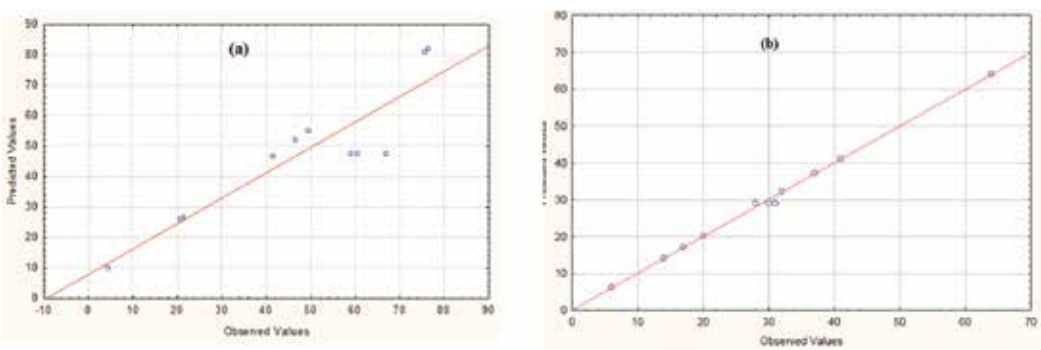

Figure 4. Calculated versus experimental values graph (a) for compressive strength (b) for setting time.

Source of variation	SS	DF	MS	Ratio	P
Compressive strength					
Regression	4237.738	4	1059.4345	4.63837	0.048
Residual	1370.437	6	228.40616		
Lack of fit	1334.403	4	333.601	18.51568	0.051897
Pure error	36,034	2	18.017		
Total	5608.174	10	1059.4345		
Setting time					
Regression	2384.625	5	476.925	56.40478	0.0000
Residual	42.277	5	8.4554		
Lack of fit	37.610	3	12.539	5.3739	0.160892
Pure error	4.667	2	2.333		
Total	2426.909	10	476.925		

Table 4. Analysis of variance.

4.2.1. Optimization

For selecting the optimal conditions we try to strike a compromise between the two responses to have good compressive strength and a suitable setting time.

By merely regarding values and signs of these significant effects, we conclude that maximization of the two responses is reached for experience number 6 (compressive strength = 76.40 MPa and setting time = 41 min):

Mass ratio of $MgCl_2.6H_2O/MgO$ (X_1): 2.22

Mixing time (X_2): 5 min

Stirring speed (X_3): 1125 rpm

The phase diagram of the ternary MOC system ($MgO-MgCl_2-H_2O$) [5] at an ambient temperature is illustrated in **Figure 5** with the composition point of the optimum which is located near phase 5 responsible for good compressive strength of the cement.

4.3. Characterization

Figure 6 shows the XRD pattern of MOC with an optimal condition. It can be found that phase 5 is present. This phase is the major product responsible for hardening and the strength of MOC. We measured porosity accessible to water, we found that the total porosity of MOC is 4% which is in good accordance with other results in literature [28].

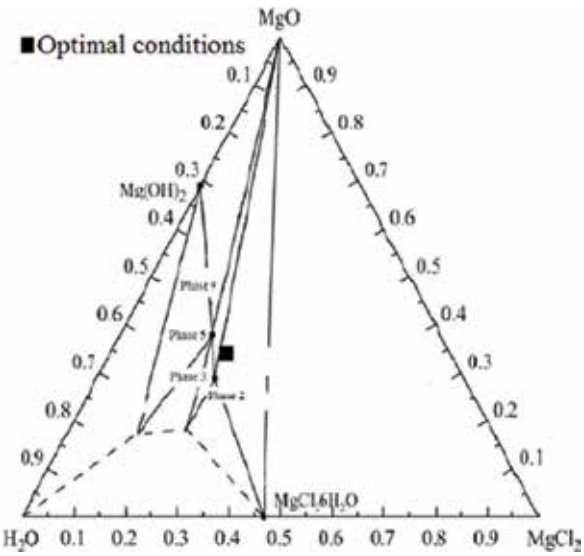

Figure 5. Phase diagram of the ternary MOC system [5].

The thermal conductivity of cement is 0.8 w/mK. The morphology of MOC is shown in **Figure 7**. We can see a rough surface with a dense network of needle-like crystals of 500 nm which has a high strength (phase 5). Thermal analysis of MOC is shown in **Figure 8**. Six endothermic events appear on the DTA curves of MOC during heating. Thermal decomposition requires a dehydration stage of the crystalline phase 5 $Mg(OH)_2MgCl_2.8H_2O$ at 179°C to obtain anhydrous materials.

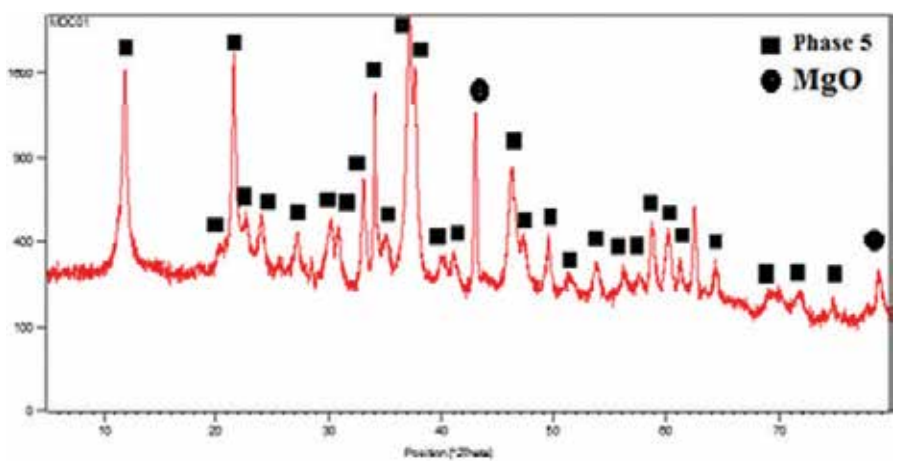

Figure 6. XRD patterns of MOC.

http://dx.doi.org/10.5772/intechopen.74315

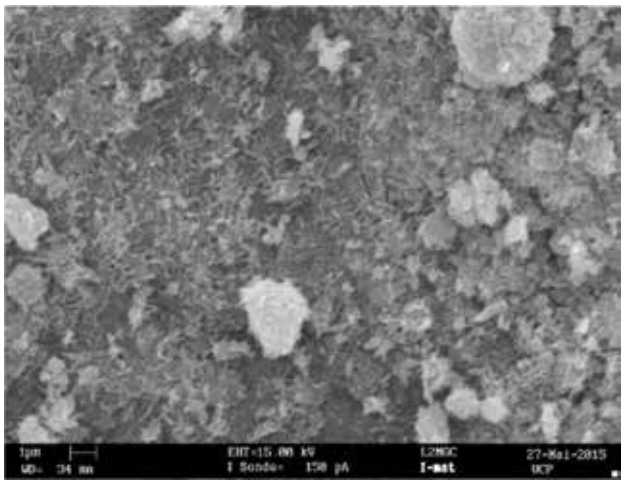

Figure 7. SEM analysis of MOC.

The other deflections in this curve at 358, 414, 484, and 711°C present the decomposition stage of 5 $Mg(OH)_2$ $MgCl_2$ and the loss of $MgCl_2$. The last deflection at 1100°C represents the decomposition to obtain the final solid product MgO.

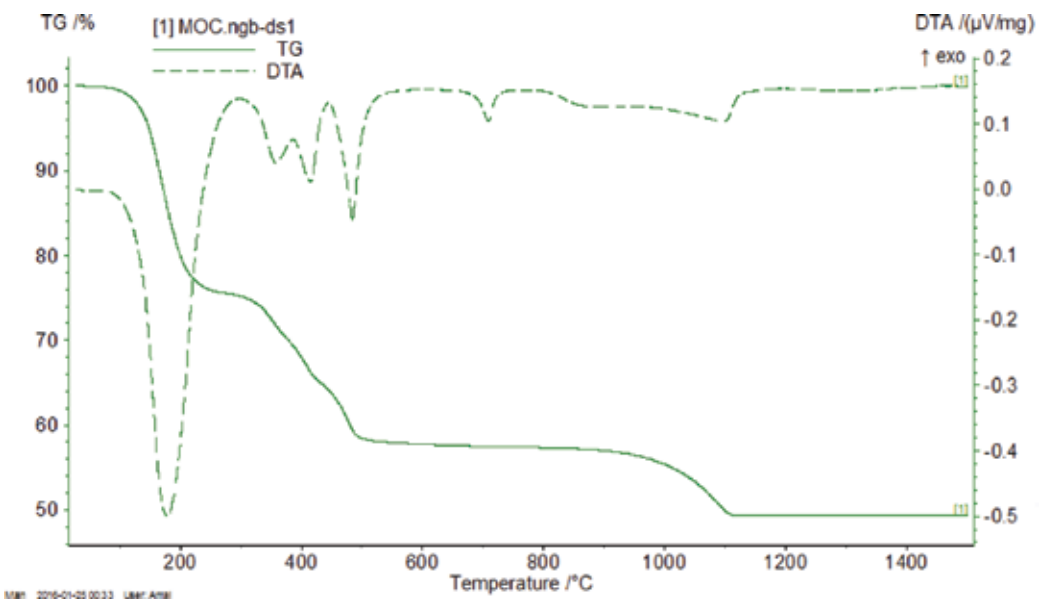

Figure 8. TG and DTA curves of MOC.

5. Conclusion

The formation of MOC from natural brines was carried out in this study using experimental design. The results showed that there is an agreement between the experimental values and those calculated from the model developed which confirms its validity. The optimal conditions are $MgCl_2.6H_2O/MgO$ (X1): 2.22, mixing time (X2): 5 min and stirring speed (X3): 1125 rpm. The responses are compressive strength = 76.40 MPa and setting time = 41 min. The interpretation of results found by DRX, IR, SEM and TG-DTA confirms the presence of phase 5 which is responsible for the good compressive strength of magnesium oxychloride cement.

Acknowledgements

This chapter was supported by a grant from Ministry of Higher Scientific Research of Tunisia. The authors would like to thank the technical team of the National Research Centre of Materials Sciences in Borj Cedria Technological Park and of L2MGC in the University of Cergy-Pontoise.

Author details

Halim Hammi[1]*, Amal Brichni[1,2], Salima Aggoun[3] and Adel Mnif[1]

*Address all correspondence to: halimhammi2015@gmail.com

1 Useful Material Valorization Laboratory, National Center for Research in Materials Sciences, Soliman, Tunisia

2 Université de Tunis El Manar, Faculté des Sciences de Tunis, Tunis, Tunisie

3 University of Cergy-Pontoise (L2MGC), Neuville Sur Oise, Cergy-Pontoise Cedex, France

References

[1] Li J, Yu Y, Li G. The influence of compound additive on magnesium oxychloride cement/urban refuse floor tile. Construction and Building Materials. 2008;**22**:521-525

[2] Montle JF, Mayhan KG. The role of magnesium oxychloride as a fireresistive material. Fire Technology. 1974;**10**:201-210

[3] Siddique R, Naik TR. Naik, Properties of concrete containing scrap-tire rubber-an overview. Waste Management. 2004;**24**:563-569

[4] Yu H. Magnesium Oxychloride Cement and Its Application. 1st ed. Beijing: China Building Materials Industry Press; 1993

[5] Zongjini L, Chau CK. Influence of molar ratios on properties of magnesium oxychloride cement. Cement and Concrete Research. 2007;**37**:866-870

[6] Deng DH, Zhang CM. The formation mechanism of the hydrate phases in magnesium oxychloride cement. Cement and Concrete Research. 1999;**29**(9):1365-1371

[7] Li Y, Yu HF, Dong JM, Wen J, S Y. Reseach Development on Hydration Product, Phase Transformation and Water Resistance Evaluation Method of Magnesium Oxychloride Cement. Journal of the Chinese Ceramic Society. 2013;**41**:1465-1473

[8] Beaudoin JJ, Ramachandran VS. Strength development in Magnesium Oxychloride and Other Cement and Concrete Research. 1975;**5**:617-630

[9] Wu CY, Zhang HF, Yu HF. The effects of aluminum-leached coal fly ash residue on magnesium oxycloride cement. Advances in Cement Research. 2013;**25**:254-261

[10] Xu K, Guo Y, Sun Q, Dong S, Li Z. Research on Chemical Intermediates. 2012;**39**:1417-1428

[11] Deng DH, Zhang CM. The effect of aluminate minerals on the phases in magnesiumoxychloride cement. Cement and Concrete Research. 1996;**26**:1203-1211

[12] Li Y, Yu H, Zheng L, Wen J, Wu C, Tan Y. Compressive strengthof fly ash magnesium oxychloride cement containing granite wastes. Construction and Building Materials. 2013;**38**:1-7

[13] M'nif A. Valorisation des saumures du sud tunisien, Habilitation. Fac. Sc. Tunis; 2001

[14] Perthuisot JP, La Sebkha El Melah de Zarzis: Genèse et Évolution d'un Bassin Paralique, École normale supérieure, Paris 1975

[15] Bûchel KH, Moretto H-H, Woditch P. Industrial Inorganic Chemistry. Weinheim: Wiley-Vch, Verlag GmbH; 2000:235

[16] Liang SHC, Gay ID. A 13C solid-state NMR study of the chemisorption and decomposition of ethanol on MgO. Journal of Catalysis. 1986;**101**:293

[17] Tsuji H, Yagi F, Hattori H, Kita H. Preparation of nanometer magnesia with high surface area and study on the influencing factors of the preparation process. Journal of Catalysis. 1994;**148**:759

[18] Copp AN. Magnesia/magnesite. American Ceramic Society Bulletin. 1995;**74**:135

[19] Wang W, Qiao X, Chen J. The role of acetic acid in magnesium oxide preparation via chemical precipitation. Journal of the American Ceramic Society. 2008;**91**:1697-1699

[20] Yuan YS, Wong MS, Wang SS. Mechanical behavior of MgO-whisker reinforced (Bi, Pb)$_2$Sr$_2$Ca$_2$Cu$_3$O$_y$ high-temperature superconducting composite. Journal of Materials Research. 1996;**11**:8

[21] Yang PD, Lieber C. Nanorod-superconductor composites: A pathway to materials with high critical current densities. Science. 1996;**273**:1836

[22] Wagner GW, Bartram PW, Koper O, Klabunde KJ. Reactions of VX, GD, and HD with nanosize MgO. The Journal of Physical Chemistry. B. 1999;**103**:3225

[23] Boldyrev AI, Simons J. Polyhedral ionic molecules. Journal of the American Chemical Society. 1997;**119**(20):4618-4621

[24] Zhou M, Zhu H, Jiao Y, Rao Y, Hark S, Liu Y, Peng L, Li Q. Optical and electrical properties of Ga-doped ZnO nanowire arrays on conducting substrates. Journal of Physical Chemistry C. 2009;**113**(20):8945-8947

[25] Sterrer M, Diwald O, Knozinger E. Vacancies and electron deficient surface anions on the surface of MgO nanoparticles. The Journal of Physical Chemistry. B. 2000;**104**:3601

[26] Mathieu D, Phan Tan Luu R. Nemrod-W Software. France: Aix-Marseille III University; 1999

[27] Goupy J. Modélisation par les plans d'expériences, Techniques de l'ingénieur. Traité Mesures et Contrôle. R 275. CFC. Paris. 2000. pp. 1-23

[28] Zhao S, Fan J, Sun W. Utilization of Iron Ore Tailings as Fine Aggregate in Ultra-High Performance Concrete. Construction and Building Materials. 2014;**50**:540-548

Calcium Phosphate Cement

Chapter 12

Calcium Phosphate Bone Cements

Erdem Şahin

Additional information is available at the end of the chapter

http://dx.doi.org/10.5772/intechopen.74607

Abstract

Biomaterials utilized in biomedical applications are of various characteristics and cements are unique in their *in situ*, biomimetic formation ability. They present the most topographically complex surfaces that usually elicit a favorable cellular response for tissue regeneration. In addition their composition may provide an effective chemical gradient around the resorbing implant to induce desired cellular activity that leads to rapid wound healing and regeneration. These are the main reasons for many cement systems to function well in the body, especially as hard tissue replacements. The properties and the setting mechanisms of the clinically most relevant cement system, calcium phosphate cements have been elucidated in this chapter.

Keywords: calcium phosphate cement, calcium orthophosphates, inorganic bone cement, cement injectability, cement setting kinetics, cement biocompatibility, orthopaedic cements

1. Introduction

In the simplest sense cement is a binder of functional solid materials. Biomedical materials that necessitate combination with a binder are usually strong, inert metals and ceramics that are implanted in order to augment defects in hard tissues such as bone and dentin. For a long time since the Second World War, this binding function had been fulfilled by organic cements that gain elasticity by crosslinking *in situ*. Polymethylmethacrylate and various other resins that display a rapid rise in viscosity and elasticity upon addition of chemicals or exposure to light have been widely accepted as effective cements despite their commonly encountered biocompatibility issues due to the release of irritating monomers and inflammatory heat of setting. Inorganic cements emerged later thanks to the advances in materials characterization techniques and understanding of the molecular mechanisms of bioactivity. Calcium sulfate,

zinc phosphate, zinc polycarboxylate, magnesium phosphate, calcium phosphate, calcium silicate and glass polyalkenoate cements all proved to be biocompatible and to some degree osteoconductive. Particularly the effectiveness of calcium phosphate cements (CPC) as biomaterials has been attributed largely to their similar composition to hard tissues, aqueous setting solutions and tailorable viscosity. In addition constant improvements in cement properties have been realized due to their biomimetic setting reactions at ambient conditions that enabled experimenting with a wide variety of chemical and biological additives. As a result, inorganic cements led in quantity by calcium phosphate cements have been applied as bulk materials to fill defects in bone and teeth, support, induce and conduct bone regeneration rather than just bind more effective biomaterials in isolation. As highlighted in the subsequent parts of this chapter, biological interaction of calcium phosphate cements with human cells have been tested extensively and provides the basis for various modification approaches to extend their applications and facilitate their evolution toward the ideal biomaterial.

Inherent solubility of most calcium compounds in water has been a major motivation for material scientists to research and discover novel cementitious systems of these materials. So was the discovery of the major class of inorganic biomedical cements, calcium phosphate cements, realized. CPCs were discovered by LeGeros, Brown and Chow in early 1980s as an alternative to bulky bone graft bioceramics to set in situ and fill bone or dental defects [1, 2]. According to Chow, the discovery of the first CPC was in fact a result of basic studies on calcium phosphate solubility behaviors for the purpose of development of a tooth remineralizing suspension similar to contemporary toothpaste formulations. Based on solubility phase diagrams, material scientists were aware of the fact that both tetracalcium phosphate (TTCP) and dicalcium phosphate anhydrate (DCP) are much more soluble than hydroxyapatite (HA) under neutral pH conditions. Further, a slurry containing appropriate amounts of these compounds can produce continuous HA precipitation while maintaining the solution composition relatively constant. Brown and Chow observed that some of the TTCP + DCP aqueous pastes became a hardened mass when left in test tubes for a few hours. Thus unaware of the beneficial biomedical consequences, they discovered a new type of bioactive, self-hardening cement that consisted of only calcium phosphates and formed HA as the product. Rigorous subsequent in vivo research on the same cement system led to the conclusion that implanted CPC was gradually replaced by new bone. This CPC composition received approval by the US Food and Drug Administration in 1996, thus becoming the first commercially available CPC for use in humans [3]. Since then, many compositions have been proposed, most of which are given in the following sections.

2. Applications

Compared to sintered calcium phosphate ceramics which are the most commonly applied materials in orthopedic surgery, calcium phosphate cements have three major advantages. Firstly, CPCs are nanocrystalline and hence have a very high specific surface area. Values as high as 100 m^2/g can be reached. In comparison, sintered ceramics have surface areas close to or below 1 m^2/g. Secondly, CPCs enable the synthesis of granules and blocks of low-temperature calcium phosphates such as dicalcium phosphate dihydrate (DCPD), dicalcium phosphate anhydrate,

octacalcium phosphate (OCP), or precipitated apatite (PHA) [4]. In addition, initial flowability of CPCs enable their convenient conveying to the surgical site by means of a pressurization equipment and easy shaping by hand to conform to the defect perfectly. Injectability and sufficient compressive strength of CPCs has expanded their use to minimally invasive surgeries like percutaneous vertebroplasty and balloon kyphoplasty where organic polymethylmethacrylate (PMMA) cements had previously been the only choice for the surgeon to fill bone defects or fix bulk implants to the defect site [5, 6]. Due to the superiority of CPCs to PMMA in many aspects including bioactivity [7–9], dimensional stability [10], and biomimetic hardening, these materials are gradually replacing the organic bone cements especially in minimally invasive operations.

Calcium phosphate bone cement pastes typically exhibit relatively low shear viscosity and elastic modulus, then gain elasticity and shear viscosity with time. The rates of growths of the elasticity and viscosity of calcium phosphate based cements are generally higher than those of conventional cements as a result of the rapid dissolution and crystallization of calcium phosphate particles in water. Their initial flowability and workability are exploited most commonly in biomedical applications for bone repair and regeneration due to their exceptional osteoconductivity especially following cancerous bone removal and for minimally invasive surgeries. The minimally invasive clinical applications of bone cement pastes include spinal fusion, vertebroplasty, khyphoplasty, cranioplasty and periodontal surgery. During surgical applications the precise placement of the bone cement paste by the surgeon is very important. Various means are available for the placement of the cement paste into the repair site. Generally a syringe with a needle can be used. Calcium phosphate cements must react slowly enough to provide enough time for the surgeon to inject and work the paste into the implantation site, and fast enough to prevent washing-out or delaying the wound closure. Also its setting time and extent of reaction should be balanced to impart strength to the final product. The initial setting time is critical as it should allow sufficient time for shaping and filling. After the filling, it is not advisable to disturb the set cement until its hardening because any mechanical strain during this period will produce cracks and adversely affect the strength. Therefore it requires the shortest possible final setting time so that the wound closure is not delayed. The initial setting time denotes the end of workability of the paste after wetting, and the final setting time indicates the hardening of the set mass [11]. An initial setting time of about 8 minutes and a final setting time of less than 15 minutes are recommended for orthopedic applications.

Typically after setting of calcium phosphate cements, aqueous setting liquid is trapped in micro-reservoirs. The release of incorporated ions enable continuous hardening for days after setting. This reservoir effect is beneficial for many aqueous inorganic cements but especially for biomedical applications because of the contribution of the material to the dynamic tissue remodeling processes. Inorganic bone cements are required to provide a temporary support for the activity of the bone microenvironment consisting of cells, proteins, growth factors and ions while simultaneously facilitating the natural remodeling process by providing a preferentially alkaline environment and an abundance of relevant ions of calcium, phosphate, carbonate, etc. An excellent explanation of the bone remodeling process from a materials scientist's perspective by Driessens *et al*. is recommended for more information [12]. Exceptional bioactivity of apatite forming CPCs is due to the alkaline microenvironment rich in calcium and phosphate

ions in ratio similar to those in the bone extracellular matrix. In addition, the inherent microporosity of these materials is beneficial for the release of drugs, and biomolecules that are proven to direct cellular activity so as to facilitate a wound healing and remodeling process close to natural as possible [13]. However macroporosity is also needed to be able to make use of these macromolecule osteoinductive factors like bone morphogenetic protein, transforming growth factor, platelet-derived growth factor, basic fibroblast growth factor and enable invasion of the material by osteoblasts [14]. Generally interconnected pores of sizes in excess of 300 μm are recommended to enhance new bone formation and the formation of capillaries [15]. Various macropore induction techniques have been applied to these biomimetically setting pastes with ease but those that work *in situ* are the most suitable for orthopedic applications [16–19]. Precise control on the porous architecture of calcium phosphate cement based scaffolds have been realized in a number of recent studies by indirect 3D printing techniques [20, 21]. The dimensional accuracy and bioactivity of such custom-fit forms of the material were found outstanding.

3. Properties

3.1. Bioactivity

As the chemical composition of the mammalian bone mineral is similar to ion-substituted, calcium-deficient hydroxyapatite (CDHA), apatite forming calcium phosphate cements have been more extensively investigated as bioactive implant materials than brushite forming CPCs. All apatite CPC formulations have precipitated hydroxyapatite (PHA) as the end-product of the reaction which has a much finer crystal structure than its sintered counterparts or other CPC setting products including brushite and monetite. High surface area and roughness are the physical requisites for osteoconduction as bone bonding is achieved by micro-mechanical interdigitation of the cement line (a thick apatite layer secreted by osteoblasts) with the material surface [22]. Also micro-topographically complex surfaces promote osteoconduction by both increasing the available surface area for fibrin attachment and providing surface features with which fibrin becomes entangled; and potentiating the activation of platelets, which produce density gradients of cytokines and growth factors that guide leukocytes and osteogenic cells during the healing process [23]. Furthermore Davies demonstrated that platelet activation on calcium phosphate surfaces is a function of the surface topography of the calcium phosphate, rather than the composition.

According to Davies, the formation of bone requires not only the recruitment and migration of a potentially osteogenic cell population but also the differentiation of this population into mature secretory cells [24]. The potentially osteogenic population migrates through the wound site and reaches the surface of bone fragments, or the implant within the wound site. This stage termed osteoconduction is the most important aspect of peri-implant healing. The implant surface design can have a profound influence on osteoconduction not only by modulating the levels of platelet activation, but also by maintaining the anchorage of the temporary scaffold of fibrin and proteins through which these cells reach the implant surface. Cells that reach the solid surface will initiate matrix synthesis by secreting the first collagenous matrix of the cement line directly on the implant surface. This new bone formation stage is generally considered as a separate and distinct phenomenon and is followed by remodeling of the bone. The bone bonding theory of Davies helps one understand how calcium phosphate and

most other inorganic cements provide the advantages of accelerating early healing and bone bonding over most other biomaterials. Calcium phosphates are known to readily adsorb proteins to their surfaces. Potentiating protein adsorption on calcium phosphate surfaces can be expected to increase the binding of fibrinogen that may lead to increased platelet adhesion and, possibly result in increased platelet activation that may accelerate healing. Increasing protein adsorption can also include an improvement in fibrin binding to the implant surface resulting in an earlier establishment of the three-dimensional matrix through which osteogenic cells have to migrate to reach the implant surface. Therefore surface micro-topography and chemistry of calcium phosphates are critical for both the osteoconduction, and also the bonding of the elaborated bone matrix to that surface.

Aside from osteoconductivity, the most important requirement for a bone substitute implant material is biocompatibility. It is defined by Williams as [25]: "The ability of a biomaterial to perform its desired function with respect to a medical therapy, without eliciting any undesirable local or systemic effects in the recipient or beneficiary of that therapy, but generating the most appropriate beneficial cellular or tissue response in that specific situation, and optimizing the clinically relevant performance of that therapy." Orthopedic and maxillofacial implants are designed for non-sustained, short-term contact meaning that the implant should degrade in time. Therefore the implant material is required to have a level of degradability in the body in addition to the appropriate beneficial cellular response to be biocompatible. The physical presence of particulate or ionic degradation products are able to stimulate inflammatory cells, especially macrophages and giant cells that may elicit a systematic response and lead to a foreign body reaction to the biomaterial. Therefore biomaterial and its degradation products have to be devoid of any potential for mutagenicity, genotoxicity, carcinogenicity, reproductive toxicity and other adverse systematic effects in order to be considered biocompatible.

In this context apatite and brushite CPCs are biocompatible and osteoconductive. Calcium phosphate cements form an apatite layer on the surface shortly after implantation in bone. However, a unique feature of cements is that the particles are mixed with each other and the force linking them is weak; therefore, these particles can easily detach from the cement body, especially after some dissolution has occurred. When this happens, the particles are easily ingested by osteoclast-like cells or by giant cells [26]. However, inflammatory reactions and cytotoxicity have been reported when large brushite CPC volumes were used, primarily due to the transformation to precipitated HA and the resultant release of phosphoric acid [27, 28]. The transformation of DCPD into PHA can be prevented by adding magnesium ions to the cement paste [29] and converting brushite to the more stable anhydrous form, monetite [30]. The latter has been achieved by various techniques including heating [31], water deficient setting [32], acidic setting [33] and high ionic strength [34]. Some inflammatory reactions due to the initial acidity of brushite cement precursors may also apparently occur when the CPC does not set since the pH gradually increases close to the physiological level upon setting. The addition of collagen to brushite cement at different powder-to-liquid ratios resulted in an up to ninefold reduction in the amount of particles released from the cement when compared to the control cement without collagen. Collagen effectively prevented particle loss from the submerged cement paste during setting. In addition brushite-collagen cement composites had a three-fold increased cell adhesion capacity [35]. Numerous other in vivo and in vitro assessments have reported that calcium phosphates always support the attachment, differentiation, and proliferation of osteoblasts and mesenchymal cells, with hydroxyapatites being

the most efficient among them [36, 37]. CPCs are not generally considered to be osteoinductive. However their drug delivery capability has been effectively exploited to impart osteoinductivity to various CPC formulations [16, 38].

3.2. Mechanical properties

The mechanical properties of calcium phosphate cements depend on two conditions: (a) the precipitate should grow in the form of clusters of crystals which have a high degree of rigidity, (b) the morphology of the crystals should enable entanglement of the clusters. In Driessen's study of 450 different CPC formulations, about 40% set in a time shorter than 60 minutes [39]. However, only part of these formulations led to cement bodies having a considerable strength. It was found that both compressive and diametral tensile strength were maximum for stoichiometric compositions with respect to the reaction products. Strength is also related to pore structure due to the size distribution of all the particles and the pressure applied to compact the particle network. Thus, the early compressive strength of the cement is mainly dependent on the quantity of the hydration products, the amount of contact points among hydrated grains, and the volume proportion of hydration product crystals [40]. In addition to the above-mentioned factors, the final compressive strength is obviously dependent on the degree of dissolution, recrystallization, growth and intergrowth of cement precursor and product crystals [41].

Both the extent of CPC conversion and the compressive strength of the cement increase drastically with time in the form of a sigmoidal function [42, 43]. In common practice, the observation of the initial plateau strength values is prevented by the requirement of sample rigidity and the finite time period of strength measurements, so that an exponential rise with time and an end plateau is reported in mechanical characterization results. The complete variation of cement strength and modulus as a function setting time can be conveniently observed using a mechanical spectrometer that is able to probe the viscoelastic character of the cement suspension [44, 45]. The compressive strength is highly correlated with the extent of conversion of the reactants to the products. After setting, CPCs can reach mechanical properties comparable to those of calcium phosphate blocks with the same porosity. Having the ceramic origin, the set products of all calcium orthophosphate cements are brittle, have both a low impact resistance and a low tensile strength within 1–10 MPa, whereas the compressive strength varies within 10–100 MPa. Brushite cements are slightly weaker than apatite cements. However their innovative modification methods result in exceptional strength because of the water consuming setting reaction of brushite cements [46]. Unlike apatite cements, which consume little (1 mole per 3 moles of powder reactant in β-tricalcium phosphate (β-TCP) systems) or no water (TTCP/DCP systems) during setting, the brushite cement system consumes a lot of water during setting reaction (up to 6 moles per 1 mole of powder reactant), theoretically allowing for the formation of cements with low or almost zero porosities. Some excellent reviews on the mechanical properties of both apatite and brushite cements are recommended for additional information [26, 47, 48]. In macroporous form apatite cement has adequate strength to replace trabecular bone. In vivo, the mechanical properties of apatite cements were found to increase, whereas those of brushite cements decreased [49, 50]. This is generally attributed to a higher bioresorbability of DCPD when compared with that of CDHA which not only depends on the inherent solubility but also on various physiological processes occurring around the implant site [51].

One of the main reasons for the weakness of CPCs is their inherent microporosity, which makes it easier for micro- and macro-cracks to run throughout the mass [14]. The pores that typically account for about 40% of hardened cement volume, originate from water reservoirs that form due to packing imperfections, shrinkage, drying and water consuming setting reaction. Porosity may be controlled to a certain extent by precompaction [52], adjusting the particle size [53, 54] and the powder/liquid (P/L) ratio [46], addition of porogens [55] and rheology enhancing chemical [56]. Combination of precompaction with citric acid due to its liquefying effect results in outstanding strength values. Unusually high strengths can also be obtained when cement P/L ratio is maximized to the limiting level of insufficient wetting. This is possible by either efficient dispersion of particle agglomerates through a liquefying effect due to electrostatic repulsion of particles or by using bimodal particle size distribution in the setting cement. Various organic and inorganic chemicals including alpha-hydroxylic acids (a.k.a. carboxylic acids), and vinylic superplasticizers have been utilized for increasing the surface charge by binding to the active surface sites [56, 57]. Bimodal particle size distributions have been shown to decrease the water demand in an α-tricalcium phosphate (α-TCP) single-component, HA-forming system where the addition of an $CaCO_3$ filler of much smaller particle size enabled higher workable P/L [58]. In the case of macropore introduction to the cement matrix by incorporation of porogens, the microporosity is simply decreased because the sample contains less CPC per unit volume due to more macroporosity. Although this is beneficial for the resorbability of the cement, mechanical properties of macroporous cement are greatly reduced compared to macropore free cements. According to Rice, strength of ceramics vary as an exponential function of porosity as given below and so does the strength of CPCs [59]:

$$\sigma = \sigma_0 \, exp(-KP) \tag{1}$$

where σ_0 is the strength of the material with zero porosity and K is a constant. This equation is modified by Le Huec to take pore size into account accordingly [60]:

$$\sigma = \left(E_0 R/(\pi c)\right)^{0.5} \exp(-KP) \tag{2}$$

where E_0 is the modulus of zero porosity, c is the average pore size and R is fracture surface energy.

Fiber reinforcement is one of the most convenient methods to compensate for the induced macroporosity in CPCs [61, 62]. Certain fibers like aramid have the property of bonding with hydroxyapatite and providing nucleation sites for set crystals. This property of aramid was made use of in the study by Xu *et al*. where fiber reinforcement imparted a substantial improvement of mechanical properties over those of fiber free porous cement, with strength increasing 3–7 times and toughness by 2 orders of magnitude [55]. The porosity values of the fiber composites were slightly less than those without fibers because the 6% mass imparted by the reinforcing fibers was fully dense.

Other factors affecting strength are the materials used in the solid phase, incorporation and particle size/shape of filler materials in the solid phase. Several researchers attempted to add

filler materials to increase the mechanical properties as in a composite matrix [63, 64]. The idea behind the use of filler particles is that if a tough filler is present in the matrix, it may stop crack Propagation. However by adding fillers porosity decreases, as does the ability of the material to allow bone ingrowth into the pores. Using bioresorbable polymers as fillers provides an effective solution to this problem [65, 66].

3.3. Injectability

Injectability of CPCs is of crucial importance for surgical procedures utilizing minimally invasive procedures such as in vertebraplasty and kyphoplasty or for delivery of the cement into a very narrow space as in root canal obturation. During the injection of the cement paste a pressure drop of the ceramic paste is developed as the paste flows out of the syringe and the needle and as it is forced into the treatment site. This pressure drop represents the bottle neck to injection and is overcome by the surgeon applying a higher pressure on the ram of the syringe that holds the cement. The applicability and the injectability of the cement suspension are governed by the time-dependent shear viscosity and elasticity of the ceramic paste (functions of all parameters affecting the setting kinetics). Once the ceramic suspension attains certain upper thresholds of viscosity and elasticity the injection of the cement paste to the treatment site is no longer possible. A rapid increase in the shear viscosity of the cement paste (transition from flowable suspension to a gel and then to a rigid solid) that is associated with the cement reaching its setting time, restricts the duration of time that the cement remains viable for injection during surgery. Usual practice for the orthopedic surgeon is to change cement formulations that include various setting retarder or promoter chemicals in addition to the setting precursors, according to the time limitations of the task. Alternatively, the setting time and flowability of calcium phosphate cements are adjustable *in situ* by the novel preshearing technology through application of oscillatory and torsional shear strains prior to pressurization and delivery to the surgical site which gives the surgeon freedom to use a wide range of cement formulations that set at various times [44].

At the initial period after mixing with the setting liquid, cements consist of dissolving particles in an aqueous solution that is gradually enriching in precursor ions. This dynamic microstructure with constantly changing maximum packing ratio and solid content typically exhibits concomitant slow alterations in the cement flow behavior according to the Krieger-Dougherty model:

$$\eta^r = \left(1 - \frac{\phi}{\phi_{max}}\right)^{-n} \tag{3}$$

where η^r is the relative viscosity (the ratio between the cement and the setting liquid viscosities), ϕ and ϕ_{max} are the volume fraction of particles in suspension and the volume fraction at which viscosity approaches infinity, respectively, and n is the intrinsic viscosity, an experimentally determinable constant (2.5 for spherical particles). Calcium phosphate cements show a shear-thinning behavior by a significant yield stress that increases with time. They are viscoplastic and can be described as Herschel-Bulkley fluids at any instant but lose their plasticity with time [67]. Furthermore, these materials are thixotropic [68]. The rheological behavior of the cement pastes are strongly influenced by the change of the surface charge during setting. The formation of agglomerates upon mixing the cement powder with the setting liquid can be minimized by taking advantage of the electrostatic repulsion between highly charged surfaces.

The Zeta potential is an important property of cement particles influencing not just particle coagulation but also ion exchange between the hydrate layer around the ceramic particle and the particle surface itself as well as the net precipitation of new material [69].

CPC injectability depends on many factors and may be quite poor in certain cases which results in liquid-solid phase separation called filter-pressing. Their capillary flow has been analyzed extensively in order to understand their injectability behavior [70, 71]. The common observation has been the overshot pressure that is needed to extrude the whole cement sample out, in other words clogging. Highly filled suspensions stably flowing inside a barrel exhibit a constant pressure vs. time curve as seen in **Figure 1a**. Binder phase migrates toward the direction of applied pressure starting at time t_0 and leaves a percolated particle network termed mat behind as shown in **Figure 1b**. Filtration of the low viscosity binder is caused by weak adhesion between the particles and the binder that may originate from improper dispersion in addition to low binder viscosity, low particle surface area and high difference between the densities of the two phases [72]. Further increasing the pressure either thickens the mat layer or discharges it (**Figure 1c**) depending on the propensity of the system to wall-slip [73–76]. The viscoplasticity of complex fluids, including gels and concentrated suspensions and cements is always accompanied by slip at the wall [77–81]. The wall-slip behavior of concentrated suspensions always occurs on the basis of the apparent slip behavior which is generated by the formation of a slip layer consisting of pure binder (which is typically 1/16th to 1/8th of particle diameter) [82–84]: Understanding the conditions necessary for the development of a contiguous slip layer at the wall is the key to prevent mat layer formation and the resulting flow instabilities including filter-pressing and clogging [85]. The development of the apparent slip layer as well as the shear viscosity of the suspension as a function of time is affected by the role that entrained air plays. Wall-slip and shear viscosity of the suspension are both intimately linked to the amount of air that is entrained during mixing and processing [86–90]. Another important factor which affects the flow and deformation behavior of concentrated suspensions is linked directly to the efficacy of the distributive and dispersive mixing of the ingredients of the formulation and the possible shear-induced migration of particles during flow [91–95].

The solid mat layer in a cement is thickened as filtration progresses, setting continues, the liquid content decreases or the solid packing increases, as a result of which the pressure required

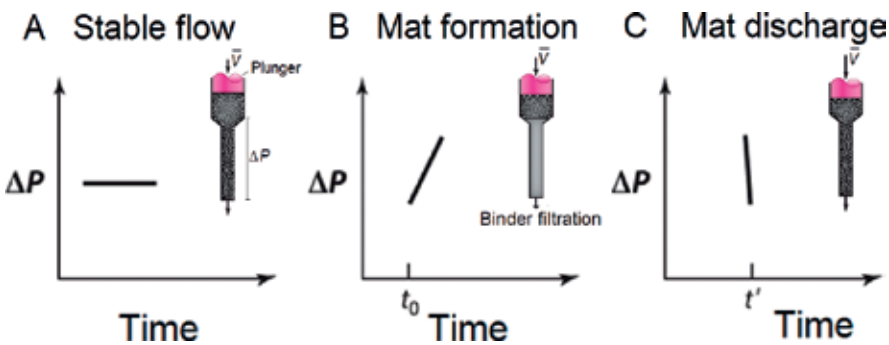

Figure 1. Stable flow (a), destabilized flow due to mat formation (b), stabilized flow due to mat formation (c) in capillary and the associated variation in the pressure drop (adapted with permission from Kalyon and Aktas et al. [72]).

to induce both liquid flow and mat discharge increases. This self-feeding loop gradually transforms the suspension to a packed bed at an increasing rate as evidenced by the exponential nature of the pressure vs. time curves of unstably flowing suspensions. Empirical attempts to tackle the filter-pressing issue shows that the injectability of CPCs is generally improved by decreasing the P/L ratio, the use of finer, round particles, the addition of electrically stabilizing groups, and the addition of viscous polymer solutions [96–101]. In addition to a large number of parameters relating to CPC composition, the injectability of a setting cement depends strongly on the post-mixing time interval relative to the cement setting time. In this regard, premixed CPCs that do not harden until being placed into the defect constitutes an advantage in that the viscoelastic properties are independent of time prior to injection [102].

3.4. Bioresorbability

Calcium phosphate cements are able to provide short-term biologically desirable properties and then be replaced by a new bone. In order to achieve optimum clinical results, an appropriate CPC resorption rate is an important parameter that may vary with the intended clinical applications. For critical applications close to vital organs like cranioplasty, rapid implant resorption and replacement by bone may not be an as important factor as implant stability and integrity, and even may not be desirable due to the sensitivity of the brain to local ionic concentration gradients. For other applications, such as periodontal bone defect repairs or sinus lift, the ability of the implant cement to be replaced quickly by bone is highly desirable. Studies on the in vivo evaluation of macroporous calcium phosphate cements revealed a higher bioresorption rate due to both a higher contact with body fluids and enhanced cellular activity due to particle degradation. When the bioresorbability of dense and macroporous α-tricalcium phosphate cement were compared, it was seen that pores formed by albumin foaming promoted bone ingrowth and replacement [103]. Introduction of macroporosity to the CPC causes a trade-off between strength and bioresorbability which should be compensated by some means of strength reinforcement such as incorporation of polymeric fibers.

The overall bioresorption behavior of calcium phosphate cement is a combination of a solution-mediated passive resorption process and a cell-mediated active resorption process. The resorption properties of bioceramics are generally believed to relate to the solubility of their constitutive phases. The much higher (3 orders of magnitude) solubility of brushite compared to hydroxyapatite translates as the much quicker resorption of brushite cements. An important in vivo characteristic of HA-forming CPC is that it does not dissolve spontaneously in a normal physiological fluid environment, yet is resorbable under cell-mediated acidic conditions. Although brushite is soluble in normal physiological fluids, studies have shown that resorption of brushite CPC was also essentially cell-mediated [3]. Phase changes often occur in brushite cements in vivo by a dissolution-reprecipitation reaction, which results in stable phases with lower solubility, thus slowing down degradation and hence bone regeneration kinetics. The kinetics of passive resorption depends on porosity of the samples, ionic substitutions, Ca:P ratio, crystallinity and pH of the cement-tissue interface. The active resorption is due to cellular activity; however, it is also related to the passive one. Serum pH near macrophages and osteoclasts can drop to 5 by the excretion of lactic acid, whereas near osteoblasts pH can become as high as 8.5 by the excretion of ammonia [12]. The micropores in hardened cements do not allow fast bone ingrowth and they are not interconnected unless special

efforts have been performed. Due to these reasons osteoclastic cells are able to degrade the hardened cements layer-by-layer only, starting at the bone cement interface. This is the main drawback of the classical cement formulations without controlled macroporous architecture. Bone substitution rate also depends on the anatomic site, age, sex, and general metabolic health of the recipient. Considering these factors, it may take 3–36 months for the cement to be completely resorbed and replaced by bone [26]. A linear degradation rate of 0.25 mm/week has been reported in literature [104].

Various ions of zinc, magnesium, fluoride and pyrophosphate have been observed to inhibit β-TCP and HA dissolution [105–107]. HA dissolution is also inhibited by the presence of compounds such as bisphosphonates, polyphosphates or pyrophosphoric acid [108]. Bisphosphonates which are metabolically stable analogs of pyrophosphate, bind strongly to hydroxyapatite crystals and suppress osteoclast-mediated bone resorption and crystal growth. The oxygen atom that binds the two phosphate groups of pyrophosphate (P—O—P) is substituted by a carbon atom (P—C—P) in bisphosphonates. Bisphosphonates are characterized by the two covalently bonded sidechains attached to the central carbon atom, termed R1 and R2. Binding to bone is enhanced when R1 is a hydroxyl group, whereas the R2 side group has some effect on binding but predominantly determines the antiresorptive potency of the bisphosphonates. Bisphosphonates with an R2 side chain containing a basic primary nitrogen atom in an alkyl chain like pamidronate and alendronate are more potent antiresorptive agents than either etidronate or clodronate, whereas compounds with more highly substituted nitrogen moieties in R2 such as ibandronate can display further increases in antiresorptive potency [109].

Resorption of calcium phosphate cements is not desired at the onset of hardening in vivo due to washout of loose calcium phosphate particles by the surrounding body fluid before maintaining mechanical rigidity. The implant should be placed into the wound site between the initial and final setting times therefore washout constitutes a problem for the cement formulations with long setting time. Besides improving the setting times, it is possible to have a coherent cement prior to implantation that sets in contact with body fluids. These are called premixed cements and are essentially pastes formed by calcium phosphate particles mixed with non-aqueous but water-miscible liquids like glycerol [100]. Also several studies show that incorporation of a gelling agent such as hydroxypropyl methylcellulose, carboxymethyl cellulose, alginate, chitosan, into CPC provides good washout resistance [110, 111]. However, generally premixed CPC have lower mechanical properties probably related to the volume initially taken up by the non-aqueous liquid [3].

4. Thermochemistry and setting kinetics

Dissolution of the initial calcium phosphates and mass transport are the primary functions of the aqueous CPC setting solution, in which the dissolved reactants form a supersaturated microenvironment with regard to precipitation of the final product. The relative stability and solubility of various calcium phosphates is the major driving force for the setting reactions that occur in various cement formulations. Mixing of calcium phosphate precursors with aqueous setting solution induces various chemical transformations, where crystals of the initial

calcium phosphates dissolve and precipitate into crystals of HA or brushite. When powders of calcium oxides are mixed with an acid-phosphate solution, they dissolve at various rates in the solvent and release calcium cations in the solution. These cations react with the phosphate anions at various rates within the solvent and form a precipitate of salt molecules. Thus, CPC setting is a result of the following three steps [112]:

I. The acid phosphates dissolve in water, release phosphate anions, and form an acid-phosphate solution of low pH.

II. The calcium oxides dissolve gradually in the low pH solution and release Ca^{2+} cations.

III. The phosphate anions react with the newly released cations and form a coordinated network and consolidate into a CPC

The conditions to form a CPC are governed by the rate of reactions that control each of these three steps. The growth kinetics is mainly controlled by phosphate incorporation step, and additives interfering with this step regulate precipitation and crystal growth. Adsorbed atoms from the solution have to be removed during crystal growth to accommodate the competing HPO_2^{4-} ion; hence, dehydration or impurity de-adsorption is an important part of the activation barrier for growth and dissolution [113]. Since acid-phosphate reactants such as DCP, monocalcium phosphate monohydrate (MCPM), or orthophosphoric acid (PA) are generally soluble, their dissolutions rates are comparatively high, hence uncontrollable. The phosphate reaction between dissolved cations and anions described in step III is also inherently fast and may be kinetically constrained to the formation of intermediate precursor phases according to the Ostwald's rule of stages. Thus, the only reaction that can be controlled is the dissolution of calcium oxides given in step II. Particle size [114, 115], crystallinity [116], powder/liquid ratio [117], precursor chemistry [105], Ca:P ratio [118], temperature [44], surface charge [69], liquid pH [119], ionic strength [34], and concentration of stabilizing, setting promoting or retarding chemicals [120–122] may significantly affect the rate of dissolution and the consequent setting time of CPC. α-TCP is a calcium oxide that dissolves fast and also reacts fast. On the other hand β-TCP dissolution rate is too low in neutral water, so that it remains mostly unreacted in a solution with a slightly acidic phosphate source. For this reason appropriate calcium oxides, based on their solubility, should be selected in combination with suitable acid-phosphate counterparts to synthesize CPCs [123].

Relative stability of different calcium phosphate salts in equilibrium with their saturated solution for different pH values can be understood from **Figure 2** showing the solubility isotherms for the ternary system $Ca(OH)_2$-H_3PO_4-H_2O at 25°C according to the solubility constants given in literature [124]. These isotherms have a negative slope in the neutral and acid regions of the solubility diagrams which point to the fact that calcium phosphates become more soluble as the pH decreases. The gradient of the slopes indicates the solubility increase of the salt as the pH decreases. Therefore the isotherm slope is considered as a measure of the salt basicity and DCPD and DCP are acid salts in comparison to OCP, α-TCP, β-TCP, HA and TTCP because they have lower negative slopes [125]. The isotherms show that the amount dissolved at equilibrium depends on the pH of the solution and the thermodynamic solubility product of the compound which is a function of both crystal and solution chemistry and physical properties.

Accordingly, HA is the least soluble salt down to a pH of 4.2; for pH values lower than this, DCP is the least soluble salt. Also, it can be observed for pH values lower than 8.5 that the most soluble salt is TTCP; and for pH values higher than 8.5 that the most soluble salt is DCPD. TTCP and DCP were used as the precursors in the first apatite CPC not fully coincidentally because these are the most soluble salts and thus would provide the greatest driving force for the HA-forming reaction. Since at a pH above 4.2, all other calcium phosphate compounds are more soluble than HA, they can be used as precursors for apatite cements. Although several calcium phosphate phases, such as OCP and whitlockite (not shown in figure), are more soluble than HA under neutral pH conditions, they have been found as the major phase in the cement products [126, 127]. This is because these metastable phases precipitate in preference to HA according to the Ostwald's rule of stages [128], and finally convert to HA. Homogeneous formation of HA at low concentrations is almost never observed due to the activation energy barrier for nucleation that should be overcome with high supersaturation. At the onset of precipitation, initial supersaturation is the thermodynamic driving force. It is demonstrated by Song *et al*. for a batch system that after the fast precipitation in the early stage, the following precipitation becomes very slow due to the decrease of supersaturation of the solution with the depletion of calcium and phosphate ions [129]. The fast precipitation cannot continue because there is no supply of extra calcium and phosphate ions. However at a semi-batch system such as that of a CPC, where time dependent dissolution of precursor calcium phosphates supplies ions for supersaturation, the fast precipitation can be kept provided that suitable pH value and concentrations of calcium and phosphate are present.

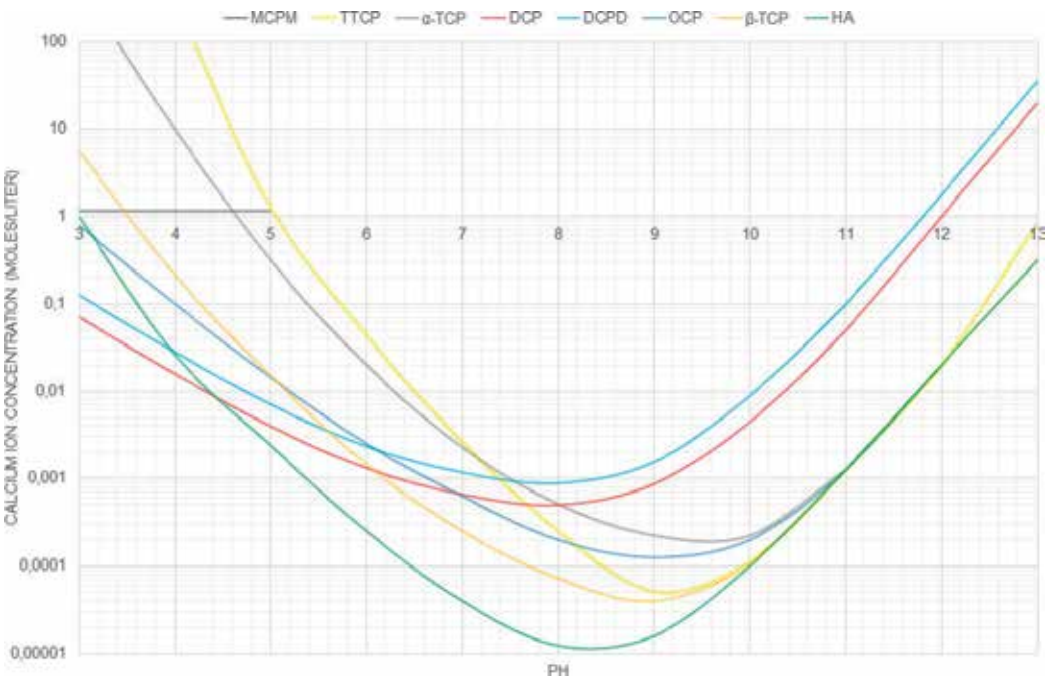

Figure 2. Calcium ion concentration of various calcium phosphate compounds as functions of solution pH.

Although the likelihood of precipitation of a particular calcium phosphate phase is ultimately determined by the thermodynamic driving force of formation, kinetic factors may be considerably more important in controlling the nature of the solids formed. Ostwald's Rule of Stages postulated in 1897 states that the crystal phase that nucleates in a supersaturated solution is not the phase that is thermodynamically stable at that temperature and pressure but rather another metastable phase that is closest in free energy to the parent phase [130]. There are also examples of phase transformations where a metastable phase exists but does not form due to immediate transformation into another phase. It is possible to observe the metastable intermediate by slowing down the kinetics of the reaction. According to the Ostwald's rule of stages, the nucleated phase is the phase that has the lowest free-energy barrier of formation of a critical radius R_c (having the lowest critical radius), rather than the phase that is thermodynamically stable (having the highest supersaturation). In classical nucleation theory [131], the free energy of formation ΔG, and the activation energy for nucleation ΔG^* are related to the surface energy γ, density ρ, and the difference between the chemical potentials of the products and the reactants $\Delta\mu$ which is basically a function of the supersaturation S with respect to the precipitating phase, which is the driving force for nucleation:

$$\Delta G = 4\pi R^2 \gamma + \frac{4}{3}\pi R^3 \rho \, \Delta\mu \tag{4}$$

$$R_c = \frac{-2\gamma}{\rho \, \Delta\mu} \tag{5}$$

where

$$\Delta\mu = -kTlnS \tag{6}$$

and

$$S = \frac{Ionic\ activity\ product}{Solubility\ product\ \left(K_{sp}\right)} \tag{7}$$

The ionic activity product of a calcium phosphate phase is the product of the concentration of the constituent ions and their activity coefficients. The activity coefficients are also complex functions of the interactions between ions in the solution as expressed by the Pitzer's thermodynamical model for electrolytes [132], hence ionic strength. Brown and Chow have shown that the thermodynamic solubility product depends on the purity of the calcium phosphate, which in turn, depends on the method of preparation [133]. Substitute ions like fluoride, carbonate and magnesium influence the structure of the calcium phosphates and therefore have specific effects on their solubilities [134].

Generally two types of CPC setting reactions are observed, the most common one is the setting reaction that occurs according to an acid-base reaction, i.e., a relatively acidic calcium phosphate phase reacts with a relatively basic one to produce a more or less neutral calcium phosphate salt [135]. Typical examples are the cement of Brown and Chow, where TTCP (basic) reacts with DCP (slightly acidic) to form PHA (slightly basic), the cement of Lemaitre where β-TCP, (slightly basic) reacts with MCPM (acidic) to form DCPD (neutral), and a variation of Lemaitre's formulation where MCPM is substituted by PA while β-TCP is replaced by CDHA according to the reactions:

$$Ca_4(PO_4)_2O + CaHPO_4 \rightarrow Ca_5(PO_4)_3OH \quad (8)$$

$$\beta - Ca_3(PO_4)_2 + Ca(H_2PO_4)_2.H_2O + 7H_2O \rightarrow 4\,CaHPO_4.2H_2O \quad (9)$$

$$Ca_9(HPO_4)(PO_4)_5OH + 3H_3PO_4 + 17\,H_2O \rightarrow 9\,CaHPO_4.2H_2O \quad (10)$$

The TTCP + DCPD and TTCP + DCP combinations have been the most studied [136]. They offer hardening at a suitable time at body or room temperature within a neutral pH range. From a theoretical standpoint, any calcium phosphate that is more acidic than HA can react directly with TTCP to form PHA or CDHA according to the following reactions:

$$7\,Ca_4(PO_4)_2O + 2\,Ca(H_2PO_4)_2.H_2O \rightarrow 6\,Ca_5(PO_4)_3OH + 3\,H_2O \quad (11)$$

$$2\,Ca_4(PO_4)_2O + Ca(H_2PO_4)_2.H_2O \rightarrow Ca_9(HPO_4)(PO_4)_5OH + 2\,H_2O \quad (12)$$

$$Ca_4(PO_4)_2O + CaHPO_4.2H_2O \rightarrow Ca_5(PO_4)_3OH + 2\,H_2O \quad (13)$$

$$3\,Ca_4(PO_4)_2O + 6\,CaHPO_4.2H_2O \rightarrow 2\,Ca_9(HPO_4)(PO_4)_5OH + 13\,H_2O \quad (14)$$

$$Ca_4(PO_4)_2O + CaHPO_4 \rightarrow Ca_5(PO_4)_3OH \quad (15)$$

$$3\,Ca_4(PO_4)_2O + 6\,CaHPO_4 \rightarrow 2\,Ca_9(HPO_4)(PO_4)_5OH + H_2O \quad (16)$$

$$3\,Ca_4(PO_4)_2O + Ca_8H_2(PO_4)_6.5H_2O \rightarrow 4\,Ca_5(PO_4)_3OH + 4\,H_2O \quad (17)$$

$$3\,Ca_4(PO_4)_2O + 3\,Ca_8H_2(PO_4)_6.5H_2O \rightarrow 4\,Ca_9(HPO_4)(PO_4)_5OH + 14\,H_2O \quad (18)$$

$$Ca_4(PO_4)_2O + 2\,Ca_3(PO_4)_2 + H_2O \rightarrow 2Ca_5(PO_4)_3OH \quad (19)$$

It is also possible to form HA from acid-base mixtures of calcium phosphates with a Ca/P lower than that of HA when an additional source of calcium ions instead of TTCP is present such as $CaCO_3$ or $Ca(OH)_2$. [137, 138] Takagi *et al*. were the first to propose a calcium phosphate cement formulation without TTCP. Different combinations of DCP and DCPD, α-TCP, amorphous calcium phosphate (ACP), calcium hydroxide and calcium carbonate have been prepared to obtain improvements in the setting time to as low as 5 minutes and tensile strengths as high as 7.5 MPa [139].

All brushite CPCs are obtained by an acid–base reaction. Because DCPD and DCP are the least soluble calcium phosphates under acidic pH (<4.2), they are the products formed by acidic CPC formulations. All other calcium phosphate phases being more soluble under these

pH conditions, can be used as precursors for the DCPD- or DCP-forming cements. Although DCP is the more stable of the two phases, it is kinetically constrained to have a higher nucleation activation energy and can only form under certain conditions as explained earlier. After setting, the pH of the cement paste slowly changes towards the equilibrium pH [140]. Up to now, several formulations have been proposed, including β-TCP + MCPM, β-TCP + H_3PO_4, and TTCP + MCPM + CaO [51, 99, 141].

The second type of setting reaction is defined as hydrolysis of a metastable calcium phosphate when the reactant and the product have the same Ca/P molar ratio. Typical examples are ACP, α-TCP, and TTCP which form CDHA upon contact with an aqueous solution:

$$Ca_x H_y (PO_4)_z.nH_2O + H_2O \rightarrow Ca_{10-x}(HPO_4)_x (PO_4)_{6-x} (OH)_{2-x} + nH_2O \quad (20)$$

$$3\,\alpha - Ca_3 (PO_4)_2 + H_2O \rightarrow Ca_9(HPO_4)(PO_4)_5 OH \quad (21)$$

$$3\,Ca_4 (PO_4)_2 O + 3\,H_2O \rightarrow Ca_9(HPO_4)(PO_4)_5 OH + 3Ca(OH)_2 \quad (22)$$

Chemical composition of calcium phosphate cements may include all ionic compounds of naturally occurring minerals in human body. The list of possible additives includes the following cations: Na^+, K^+, Mg^{2+}, Ca^{2+}, H^+, Sr^{2+}, Si^{4+}, Fe^{2+}, Ag^+, and anions: PO_4^{3-}, HPO_4^{2-}, H_2PO^{4-}, CO_3^{2-}, HCO_3^-, SO_4^{2-}, HSO_4^-, Cl^-, F^-, SiO_4^{4-}. Therefore, mixed-type cements consisting of calcium phosphates and other calcium salts like gypsum, calcium sulfate hemihydrate, calcium pyrophosphate, calcium polyphosphates, calcium carbonate, calcium oxide, calcium hydroxide, calcium aluminate, calcium silicate, strontium phosphate, as well as cements made of ion substituted calcium phosphates such as $Ca_2KNa(PO_4)_2$, $NaCaPO_4$, $Na_3Ca_6(PO_4)_5$, magnesium-substituted calcium deficient hydroxyapatite (CDHA), strontium-substituted CDHA are possible [142].

CO_3^{2-} ions have the most significant effect on CPC microstructure such that incorporation of carbonate in the apatite cement causes a decrease in the precipitated crystallite size and reduces the setting rate as well as the attained compressive strength. According to the study by Khairoun *et al*. $CaCO_3$ addition extended the initial setting times but significantly shortened the final setting times of single component HA cement. Furthermore its accelerating effect was more pronounced at higher concentrations [137]. Morphological studies reveal that the size and shape of the crystallites change from long needles to smaller rods to tiny spheroids [18, 102]. Carbonate ions can incorporate into apatite and substitute for PO_4^{3-} or OH^- in the apatite crystal structure and subsequently change its properties. It is reported that the supersaturation required for precipitation of slightly carbonated apatite was higher than that of apatite in simulated body fluid [143]. Carbonate ions disturb the crystallization of the growing apatite crystallites to such an extent that, depending upon the amount of carbonate added, the material may give an amorphous X-ray diffraction pattern. A submicron structure of interconnected microcrystals are responsible for the improved final mechanical properties of the cement formulation with addition of calcium carbonate. Moreover, carbonate ions cause the bonding in the apatite to become weaker and more isotropic, which results in the small spheroidal crystals and in faster dissolution rates [42].

Similarly, many carboxyl group containing acids and salts have significant effect on hydroxyapatite microstructure and in general setting kinetics of calcium phosphate cements. A number of α-hydroxylated carboxylic acids and salts readily form calcium complexes as well as relatively insoluble and often amorphous Ca-carboxylate compounds [56]. These include glycolic, citric, tartaric, malonic, malic, succinic, lactic and maleic acids. Upon application of precompaction, compressive strength of TTCP-DCP cement increased fourfold to 184 MPa with sodium citrate concentration up to 500 mM compared to plain water and citric acid cement liquid [144]. Sodium citrate addition changed the surface zeta potentials of TTCP and DCP to −50.6 and −50.1 mV with 50 mM sodium citrate from −15.0 and −18.4 mV with water.

5. Phase evolution during setting

The powder of the original calcium phosphate cement formulation proposed by Brown and Chow consists of an equimolar mixture of TTCP and DCP. The setting reaction of calcium phosphate cements starts with ordered dissolution of the salts in the aqueous system. This supplies Ca^{2+} and PO_4^{3-} ions, which precipitate in the form of HA. Epitaxial enlargement of petal or needle-like crystals after initial setting is responsible for the adherence and interlocking of the crystalline grains, which result in hardening [26]. Detailed investigations of the setting of various CPC formulation using various molar ratios, particle sizes, P/L ratios reveal that the reaction proceeds by complete dissolution of the acidic phases DCP or MCPM and partial dissolution of the basic TTCP or β-TCP particles. The specific surface area and the resulting solubility of the basic phase has a much greater effect on the setting rate as increasing its specific surface area leads to an increase in pH, and results in a sharp rise in the solubility of the acidic particles and the supersaturation of HA in the solution [40]. For apatite cement setting is controlled by the dissolution of reactant particles in the first 4-h period, and since the rate of dissolution is proportional to the surface area of the particles which is basically constant in CPC specimens in the earlier stage, the precipitation rate of HA is linear with time. HA forms among the reactant particles which enhances the joint of solids, or around the particles which reduces the distance between grains [42]. Setting is controlled by diffusion through the HA layer at later stages. At 24 hours, the crystals are completely formed, being highly compacted in some areas of high density and well separated in areas with more porosity. Precipitated HA either in stoichiometric or calcium deficient form, nucleate and grow on TTCP particles, thereby reducing their dissolution rate at the final stages [145]. When such a shell is formed around the reactants, the rate of HA formation is controlled by the transport of water and ions through the shell and decrease with an increase of its thickness. Since the densities of DCP and HA are different, the hydration of the residual DCP engulfed by the shell to HA leads to volume expansion and internal stress which is harmful to the compressive strength.

Liu *et al*. describes the thermodynamics of apatite cement setting clearly [118]. Calcium phosphate cement setting reactions are generally exothermic reactions consisting of several steps. In the short initiating period, water is absorbed and wets the surface of the grains upon mixing calcium phosphate powder with water. This is a physical exothermic process. In the inducing

period or latency, the particle dissolution which is also exothermic contributes to a rise in concentration of the calcium and phosphate ions in the solution. With the different dissolution rates of the basic and acidic precursors and the latter being faster, initially acidic pH translates toward the neutral or basic region until the solution is supersaturated, and then DCPD or HA crystallizes from the solution. The accelerating period is a fast, reaction controlled region. In the decelerating period, setting reaction decreases and the reaction process converts from surface reaction-controlled to diffusion-controlled after the setting product grows around the particle surface of the raw materials. Finally, the precipitate product layer may be destroyed by osmotic pressure and crystallization interior stress, which may lead to the increase of the reaction rate and another slight exothermic peak.

The phase evolution of brushite forming β-TCP—MCPM system has been monitored by various techniques including FTIR spectroscopy [146], DS calorimetry [117], pH-stat base titration [33, 34] and small amplitude oscillatory rheometry [44]. The observations confirm the above-mentioned general thermodynamic changes in the state of the CPC. Upon mixing the cement precursors with excess setting liquid, MCPM instantly dissolves and supplies $H_2PO_4^-$ and Ca^{2+} ions to the solution. A small fraction of $H_2PO_4^-$ is expected to dissociate into H^+ and HPO_4^{2-} ions due to its relative stability among phosphoric acid species in water at room temperature [83]. β-TCP dissolves simultaneously to release $3Ca^{2+}$ and $2PO_4^{3-}$ that can form brushite $CaHPO_4{\cdot}2H_2O$ provided that stoichiometric H^+ ions are removed from the solution to first form HPO_4^{2-}groups, resulting in an initial rise in solution pH that is an indication of supersaturation build-up. At this stage cement injectability is maximum. Subsequent to this period, the injectability of CPC gradually diminishes as crystal domains start to expand and intergrow with increasing β-TCP dissolution. Built-up supersaturation can quickly relax by crystal growth in the presence of brushite seeds. As crystals intergrow into small domains, cements gain dough consistency and elasticity develops as seen in **Figure 3**. With increasing intergrowth of the crystalline phase the suspension becomes thicker, i.e., more viscous and more elastic as defined by the increases of the storage modulus, G′ and the magnitude of complex viscosity, η* occurring between the dough time and the initial setting time. CPC is workable by hand prior to the dough time as it lacks stiffness and rigidity. Subsequent precipitation and β-TCP dissolution act to balance the supersaturation and pH until the rate of one weakens relative to the other [147]. This interplay between dissolution and precipitation continues indefinitely until the consumption of precursors.

After the working period a particle to particle network develops and the injectability of the doughy cement suspension becomes modestly more difficult as the initial setting time is approached [148]. Bone cements with various solid contents have been reported to be injectable well beyond their dough time [67] which is most likely due to the active wall-slip mechanism that enables stable flow of doughy pastes. Cement suspension can be shaped by hand at this working period when it has a dough consistency and does not stick to surgical gloves. At the initial setting time a solid network structure or gelling starts to develop in cement microstructure when elasticity and viscosity starts to overshoot asymptotically. The viscoelastic properties change abruptly during this setting period with a sudden transition from

http://dx.doi.org/10.5772/intechopen.74607

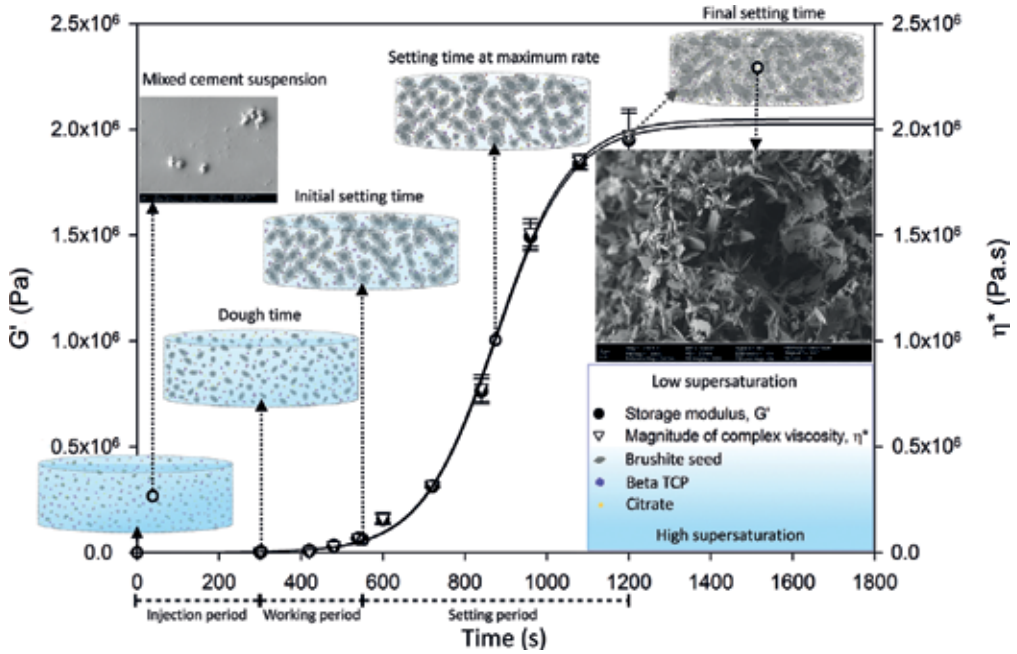

Figure 3. Schematics of calcium phosphate cement setting as represented by the dynamic rheological properties (Şahin and Kalyon [44]).

viscous to elastic flow behavior and elasticity increases at a decreasing rate as a function of the dissolution rate which depends on the β-TCP and water content. Flow instabilities naturally build pressure drop up constantly beyond that point as a result of which injection becomes impractical.

A recent development on improvement of injectability or extrudability of calcium phosphate cements was introduced by our research group so that the inherent injectability problem can be solved by conditioning the cement prior to injection by preshearing. [44]. Our observation that application of oscillatory and steady shear strains i.e. preshearing alters both the setting kinetics and the microstructure, enables tailoring of the cement viscosity and the injection, working and setting periods. The rheology of fast-setting brushite cement was also characterized (**Figure 3**) including the linear viscoelastic strain limit which was characterized for inorganic cements as a function of setting time for the first time. A preshearing apparatus akin to a syringe with the capability to not only pressurize but also mix, preshear and dispense cements *in situ* is designed to facilitate their effective handling and injection. This novel mechanical modification technique is applicable to most inorganic cements and opens an avenue for further research on modification of cement properties, especially rheology without resorting to chemical additives that may compromise the bioactivity and other favorable properties. The beneficial effects of preshearing on workability and extrudability of inorganic cements promise exciting new applications for them such as direct 3D printing of micro- and macroporous scaffolds for bone regeneration.

Author details

Erdem Şahin

Address all correspondence to: erdemsahin@mu.edu.tr

Department of Metallurgical and Materials Engineering, Muğla Sıtkı Koçman University, Muğla, Turkey

References

[1] LeGeros RZ, Chohayeb A, Shulman A. Apatitic calcium phosphates: Possible dental restorative materials. Journal of Dental Research. 1982;**61**(1):343-347

[2] Chow LC, Takagi S. A natural bone cement, "a laboratory novelty led to the development of revolutionary new biomaterials". Journal of Research of the National Institute of Standards and Technology. 2001;**106**:1029-1033

[3] Chow LC. Next generation calcium phosphate-based biomaterials. Dental Materials Journal. 2009;**28**(1):1-10

[4] Bohner M, Gbureck U, Barralet JE. Technological issues for the development of more efficient calcium phosphate bone cements: A critical assessment. Biomaterials. 2005;**26**: 6423-6429

[5] Bai B et al. The use of an injectable, biodegradable calcium phosphate bone substitute for the prophylactic augmentation of osteoporotic vertebrae and the management of vertebral compression fractures. Spine. 1999;**24**(15):1521

[6] Korovessis P, Hadjipavlou A, Repantis T. Minimal invasive short posterior instrumentation plus balloon kyphoplasty with calcium phosphate for burst and severe compression lumbar fractures. Spine. 2008;**33**(6):658-667

[7] Ooms EM et al. Histological evaluation of the bone response to calcium phosphate cement implanted in cortical bone. Biomaterials. 2003;**24**(6):989-1000

[8] Xin L et al. Decreased extrusion of calcium phosphate cement versus high viscosity PMMA cement into spongious bone marrow—An ex vivo and in vivo study in sheep vertebrae. The Spine Journal. 2016;**16**(12):1468-1477

[9] Grafe IA et al. Calcium-phosphate and polymethylmethacrylate cement in long-term outcome after kyphoplasty of painful osteoporotic vertebral fractures. Spine. 2008;**33**(11): 1284-1290

[10] Fernández E et al. Dimensional and thermal behaviour of calcium phosphate cements during setting compared to PMMA bone cements. Journal of Materials Science Letters. 1995;**14**(1):4-5

[11] Komath M, Varma HK, Sivakumar R. On the development of an apatitic calcium phosphate bone cement. Bulletin of Materials Science. April 2000;**23**(2):135-140

[12] Driessens FCM, Wolke JGC, Jansen JA. A new theoretical approach to calcium phosphates, aqueous solutions and bone remodeling. Journal of the Australian Ceramic Society. 2012;**48**:144-149

[13] Ginebra M-P, Traykova T, Planell JA. Calcium phosphate cements as bone drug delivery systems: A review. Journal of Controlled Release. 2006;**113**(2):102-110

[14] Espanol M et al. Intrinsic porosity of calcium phosphate cements and its significance for drug delivery and tissue engineering applications. Acta Biomaterialia. 2009;**5**(7): 2752-2762

[15] Karageorgiou V, Kaplan D. Porosity of 3D biomaterial scaffolds and osteogenesis. Biomaterials. 2005;**26**(27):5474-5491

[16] Ginebra M-P et al. New processing approaches in calcium phosphate cements and their applications in regenerative medicine. Acta Biomaterialia. 2010;**6**(8):2863-2873

[17] Chevalier E et al. Fabrication of porous substrates: A review of processes using pore forming agents in the biomaterial field. Journal of Pharmaceutical Sciences. 2008;**97**(3): 1135-1154

[18] Takagi S, Chow LC. Formation of macropores in calcium phosphate cement implants. Journal of Materials Science: Materials in Medicine. 2001;**12**(2):135-139

[19] Barralet JE, Grover L, Gaunt T, Wright AJ, Gibson IR. Preparation of macroporous calcium phosphate cement tissue engineering scaffold. Biomaterials. 2002;**23**(15):3063-3072

[20] Klammert U et al. 3D powder printed calcium phosphate implants for reconstruction of cranial and maxillofacial defects. Journal of Cranio-Maxillofacial Surgery. 2010;**38**(8): 565-570

[21] Habibovic P et al. Osteoconduction and osteoinduction of low-temperature 3D printed bioceramic implants. Biomaterials. 2008;**29**(7):944-953

[22] Davies JE. Bone bonding at natural and biomaterial surfaces. Biomaterials. 2007;**07**:049

[23] Davies JE. Understanding Peri-implant endosseous healing. Journal of Dental Education. 2003;**67**:8

[24] Davies JE. In vitro modeling of the bone-implant Interface. The Anatomical Record. 1996;**245**:426-445

[25] Williams DF. On the mechanisms of biocompatibility. Biomaterials. 2008;**29**:2941-2953

[26] Ambard AJ, Mueninghoff L. Calcium phosphate cement: Review of mechanical and biological properties. Journal of Prosthodontics. 2006;**15**(5):321-328

[27] Dorozhkin SV. Calcium orthophosphate cements for biomedical application. Journal of Materials Science. 2008;**43**:3028-3057

[28] Meininger S et al. Phytic acid as alternative setting retarder enhanced biological performance of dicalcium phosphate cement in vitro. Scientific Reports. 2017;**7**

[29] Lee D, Kumta PN. Chemical synthesis and stabilization of magnesium substituted brushite. Materials Science and Engineering: C. 2010;**30**(7):934-943

[30] Tamimi F, Sheikh Z, Barralet J. Dicalcium phosphate cements: Brushite and monetite. Acta Biomaterialia. 2012;**8**(2):474-487

[31] Tamimi F et al. The effect of autoclaving on the physical and biological properties of dicalcium phosphate dihydrate bioceramics: Brushite vs. monetite. Acta Biomaterialia. 2012;**8**(8):3161-3169

[32] Tas AC. Monetite (CaHPO4) synthesis in ethanol at room temperature. Journal of the American Ceramic Society. 2009;**92**(12):2907-2912

[33] Şahin E, Çiftçioğlu M. Monetite promoting effect of citric acid on brushite cement setting kinetics. Materials Research Innovations. 2014;**18**(3):138-145

[34] Şahin E, Çiftçioğlu M. Monetite promoting effect of NaCl on brushite cement setting kinetics. Journal of Materials Chemistry B. 2013;**1**(23):2943-2950

[35] Tamimi F et al. Brushite–collagen composites for bone regeneration. Acta Biomaterialia. 2008;**4**(5):1315-1321

[36] Rezwan K et al. Biodegradable and bioactive porous polymer/inorganic composite scaffolds for bone tissue engineering. Biomaterials. 2006;**27**(18):3413-3431

[37] Theiss F et al. Biocompatibility and resorption of a brushite calcium phosphate cement. Biomaterials. 2005;**26**(21):4383-4394

[38] Lee G-S et al. Direct deposited porous scaffolds of calcium phosphate cement with alginate for drug delivery and bone tissue engineering. Acta Biomaterialia. 2011;**7**(8):3178-3186

[39] Driessens FCM et al. Effective formulations for the preparation of calcium phosphate bone cements. Journal of Materials Science: Materials in Medicine. 1994;**5**(3):164-170

[40] Liu C, Shao H, Chen F, Zheng H. Effects of the granularity of raw materials on the hydration and hardening process of calcium phosphate cement. Biomaterials. 2003;**24**:4103-4113

[41] Fernandez E, Ginebra MP, Boltong MG, Driessens FCM, Ginebra J, De Maeyer EAP, Verbeeck RMH, Planell JA. Kinetic study of the setting reaction of a calcium - phosphate bone cement. Journal of Biomedical Materials Research. 1996;**32**:367-374

[42] Liu C, Shen W, Gu Y, Hu L. Mechanism of the hardening process for a hydroxyapatite cement. Journal of Biomedical Materials Research. 1997;**35**:75-80

[43] Fernandez E, Gil FJ, Best SM, Ginebra MP, Driessens FCM, Planell JA. Improvement of the mechanical properties of new calcium phosphate bone cements in the $CaHPO_4$-α-$Ca_3(PO_4)_2$ system: Compressive strength and microstructural development. Journal of Biomedical Materials Research. 1998;**41**:560-567

[44] Şahin E, Kalyon DM. The rheological behavior of a fast-setting calcium phosphate bone cement and its dependence on deformation conditions. Journal of the Mechanical Behavior of Biomedical Materials. 2017;**72**:252-260

[45] Combes C et al. Rheological properties of calcium carbonate self-setting injectable paste. Acta Biomaterialia. 2010;**6**(3):920-927

[46] Hofmann MP, Mohammed AR, Perrie Y, Gbureck U, Barralet JE. High-strength resorbable brushite bone cement with controlled drug-releasing capabilities. Acta Biomaterialia. 2009;**5**:43-49

[47] Charriere E. Mechanical characterization of brushite and hydroxyapatite cements. Biomaterials. 2001;**22**:2937-2945

[48] Zhang J et al. Calcium phosphate cements for bone substitution: Chemistry, handling and mechanical properties. Acta Biomaterialia. 2014;**10**(3):1035-1049

[49] Constantz BR et al. Histological, chemical, and crystallographic analysis of four calcium phosphate cements in different rabbit osseous sites. Journal of Biomedical Materials Research Part A. 1998;**43**(4):451-461

[50] Frayssinet P et al. Short-term implantation effects of a DCPD-based calcium phosphate cement. Biomaterials. 1998;**19**(11-12):971-977

[51] Grover LM et al. In vitro ageing of brushite calcium phosphate cement. Biomaterials. 2003;**24**(23):4133-4141

[52] Barralet JE et al. Effect of porosity reduction by compaction on compressive strength and microstructure of calcium phosphate cement. Journal of Biomedical Materials Research Part A. 2002;**63**(1):1-9

[53] Almirall A, Larrecq G, Delgado JA, Martinez S, Planell JA, Ginebra MP. Fabrication of low temperature macroporous hydroxyapatite scaffolds by foaming and hydrolysis of an α-TCP paste. Biomaterials. 2004;**25**:3671-3680

[54] Ginebra MP, Driessens FCM, Planell JA. Effect of the particle size on the micro and nanostructural features of a calcium phosphate cement: A kinetic analysis. Biomaterials. 2004;**25**(17):3453-3462

[55] Xu HHK et al. Strong and macroporous calcium phosphate cement: Effects of porosity and fiber reinforcement on mechanical properties. Journal of Biomedical Materials Research Part A. 2001;**57**(3):457-466

[56] Barralet JE et al. High-strength apatitic cement by modification with α-hydroxy acid salts. Advanced Materials. 2003;**15**(24):2091-2094

[57] Fernandez E, Sarda S, Hamcerencu M, Vlad MD, Gel M. High-strength apatitic cement by modification with superplasticizers. Biomaterials. 2005;**26**:2289-2296

[58] Gbureck U, Spatz K, Thull R, Barralet JE. Rheological enhancement of mechanically activated a-tricalcium phosphate cements. Journal of Biomedical Materials Research Part B: Applied Biomaterials. 2005;**73B**:1-6

[59] Rice RW. Porosity of Ceramics, Chapter 2- Evaluation of the Porosity Dependence of Properties. New York: M. Dekker; 1998

[60] Le Huec JC, Schaeverbeke T, Clement D, Faber J, Le Rebeller A. Influence of porosity on the mechanical resistance of hydroxyapatite ceramics under compressive stress. Biomaterials. 1995;**16**(2):113-118

[61] Xu HHK, Eichmiller FC, Giuseppetti AA. Reinforcement of a self-setting calcium phosphate cement with different fibers. Journal of Biomedical Materials Research. 2000;**52**: 107-114

[62] Xu HHK, Quinn JB. Calcium phosphate cement containing resorbable fibers for short-term reinforcement and macroporosity. Biomaterials. 2002;**23**:193-202

[63] Muller FA, Gbureck U, Kasuga T. Whisker-reinforced calcium phosphate cements. Journal of the American Ceramic Society. 2007;**90**(11):3694-3697

[64] Link DP. Mechanical evaluation of implanted calcium phosphate cement incorporated with PLGA microparticles. Biomaterials. 2006;**27**:4941-4947

[65] Xu HHK, Quinn JB, Takagi S, Chow LC. Processing and properties of strong and non-rigid calcium phosphate cement. Journal of Dental Research. 2002;**81**:219

[66] Sun L, Xu HHK, Takagi S, Chow LC. Fast setting calcium phosphate cement-chitosan composite: Mechanical properties and dissolution rates. Journal of Biomaterials Applications. 2007;**21**:299

[67] Wang X, Ye J, Wang H. Effects of additives on the rheological properties and injectability of a calcium phosphate bone substitute material. Journal of Biomedical Materials Research Part B: Applied Biomaterials. 2006;**78**(2):259-264

[68] Liu C et al. Rheological properties of concentrated aqueous injectable calcium phosphate cement slurry. Biomaterials. 2006;**27**(29):5003-5013

[69] Gbureck U, Probst J, Thull R. Surface properties of calcium phosphate particles for self setting bone cements. Biomolecular Engineering. 2002;**19**:51-55

[70] O'Neill R, McCarthy HO, Cunningham E, Montufar E, Ginebra M-P, Wilson DI, Lennon A, Dunne N. Extent and mechanism of phase separation during the extrusion of calcium phosphate pastes. Journal of Materials Science. Materials in Medicine. 2016;**27**:29

[71] O'Neill R, McCarthy H, Montufar E, Ginebra M-P, Wilson D, Lennon A, Dunne N. Critical review: Injectability of calcium phosphate pastes and cements. Acta Biomaterialia. 2016

[72] Kalyon DM, Seda A. Factors affecting the rheology and processability of highly filled suspensions. Annual Review of Chemical and. Biomolecular Engineering. 2014;**5**:229-254

[73] Yilmazer U, Gogos CG, Kalyon DM. Mat formation and unstable flows of highly filled suspensions in capillaries and continuous processors. Polymer Composites. 1989;**10**(4): 242-248

[74] Yaras P, Kalyon DM, Yilmazer U. Flow instabilities in capillary flow of concentrated suspensions. Rheologica Acta. 1994;**33**:48-59

[75] Kalyon D, Malik M. Axial laminar flow of viscoplastic fluids in a concentric annulus subject to wall slip. Rheologica Acta. 2012;**51**:805-820

[76] Aral B, Kalyon DM. Effects of temperature and surface roughness on time-dependent development of wall slip in torsional flow of concentrated suspensions. Journal of Rheology. 1994;**38**(4):957-972

[77] Medina-Bañuelos EF, Marín-Santibáñez BM, Pérez-González J, Malik M, Kalyon DM. Couette flow of a viscoplastic microgel with wall slip. Journal of Rheology. 2017;**61**: 1007-1022

[78] Fabian Ortega-Avila J, Pérez-González J, Marín-Santibáñez BM, Rodríguez-González F, Aktas S, Malik M, Kalyon DM. Axial annular flow of a viscoplastic microgel with wall slip. Journal of Rheology. 2016;**60**(3):503-515

[79] Aktas S, Kalyon DM, Marín-Santibáñez BM, Pérez-González J. Shear viscosity and wall slip behavior of a viscoplastic hydrogel. Journal of Rheology. 2014;**58**(2):513-535

[80] Kalyon D. An analytical model for steady coextrusion of viscoplastic fluids in thin slit dies with wall slip. Polymer Engineering and Science. 2010;**50**(4):652-664

[81] Lawal A, Kalyon DM. Squeezing flow of viscoplastic fluids subject to wall slip. Polymer Engineering and Science. 1998;**38**(11):1793-1804

[82] Kalyon D, Yaras P, Aral B, Yilmazer U. Rheological behavior of concentrated suspensions. Journal of Rheology. 1993;**37**:35-53

[83] Suwardie H, Yazici R, Kalyon DM, Kovenklioglu S. Capillary flow behavior of microcrystalline wax and silicon carbide suspension. Journal of Materials Science. 1998;**33**: 5059-5067

[84] Kalyon D. Apparent slip and viscoplasticity of concentrated suspensions. Journal of Rheology. 2005;**49**(3):621-640

[85] Tang HS, Kalyon DM. Time-dependent tube flow of compressible suspensions subject to pressure dependent wall slip: Ramifications on development of flow instabilities. Journal of Rheology. 2008;**52**(5):1069-1090

[86] Lu G, Kalyon D, Yilgor I, Yilgor E. Rheology and processing of BaSO4 filled medical-grade thermoplastic polyurethane. Polymer Engineering and Science. 2004;**44**(10):1941-1948

[87] Aral B, Kalyon DM. Rheology and extrudability of very concentrated suspensions: Effects of vacuum imposition. Plastics Rubber and Composites Processing and Applications. 1995;**24**:201-210

[88] Kalyon DM, Gokturk H, Yaras P, Aral B. Motion analysis of development of wall slip during die flow of concentrated suspensions. Society of Plastics Engineers ANTEC Technical Papers. 1995;**41**:1130-1134

[89] Kalyon DM, Jacob C, Yaras P. An experimental study of the degree of fill and melt densification in fully-intermeshing, co-rotating twin screw extruders. Plastics Rubber and Composites Processing and Applications. 1991;**16**(3):193-200

[90] Kalyon DM, Yazici R, Jacob C, Aral B, Sinton SW. Effects of air entrainment on the rheology of concentrated suspensions during continuous processing. Polymer Engineering and Science. 1991;**31**:1386-1392

[91] Kalyon DM, Dalwadi D, Erol M, Birinci E, Tsenoglou C. Rheological behavior of concentrated suspensions as affected by the dynamics of the mixing process. Rheologica Acta. 2006;**45**:641-658

[92] Erol M, Kalyon D. Assessment of the degree of mixedness of filled polymers: Effects of processing histories in batch mixer and co-rotating and counter-rotating twin screw extruders. International Polymer Processing. 2005;**20**:228-237

[93] Feger C, Gelorme JD, McGlashan-Powell M, Kalyon D. Mixing, rheology and stability of highly filled thermal pastes. IBM Journal of Research and Development. 2005;**49**(4/5):699-707

[94] Allende MM, Kalyon D. Assessment of particle-migration effects in pressure-driven viscometric flows. Journal of Rheology. 2000;**44**(1):79-90

[95] Lawal A, Kalyon DM. Simulation of the intensity of segregation distributions using three-dimensional fem analyses: Applications to co-rotating twin screw extruders. Journal of Applied Polymer Science. 1995;**58**:1501-1507

[96] Habib M et al. Mechanisms underlying the limited injectability of hydraulic calcium phosphate paste. Acta Biomaterialia. 2008;**4**(5):1465-1471

[97] Montufar EB, Maazouz Y, Ginebra MP. Relevance of the setting reaction to the injectability of tricalcium phosphate pastes. Acta Biomaterialia. 2013;**9**(4):6188-6198

[98] Leroux L et al. Effects of various adjuvants (lactic acid, glycerol, and chitosan) on the injectability of a calcium phosphate cement. Bone. 1999;**25**(2):31S-34S

[99] Barralet JE, Grover LM, Gbureck U. Ionic modification of calcium phosphate cement viscosity. Part II: Hypodermic injection and strength improvement of brushite cement. Biomaterials. 2004;**25**(11):2197-2203

[100] Chow LC, Markovic M, Takagi S. Injectable calcium phosphate cements. Society for Biomaterials. 2016

[101] Bohner M, Baroud G. Injectability of calcium phosphate pastes. Biomaterials. 2005;**26**(13): 1553-1563; ISSN 0142-9612

[102] Takagi S et al. Premixed calcium–phosphate cement pastes. Journal of Biomedical Materials Research Part B: Applied Biomaterials. 2003;**67**(2):689-696

[103] Mino-Farina N. Quantitative analysis of the resorption and osteoconduction of a macroporous calcium phosphate bone cement for the repair of a critical size defect in the femoral condyle. The Veterinary Journal. 2009;**179**:264-272

[104] Ohura K et al. Resorption of, and bone formation from, new β-tricalcium phosphate-monocalcium phosphate cements: An in vivo study. Journal of Biomedical Materials Research Part A. 1996;**30**(2):193-200

[105] Nancollas GH, Wang L. Calcium orthophosphates: Crystallization and dissolution. Chemical Reviews. 2008;**108**:4628-4669

[106] Grases F, Ramis M, Costa-Bauza A. Effects of phytate and pyrophosphate on brushite and hydroxyapatite crystallization. Urological Research. 2000;**28**:136-140

[107] Termine JD, Peckauskas RA, Posner AS. Calcium phosphate formation in vitro: II. Effects of environment on amorphous-crystalline transformation. Archives of Biochemistry and Biophysics. 1970;**140**(2):318-325

[108] Panzavolta S, Torricelli P, Bracci B, Fini M, Bigi A. Alendronate and Pamidronate calcium phosphate bone cements: Setting properties and in vitro response of osteoblast and osteoclast cells. Journal of Inorganic Biochemistry. 2009;**103**:101-106

[109] Nancollas GH, Tang R, Phipps RJ, Henneman Z, Gulde S. Novel insights into actions of bisphosphonates on bone: Differences in interactions with hydroxyapatite. Bone. 2006;**38**:617-627

[110] Cherng A, Takagi S, Chow LC. Effects of hydroxypropyl methylcellulose and other gelling agents on the handling properties of calcium phosphate cement. Journal of Biomedical Materials Research Part A. 1997;**35**(3):273-277

[111] Perez RA, Kim H-W, Ginebra M-P. Polymeric additives to enhance the functional properties of calcium phosphate cements. Journal of Tissue Engineering. 2012;**3**(1):1-20

[112] Giocondi JL et al. Molecular mechanisms of crystallization impacting calcium phosphate cements. Philosophical Transactions of the Royal Society of London A: Mathematical, Physical and Engineering Sciences. 2010;**368**(1917):1937-1961

[113] Alkhraisat MH et al. Beta-tricalcium phosphate release from brushite cement surface. Journal of Biomedical Materials Research Part A. 2008;**84**(3):710-717

[114] Mersmann A. Crystallization Technology Handbook, Chapter: 11. 2nd ed. Marcel-Dekker, Inc.; 2001

[115] Bohner M, Brunner TJ, Stark WJ. Controlling the reactivity of calcium phosphate cements. Journal of Materials Chemistry. 2008;**18**:5669-5675

[116] Bohner M. Reactivity of calcium phosphate cements. Journal of Materials Chemistry. 2007;**17**:3980-3986

[117] Hofmann MP, Nazhat SN, Gbureck U, Barralet JE. Real-time monitoring of the setting reaction of brushite-forming cement using isothermal differential scanning calorimetry. Journal of Biomedical Materials Research Part B: Applied Biomaterials. 2006;**79B**:360-364

[118] Liu C, Gai W, Pan S, Liu Z. The exothermal behavior in the hydration process of calcium phosphate cement. Biomaterials. 2003;**24**:2995-3003

[119] Song Y, Hahn HH, Hoffmann E. The Effects of pH and Ca/P Ratio on the Precipitation of Calcium Phosphate. Chemical Water and Wastewater Treatment VII; 2002

[120] Johnsson MSA, Nancollas GH. The role of brushite and octacalcium phosphate in apatite formation. Critical Reviews in Oral Biology and Medicine. 1992;**3**(1/2):61-82

[121] Bohner M. New hydraulic cements based on α-tricalcium phosphate–calcium sulfate dihydrate mixtures. Biomaterials. 2004;**25**:741-749

[122] Sarda S et al. Kinetic study of citric acid influence on calcium phosphate bone cements as water-reducing agent. Journal of Biomedical Materials Research Part A. 2002;**61**(4):653-659

[123] Wagh AS. Chemically Bonded Phosphate Ceramics, Chapter 5 – Dissolution Characteristics of Metal Oxides and Kinetics of Ceramic Formation; 2004

[124] Layrolle P, Daculsi G. Physicochemistry of apatite and its related calcium phosphates. In: Thin Calcium Phosphate Coatings for Medical Implants. Springer New York; 2009. pp. 19-21

[125] Fernandez E, Gil FJ, Ginebra MP, Driessens FCM, Planell JA. Calcium phosphate bone cements for clinical applications part I: Solution chemistry. Journal of Materials Science: Materials in Medicine. 1999;**10**:169-176

[126] Bermudez O et al. Development of an octocalcium phosphate cement. Journal of Materials Science: Materials in Medicine. 1994;**5**(3):144-146

[127] Nakano Y et al. In vitro and in vivo characterization and mechanical properties of α-TCP/OCP settings. Bioceramics. 1999;**12**:315-318

[128] Wolde t, Rein P, Frenkel D. Homogeneous nucleation and the Ostwald step rule. Physical Chemistry Chemical Physics. 1999;**1**(9):2191-2196

[129] Song Y, Hahn HH, Hoffmann E. The Effects of pH and Ca/P Ratio on the Precipitation of Calcium Phosphate. Chemical Water and Wastewater Treatment VII; 2002

[130] Ostwald W. Studien über die Bildung und Umwandlung fester Körper. Zeitschrift für Physikalische Chemie. 1897;**22**(1):289-330

[131] Balluffi RW, Allen SM, Carter WC. Kinetics of Materials, Chapter 19: Nucleation. John Wiley & Sons; 2005

[132] Pitzer KS. Thermodynamics of electrolytes. I. Theoretical basis and general equation. The Journal of Physical Chemistry. 1973;**77**(2)

[133] Brown WE, Chow LC. Thermodynamics of apatite crystal growth and dissolution. Journal of Crystal Growth. 1981;**53**(1):31-41

[134] Tung MS, Chow LC, Brown WE. Basic biological sciences hydrolysis of dicalcium phosphate dihydrate in the presence or absence of calcium fluoride. Journal of Dental Research. 1985;**64**(1):2-5

[135] Bohner M. Calcium orthophosphates in medicine: From ceramics to calcium phosphate cements. Injury - International Journal of the Care of the Injured. 2000;**3I**:S-D3747

[136] Hirayama S, Takagi S, Markovic M, Chow LC. Properties of calcium phosphate cements with different tetracalcium phosphate and dicalcium phosphate anhydrous molar ratios. Journal of Research of the National Institute of Standards and Technology. 2008;**113**:311-320

[137] Khairoun I, Boltong MG, Driessens FCM, Planell JA. Effect of calcium carbonate on the compliance of an apatitic calcium phosphate bone cement. Biomaterials. 1997;**18**:1535-1539

[138] Monma H. Chemical and biomaterials aspects of calcium phosphate cement. Phosphorous Research Bulletin. 2006;**20**:41-46

[139] Takagi S, Chow LC, Ishikawa K. Formation of hydroxyapatite in new calcium phosphate cements. Biomaterials. 1998;**19**:1593-1599

[140] Bohner M et al. Composition effects on the pH of a hydraulic calcium phosphate cement. Journal of Materials Science: Materials in Medicine. 1997;**8**(11):675-681

[141] Grover LM, Gbureck U, Wright AJ, Tremaynec M, Barralet JE. Biologically mediated resorption of brushite cement in vitro. Biomaterials. 2006;**27**:2178-2185

[142] Dorozhkin SV. Self-setting calcium orthophosphate ($CaPO_4$) formulations. In: Developments and Applications of Calcium Phosphate Bone Cements. Singapore: Springer; 2018. pp. 41-146

[143] Lu X, Leng Y. Theoretical analysis of calcium phosphate precipitation in simulated body fluid. Biomaterials. 2005;**26**:1097-1108

[144] Gbureck U et al. Ionic modification of calcium phosphate cement viscosity. Part I: Hypodermic injection and strength improvement of apatite cement. Biomaterials. 2004;**25**(11):2187-2195

[145] Ishikawa K, Takagi S, Chow LC, Suzuki K. Reaction of calcium phosphate cements with different amounts of tetracalcium phosphate and dicalcium phosphate anhydrous. Journal of Biomedical Materials Research. 1999;**46**:504-510

[146] Hofmann MP et al. FTIR-monitoring of a fast setting brushite bone cement: Effect of intermediate phases. Journal of Materials Chemistry. 2006;**16**(31):3199-3206

[147] Bohner M, Gbureck U. Thermal reactions of brushite cements. Journal of Biomedical Materials Research Part B: Applied Biomaterials. 2008;**84**(2):375-385

[148] Sarda S, Fernandez E, Llorens J, Martinez S, Nilsson M, Planell JA. Rheological properties of an apatitic bone cement during initial setting. Journal of Materials Science: Materials in Medicine. 2001;**12**(10-12):905-909

Chapter 13

Cements for High-Temperature Geothermal Wells

Tatiana Pyatina and Toshifumi Sugama

Additional information is available at the end of the chapter

http://dx.doi.org/10.5772/intechopen.74108

Abstract

Geothermal environments are among the most difficult conditions for cements to survive. Normally accepted for high-temperature oil wells silica-modified Portland-based cement formulations are not durable in hostile geothermal environments failing to provide good zonal isolation and metal casing corrosion-protection. High-temperature well cement compositions based on calcium-aluminate cements have been designed to seal such wells. Two types of calcium-aluminate cement are of particular interest for geothermal applications. One is–chemical type, calcium-aluminate-phosphate cement (CaP) already used in the field and the other, alkali-activated calcium-aluminate type (thermal shock resistant cement, (TSRC), has been recently developed. The CaP cements were designed as CO_2-resistant cements for use in mildly acidic (pH ~ 5.0) CO_2-rich downhole environments. TSRC was formulated to withstand dry-heat – cold water cycles of more than 500°C. This chapter includes information and discussions of cement forming mechanisms, cements mechanical properties, resistance to mild and strong acids, cement-carbon steel bonding and self-recovery of mechanical strength and fractures closure after imposed damage. Performance of common high-temperature OPC-based composites is discussed for comparison.

Keywords: geothermal cements, chemical cement, calcium-aluminate phosphate cement, alkali activated cement, durability, cement-metal interface, acid resistance, cement corrosion protection, self-healing cement composites, well integrity

1. Introduction

Geothermal resources exist throughout the world. To recover geothermal energy subterranean wells are installed, fluids heated by geothermal formations are produced to the surface, the heat is used to power turbines to generate electrical power and the spent fluid is injected back into the reservoir through injection wells. The formation fluids are often very saline and

corrosive with high concentrations of toxic metals so most of the time cannot be used outside of the geothermal systems. In regions where there is no fluid at geothermal formations, conditions called "hot dry rock", fluids from the surface are pumped down an injection well, superheat at hot dry rocks and are returned to the surface through production wells. Although the geothermal wells are constructed in the way similar to regular oil and gas wells the conditions to which cement is exposed are often much more severe and some failures of geothermal wells were directly attributed to cement failures [1]. In addition to highly acidic and saline fluids geothermal cements may be exposed to temperatures above 500°C [2] and temperature fluctuations of more than 1100°C [3]. To address such conditions new cement formulations were designed and developed. Because of the most difficult conditions to survive geothermal cements have the most stringent requirements. They are usually designed to have a low water permeability of less than 0.1 mD and compressive strength of at least 7 MPa (API Task Group on Cements for Geothermal Wells, 1985) [4]. The set cement must be stable in saline brines and CO_2-rich environments, resistant to acidic gases and fluids. In addition, geothermal cements must withstand thermal shock conditions where they encounter large temperature variations and provide good corrosion protection of the casing. The majority of geothermal wells are cemented with silica-stabilized Portland cement composites.

Portland cement systems have difficulties with carbonate present in many geothermal wells. Calcium silicate hydrates convert to calcium carbonate and amorphous silica at high carbonate concentrations even at low temperature [5]. Even the systems with low calcium-to-silica ratios traditionally used to withstand carbonate attacks are not stable under geothermal conditions with high CO_2 content [6, 7]. Both high-temperature calcium-silicate hydrates formed at low calcium-to-silica ratios, tobermorite and xonotlite, are sensitive to carbonation. Decrease of silica, proposed as a measure to improve resistance of Portland cement-silica blends to carbonate, produces weaker cement but allows calcium hydroxide formed at low silica content to react with carbonate and form a dense protective layer that slows down cement degradation [8–10]. Various organically-modified Portland-based systems or "synthetic cements" have been proposed for the use in aggressive geothermal environments but their applications are limited by polymers high temperature stabilities [11–13]. To address the difficulties of cementing geothermal wells oil well cements modified with alumina [14] and alternative, calcium-aluminate-cement (CAC) based systems were studied and developed specifically for geothermal well applications [15–19]. Chemical bond calcium phosphate blends (CaP) consisting of calcium-aluminate cement, fly ash, type F and sodium polyphosphate have been successfully used for cementing geothermal wells [20].

Studies on alkali-activated cement composite of calcium aluminate cement and fly ash F (thermal shock resistant cement, (TSRC)) demonstrated excellent performance under various stresses of simulated geothermal environments [21, 22], and outstanding CS bond durability [23]. Further work showed that TSRC has self-healing properties, which is ability to recover its compressive strength and seal the cracks at temperatures up to 300°C [24].

In this chapter the properties of chemical bond calcium phosphate cement and alkali-activated cement composites have been revisited and updated to allow for better understanding of cement behavior under conditions of geothermal wells and in other applications in aggressive environments. Properties of the blend of class G oil well Portland cement modified with silica are presented as a benchmark.

2. CaP cement and TSRC performance under stresses

2.1. Chemistries and mechanisms of CO_2- and acid-resistance: cement matrix

Both CaP cement and TSRC major components are CAC (Secar #51 and Secar #80 respectively) and fly ash F (FAF). **Table 1** shows oxides composition of these CACs, class G cement and fly ash F. The XRD data identify three crystalline phases in CAC #80, corundum (α-Al_2O_3), calcium monoaluminate ($CaO{\cdot}Al_2O_3$, CA), and calcium dialuminate ($CaO{\cdot}2Al_2O_3$, CA_2) and #51 CAC has CA as its dominant phase, coexisting with gehlenite [$Ca_2Al(Al, Si)_2O_7$] and corundum as the secondary components.

CaP is formed by chemical reactions between #51 CAC, FAF, and sodium hexametaphosphate [SHMP: $(NaPO_3)_6$]. These reactions take place in two stages – firstly, a fast chemical reaction between sodium polyphosphate and calcium ions released from calcium aluminate cement takes place with formation of calcium hydrogen phosphate. It further reacts with calcium aluminate cement forming hydroxyapatite. Aluminum released by CAC forms aluminum oxide hydroxide, boehmite. Secondly, the fly ash reacts with sodium ions from sodium polyphosphate at high temperatures with formation of analcime. The reactions may be summarized by the following equation:

$$\begin{aligned} &CaO \cdot Al_2O_3(CaO \cdot 2Al_2O_3) + Al_2O_3 \cdot 2SiO_2\,(SiO_2) + [NaPO_3]_n \rightarrow \\ &Ca_5\,(PO_4)_3(OH) + Na_8Al_8Si_{16}O_{48}(H_2O)_8 + AlOOH \end{aligned}$$

Carbonation of CaP cement matrix proceeds with formation of very stable carbonated apatite from apatite and cancrinite from analcime. The analcime → cancrinite transition results in increased matrix porosity and some loss of the strength, which however stabilizes after longer curing times [16].

$$Ca_5\,(PO_4)_3(OH) + H_2CO_3 \rightarrow Ca_5\,(PO_4)_3 \cdot CO_3 + H_2O$$

$$Na_8Al_8Si_{16}O_{48}(H_2O)_8 + H_2CO_3 \rightarrow Na_8\left[(AlSi)_{12}O_{24}CO_3\right] \cdot 3H_2O$$

Since CaP cement generally develops high initial compressive strength of more than 35 MPa, the reduced strength of about 20 MPa after the carbonation is still more than sufficient for all the cement functions in a well.

Component	Oxide composition, wt%							
	Al_2O_3	CaO	SiO_2	Fe_2O_3	Na_2O	K_2O	TiO_2	SO_3
Class G cement	2.9	66.0	18.0	3.8	0.3	1.3		5.4
CAC, #80	75.2	24.7	—	0.1	—	—	—	
CAC, #51	45.1	49.7	—	2.8	—	—	2.4	
FAF	35	2.7	50.0	7.1	0.30	3.1	1.6	

Table 1. Oxide compositions of cement blends' starting materials.

TSRC is formed by reactions of CAC#80, FAF and sodium meta-silicate. In the case of TSRC reactions are more concomitant than in the case of CaP cement. CAC and SMS-activated FAF react with formation of aluminum oxide hydroxide from Al of CAC, calcium-aluminum-silicates from ions released by all cement components and zeolites from FAF and SMS reactions. The reaction with formation of calcium-aluminum-silicate, high-temperature zeolites, analcime and hydroxysodalite, at 300°C can be written as follows:

$$CaO \cdot Al_2O_3\,(CaO \cdot 2Al_2O_3) + Al_2O_3 \cdot 2SiO_2\,(SiO_2) + Na_2O \cdot nSiO_2 \rightarrow$$
$$CaAl_2Si_2O_8 + Na_8Al_8Si_{16}O_{48}\,(H_2O)_8 + Na_4Al_3Si_3O_{12}(OH) + AlOOH$$

Katoite and katoite silician, hydrogrossular and other zeolites (thomsonite, garronite, Lind A) form at lower curing temperatures.

Wet carbonation of TSRC matrix proceeds with formation of carbonated zeolite, cancrinite as in the case of CaP cement:

$$Na_8Al_8Si_{16}O_{48}\,(H_2O)_8 + H_2CO_3 \;\rightarrow\; Na_8\left[(AlSi)_{12}O_{24}CO_3\right] \cdot 3H_2O$$

Since CaP and TSRC are both blends of CAC and FAF many of their hydration products are similar. Specifically, the hydration products of the common phases (CAC and FAF), such as boehmite, calcium-aluminate, katoite, calcium-aluminum silicates dmisteinbergite/anorthite, and analcime are present in both cements. Some other products are specific for the reactant (sodium polyphosphate)/activator (sodium meta-silicate) used in the blends. They are apatite (a product of CAC and polyphosphate reaction) in CaP cement blend, silicon-rich phases such as katoite silician and more zeolites because of the faster alkali activation of FAF by sodium-meta-silicate in TSRC. These zeolites are more silica-rich than for CaP cement. They include Lind A, thomsonite and sodalite depending on hydration temperature. As a result of similar mineralogical composition, the responses of these two cements to many stress environments are also similar.

Specifically, in carbonate-rich environment one of the main carbonation products is stable CO_3-contaning mineral cancrinite [16, 24]. CaP also forms carbonated apatite. In the case of sulfuric acid attack calcium reacts with sulfates forming anhydrate in both cements and the remaining alkali aluminum-silicates provides structural stability of the acid-treated matrix [22].

A noticeable difference in the phase composition development of the two cements is fast formation of $CaHPO_4(H_2O)_x$, chemical reaction product in CaP at 90–101°C and no visible reaction of FAF for the first 25 days under these conditions. In fact FAF has a low reactivity at low pH (~6.6) of CaP cement. On the other hand TSRC hydration products include crystalline zeolite (zeolite A, gismondine) already after 22 days at 85°C due to the fly ash F activation by sodium meta-silicate present in the composition of that cement [25]. Due to the dissolution of sodium meta-silicate with release of sodium ions TSRC slurry is highly alkaline (pH~13). While fast chemical reactions of CaP cement allow fast early strength development, faster FAF reactions in TSRC may be important in acidic environments where low permeability is required to limit acid penetration into the cement matrix causing its deterioration. In the case of CaP cement such penetration may take place along the non-reacted FAF particles at early hydration times.

The phase compositions of the cements depend on temperature, curing time and curing regime (how fast the final temperature is reached). If the cement sets and rests for some time at lower temperature (e.g. pumping temperature of below 100°C) before the high final temperature is reached, the low-temperature stable phases may still be present after high-temperature curing. For example, Linde A zeolite that forms in TSRC cured for 3 days at 85°C persists after 7-day curing at 200°C but disappears if the sample is cured at 300°C [25]. Another important factor of the curing regime is whether CAC and FAF react consecutively or simultaneously. At lower temperatures the hydration starts with more reactive CAC especially in the case of CaP cement that does not have alkali activator for FAF. As a result calcium aluminate hydrates (katoite) and chemical reaction products (calcium-hydrogen phosphate and apatite) form when the temperature increase is slow. If the temperature rises fast enough for both CAC and FAF to react simultaneously or close in time mixed products containing starting materials from both CAC and FAF form (dmisteinbergite) along with the reaction products of CAC (apatite), and FAF (analcime) reacting separately. **Table 2** summarizes possible crystalline phase compositions of CaP and TSRC at different temperatures after short curing times (<5 d). It can be seen that in the case of CAP cement zeolite analcime becomes one of the major phases only at high temperature of 300°C.

2.2. Thermal shock and corrosion protection: cement-carbon steel interface

Portland cement modified with crystalline silica for high-temperature cementing applications in underground wells generally demonstrates a poor bonding to CS casings. The annuluses formed along the cement-casing interface because of the poor cement bonding may cause fluids and gas migration, contamination of underground formations, severe casing corrosion, and, in the worst case scenario, catastrophic well collapse events. To overcome the problem slurries are modified with organic additives such as latex-based bonding aids/gas migration

Temp.	Major phases		Minor phases	
	CaP	TSRC	CaP	TSRC
~100°C	Hydroxyapatite	Gibbsite, Linde A	Boehmite, calcium hydrogen phosphate	Katoite, gismondine
~200°C	Hydroxyapatite	Katoite, thomsonite, gismondine;	Katoite, boehmite; calcium hydrogen phosphate; P-type zeolite; analcime	Sodalite/hydroxysodalite, dmisteinbergite, boehmite; analcime
~300°C	Dmisteinbergite hydroxyapatite, analcime	Dmisteinbergite, analcime, hydroxysodalite, boehmite	Anorthite, calcium hydrogen phosphate, Boehmite	Boehmite, gismondine, muscovite, margarite

Table 2. Short-term crystalline-phase compositions of TSRC and CaP cement at different temperatures.

prevention products. Although costly, such additives noticeably improve bonding strength of cement but also impose temperature limitations. The products does not survive temperatures above ~200°C on one hand and slow down cement hydration and, as a result, compressive strength development at ~60–85°C. Set retardation of latex-modified slurries at temperatures above ~120°C for placement in the wells may be also problematic.

Calcium-aluminate-cement containing blends have stronger CS bond and bond durability under various stress environments [23]. Further work showed that TSRC is able to recover its compressive strength and seal the cracks after imposed damage at temperatures up to 300°C [24]. It was demonstrated that the strength recovery of TSRC could be further enhanced to above 100% by addition of micro glass fibers (MGF, see below). Performance of MGF-modified TSRC, CaP and G/SiO_2 blend sheath samples with CS in thermal shock tests was evaluated. In these tests all the blends were modified with 5% by weight carbon micro fibers (for more information see [23, 26]) and with 5% micro glass fibers (Fiber Glast Development Corporation, part #38; 16 × 230 micron diameter × length) to improve their "self-healing" performance. Thermal-shock tests were performed on samples of carbon steel tube surrounded by cement sheath. After a day of curing in water at 300°C the samples were dry heated to 350°C for 24 hours and then cold water of about 20°C passed through the tube. The dry heat-cold water cycles were repeated up to 7 times. The thermal shock tests reduced the bond strength of all tested composites consistent with earlier reports [23, 26]. After 7 cycles the TSRC and CaP samples developed very thin cracks ("hair cracks"). The G/SiO_2 formulation developed noticeable wide crack that was getting wider during the heating period and narrower during the cooling (**Figure 1**). As expected both calcium-aluminate cement-based blends showed a stronger initial bonding and significantly better thermal shock resistance than class G blend. Furthermore, TSRC, developed to withstand large temperature variations, outperformed CaP in both the initial shear bond strength and the strength remaining after the tests. The composition difference that allows the better performance of TSRC at the interface with CS and in thermal shock tests is higher alkalinity of the slurries due to the presence of sodium-meta-silicate and as a result faster activation of fly ash F than in CaP cement blends. It was reported that the presence and reactions of FAF mostly contribute to the thermal shock resistance of blend cements [27].

High pH of TSRC slurries also helps corrosion protection of the CS. **Figure 2** shows CS corrosion rates, cement layer thickness and appearance of CS plates after the corrosion tests for CaP, TSRC and G/SiO_2 blends. The samples cured at 300°C for 1 d before the lap-shear bond strength tests (two CS plates bound by a thin layer of set cement are pulled apart) were exposed for 5 more days to the curing environment. Then electrochemical measurements were taken on three different locations for each sample to obtain corrosion rate. In addition, cement layer thickness was measured. During the lap-shear bond strength tests the samples underwent different failure mechanisms. In the case of class G/SiO_2 blend the bond between the cement layer and CS broke leaving CS plate for the most part free of cement and exposed to corrosion (adhesive failure). For TSRC the break happened inside the cement layer (cohesive failure) with some cement left on the CS plate providing its corrosion protection. CaP cement underwent mixed failure mechanism with partial cement coverage left on the plate after the bond tests.

http://dx.doi.org/10.5772/intechopen.74108

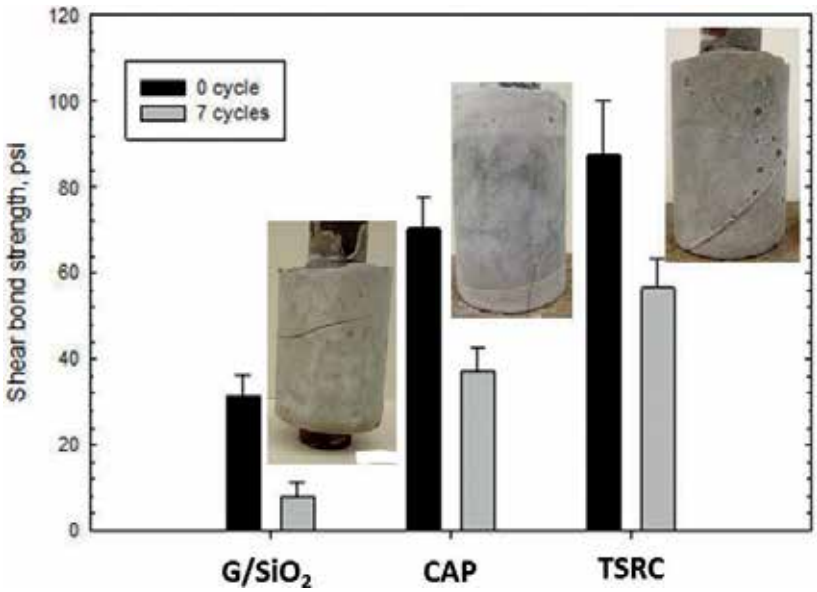

Figure 1. Shear bond strength and appearance of cement-CS sheath samples hydrothermally cured at 300°C and subjected to 7 cycles of thermal shock tests.

The appearances of the samples show clear signs of corrosion of class G/SiO_2 covered CS plate and some corrosion spots on the plate with CaP cement. TSRC samples do not have signs of corrosion. This observation is confirmed by corrosion rate and cement thickness data – showing the lowest corrosion rate and the thickest cement layer for the plate with TSRC. Class G cement blend provides the least corrosion protection of carbon steel. **Figure 3** gives microphotographs and elemental composition of TSRC and G/SiO_2 cement covering carbon steel plates. The measurements of iron from the underlying plates are consistent with the cement layer thickness data – the level of iron from CS measured at the G/SiO_2 blend is 5 times higher than that at TSRC suggesting thinner more porous cement layer for the Portland cement-based blend than for alkali activate FAF/CAC cement.

An important observation is high levels of Al in the interface layers. Class G cement is relatively poor in aluminum, so the amorphous, aluminum-rich layer protecting carbon steel is thin. On top of it calcium-silicate hydrate, xonotlite, with short parallel needles is sparingly spread. In general, the samples with needle-shaped xonotlite crystals exhibit higher permeabilities [7]. TSRC on the other hand forms thick aluminum-rich amorphous layer covered with intertwined rods of zeolite crystals (the bottom part of the microphotograph) acting as a self-reinforcing material.

In summary, calcium-aluminate cement blends with fly ash F significantly outperformed high temperature class G/SiO_2 Portland cement-based blend in bond strength with CS and its resistance to large temperature variations under the thermal shock conditions. Dense and thick aluminum-rich amorphous TSRC layer formed on the surface of CS plate and highly alkaline environment of its slurry provided excellent corrosion protection of CS. Randomly

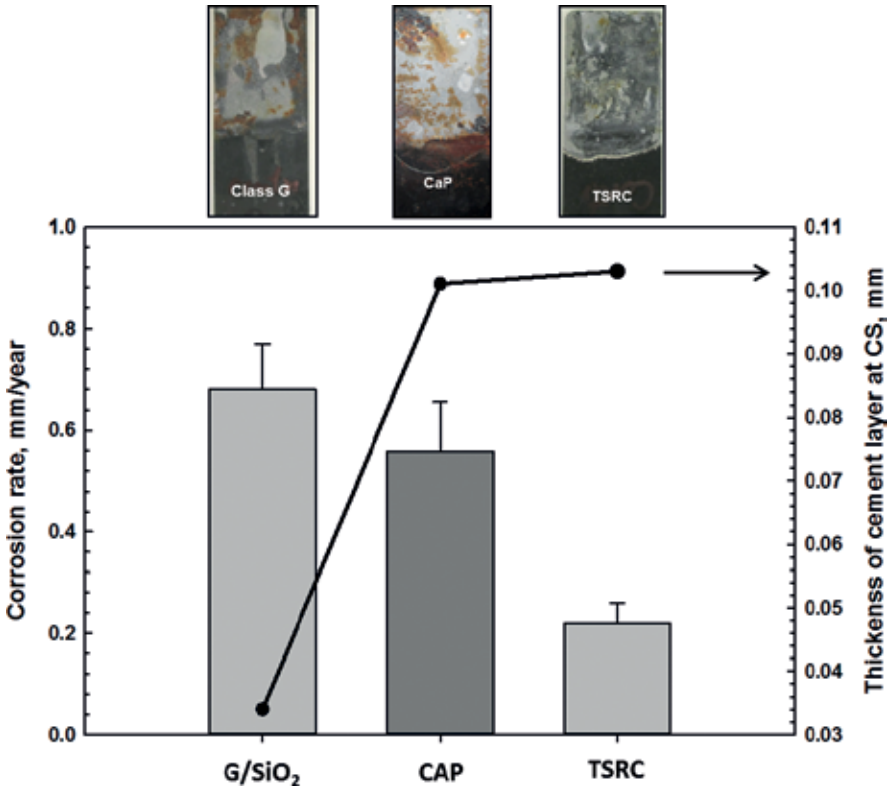

Figure 2. Corrosion rate, cement layer thickness and appearance of carbon steel samples with cement layer after hydrothermal curing for total 6 d at 300°C.

oriented zeolite crystals with rode-morphology provided self-reinforced cement on top of the amorphous phase in contact with the CS plate. As expected, Portland cement-based blends underwent adhesive failure in lap shear bond tests. With little cement left on CS the corrosion protection was poor. The spots of CS covered with remaining G/SiO_2 blend had thin amorphous layer covered with needle-like xonotlite crystals that are known to exhibit high permeability.

2.3. Strength recovery after compressive damage

Although strong, cements are brittle and, as a result, are likely to be damaged under various stresses of geothermal wells. To locate and repair such damage in underground constructions is very difficult and costly. That is why cements self-healing properties are of particular interest for underground applications. The subterranean geothermal environments offer some special conditions for cement self-healing. Particularly, cements are exposed to fluids necessary for reaction of latent components of cementitious blends and these fluids are rich in ions, both cations and anions that may participate in formation of new phases contributing to healing of damaged cements. Dissolution of slow-reacting volcanic ash components in interstitial water with release of hydroxyl ions and solution enrichment in Na, K, Ca, and Si was shown to result

http://dx.doi.org/10.5772/intechopen.74108

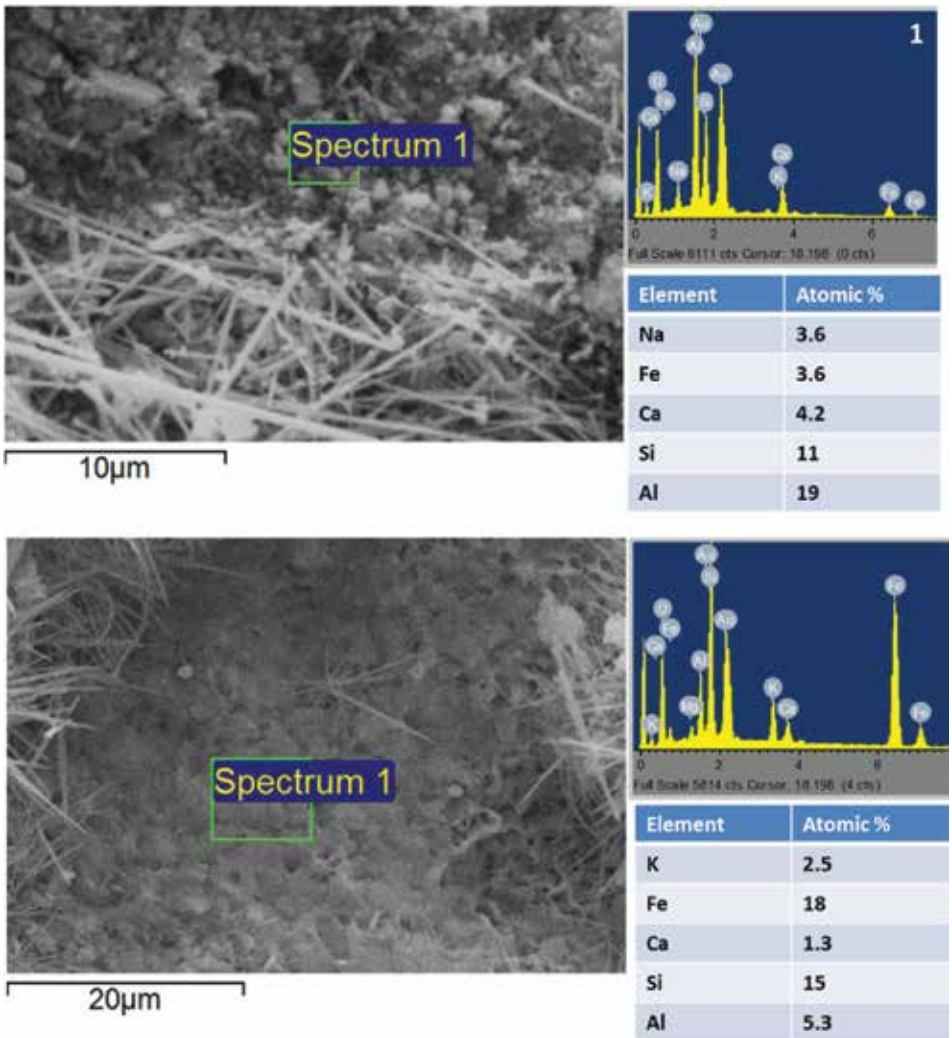

Figure 3. Microphotographs and elemental compositions of TSRC (top) and G/SiO_2 layers on carbon steel plates after 6 d hydrothermal curing at 300°C.

in long-term crystallization of zeolite, Al-tobermorite, and stratlingite reinforcing Roman marine concretes [28]. Such authigenic mineral cycling when new minerals form through in-situ precipitation and recrystallization may regenerate geothermal cements with FAF pozzolanic component in their composition. High temperatures help to accelerate the process.

Table 3 shows strength recoveries of the three blends after repeated damage and two 5-day healing periods. Detailed information on experimental set up can be found elsewhere [24]. The brine composition is given in [29]. In these tests 1-day cured samples were compressively damaged or broken (the compression tests were stopped at the maximum yield point) and then exposed to the curing conditions for 5 more days. The compressive strength was retested

Cement system	Curing environment (300°C)		
	Water	Alkali carbonate 0.05 M $NaCO_3$	Hypersaline brine
Class G/SiO_2	C	B	B
TSRC	A	A	A
CaP cement	C	C	A

Table 3. Cement strength recoveries after repeated compressive damage and two 5 d healing periods. Average recovery rates after 1st and 2nd compressive breaks for 1 d 300°C- cured samples: A 80–99%; B 60–79%; C < 60%.

after the 5-day healing period. The damage-healing cycle was repeated and the compression strength recovery data averaged.

The data show that at short curing times TSRC may successfully recover its strength after repeated damage in different environments. The recoveries of class G and CaP cement blends are not as good with the exception of CaP cement in hypersaline brine.

As mentioned above one possible mechanism of strength recovery are FAF reactions contributing to the "healing" process of damaged cements. However, although both CaP cement and TSRC contain FAF strength recoveries of CaP cement are inferior to those of TSRC and in the environment of alkali carbonate even to class G blend. One of the reasons for poor strength recoveries is the brittleness and the strong bond nature (chemical bond) of the CaP blend. Fast early compressive strength development through chemical reactions of sodium phosphate with calcium aluminate makes this cement strong but brittle. So the Young's modulus of the control CaP blend after 1 d curing at 300°C is 1896 MPa, while for TSRC it is 971 MPa. As a result wide cracks and fractures form under the compressive damage, making the repairs problematic. Another possible cause of lower healing performance of CaP cement could be its lower alkalinity in comparison with TSRC and G/SiO_2 blends. Under conditions of low alkalinity dissolution of fly ash and crystallization of healing phases requires longer times or may not happen at all.

Addition of slowly-reacting components, such as MGF, to the blends helps to improve strength recoveries (**Table 4**). MGF react under alkaline conditions contributing sodium, aluminum, and silicon to the pore water of the blends. These ions favor formation of zeolites that at later times may alter to other more stable zeolites or feldspar minerals [30].

In case of MGF additions strength recoveries are improved to above 100% (higher strength of damaged samples after the healing than the original strength) for TSRC and to 80–99% for class G/SiO_2 blend. In addition to the exceptional strength recoveries of TSRC samples optimal selection of pozzolanic materials allows binding cement pieces completely broken off the samples. The bond strength of such re-adhered pieces can be evaluated from the stress–strain curves of compressive strength tests. An example of such curve for a TSRC sample broken into two pieces and then cured at 300°C for 5 days in alkali carbonate environment is shown in **Figure 4**. On the curve the yield point (YP) compressive strength is 17.3 MPa. However, the initial failure (IF) of the sample where the re-adhered piece breaks off can be seen as a left shoulder with the failure point at 10.8 MPa. Such points of IF allow evaluation of the

Cement system	Curing environment (300°C)		
	Water	Alkali carbonate 0.05 M $NaCO_3$	Hypersaline brine
Class G/SiO_2	A	A	A
TSRC	A+	A+	A+
CaP cement	C	B	A

Table 4. Cement strength recoveries for blends reinforced with MGF after repeated compressive damage and two 5 d healing periods. Average recovery rates after 1st and 2nd compressive breaks for 1 d 300°C-cured samples: A+ > 100%; A 80–99%; B 60–79%; C < 60%.

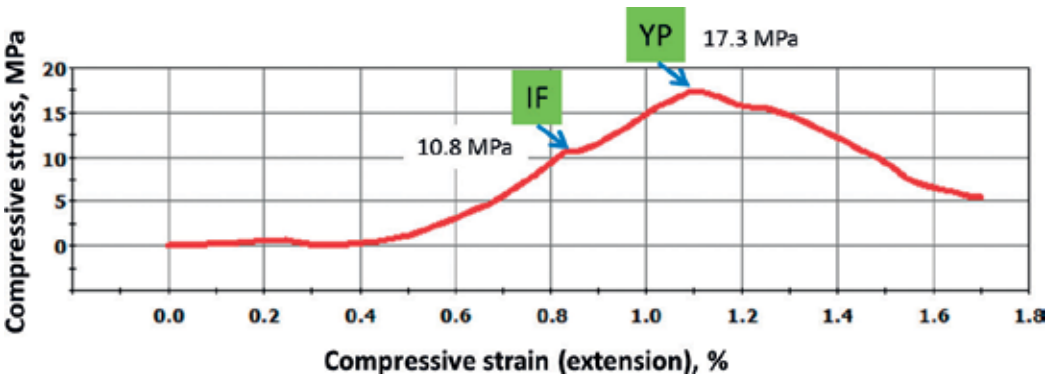

Figure 4. Strain–stress compressive curve for TSRC sample broken into two pieces and re-bound in alkali carbonate (0.05 M $NaCO_3$) at 300°C for 5 days; points of breaking off the re-adhered piece (initial failure, IF) and the yield point (YP) of the sample are shown.

recovered bond strength between broken off cement pieces and cement matrix. In the TSRC example the recovered strength (10.8 MPa) was above that required by the API task group on cements for geothermal wells (7 MPa).

The recoveries do not improve as much for CaP blend as for TSRC. This is likely due to significantly lower alkalinity of that slurry (pH~6.6), which does not allow fast MGF reactions and, on the other hand, fast chemical reactions resulting in stable products with little phase transitions that could help strength recoveries. As mentioned above another reason for lower strength recoveries in the case of CaP cement is its brittle nature that causes formation of large, smooth, difficult-to-repair cracks under compressive stresses.

3. Conclusions

Two types of calcium-aluminate cement – fly ash F blends, chemical (CaP) and alkali activated (TSRC), noticeably outperform common high-temperature well-cement blends of Portland cement and silica. The factors that contribute to their good performance under conditions of thermal shock, CO_2-rich- and strong-acid environments are as follows.

Good acid and thermal shock resistance of fly ash F reaction products, formation of stable carbonation phases, including carbonated apatite from apatite in CaP cement and cancrinite from zeolites in both CaP cement and TSRC.

The differences in the performance of these blends come from the minor components, sodium polyphosphate (CaP) and sodium-meta-silicate activator (TSRC). In CaP cement fast chemical reactions of sodium polyphosphate produce calcium phosphate-containing phases at early curing times, contributing to the early strength development and CO_2-resistance through formation of stable carbonated apatite phase. The reactions of fly ash F are delayed in CaP cement because of low ash reactivity at low pH of the interstitial water of this cement. This, along with the brittle cement nature limits early strength recoveries after cement damage. The low pH is also unfavorable for corrosion protection of carbon steel.

On the other hand, in TSRC samples sodium meta-silicate creates highly alkaline slurries that promote fly ash F reactions at earlier curing times than in the case of CaP. Fly ash F reaction products contribute to strong acid-, thermal shock resistance and high pH favorably changes the environment for corrosion protection of carbon steel. Excellent strength recoveries for damaged or broken TSRC samples are possible thanks to the cement's ductile nature and highly alkaline pH of its interstitial solution promoting fly ash F reactions with formation of new healing phases. However, the relatively high (>100°C) temperatures are necessary for fast early strength development of TSRC, while chemical reactions with the formation of phosphate in CaP cement allow fast early strength development over a wide temperature range.

This different natures of the two discussed calcium-aluminate cements may provide important advantages when specific properties are required under aggressive environments – whether it is fast early compressive strength development or formation of tough composites with regenerative potential.

Acknowledgements

This publication was based on the work supported by the Geothermal Technologies Office in the US Department of Energy (DOE) Office of Energy Efficiency and Renewable Energy (EERE), under the auspices of the US DOE, Washington, DC, under contract No. DE-AC02-98CH 10886. Research was carried out in part at the Center for Functional Nanomaterials, Brookhaven National Laboratory, which is supported by the US Department of Energy, Office of Basic Energy Sciences, under Contract No. DE-SC0012704.

Author details

Tatiana Pyatina* and Toshifumi Sugama

*Address all correspondence to: tpyatina@bnl.gov

Brookhaven National Laboratory, Upton, USA

References

[1] Nelson E, Barlet-Gouedard V. Thermal cements. In: Nelson E, Guillot D, editors. Well Cementing. 2nd ed. Sugar Land, Texas, USA: Schlumberger; 2006. pp. 319-341

[2] Uchida T, Akaku K, Yanagisawa N, Kamenosono H, Sasaki M, Miyazaki S, Doi N. Deep geothermal resources survey project in the Kakkonda geothermal field. Journal of Energy Recourses. 1998;**20**:215-222

[3] Bensted J. Current calcium aluminate cement applications in well plugging. In: Fentiman C, Mangabhai R, Scrivener K, editors. Calcium Aluminate Cements. Proceedings of the Centenary Conference. HIS: bre press; 2008. p. 345-356

[4] API Task Group on Cements for Geothermal Wells. API Work group reports field tests of geothermal cements. Oil and Gas Journal. 1985;**83**:93-97

[5] Taylor H. The Chemistry of Cements. London, England: Academic Press Press Inc. Ltd.; 1964

[6] Hedenquest J, Stewart M. Natural CO_2-rich steam-heated water in the Broadlands-Okaaki geothermal system, New Zealand: their chemistry distribution and corrosive nature. In: GRC Transactions. 1985 Davis, CA

[7] Grabowski E, Gillot JE. Effect of replacement of silica flour with silica fume on engineering properties of oil well cements at normal and elevated temperatures and pressures. Cement and Concrete Research. 1989;**19**:333-344

[8] Milestone N, Sugama T, Kukacka L, Carciello N. Carbonation of geothermal grouts — Part 3: CO_2 attack on grouts containing bentonite. Cement and Concrete Research. 1987;**17**:295-306

[9] Milestone N, Sugama T, Kukacka L, Carciello N. Carbonation of geothermal grouts — Part 2: CO_2 attack at 250°C. Cement and Concrete Research. 1987;**17**:37-46

[10] Milestone N, Sugama T, Kukacka L, Carciello N. Carbonation of geothermal grouts — Part 1: CO_2 attack at 150°C. Cement and Concrete Research. 1986;**16**:941-950

[11] Zeldin A, Kukacka L. Polymer Cement Geothermal Well Completion Materials. Brookhaven National Laboratory report BNL 51287. Upton, NY: Brookhaven National Laboratory; 1980

[12] Pettit R. Completion of hot dry rock geothermal well systems. Paper SPE 8267 SPE Annual Technical Conference and Exhibition, 23-26 September, Las Vegas, NV, USA; 1979

[13] Degouy D, Martin M. Characterization of the evolution of cementing materials after aging under severe bottomhole conditions. Paper SPE 20904 SPE European Petroleum Conference, 22-24 October, The Hague, The Netherlands; 1990

[14] Meller N, Kyrtsis K, Hall C. The minerology of the CaO-Al_2O_3-SiO_2-H_2O (CASH) hydroceramic system from 200 to 350°C. Cement and Concrete Research. 2009;**39**:45-53

[15] Roy D, White C, Langton E, Grutzeck M. New high temperature cementing materials for geothermal wells: stability and properties. Brookhaven National Laboratory report BNL 51249. 1980; Brookhaven National Laboratory, Upton, NY, USA

[16] Sugama T, Weber L, Brothers L. Sodium-polyphosphate-modified fly ash/calcium aluminate blend cement: durability in wet harsh geothermal environments. Materials Letters. 2000;**44**:45-53

[17] Sugama T, Brothers L, Weber L. Calcium aluminate cements in fly ash/calcium aluminate blend phosphate cement systems: Their role in inhibiting carbonation and acid corrosion at a low hydrothermal temperature of 90°C. Journal of Materials Science. 2002;**37**:3163-3173

[18] Sugama T, Brothers L, Van de Putte T. Air-foamed calcium aluminate phosphate cement for geothermal wells. Cement and Concrete Composites. 2005;**27**:758-768

[19] Sugama T, Weber L, Brothers L. Resistance of sodium polyphosphate-modified fly ash/calcium aluminate blend cements to hot H_2SO_4 solution. Cement and Concrete Research. 1999;**29**:1969-1976

[20] Brookhaven National Laboratory. Brookhaven Lab., Halliburton Company, and Unocal Corporation Win R&D 100 Award for High-Performance Cement. Press release 00-56. 2000

[21] Sugama T, Gill S, Muraca A, Pyatina T. Corrosion-resistant foamed cement for carbon steels in enhanced geothermal systems. In: GRC Transactions, vol. 37, 29 September-2 October 2013; Las Vegas, NV

[22] Pyatina T, Sugama T. Acid resistance of calcium-aluminate cement- fly ash F blends. Advances in Cement Research. 2016;**28**:433-457

[23] Sugama T, Pyatina T. Bond durability of carbon-microfiber-reinforced alkali-activated high-temperature cement adhering to carbon Steel. Engineering. 2017;**9**:142-170

[24] Pyatina T, Sugama T, Ronne A. Self-repairing geothermal well cement composites. In: GRC Transactions, vol. 40, 23-26 October 2016, Sacramento, CA, USA

[25] Pyatina T, Sugama T, Moon J, James S. Effect of tartaric acid on hydration of a sodium-metasiliscate-activated blend of calcium aluminate cement and fly ash F. Materials. 2017;**10**:342-362

[26] Pyatina T, Sugama T. Use of carbon microfibers for reinforcement of calcium aluminate-class F fly ash cement activated with sodium meta-silicate at up to 300°C In: GRC Transactions, vol. 39, 20-23 September 2015, Reno, NV, USA

[27] Gill S, Pyatina T, Sugama T. Thermal shock resistant cement. In: GRC Transactions, vol. 36, 30 September-3 October 2012, Reno, NV, USA

[28] Jackson M, Mulcahy S, Chen H, Li Y, Li Q, CaPpelletti P, Wenk H. Phillipsite and Al-tobermorite mineral cements produced through low-temperature water-rock reactions in Roman marine concrete. American Mineralogist. 2017;**102**:1435-1450

[29] Sugama T, Pyatina T, Redline E, McElhanon J, Blankenship D. Degradation of different elastomeric polymers in simulated geothermal environments at 300°C. Polymers Degradation and Stability. 2015;**120**:328-339

[30] Hay R, Sheppard RA. Occurence of zeolites in sedimentary rocks: an overview. Reviews in Mineralogy and Geochemistry. 2001;**45**:217-234

Section 4

Alkali Activated Cements

Chapter 14

Clay-Based Materials in Geopolymer Technology

Mohd Mustafa Al Bakri Abdullah, Liew Yun Ming,
Heah Cheng Yong and
Muhammad Faheem Mohd Tahir

Additional information is available at the end of the chapter

http://dx.doi.org/10.5772/intechopen.74438

Abstract

The term "geopolymer" was introduced by Davidovits in the 1970s. The prefix "geo" was selected to symbolize the constitutive relationship of the binders to geological materials, natural stone and/or minerals. Geopolymer is mineral polymers of inorganic polymer glasses with structure resembling natural zeolitic materials. Previously, geopolymer formation used source materials such as clay (e.g. kaolin and calcined kaolin) or industrial by-product (e.g. slag and fly ash). The precursor material plays an important role in the formation of geopolymer. The source material provides silicon (Si) and aluminum (Al) for reaction by an alkali activator solution. The Si and Al contents in the source materials dissolve in the alkaline activator solution and then polymerize to form a polymeric Si-O-Al-O framework which becomes the binder. Geopolymeric materials are attractive because of their excellent mechanical properties; durability and thermal stability can also be achieved. Owing to their low calcium content, they are more resistant to acid attack than materials based on Portland cement. In addition, they are of great interest because of the reduced energy requirement for their manufacture and the higher sustainability. Recently the search for alternative low cost and easily available materials led among others to Clay. Clay generally consists of a mixture of different clay minerals and associated minerals, which are strongly affected by the nature of the parent rocks. These materials are extensively distributed over the surface of the world and may show certain reactivity after a thermal activation process shows a great potential to be utilized in geopolymer technology. This article presents the potential of different types of clay as the source materials for geopolymerization reaction in terms of morphological properties. Moreover, the mechanical and microstructural properties of geopolymer made with various kinds of clay and its potential application are also presented.

Keywords: geopolymer, inorganic polymer, clay

1. Introduction

In 1978, the word "geopolymer" was introduced by Davidovits [1]. In general, geopolymer is an inorganic polymeric material formed through the reaction between aluminosilicate sources and highly alkaline silicate solution, followed by curing at ambient or slightly higher temperature [2]. The formation process is termed as geopolymerization reaction.

Geopolymer has an empirical formula of:

$$M_n\{-(SiO_2)_z - AlO_2\} \cdot w\,H_2O \quad (1)$$

where M is cation such as K^+, Na^+ or Ca^{2+}; n is the degree of polycondensation; z is 1, 2, 3 and w is the amount of binding water. It has three-dimensional Si-O-Al polymeric networks ranging from amorphous to semi-crystalline. Tetrahedral SiO_4 and AlO_4 are linked alternately by sharing oxygen atom as shown in **Figure 1**. As refer to **Figure 1**, the terminology of geopolymers can be categorized into three forms which are poly(sialate), poly (sialate-siloxo) and poly (sialate-disiloxo). The Al is in IV-fold coordination [3, 4]. This leaves a negative charge in the IV-fold coordinated Al that is charge-balanced by cations (Na^+, K^+, Li^+, Ca^{2+}, Ba^{2+}, NH^{4+} and H_3O^+). The charge-balancing by cations is important in determining the structural integrity and fragility of geopolymers [5].

The cations is usually contributed by alkaline silicate solution which is a mixture of alkali hydroxides (NaOH or/and KOH) and silicate solution (Na_2SiO_3 or/and K_2SiO_3) [6–8]. The alkali hydroxide is required for the dissolution of aluminosilicates while alkali silicate acts as binder, alkali activator and dispersant or plasticizer [9]. The alkali silicate solution contributes certain amount of SiO_2 for the geopolymerization reaction [10].

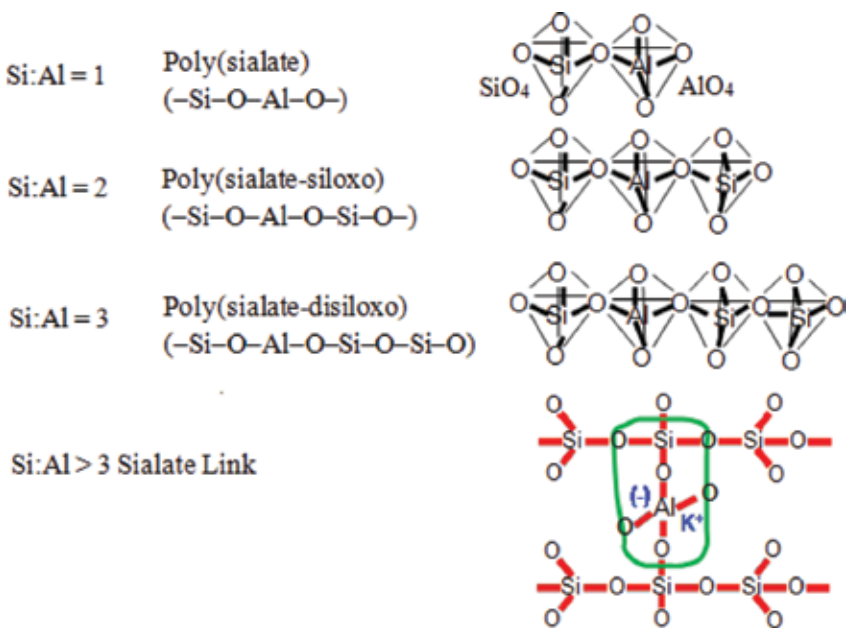

Figure 1. Geopolymer systems based number of siloxo Si-O units [2].

http://dx.doi.org/10.5772/intechopen.74438

2. Aluminosilicates

The aluminosilicate sources are materials rich in alumina and silica content (e.g. ashes [11–14], clays [15, 16] or slag [17, 18]). Some other natural and artificial silicoaluminates such as zeolite [19] and magnesium-contained minerals [20] have also been used as an important source of Si^{4+} and Al^{4+} ions in the geopolymer binding system. Normally, the total composition of Al_2O_3 and SiO_2 is more than 70%, preferable in reactive amorphous phase [3, 21]. In this book chapter, the utilization of clay or clay minerals in geopolymer formation is discussed.

3. Kaolin/kaolinite

Kaolinite is the most common clay mineral used in geopolymer synthesis. It has 1:1 uncharged dioctahedral layer structure (**Figure 2a**) whereby the layers are $(Si_2O_5)_n^{2-}$ sheet and the $Al(OH)_3$ (gibbsite) sheet linked by sharing oxygen atoms. The layers are held together by weak van der waals and hydrogen bonds leading to the layered structure (**Figure 2b**).

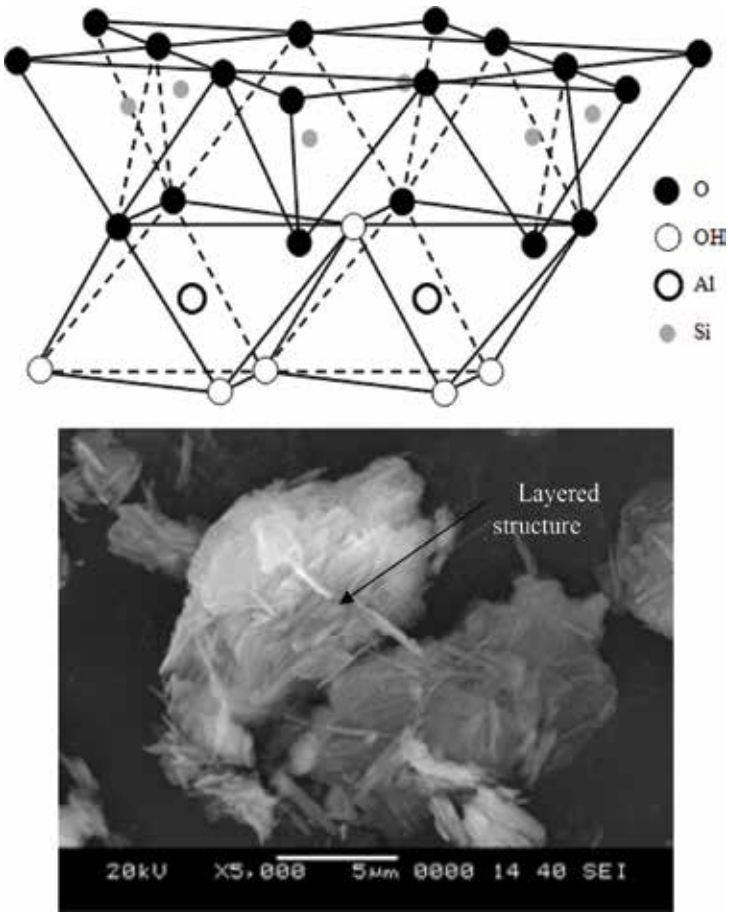

Figure 2. Structure of kaolinite (above) and microstructure of kaolinite (below) [22].

4. Metakaolin

Thermal treatment of kaolinite leads to the transformation of crystalline phases into reactive amorphous phases [7], which is the active constituent that determines the final strength of geopolymers. The thermal treatment is usually carried out at temperature in the range of 550–800°C which accompanied by dehydroxylation of strongly bounded hydroxyl ions on the Al-constitutive layer. Thus, kaolinite is transformed into metakaolin.

Metakaolin also has layered structure as kaolinite even after the thermal treatment process. However, the layer structure appeared more open than kaolinite (**Figure 3**) [23, 24].

Also, the thermal treatment destroys the hexagonal layer of kaolinite and causes atomic arrangement that converted the hexa-coordinated Al ions of kaolinite are converted into penta- and tetra-coordinated Al ions [25]. The amount of penta- and tetra-coordinated Al ions reflects the reactivity of metakaolin [24].

4.1. Clay-based geopolymers

Clays are frequently used as the source materials in geopolymer formation. They have a total composition of Al_2O_3 and SiO_2 in the range between 70 and 90% (**Table 1**) wherein the composition of clay is dependent on the origin and the geology of the location. Initially, in the early stage of geopolymer development, kaolin/kaolinite is mostly used as the aluminosilicate sources [2, 6, 32, 33]. Later, the experimental work has expanded to calcined clays, ashes and slag. This is because kaolin/kaolinite shows low reactivity with alkaline silicate solution causing low strength products. It is deemed that the near zero charge between layers and the layered structure that does not permit the exchange of ions or other element. Hence, kaolin/kaolinite has low surface area for geopolymerization reaction. According to Heah et al. [34], the low surface area limits the dissolution of kaolin/kaolinite to provide Si^{4+} and Al^{4+} ions for further reaction. Comparatively, fly ash has greater surface area as they have spherical-shaped particles.

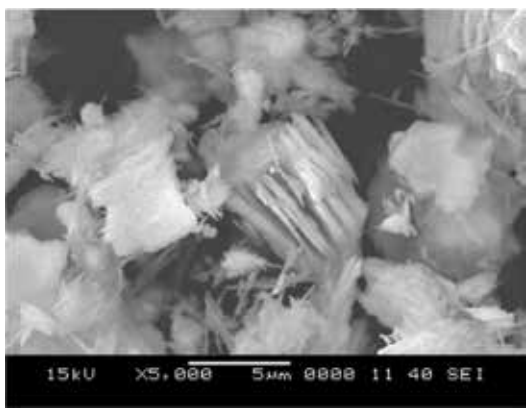

Figure 3. SEM micrograph of metakaolin (800°C for 2 hours) [23].

Clay/clay mineral	SiO_2	Al_2O_3	Fe_2O_3	TiO_2	MgO	P2O5	Na2O	CaO	K2O	MnO	SO3	LOI
Metakaolin [26]	51.35	44.24	0.98	0.90	0.48	0.45	0.16	0.13	0.08	0.01	—	0.72
Metakaolin [27]	52.1	43.0	0.7	—	0.3	—	0.12		2.5	—	—	1.0
Metakaolin [28]	59.7	34.1	0.9	—		—	0.2	0.1		—	0.1	1.2
Clay sediment from Occhito reservoir, Italy [29]	47.5	15.6	6.7	—	2.4	—	0.3	10.2	1.9	—	—	15.4
Clay sediment from Sabetta reservoir, Italy [29]	50.0	15.9	5.7	—	1.9	—	0.3	6.9	1.7	—	—	17.5
Kaolinite from Hiswa, Jordan [30]	48.92	25.16	7.52	0.86	0.21	0.16	0.21	0.68	1.4	0.01	2.94	11.93
Kaolinite [31]	49.35	36.03	0.20	0.02	0.02	—	0.04	0.02	2.29	—	—	11.94
Kaolinite [31]	40.86	39.87	0.39	0.46	0.12	—	0.01	0.12	0.17	—	—	17.91
Kaolinite [31]	42.66	40.92	1.12	0.45	0.04	—	0.14	0.14	0.09	—	—	14.13
Halloysite [31]	48.12	36.33	0.33	0.16	—	—	0.05	0.04	0.03	—	—	14.8

Table 1. Chemical composition of clays from different origins.

Summary of the compressive strength of geopolymers based on clay/clay minerals is tabulated in **Table 2**. The strength achieved by geopolymers based on clay/clay minerals is low. The addition of kaolinite as secondary source of aluminosilicate is necessary in order to achieve strength. Unfortunately, the use of kaolinite alone in geopolymer is not preferable as it will produce weak structure [35]. The statement is further supported by van Jaarsveld et al. [38] who concluded the strength of fly ash geopolymers degraded as the result of high kaolinite content (41%) addition. The main reason for the deterioration in strength is because not all kaolinite reacted in the reaction.

If the clays/clay minerals are heat-treated, the mechanical strength of the final products would increase [35, 39]. Pre-treatment is crucial to increase the reactivity of clays/clay minerals. The pre-treatment methods include mechanochemical, chemical and thermal treatments. MacKenzie et al. [40] reported that typical characteristic geopolymers are produced with heat-treated (200–1000°C for 2 hours) halloysite. Mechanochemical-treated (high-energy grinding for 20 hours at 400 rpm) halloysite showed less complete geopolymer formation. For acid-treated (0.1 M HCl) halloysite, the resulting geopolymers were poorly set while alkaline-treated (0.1 M NaOH) halloysite caused the formation of crystalline zeolites. Thermal treatment is the most used methods. Successfully calcined clays lead to highly pozzolanic amorphous phase. For instance, geopolymers from clay sediments treated at 750°C for 2 hours showed greater compressive strength (6–12 MPa) than those treated at 400°C (1–4 MPa) [29].

Clay/Clay minerals	Strength (MPa)		Ref.
	KOH	NaOH	
Almandine	10.3[c]	8.5[c]	[35]
Grossular	16.7[c]	14.5[c]	[35]
Sillimanite	12.7[c]	6.5[c]	[35]
Andalusite	11.1[c]	8.8[c]	[35]
Kyanite	6.8[c]	6.3[c]	[35]
Pumpellyite	10.8[c]	8.8[c]	[35]
Spodumene	13.1[c]	5.0[c]	[35]
Augite	6.7[c]	5.0[c]	[35]
Lepidolite	4.3[c]	2.5[c]	[35]
Illite	7.1[c]	5.8[c]	[35]
Celsian	9.7[c]	8.7[c]	[35]
Sodalite	15.0[c]	10.3[c]	[35]
Stilbite	18.9[c]	14.2[c]	[35]
Heulandite	7.4[c]	5.6[c]	[35]
Anorthite	14.4[c]	6.0[c]	[35]
Kaolin	-	2 – 10[c]	[37]
Clay residues		5.76 – 5.98[f]	[38]

[c]compressive strength;
[f]flexural strength

Table 2. Strength result of clay/clay minerals geopolymers.

According to the author, thermally treated clay sediments exhibited improved surface area toward dissolution and geopolymerization reaction. Apart from the purely clay geopolymers, blended geopolymers are also produced with the addition of other materials such as calcium hydroxide, slag and ashes with the clay materials as the starting source material. When calcium hydroxide is added, the strength of the blended geopolymers does not degrade [41, 42]. Similarly, the addition of 30% slag in metakaolin geopolymers showed improvement in the mechanical strength. Slag acted as filler in the geopolymer structure and enhanced the mechanical properties. However, the slag addition is limited to below 50% as it will greatly deteriorate the strength at content beyond 50% [43]. The high calcium content in both calcium hydroxide and slag caused the formation of geopolymer matrix as the main phases and the calcium silicate hydrates (CSH) phases as the secondary phases [27, 43]. This can be clearly shown in **Figure 4**.

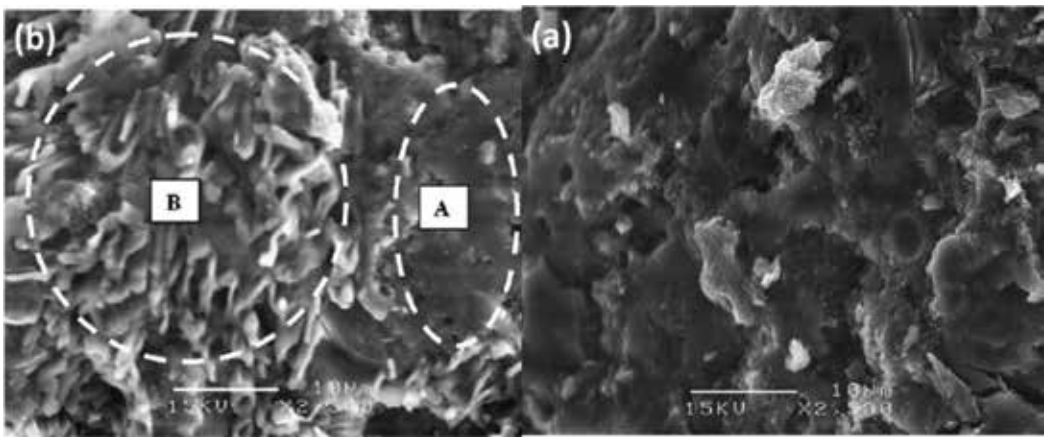

Figure 4: SEM micrographs of (a) pure metakaolin; and (b) metakaolin-50% slag geopolymer (a—Geopolymer matrix and B—CSH phases) [43].

5. Geopolymerization mechanism

Geopolymer formation involves chemical reaction that transforms partially or totally amorphous aluminosilicates into three-dimensional polymeric networks. The geopolymerization reaction is exothermic. Under strong alkaline medium, the aluminosilicate sources dissolve into SiO4 and AlO4 tetrahedral units which later on participate in the polycondensation process [44, 45].

The chemical attack of kaolinite starts from the surface and edge and continues layer by layer inside the structure (**Figure 5**) [46]. The Al-substituted silicate layers formed and the structural deformed Al sites transformed into tetra-coordinated Al sites after attack by alkali hydroxide (**Figure 6**) [47].

Davidovits proposed the reaction mechanism as shown in **Figure 7**. The reaction aluminosilicates and alkali silicate solution produced geopolymers with Si-O-Al backbone.

In general, the geopolymerization mechanism is similar for all types of aluminosilicates. Most researchers agreed that the geopolymerization reaction involves dissolution, polycondensation and hardening process. The dissolution of aluminosilicates is initiated by presence of hydroxyl ions in the alkaline silicate solution which releases Si and Al species for further polycondensation reaction [9, 49]. The geopolymerization reaction is deemed occurs in multistep simultaneously [38, 42, 50] such as reorganization and diffusion of dissolved ions with formation of small coagulated structures, solid state transformation and hardening to form hard solid polycondensation to form aluminosilicate gel phases and dissolution of aluminosilicates in highly alkaline medium.

In addition, Xu and Van Deventer [51] suggested that geopolymer is formed through Eqs. (2)–(4). Eq. (1) represents the mixing of aluminosilicates with alkali silicate solution. Geopolymer gel is formed in Eq. (3), while Eq. (4) shows the formation of geopolymer rigid solid.

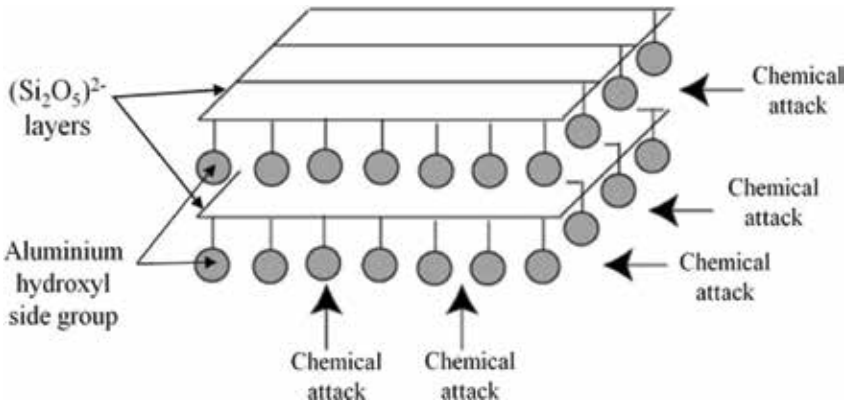

Figure 5. Reaction of kaolinite under alkaline medium (gray circle denotes the aluminum hydroxyl side groups) [46].

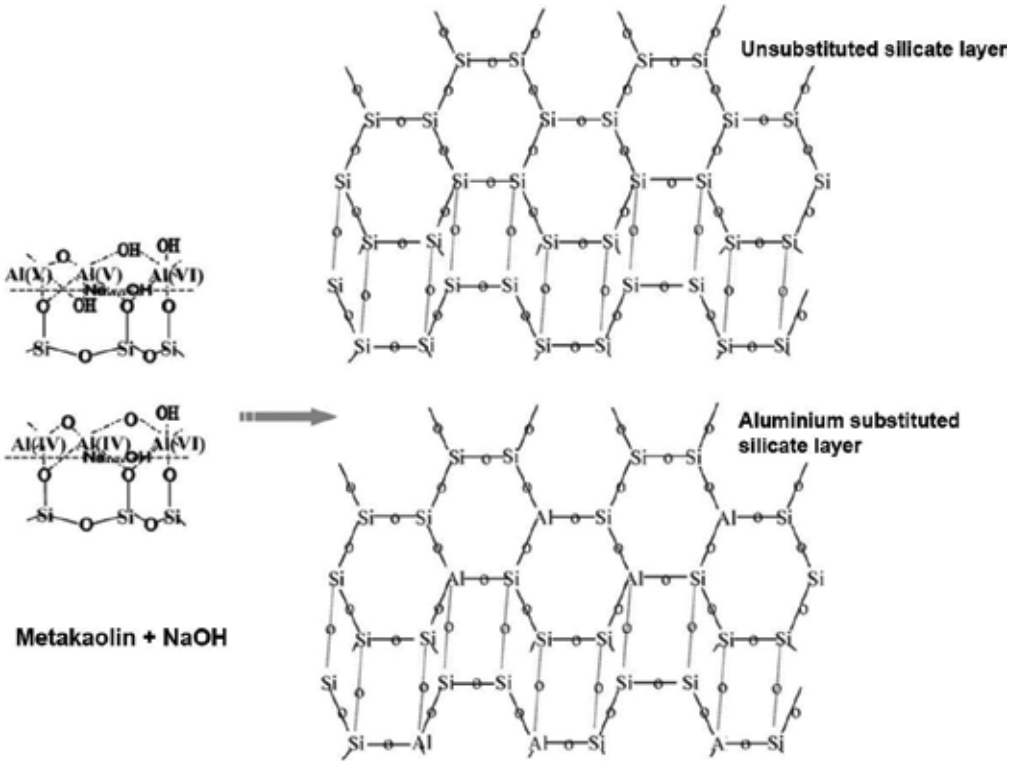

Figure 6. Formation of aluminum substituted silicate layer in metakaolin after attack by NaOH solution [47].

$$\text{Al–Si material (s)} + \text{MOH (aq)} + \text{Na}_2\text{SiO}_3\text{ (s or aq)}\downarrow \tag{2}$$

$$\text{Al–Si material (s)} + \left[\text{M}_z\left(\text{AlO}_2\right)_x\left(\text{SiO}_2\right)_y \cdot n\text{MOH} \cdot m\,\text{H}_2\text{O}\right]\text{gel}\downarrow \tag{3}$$

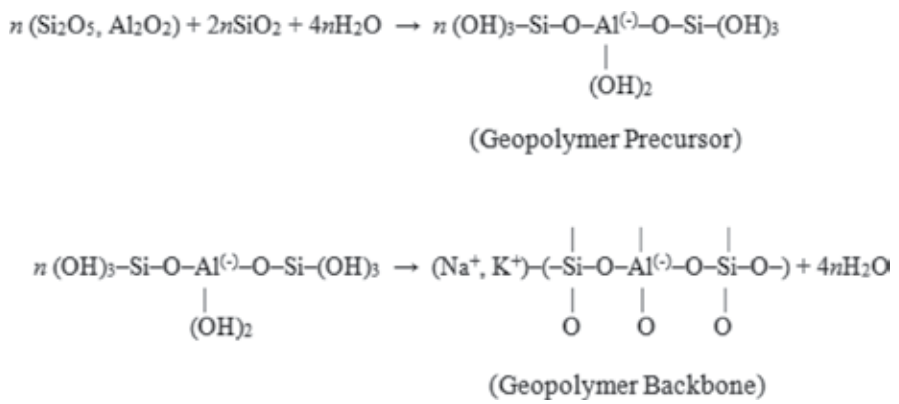

Figure 7. Schematic diagram of geopolymer formation [48].

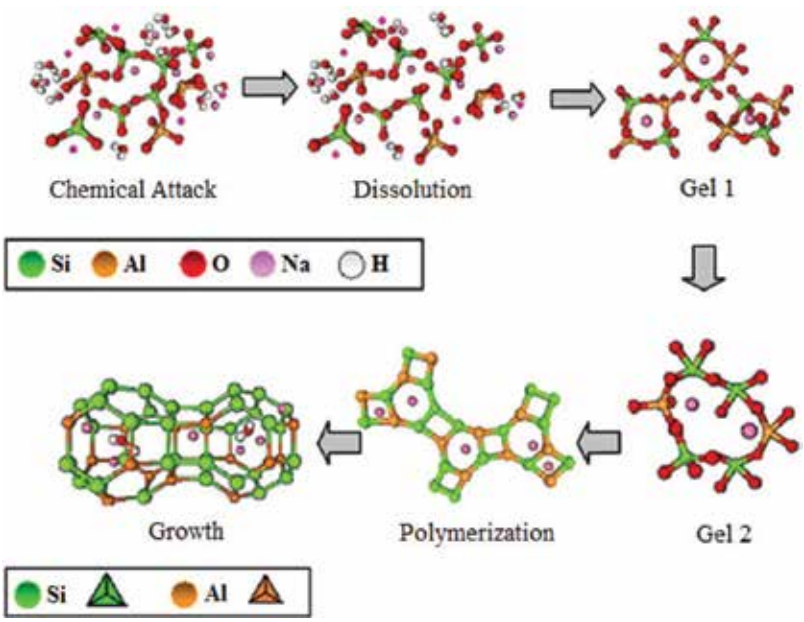

Figure 8. Graphic model of alkali activation of geopolymers [54].

$$\text{Al–Si material (s)} \left[M_a \left((AlO_2)_a (SiO_2)_b \right) n\text{MOH} \cdot \text{m}H_2O \right] \quad (4)$$

According to Provis et al. [52, 53], the final geopolymer gel phase after extended curing process is different from the initial gel phase. The curing process allows continuous rearrangement of geopolymer gel phase toward more crosslinking and some zeolite crystals (more ordered phases) are formed in the geopolymer structure. Similar model is illustrated by Duxson et al. [54] in **Figure 8**. The intermediate product (Gel 1) having high Al contents transformed into

Gel 2 with high Si content as the reaction progresses and finally rearranged forming three-dimensional geopolymer frameworks.

5.1. Clay-based geopolymer formation

Most usual method to form geopolymer is direct mixing of aluminosilicate with alkali silicate solution. After mixing, the geopolymer paste is compacted in molds and cured at room temperature or slightly higher temperature (20–80°C). To avoid extensive loss of moisture, the geopolymer paste is covered with a thin plastic film during the curing process. Besides, other mixing method has also been studied with different mixing sequences. The aluminosilicate is firstly mixed with liquid sodium silicate and the NaOH solution is added afterwards.

Based on Lecomte et al. [25], the normal mixing and separate mixing did not lower the degree of geopolymerization reaction of kaolin/white clay-slag blended geopolymers. However, separate mixing required additional water for mixing and hence detrimental to the mechanical strength. A contradict result is reported by Rattanasak & Chindaprasirt [55] based on fly ash geopolymer. The separate mixing permits more time for dissolution of aluminosilicates providing more dissolved species for the polycondensation process. This in turn leads to formation of stronger geopolymers. On top of that, the homogeneity of the geopolymer mixtures is crucial in order to attain high strength.

Regardless of the different mixing sequence, workability is an important criterion to be taken into consideration during geopolymer formation. Serious workability problem leads to compaction difficulty and produce weak geopolymer structure [23, 34]. For geopolymer based on clay, it usually requires excess water during the mixing process in order to achieve certain consistency. The addition of excess water will definitely decrease the mechanical strength of the final product. Comparison with fly ash geopolymers, the mixture of clay-based geopolymer is usually highly viscous and sticky [56]. The layer structure of clay induces greater inter-particle friction which limits the flowability of mixture. Unlike clay, fly ash has spherical-shaped particles. The imposed inter-particle friction is lesser and can acquire adequate consistency without addition of excess water.

6. Characterization of clay-based geopolymers

6.1. Morphology

As aforementioned, the kaolinite and metakaolin appears plate-like or layer-like structure. After the geopolymerization reaction, this layer-like structure changed. The morphology of clay-based geopolymer appeared sponge-like with globular units (**Figure 9**). The microstructure grows and develops over time starting from the precipitation of loosely-packed globular units on the metakaolin's particle surface and densification of geopolymer matrix inside and outside voids [57, 58]. At the beginning the K/Al and Si/Al molar ratios are high due to leaching of Si from liquid sodium silicate. As time passed, more dissolved Al entered the geopolymer system and lowered the molar ratios [57]. Instead of globular units of geopolymer matrix,

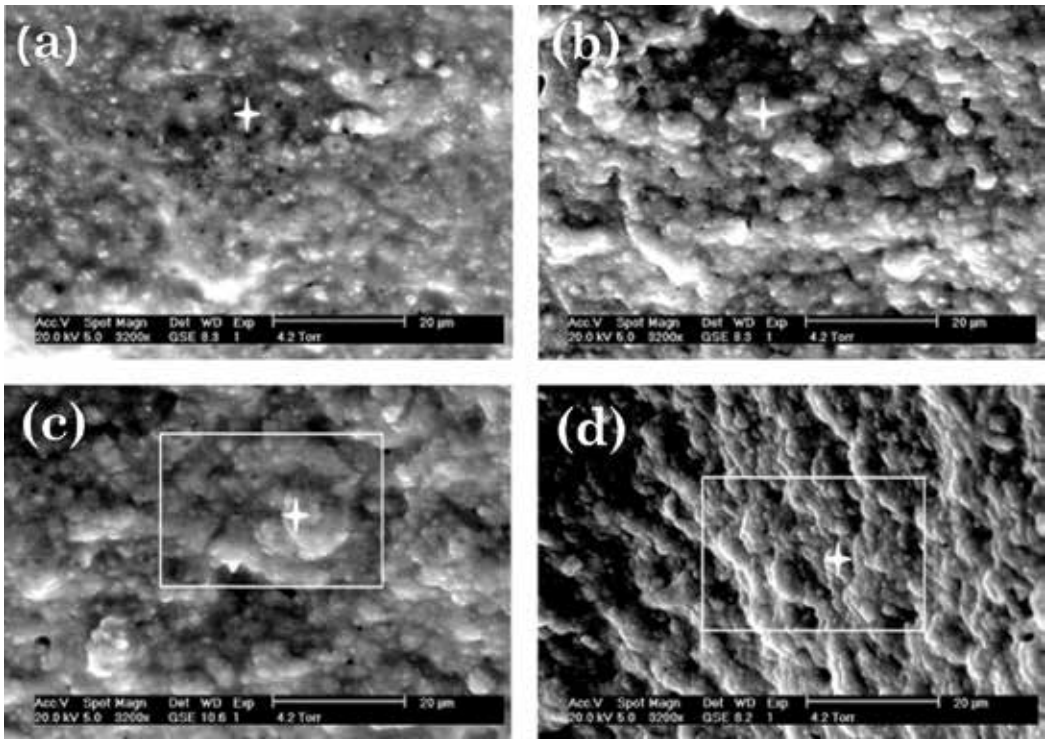

Figure 9. ESEM micrographs of metakaolin geopolymers after (a) 10 minutes, (b) 3 hours, (c) 6 hours, and (d) 9 hours of mixing [57].

fly ash-based geopolymers revealed smooth heterogeneous geopolymer matrix with remnant fly ash particles in the hollow cavities due to partially dissolution (**Figure 10**).

Differently, Wang et al. [59] observed that the metakaolin geopolymers are not compact. The layer structure is remained in the geopolymer matrix after geopolymerization reaction (**Figure 11**). The remnant metakaolin geopolymer might have left and embedded in the geopolymer structure. Based on Rowles et al. [60], the residual raw particles in geopolymer structure may weaken the structure. This is because the residual particles act as stress concentration point that permit propagation of cracks and fractures. To our knowledge, complete geopolymerization reaction is not achieved. There must be come residual raw materials left in the structure after the chemical reaction.

The mechanical strength of geopolymer is affected significantly by the density and porosity in the structure. High strength geopolymer is associated with low porosity, high dense and fine-grained microstructure [61].

6.2. Mineralogy of clay-based geopolymers

The X-ray diffraction (XRD) pattern of kaolinite consists mainly of crystalline phases [34]. The thermal treatment of kaolinite transformed the crystalline phases into amorphous phases.

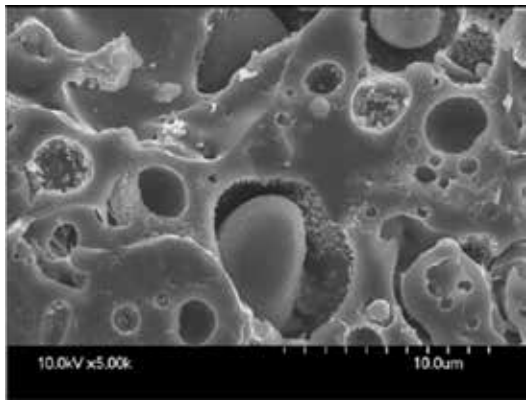

Figure 10. SEM micrographs of fly ash geopolymers cured at room temperature for 24 hours and at 80°C for another 24 hours [15].

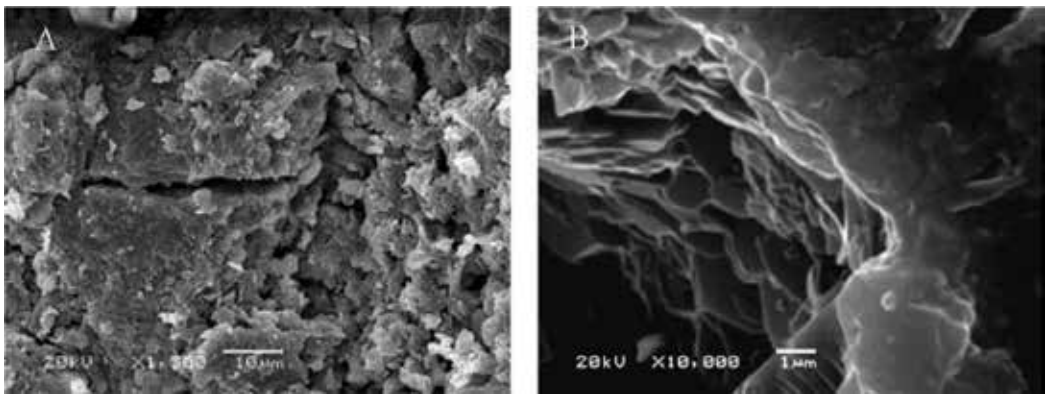

Figure 11. SEM micrographs of metakaolin geopolymers [59].

The metakaolin retains some long-range order as result of stacking of the hexagonal layers [62]. Therefore, metakaolin shows semi-crystalline to amorphous pattern with a halo at 2θ between 15 and 30° [56]. This diffuse halo represents the amorphous silica in metakaolin [63]. Marked shift in the scattering peak is observed after the geopolymer formation. The diffuse halo in metakaolin shifted to higher angle. Generally, geopolymers show completely amorphous X-ray diffraction (XRD) pattern with a diffuse halo peak at 2θ between 27 and 30° [25, 48, 57, 64, 65]. The primary binder phase in geopolymer matrix contributes to the amorphous characteristic and determines the strength of geopolymers. Also, in a study carried out by Wang et al. [59], the halo diffuse peak of metakaolin geopolymer fell at 2θ between 18 and 25°. Increasing Si/Al ratio reduces the angle of diffuse halo [65].

Crystalline phases, particularly zeolites, are usually grown in geopolymers in conjunction with the amorphous binder phases (**Figure 12**) [46, 66]. As zeolites have similar chemical composition with geopolymers, geopolymers are usually deemed as the zeolitic precursor. The

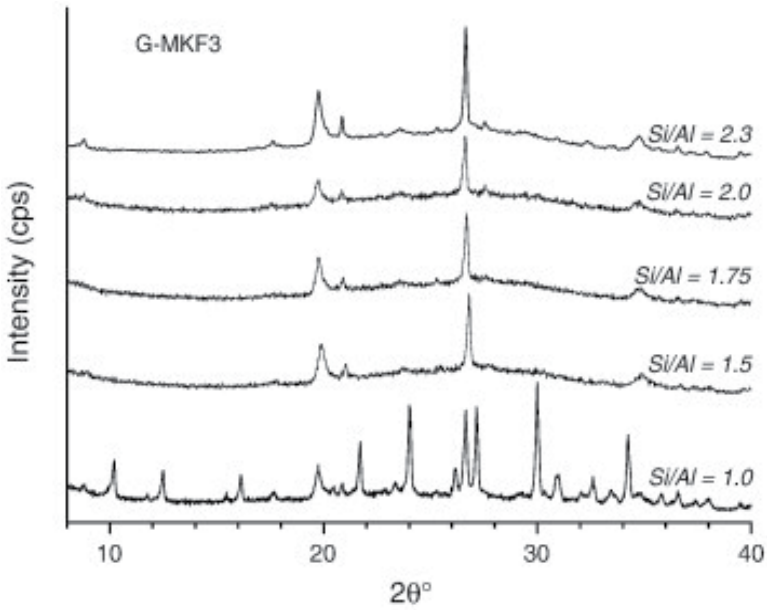

Figure 12. XRD patterns of geopolymers from Algerian metakaolin, activated with alkaline sodium silicate solution and cured at 50°C for 24 h with various Si/Al ratios [66].

main difference between them is that zeolite is crystalline while geopolymer is amorphous. The growth of crystalline phases is facilitated by the high water content, high curing temperature, aging and also extended curing period [4, 67]. Zeolites are highly porous and have poor mechanical properties. Some researches [68, 69] claimed that zeolite crystallites reinforce and improve strength of clay geopolymers. Yet, the long-term strength reduced. Even so, it is strongly believed that there is a tolerance limit on the crystalline phase's content within the geopolymer matrix. Similar trend was reported for fly ash geopolymers [70].

7. Functional group identification

Kaolinite shows FTIR bands around 1113 cm^{-1} (Si-O bonds in SiO_4 molecules); 994 cm^{-1} (Si-O bonds in SiO_4 molecules); 907 cm^{-1} (Al^{IV}-OH vibrations); 799 cm^{-1} (SiO-symmetric stretching) and 537 cm^{-1} (Si-O-Al^{VI}) [24, 38, 71, 72]. On the other hand, as the kaolinite is thermally treated, the band at 1113 cm^{-1} shifted to lower wavenumber (~ 1031 cm^{-1}) [23]. This is related to the amorphous SiO_2 [25]. The FTIR bands associated with VI-fold coordinated Al vanished after calcination as a result of distortion of tetrahedral and octahedral sheets of kaolinite [24]. The band at around 781 cm^{-1} appears in metakaolin as the Al-O stretching vibration in AlO_4 tetrahedral [73].

As the geopolymerization reaction progresses, shift of bands are observed. Clay-based geopolymer exhibits main FTIR absorption band at 990 cm^{-1} associated with the asymmetrical

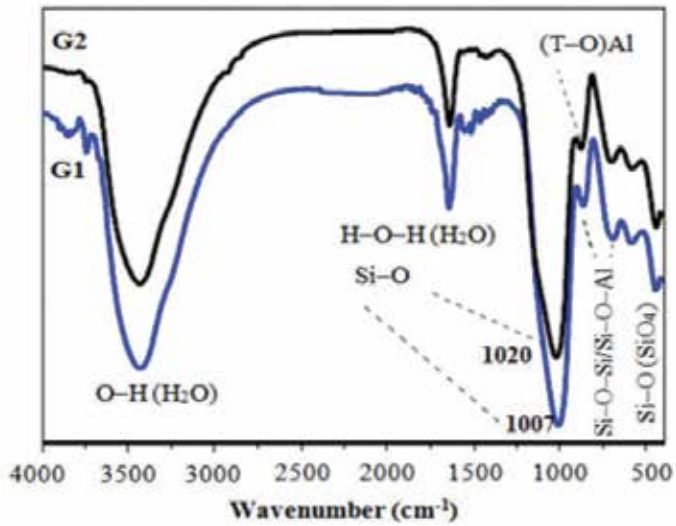

Figure 13. Shifts of FTIR bands from Gel 1 (G1) to Gel 2 (G2) [75].

stretching of Si-O-Si and Si-O-Al bonds [42, 74]. This band is shifted from the band at 1031 cm^{-1} in metakaolin. In addition, this FTIR band becomes more intense as the reaction proceeds indicating more geopolymer networks are formed. The band is usually shifted to lower wavenumber from raw materials and further shifted to higher wavenumber as a consequence of curing process. This is because of the changes in the silicate network with more substitution of non-bridging oxygen and increasing substitution of Al in the silicate sites. This is proved by the model by Duxson et al. [54] who proposed the transformation from Gel 1 to Gel 2 over time, aforementioned. This band shift is also observed in fly ash geopolymers (**Figure 13**) [75].

Another bands at 720 cm^{-1} (Si-O-Si/ Si-O-Al stretching), 560 cm^{-1} (tetrahedral aluminum stretching bands) and 690-440 cm^{-1} (Si-O-Si/ Si-O-Al bending vibrations) are also present in clay-based geopolymers [41, 42, 56]. High Si content in geopolymer structure produces stronger geopolymers as the Si-O-Si bonds are stronger than Si-O-Al bonds [76].

8. Properties of clay-based geopolymer

Geopolymers exhibit excellent mechanical and physical properties, such as low density, good chemical, fire and thermal resistance, high mechanical strength, and so on. Therefore, they are widely applied in various fields as new materials with high tech application. Geopolymers harden rapidly. In general, metakaolin geopolymers set and harden within 24 h. Short set time of 4 h has been reported by De Silva et al. [77] cured at 40°C. Fpr fly ash based geopolymer paste, in another way, sets and hardens faster compared to metakaolin geopolymers. Accordance to Hardjito et al., fly ash geopolymer can be hardened up to 2 h when cured at 65 and 80°C [78]. However, setting time is significantly dependent on the curing temperature. The geopolymer will set faster when cured at higher temperature. At 50°C, geopolymerization process required 4 h. Furthermore, geopolymerization process needed 1.5 h and 0.5 h

at 85 and 95°C, respectively [2]. If the geopolymer paste is cured at temperatures lower than ambient temperature, it might need more than 1 day to set. No degradation in the strength of geopolymers at 28 days even they set at a longer time, as reported by Rovnanik [74].

The bulk density of metakaolin geopolymers is reported in the range between 1.20 and 1.80 g/cm^3. Thus, lightweight products can be made out of geopolymers. The bulk density reported is lower than ordinary Portland cement paste and almost or even lower than geopolymers based on slag and fly ash . For instance, ordinary Portland cement paste has density of more than 1.80 g/cm^3 [35] while coal fly ash geopolymers have density in the range between 1.40 to 1.80 g/cm^3 [79, 80]. Bulk density is mainly affected by the curing condition as well as other synthesis parameters, such as the nature of alkali metal silicate, the type of geopolymers and alkali concentration. Bulk density decreases with increasing curing temperature [74]. Compressive strength increses with the increases of bulk density. Almost similar bulk density values were recorded for K-based (1.39–1.82 g/cm^3) and Na-based (1.25–1.72 g/cm^3) metakaolin geopolymers. Na-based geopolymers are generally lighter than K-based geopolymers. This is due to K-based geopolymers are denser and contain fewer pores as aforementioned [65].

From the result obtained by De Silva et al. [77] in **Figure 14**, high SiO_2/Al_2O_3 ratio in the initial composition shows longer setting and hardening times. Strength development of metakaolin geopolymers with SiO_2/Al_2O_3 of 3.81 became high and stabilized at a later age, even though the setting time was longer. Setting time is short providing that there is high Al_2O_3 content; however, it will deteriorate strength due to low SiO_2 content. Besides, the calcium content in the precursor materials would definitely affect the setting time. This is due to the fact that the Ca content provides extra nucleation sites for precipitation of dissolved species and hence leads to setting and hardening at a faster rate [55].

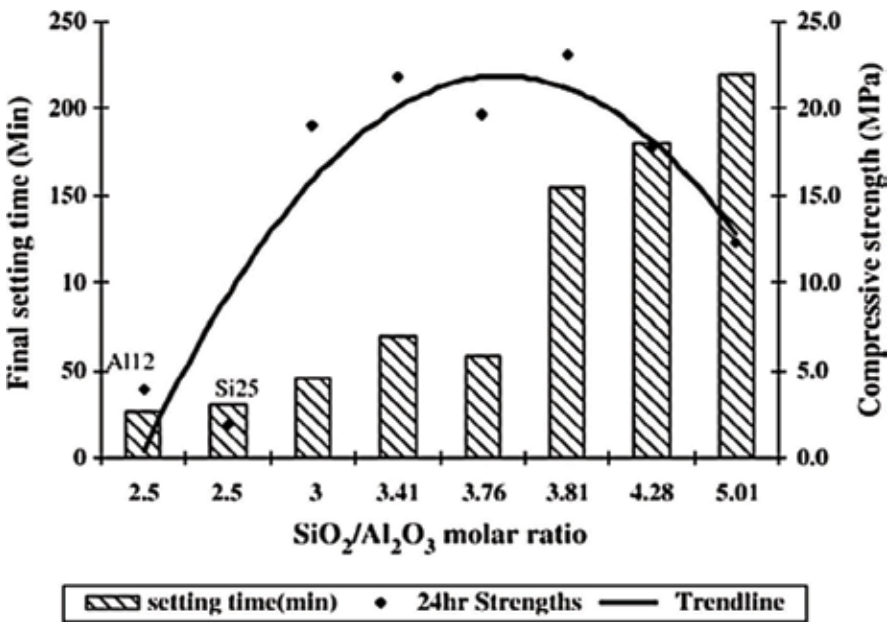

Figure 14. Final setting times and compressive strength of metakaolin geopolymers with varying SiO_2/Al_2O_3 molar ratios at constant H_2O/Na_2O molar ratio of 13.6 [81].

Geopolymers achieve compressive strength of 20 MPa after only 4 h at 20°C. The 28-day compressive strength of geopolymers could be as high as 70–100 MPa [1]. High strength means the easier or higher dissolution of source materials, generating more aluminosilicate species, which are the most important ingredients for geopolymerization process. The reaction extent of source materials can be measured directly by the compressive strengths of prepared geopolymers. The strength of geopolymers is dependent on the strength of gel phase, the amount of gel phase formed and amorphous nature of the reaction products [73].

On the other hand, geopolymers have excellent thermal stability with low shrinkage (2%). Geopolymers are stable up to 1000–1200°C [4, 58, 82, 83] and have ceramic-like structure [3]. Geopolymers are dimensionally stable in the working range between 250 and 800°C, accordance to Subaer and van Riessen [84]. In order to improve the thermal properties of geopolymers, filler (e.g. granite or quartz) and foaming agents (e.g. Al powder, hydrogen peroxide) have been added during geopolymer mixing. Addition of quartz or granite reduced shrinkage to 1% [85]. In addition, based on Rickard et al. [86], foamed geopolymers reinforced with polypropylene fibers achieved fire rating of at least 1 h (**Figure 15**).

Foamed geopolymers have good potential for ambient application as thermal insulator while exhibiting low density and compressive strength. For fire resistance application, materials must have very low thermal conductivity and resistance to thermal damage as to achieve the similar fire rating. Contradict result was reported by Elimbi et al. [87], whereby metakaolin geopolymers decreased in strength when heated between 300 and 900°C. It was explained due to the progressive transformation of geopolymer matrix into crystalline phases. The metakaolin geopolymers were warped and glazed with cracks at 1000°C.

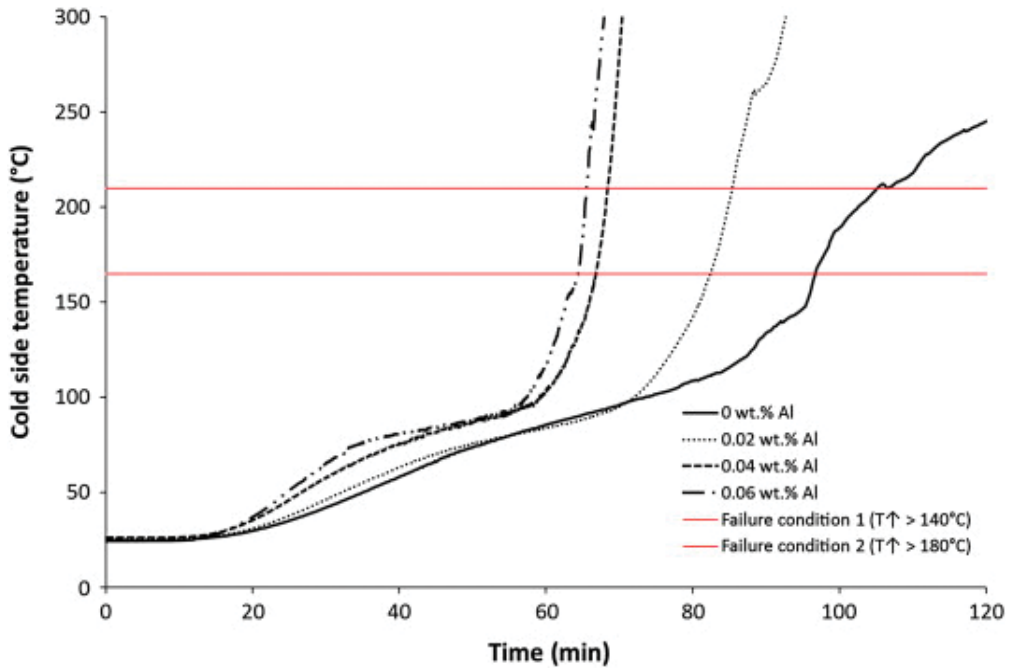

Figure 15. Cold side temperatures during the fire testing of four mixes of metakaolin geopolymers [86].

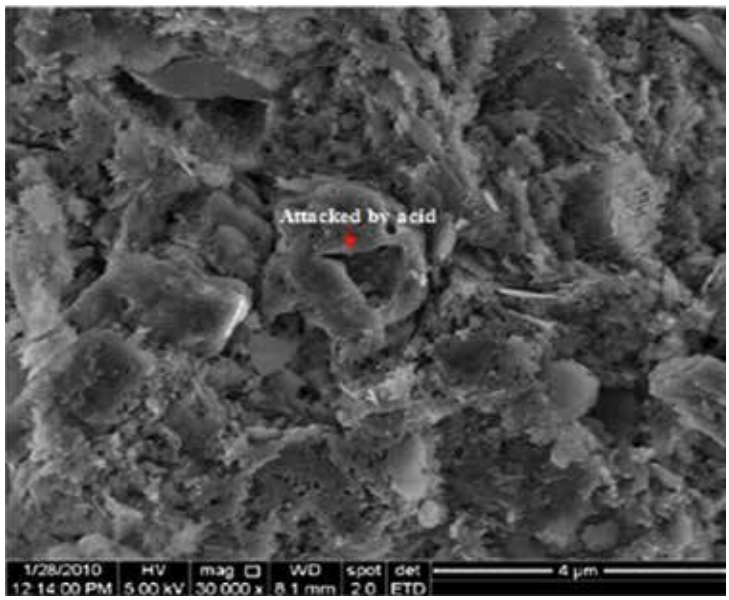

Figure 16. SEM micrograph of kaolinite geopolymers subjected to acid attack test after 90 days [30].

Geopolymers possess high perseverance in acidic and alkaline media [68, 88]. Comparatively, they are more stable under alkaline medium. No deterioration in mechanical properties when immersed in sea water (pH = 8) and sodium sulfate solution (5% Na_2SO_4) up to 360 days. On the other hand, geopolymers were severely attacked when immersed in HCl solution for long period. Compression strength decreased while mass loss of samples increased. This was probably due to the de-aluminum of geopolymer structure in highly acidic medium. De-aluminum leads to mass loss of geopolymer structure as the consequences of SiAOAAl bonds break that form more silicic acid ions in acid medium. The microstructure of the produced geopolymers became more porous (**Figure 16**) [30].

Drying shrinkage is shrinkage of the geopolymer matrix as a result of the loss of unbounded water during the curing process. As aforementioned, the addition of filler minimizes shrinkage of geopolymer samples. In general, shrinkage occurs in greater tendency in materials with higher content of finer materials than those with high content of coarser materials [89]. For instance, for geopolymers with sand filler, the drying shrinkage recorded was 0.01% at 180 days. However, for geopolymers without sand filler, the drying shrinkage fluctuated between 0.03 and 0.04% [30].

9. Applications of geopolymers

Geopolymers have great potential for variety of applications. Some applications have been successfully commercialized and marketed such as PYRAMENT blended cement and GEOPOLYMITE binders. GEOPOLYMITE binders have been used in several fields such as molding, tooling, foundry work, building's thermal insulation and furnace insulation while

PYRAMENT blended cement has been adapted in civil engineering in the production of prestressed and precast concrete [90].

Besides, geopolymers have been used to produce high-quality brick and tiles. Previously, kaolinite geopolymers are formed through low-temperature geopolymeric setting (L.T.G.S.) followed by ultra-rapid fire at 1000–1200°C to form bricks and tiles [4]. Up to now, this similar method has still being investigated by several researchers [91]. The geopolymer ceramics are non-burning and fire resistant. Furthermore, a new development of ceramic materials is compressing geopolymer powder using powder metallurgy method followed by sintering at 1000–1200°C [92].

In 1994, fireproof geopolymer fiber-reinforced composites have been used for aviation applications as aircraft composites and cabin interiors (floor panels, sidewalls, ceiling and partitions) to eliminate cabin fire during the aircraft accidents. The idea was arised from the problem of the existing plastic materials that were combustible and emitted flammable gases when they burnt. Besides, geopolymers have been used by Formula One teams in car manufacturing due to its corrosive, fire and heat resistance [4].

Concern toward lightweight materials for easy transportation and less energy consumption has led to lightweight concrete materials from geopolymers in civil engineering [93]. Furthermore, the lightweight concrete facilitates structural loading bearing and acts as thermal insulator [94]. Studies on foamed geopolymers in thermal insulation materials for housing construction have also been studied [95]. Zhang et al. [96] made reflective and heat insulative coating from geopolymers. With the addition of pigments and fillers (such as hollow glass microspheres, talc powder and titanium dioxide), wetting agent, dispersing agent and water-retaining agent, the coating produced has 90% reflectivity and thermal insulation performance up to 24°C. Apart from thermal insulative properties, the synthesis of geopolymer for acoustic insulation has been reported by Hung et al. [97]. Geopolymers can adequately and potentially become sound insulating materials in construction and buildings. The density of geopolymer matrix affects the noise reduction coefficient.

In addition, according to Temuujin et al. [98], geopolymers are capable of anti-ultraviolet and anti-aging, which made them suitable as coating for exterior wall building to conserve energy. The studies on the thermal and fire performance of geopolymers have also been reported elsewhere [81, 99–101]. As mentioned earlier, geopolymers have molecular structures to resemble zeolitic materials. As such, they are able to immobilize toxic waste or heavy metals as they can absorb and solidify toxic chemical waste. This is beneficial to the immobilization technology [84, 102].

Porous geopolymers were prepared by Okada et al. [89] for use in cooling system. This idea was come about due to high water retention properties or slow water releasing properties of geopolymers. This makes geopolymers suitable for surface cooling by water evaporation that helps to curb the rising earth temperature due to human activities and country development. Potential use of geopolymer in infrastructure rehabilitation was suggested by Pacheco-Torgal et al. [103]. Geopolymer paste can function as sealer for structures and replaced epoxy adhesives in fiber-reinforced polymer retrofiting. Almost similar research was carried out by Geraldes et al. [104], whereby geopolymers are used as restoration materials for tiles. In

order to further enhance the usage of geopolymers in civil engineering, researchers have investigated on one-part geopolymer system [105–107], whereby geopolymer mixture can be prepared by just adding water. The interest of this study is caused by the limitation of geopolymer technology for in-situ application which lowers its economical value.

n recent year, the study on geopolymers moves toward application as biomaterials. As proven by Pangdaeng et al. [28], geopolymer has good bioactivity and it is improved by the addition of white Portland cement. On the other hand, geopolymer as drug delivery system has also been studied by Jamstorp et al. [108] and Cai et al. [109]. Based on them, geopolymers possess variable pore-structure for the release of drug at target cell. This again extends the application of geopolymers in the medical fields.

Author details

Mohd Mustafa Al Bakri Abdullah*, Liew Yun Ming, Heah Cheng Yong and Muhammad Faheem Mohd Tahir

*Address all correspondence to: mustafa_albakri@unimap.edu.my

Center of Excellence Geopolymer & Green Technology, School of Materials Engineering, Universiti Malaysia Perlis (UniMAP), Kangar, Perlis, Malaysia

References

[1] Davidovits J. Geopolymers and geopolymeric new materials. Journal of Thermal Analysis. 1989;**35**(2):429-441

[2] Davidovits J. 30 years of successes and failures in geopolymer applications. Market trends and potential breakthroughs, in Geopolymer 2002 Conference. 2002, Geopolymer institute, Saint-Quentin, France: Melbourne, Australia

[3] Davidovits J. Geopolymers: Inorganic polymeric new materials. Journal of Thermal Analysis. 1991;**37**:1633-1656

[4] Provis JL, Lukey GC, van Deventer JSJ. Do geopolymers actually contain nanocrystalline zeolites? A reexamination of existing results. Chemistry of Materials. 2005; **17**:3075-3085

[5] Saidi N, Samet B, Baklouti S. Effect of composition on structure and mechanical properties of Metakaolin based PSS-Geopolymer. International Journal of Material Science. 2013;**3**(4):145-151

[6] Barbosa VFF, MacKenzie KJD, Thaumaturgo C. Synthesis and characterisation of materials based on inorganic polymers of alumina and silica: Sodium polysialate polymers. International Journal of Inorganic Materials. 2000;**2**(4):309-317

[7] Xu H, van Deventer JSG. Geopolymerization of multiple minerals. Minerals Engineering. 2002:**15**:1131

[8] Davidovits J. Chemistry of geopolymeric systems. Terminology. In Second International Conference Geopolymere'99. 1999. Saint-Quentin

[9] Komnitsas K, Zaharaki D. Geopolymerisation: A review and prospects for the minerals industry. Minerals Engineering. 2007;**20**:1261-1277

[10] Singh PS et al. Geopolymer formation process at room temperature studied by ^{29}Si and ^{27}Al MAS-NMR. Materials Science and Engineering A. 2005;**396**:392-402

[11] van Jaarsveld JGS. The physical and chemical characterisation of fly ash based geopolymers, in Department of Chemical Engineering. 2000, University of Melbourne: Victoria, Australia

[12] Temuujin J, Riessen Av, MacKenzie KJD. Preparation and characterisation of fly ash based geopolymer mortars. Construction and Building Materials. 2010;**24**:1906-1910

[13] Chindaprasirt P et al. Comparative study on the characteristics of fly ash and bottom ash geopolymers. Waste Management. 2009;**29**:539-543

[14] Hardjito D, Shaw Shen F. Fly ash-based geopolymer mortar incorporating bottom ash. Modern Applied Science. 2012;**4**:44-52

[15] Kong DLY, Sanjayan JG, Sagoe-Crentsil K. Comparative performance of geopolymers made with metakaolin and fly ash after exposure to elevated temperatures. Cement and Concrete Research. 2007;**37**:1583-1589

[16] Yunsheng Z, Wei S, Zongjin L. Composition design and microstructural characterization of calcined kaolin-based geopolymer cement. Applied Clay Science. 2010;**47**(3-4):271-275

[17] Wang SD, Scrivener KL, Pratt PL. Factors affecting the strength of alkali-activated slag. Cement & Concrete Research. 1994;**24**:1033-1043

[18] Cheng TW, Chiu JP. Fire-resistant geopolymer produced by granulated blast furnace slag. Minerals Engineering. 2003;**16**:205-210

[19] Villa C et al. Geopolymer synthesis using alkaline activation of natural zeolite. Construction and Building Materials. 2010;**24**(11):2084-2090

[20] MacKenzie KJD et al. Magnesium analogues of aluminosilicate inorganic polymers (geopolymers) from magnesium minerals. Journal of Materials Science. 2013;**48**:1787-1793

[21] Cioffi R, Maffucci L, Santoro L. Optimization of geopolymer synthesis by calcination and polycondensation of a kaolinitic residue. Resources Conservation and Recycling. 2003;**40**:27-38

[22] Varga G. The structure of kaolinite and metakaolinite. Epitoanyag. 2007;**59**:6-9

[23] Liew YM et al. Processing and characterization of calcined kaolin cement powder. Construction and Building Materials. 2012;**30**:794-802

[24] Cristobal AGS et al. Zeolites prepared from calcined and mechanically modified kaolins: A comparative study. Applied Clay Science. 2010;**49**:239-246

[25] Lecomte I et al. Synthesis and characterization of new inorganic polymeric composites based on kaolin or white clay and on ground-granulated blast furnace slag. Journal of Materials Research. 2003;**18**:2571-2579

[26] Zhang HY et al. Development of metakaolin–fly ash based geopolymers for fire resistance applications. Construction and Building Materials. 2014;**55**:38-45

[27] Buchwald A, Hilbig H, Kaps C. Alkali-activated metakaolin-slag blends—Performance and structure in dependence of their composition. Journal of Materials Science. 2007;**42**:3024-3032

[28] Pangdaeng S et al. Apatite forming on calcined kaolin-white Portland cement geopolymer. Materials Science and Engineering C; 2015

[29] Ferone C et al. Thermally treated clay sediments as geopolymer source material. Applied Clay Science. 2015;**107**:195-204

[30] Slaty F et al. Durability of alkali activated cement produced from kaolinitic clay. Applied Clay Science. 2015;**104**:229-237

[31] Takeda H et al. Characterization of zeolite in zeolite-geopolymer hybrid bulk materials derived from kaolinitic clays. Materials. 2013;**6**:1767-1778

[32] Davidovits J, Sawyer JL. Early High-Strength Mineral Polymer. United States: Pyrament Inc, Houston, Tex; 1984

[33] Davidovits J. Mineral Polymers and Methods of Making Them. United States; 1982

[34] Heah CY et al. Study on solids-to-liquid and alkaline activator ratios on kaolin-based Geopolymers. Construction and Building Materials. 2012;**35**:912-992

[35] Xu H, van Deventer JSJ. The geopolymerisation of alumino-silicate minerals. International Journal of Mineral Processing. 2000;**59**(3):247-266

[36] Heah CY et al. Effect of curing profile on kaolin-based geopolymers. Physics Procedia. 2011;**22**:305-311

[37] Kovarik T et al. A novel approach to polyaluminosialates curing process using electric boosting and temperature profile investigation by DSC. Journal of Thermal Analysis Calorimetry. 2015;**121**:517-524

[38] van Jaarsveld JGS, van Deventer JGS, Lukey GC. The effect of composition and temperature on the properties of fly-ash and kaolinite-based geopolymers. Chemical Engineering Journal. 2002;**89**:63-73

[39] Pacheco-Torgal F, Castro-Gomes J, Jalali S. Alkali-activated binders: A review. Part 2. About materials and binders manufacture. Journal of Construction and Building Materials. 2008;**22**:1315-1322

[40] MacKenzie KJD et al. Formation of aluminosilicate geopolymers from 1:1 layer-lattice minerals pre-treated by various methods: A comparative study. Journal of Materials Science. 2007;**42**:4667-4674

[41] Alonso S, Palomo A. Alkaline activation of metakaolin and calcium hydroxide mixtures: Influence of temperature, activator concentration and solids ratio. Materials Letters. 2001;**47**(1-2):55-62

[42] Alonso S, Palomo A. Calorimetric study of alkaline activation of calcium hydroxide-metakaolin solid mixtures. Cement and Concrete Research. 2001;**31**(1):25-30

[43] Yunsheng Z et al. Synthesis and heavy metal immobilization behaviours of slag based geopolymer. Journal of Hazardous Materials. 2007;**143**:206-213

[44] Davidovits J. High-alkali cements for 21st century concretes. In Concrete Technology, Past, Present and Future. 1994: Metha PK, Farmington Hills: American concrete institute

[45] Yip CK, Lukey GC, van Deventer JSJ. The coexistence of geopolymeric gel and calcium silicate hydrate at the early stage of alkaline activation. Cement and Concrete Research. 2005;**35**(9):1688-1697

[46] Davidovits J. Geopolymer chemistry and applications. 2nd ed. 16 Rue Galilee, 02100 Saint Quentin, France: Institute Geopolymere; 2008

[47] Singh PS, Bastow T, Trigg M. Structural studies of geopolymers by ^{29}Si and ^{27}Al MAS-NMR. Journal of Material Sciences. 2005;**40**:3951-3961

[48] Davidovits J. Geopolymers: Inorganic polymeric new materials. Journal of material. Education. 1994;**16**:91-139

[49] Davidovits J. Proceeding of the 1st International Conference on Geopolymer '88. 1988: Geopolymere, 16 Rue Galilee, 02100 Saint Quentin, France

[50] Dimas D, Giannopoulou L, Panias D. Polymerization in sodium silicate solutions: A fundamental process in geopolymerization technology. Journal of Material Sciences. 2009;**44**:3719-3730

[51] Xu H, van Deventer JSJ. The effect of alkali metals on the formation of geopolymeric gels from alkali-feldspars. Colloids and Surfaces A: Physicochemical and Engineering Aspects 2003;**216**:27

[52] Provis JL et al. Modeling the formation of geopolymers, in Department of Chemical and Biomolecular Engineering. Victoria, Australia: The University of Melbourne; 2006

[53] Provis JL, Deventer JSJv. Geopolymerisation kinetics. 2. Reaction kinetic modelling. Chemical Engineering Science. 2007;**62**:2318-2329

[54] Duxson P et al. Geopolymer technology: The current state of the art. Journal of Material. Sciences. 2007;**42**:2917-2933

[55] Rattanasak U, Chindaprasirt P. Influence of NaOH solution on the synthesis of fly ash geopolymer. Minerals Engineering. 2009;**22**(12):1073-1078

[56] Liew YM et al. Optimization of solids-to-liquid and alkali activator ratios of calcined kaolin geopolymeric powder. Construction and Building Materials. 2012;**37**:440-451

[57] Zhang YS, Sun W, Li ZJ. Hydration process of potassium polysialate (K-PSDS) geopolymer cement. Advances in Cement Research. 2005;**17**:23-28

[58] Sun W et al. In situ monitoring of the hydration process of K-PS geopolymer cement with ESEM. Cement and Concrete Research. 2004;**34**:935-940

[59] Wang H, Li H, Yan F. Synthesis and mechanical properties of metakaolinite-based geopolymer. Colloids and Surfaces A: Physicochemical and Engineering Aspects. 2005;**268**(1-3):1-6

[60] Rowles MR et al. ^{29}Si, ^{27}Al, ^{1}H and ^{23}Na MAS NMR study of the bonding character in aluminosilicate inorganic polymers. Applied Magnetic Resonance. 2007;**32**:663-689

[61] Steveson M, Sagoe-Crentsil K. Relationships between composition, structure and strength of inorganic polymers. Part 1: Metakaolin-derived inorganic polymers. Journal of Materials Science. 2005;**40**:2023-2036

[62] Wong H et al. Characterization and thermal behaviour of kaolin. Journal of Thermal Analysis and Calorimetry. 2011;**105**:157-160

[63] Belver C, Banares MA, Vicente MA. Preparation of porous silica by acid activation of metakaolins. In: 6th International Symposium on the Characterization of Porous Solids (COPS-VI). 2002. Alicante, Spain: Elsevier Science B.V.

[64] Davidovits J. Properties of geopolymer cements. In: Proceedings First International Conference. 1994. Kiev, Ukraine: Geopolymer Institute, Saint-Quentin, France

[65] Lizcano M et al. Mechanical properties of sodium and potassium activated metakaolin-based geopolymers. Journal of Materials Science. 2012;**47**:2607-2616

[66] Zibouche F et al. Geopolymers from Algerian metakaolin. Influence of secondary minerals. Applied Clay Science. 2009;**43**:453-458

[67] Duxson P et al. The effect of alkali and Si/Al ratio on the development of mechanical properties of metakaolin-based geopolymers. Colloids and Surfaces A: Physicochem. Eng. Aspects. 2007;**292**:8-20

[68] Palomo A et al. Chemical stability of cementitious materials based on metakaolin. Cement and Concrete Research. 1999;**29**:997-1004

[69] Kolousek D et al. Preparation, structure and hydrothermal stability of alternative (sodium silicate-free) geopolymers. Journal of Materials Science. 2007;**42**:9267-9275

[70] Criado M et al. An XRD study of the effect of the SiO_2/Na_2O ratio on the alkali activation of fly ash. Cement and Concrete Research. 2007;**37**:671-679

[71] Granizo ML, Blanco-Varela MT, Martinez-Ramirez S. Alkali activation of metakaolins: Parameters affecting mechanical, structural and microstructural properties. Journal of Material Sciences. 2007;**42**:2934-2943

[72] Galan E et al. Technical properties of compounded kaolin sample from Griva (Macedonia, Greece). Applied Clay Science. 1996;**10**:477-490

[73] Ilic BR, Mitrovic AA, Milicic LR. Thermal treatment of kaolin clay to obtain metakaolin. Hemijska Industrija. 2010;**64**:351-356

[74] Rovnanik P. Effect of curing temperature on the development of hard structure of metakaolin-based geopolymer. Construction and Building Materials. 2010;**24**:1176-1183

[75] Criado M, Fernandez-Jimenez A, Palomo A. Alkali activation of fly ash: Effect of the SiO_2/Na_2O ratio. Part 1: FTIR study. Microporous and Mesoporous. 2007;**106**:180-191

[76] Duxson P et al. Understanding the relationship between geopolymer composition, microstructure and mechanical properties. Colloids and Surfaces A: Physicochem. 2005;**269**:47-58

[77] De Silva P, Sagoe-Crenstil K, Dirivivatnanon V. Kinetics of geopolymerization: role of Al_2O_3 and SiO_2. Cement Concrete Research. 2007;**37**:512-518

[78] Hardjito D, Cheak CC, Ing CHL. Strength and setting times of low calcium fly ash-based geopolymer mortar. Modern Applied Science. 2008;**2**:3-11

[79] Andini S et al. Coal fly ash as raw material for the manufacture of geopolymer-based products. Waste Management. 2008;**28**:416-423

[80] Swanepoel JC, Strydom CA. Utilisation of fly ash in a geopolymeric material. Appl-Geochem. 2002;**17**(8):1143

[81] Kamseu E et al. Insulating behavior of metakaolin-based geopolymer materials assess with heat flux meter and laser flash techniques. Journal of Thermal Analysis and Calorimetry. 2012;**108**:1189-1199

[82] Davidovits J. Geopolymer chemistry and properties. In: Davidovits J, Orlinski J, editors. Proceedings of the 1st International Conference on geopolymer'88. Compiegne, France. p. 25-48

[83] Schmucker M, MacKenzie KJD. Microstructure of sodium polysialatesiloxogeopolymer. Ceramics International. 2005;**31**:433-437

[84] Chequer CD-L, Frizon F. Impact of sulfate and nitrate incorporation on potassium and sodium-based geopolymers: Geopolymerization and materials properties. Journal of Materials Science. 2011;**46**:5657-5664

[85] Subaer v RA. Thermo-mechanical and microstructural characterisation of sodium-poly (sialate-siloxo) (Na-PSS) geopolymers. Journal of Materials Science. 2007;**42**:3117-3123

[86] Rickard WDA, Vickers L, van Riessen A. Performance of fibre reinforced, low density metakaolin geopolymers under simulated fire conditions. Applied Clay Science 2013;**73**:71-77

[87] Elimbi A et al. Thermal behavior and characteristics of fired geopolymers produced from local Cameroonian metakaolin. Ceramics International. 2014;**40**:4515-4520

[88] Davidovits J. Recent progresses in concretes for nuclear waste and uranium waste containment. Concrete International. 1994;**16**(12):53-58

[89] Okada K et al. Water retention properties of porous geopolymers for use in cooling applications. Journal of the European Ceramic Society. 2009;**29**:1917-1923

[90] Davidovits J, Davidovics M. Geopolymer: Ultra-high temperature tooling material for the manufacture of advanced composites. SAMPE Symposium Exhibition. 1991;**36**:1939-1949

[91] Kuenzel C et al. Production of nepheline/quartz ceramics from geopolymer mortars. Journal of the European Ceramic Society. 2013;**33**:251-258

[92] Jaya NA, Abdullah MMAB, Ahmad R. Reviews on clay geopolymer ceramic using powder metallurgy method. Materials Science Forum. 2014;**803**:81-87

[93] Pimraksa K et al. Lightweight geopolymer made of highly porous siliceous materials with various Na_2O/Al_2O_3 and SiO2/Al2O3 ratios. Material Science Engineering, A. 2011;**528**:6616-6623

[94] Aguilar RA, Diaz OB, Garcia JIE. Lightweight concretes of activated metakaolin-fly ash binders, with blast furnace slag aggregates. Construction and Building Materials. 2010;**24**(7):1166-1175

[95] Prudhomme E et al. In situ inorganic foams prepared from various clays at low temperature. Applied Clay Science. 2011;**51**:15-22

[96] Zhang Z et al. Preparation and characterization of a reflective and heat insulative coating based on geopolymers. Energy and Buildings. 2015;**87**:220-225

[97] Hung T-C et al. Inorganic polymeric foam as a sound absorbing and insulating material. Construction and Building Materials. 2014;**50**:328-334

[98] Temuujin J, Minjigmaa A, Rickard W. Preparation of metakaolin based geopolymer coatings on metal substrates as thermal barriers. Applied Clay Science. 2009;**46**(3):265-270

[99] Henon J et al. Potassium geopolymer foams made with silica fume pore forming agent for thermal insulation. Journal of Porous Materials. 2013;**20**:37-46

[100] Temuujin J et al. Thermal properties of spray-coated geopolymer-type compositions. Journal of Thermal Analysis and Calorimetry. 2012;**107**:287-292

[101] Sukontasukkul P et al. Use of phase change material to improve thermal properties of lightweight geopolymer panel. Materials and Structures. 2016;**49**:4637-4645

[102] Ponzoni C et al. Chromium liquid waste inertization in an inorganic alkali activated matrix: Leaching and NMR multinuclear approach. Journal of Hazardous Materials. 2015;**286**:474-483

[103] Pacheco-Torgal F et al. An overview on the potential of geopolymers for concrete infrastructure rehabilitation. Construction and Building Materials. 2012;**36**:1053-1058

[104] Geraldes CFM et al. Geopolymers as potential repair material in tiles conservation. Applied Physics A Material Science Process. 2016;**122**:197

[105] Sturm P et al. Degree of reaction and phase content of silica-based one-part geopolymers investigated using chemical and NMR spectroscopic methods. Journal of Materials Science. 2015;**50**:6768-6778

[106] Ke X et al. One-part geopolymers based on thermally treated red mud/NaOH blends. Journal of the American Ceramic Society. 2015;**98**:5-11

[107] Peng MX et al. Synthesis, characterization and mechanisms of one-part geopolymeric cement by calcining low-quality kaolin with alkali. Materials and Structures. 2015;**48**:699-708

[108] Jamstorp E et al. Mechanically strong geopolymers offer new possibilities in treatment of chronic pain. Journal of Controlled Release. 2010;**146**:370-377

[109] Cai B, Engqvist H, Bredenberg S. Evaluation of the resistance of a geopolymer-based drug delivery system to tampering. International Journal of Pharmaceutics. 2014;**465**:169-174

Edited by Hosam El-Din M. Saleh and Rehab O. Abdel Rahman

Cement-based materials have been used by humans nearly since the dawn of civilization. The Egyptians used lime and gypsum cement to bind their aggregate materials, mud and straw, resulting in bricks that are used for building their famous Egyptian pyramids (between 3000 and 2500 BC).

Hydrated cement is a cement material bonded together with water and used for building construction; it is characterized by acceptable chemical, physical, thermal, mechanical, and structural stability. It plays a main role in the creation of vessels for storage, roads to travel on, weather-resistant structure for protection, inert hard stabilizer for hazardous wastes, and so on.

Due to the composition of these materials and their advantages, it has been practiced in different applications. Cement is an essential component of making concrete, the single most prevalent building material used worldwide for construction, skyscrapers, highways, tunnels, bridges, hydraulic dams, and railway ties.

Besides their numerous desired properties, there are some undesirable features. To overcome these disadvantages, several studies were established to prepare, improve, and evaluate innovative cement-based materials.

Despite its oldness and deep research, every year several methods and materials evolve and so do cement technology. This book intends to provide a comprehensive overview on recent advances in the evaluation of these materials.

Published in London, UK

IntechOpen

ISBN 978-1-83881-514-1